Marine biodiversity during the latest Cretaceous in Antarctica and the nature of the Cretaceous–Paleogene mass extinction

James David Witts

Submitted in accordance with the requirements for the degree of Doctor of Philosophy

The University of Leeds

School of Earth and Environment

June, 2016

The candidate confirms that the work submitted is his/her own, except where work which has formed part of jointly-authored publications has been included. The contribution of the candidate and the other authors to this work has been explicitly indicated below. The candidate confirms that appropriate credit has been given within the thesis where reference has been made to the work of others.

In the case of each data chapters outlined below, the candidate was the primary and corresponding author of material written for publication. Additional edits, extensive discussions, and reviews were provided by all co-authors at all stages during the PhD.

Chapter 3: Witts, J.D., Bowman, V.C., Wignall, P.B., Crame, J.A., Francis, J.E., Newton, R.J. Evolution and extinction of Maastrichtian (Late Cretaceous) cephalopods from the López de Bertodano Formation, Seymour Island, Antarctica. **Published** – *Palaeogeography, Palaeoclimatology, Palaeoecology*. 418 (January 2015), 193-212.

The candidate is the lead author and is responsible for all data analysis, interpretation, and for writing the manuscript. Fossil identifications were made by the candidate with help from Crame. Major editorial changes to the manuscript were contributed by all co-authors of the manuscript. Crame, Francis, and Bowman were responsible for field data collection in Antarctica.

Chapter 4: Witts, J.D., Whittle, R.J., Wignall, P.B., Crame, J.A., Francis, J.E., Newton, R.J., Bowman, V.C. Macrofossil evidence for a rapid and severe Cretaceous–Paleogene (K–Pg) mass extinction event in Antarctica. **Published** – *Nature Communications*. 7 (May 2016), March 2016.

Fieldwork and fossil sampling on Seymour Island was conducted by Crame, Whittle, Francis, and Bowman. Macrofossil identifications were made by the candidate with assistance from Whittle and Crame. The candidate analysed and interpreted the data, and wrote the manuscript with contributions and editorial changes from all co-authors.

Chapter 5: Witts, J.D., Newton, R.J., Wignall, P.B., Bottrell, S.H., Hall, J.L.O., Francis, J.E., Crame, J.A. A biogenic and sedimentary sulphur isotope record across the Cretaceous–Paleogene (K–Pg) boundary in Antarctica: relationship to environmental change, mass extinction and recovery. **Formatted for submission** – *Geochemica Cosmochemica Acta*.

The candidate prepared the samples, analysed the data, and is responsible for writing the manuscript. Fossil sampling and fieldwork in Antarctica was conducted by Francis and Crame. Newton and Bottrell provided laboratory facilities and analytical assistance, and Hall provided additional isotope data from fossil molluscs for comparison. All co-authors of the manuscript provided intellectual input and editorial changes to the draft manuscript.

Two additional manuscripts are appended to the thesis. These represent papers where the candidate is not the lead author, but did contribute data and expertise.

Acknowledgements

Firstly I would like to thank my supervisors; Paul Wignall, Jane Francis, Rob Newton, and Alistair Crame, for all their help, advice, and the benefit of their extensive scientific knowledge during the course of this long project. I would also like to thank two co-authors, de-facto supervisors, and good friends; Vanessa Bowman and Rowan Whittle. I feel extremely lucky to have had the opportunity to work with and learn from all of them.

I thank all the people I have shared an office with in Leeds over the years; Andy, Santi, Matt, Abi, Nick, Jon, Dawn, Laura, Rhian, Maggie, Chris, Jo, Autumn, and of course Tom Fletcher. Thank you all for your help, advice, patience, humour, and good company. I can only apologise for the years of heavy sighing, occasional bad language, and disruption from procrastination!

It is a bit of a cliché, but there really are too many people to thank for making the nearly seven years working and studying in Leeds such a great experience. I would like to single out Graham McLeod, for all the hilarious (and not so hilarious) fieldtrip memories, and the many hours of long drives in a Ford Tourneo/musical/philosophical education. Lyndsey Fox, a faithful tea break companion, fellow gin enthusiast, and baker of the worlds best chocolate foram cake. Steffi Lutz, who taught me that Germans do have a sense of humour (just don't mention ze war). Vern Manville, Phil Murphy, Nigel Mountney, Dan Morgan, Cris Little, Jacqui Houghton and others, taught me 'how to teach geology and get away with it' and supported me throughout my part-time teaching, part-time PhD role.

Completion of this thesis really would have been impossible without the help and unfailing support of my wonderful girlfriend, Aislinn Boylan. Thank you for everything.

Finally, I would like to thank my family for their continued love and encouragement. In particular, Steve Witts, Sarah Witts, and Sophie Witts. I would like to dedicate this thesis to my amazing parents, without whom none of this would have been possible.

The lost world of the Mesozoic: A typical scene in the shallow water, Maastrichtian oceans of the James Ross Basin, Antarctica ~66 million years ago. Now represented by rocks and fossils of the López de Bertodano Formation, outcropping on Seymour Island and the subject of this thesis.

At the height of the Antarctic summer, a group of heteromorph ammonites (*Diplomoceras cylindraceum*) drift through the shallows searching for food.

These 2 meter-long giants have attracted the attention of some planispiral ammonites (*Maorites densicostatus*) (middle right). In the background to the left, a pair of *Eutrephoceras* nautiloids forage in the silt of the sea bed, which is colonised by cidaroid echinoids and the coiled shells of the serpulid *Rotularia*.

(Painting by James McKay).

Abstract

The Cretaceous–Paleogene (K–Pg) mass extinction event occurred 66 million years ago, the most recent of the 'Big Five' extinction crises of the last 540 million years. This event had a profound effect on both life and the broader Earth system, with the extinction of up to 75% of life. Despite years of detailed research, debate continues as to the nature and timing of the extinction. Ideas for an abrupt crisis, triggered by bolide impact at Chicxulub in the Gulf of Mexico, contrast with those suggesting a more gradual extinction, involving volcanism from the Deccan Traps Large Igneous Province in India and/or climatic changes. Evidence from the high latitudes has been used to suggest that the fossil record from Antarctica is incompatible with models for a single, sudden event, and that extinction intensity declined at high latitudes. This thesis presents a detailed study of extensive fossil and sediment collections from the highest southern latitude onshore outcrop containing the K–Pg transition; the highly expanded and fossiliferous López de Bertodano Formation of Seymour Island, James Ross Basin, located at 65°S today, and during the Cretaceous. New biostratigraphic and diversity data for the molluscan (bivalves, gastropods, cephalopods) faunas of the López de Bertodano Formation, and geochemical datasets (seawater sulphur and pyrite sulphur isotopes) are compared to published records, and evidence for palaeoenvironmental change. They suggest a single, rapid extinction event coincident with the K–Pg boundary, with no precursor decline. The magnitude of the extinction in Antarctica is also consistent with lower latitudes, suggestive of a global, catastrophic trigger for the K–Pg extinction, such as bolide impact. Sulphur isotope data suggest the K–Pg sulphur cycle was able to respond to rapid environmental changes before, and after the K–Pg mass extinction. A decoupling of the carbon and sulphur cycle occurred during the latest Cretaceous, but productivity collapse after the K–Pg extinction also affected the sulphur cycle. The recovery to pre-extinction values was achieved on the same timescale as carbon cycle and initial ecological recovery, suggesting close geosphere-biosphere links at this time.

Table of Contents

List of Tables

List of Figures

Chapter 1 : Introduction

1.1 Thesis rationale

It is widely accepted that five major Mass Extinction events have shaped and altered the course of life on Earth over the past ~540 million years (Raup and Sepkoski, 1982; Hallam and Wignall, 1997; Bambach, 2006). The youngest, and also the most intensively studied of these 'Big Five' events is the Cretaceous–Paleogene (K–Pg) extinction of 66 million years ago (Ma), famed for its most high profile victims; non-avian dinosaurs and flying reptiles on land, and ammonoid cephalopods and marine reptiles in the oceans (e.g. MacLeod et al., 1997; Brusatte et al., 2014; Landman et al., 2015). This extinction event led to a fundamental restructuring of global ecosystems, and ultimately to the rise of modern fauna and flora (Alroy, 1998; Krug et al., 2009).

It is now over thirty-five years since the landmark study of Alvarez et al. (1980) ignited significant research interest into events that occurred during the K–Pg crisis. As per the original 'Alvarez Hypothesis', a significant body of work suggests that the extinction occurred geologically rapidly (Arenillas et al., 2006; Renne et al., 2013), and is coincident with evidence globally for rapid environmental deterioration following the impact of a large (~10 km diameter) bolide, producing the ~180–200 km wide Chicxulub crater in the Gulf of Mexico (Hildebrand et al., 1991; Ocampo et al., 2006; Schulte et al., 2010). However, disagreement remains as to the precise timing and magnitude of the extinction, as well as the contributions of a variety of other potential driving mechanisms including Large Igneous Province (LIP) volcanism represented by the Deccan Traps in India – now thought to have erupted in a 750 kyr 'window' around 66 Ma (Courtillot and Fluteau, 2010; Richards et al., 2014; Renne et al., 2015) – and other changes to the Earth system such as relatively rapid temperature and/or sea level oscillations which are apparent worldwide

during the latest Cretaceous (Archibald et al., 2010; Keller et al., 2010; Renne et al., 2013).

There are also persistent suggestions of a latitudinal gradient to the crisis, with a variety of faunal and floral groups appearing to show higher extinction rates at sites closer to the equator relative to sites located at high latitudes (Zinsmeister et al., 1989; Jiang et al., 2010; Vilhena et al., 2013). In addition, biotic and environmental recovery following the mass extinction is also hypothesised to have proceeded more rapidly at high latitudes in both marine and terrestrial settings (Sepúlveda et al., 2009; Jiang et al., 2010; Barreda et al., 2012).

Much of the ongoing debate surrounding the K–Pg extinction is at least partly due to the relative rarity of sites (particularly in shallow marine and terrestrial settings) which provide a complete record of events during the critical time intervals leading up to, and in the immediate aftermath of the extinction event. It is also apparent that an even smaller number of onshore locations provide adequate stratigraphic and temporal coverage to truly evaluate the palaeoenvironmental context in which the extinction took place, and especially at a resolution that allows hypotheses surrounding the cause and effects to be examined in a satisfactory way (e.g. Hart et al., 2012). There is a clear need for detailed, stratigraphically constrained datasets from such locations to assess how global ecosystems and the wider Earth system were affected by the various environmental changes during the Cretaceous–Paleogene time interval.

1.2 Aims and objectives

This thesis aims to examine one such stratigraphic succession which includes a record of the K–Pg extinction event; represented by the shallow marine sediments of the highly expanded López de Bertodano Formation from the high southern latitude location of Seymour Island, Antarctica (65°S).

The overall aims are to provide a detailed, and where possible quantitative, assessment of the K–Pg extinction event on the high latitude shallow marine

2

biota, by utilising extensive macrofossil collections (primarily based on marine molluscs – ammonoid and nautiloid cephalopods, bivalves and gastropods) taken from a series of detailed measured sedimentary sections across southern Seymour Island. By examining the pre-boundary Maastrichtian community, faunal changes during the boundary interval, and the earliest Paleocene fauna, this study will also provide a longer-term record of macrofaunal diversity change at high latitudes through this critical time interval.

In addition, generation of stable isotope records (sulphur isotopes) and assessment of the sedimentary geochemistry of the López de Bertodano Formation allows the record of marine biodiversity to be placed in context alongside evidence for other palaeoenvironmental changes occurring in Antarctica, and worldwide, during this time.

Specifically, this thesis aims to answer the following broad research questions:

1. What is the nature, rate, and timing of the Cretaceous–Paleogene extinction event in Antarctica? Is there evidence for a single, catastrophic event, a gradual diversity drawdown through the Late Cretaceous, or is the extinction in Antarctica the sum of multiple, different events?

2. How do hypothesised Earth system changes (e.g. sea level, climate changes) occurring at high latitudes during the Cretaceous–Paleogene interval affect marine biodiversity?

3. How does the record of environmental and biotic change recorded in the López de Bertodano Formation compare with existing records from contemporaneous lower latitude sections?

4. How do these new data from Antarctica add to the various hypotheses surrounding the K–Pg mass extinction event and its probable causes, effects, and the subsequent recovery of life?

1.3 Thesis structure and publications

To answer these questions, this thesis is divided into six chapters. Following an overview of the thesis rationale and structure in the remainder of **Chapter 1**, **Chapter 2** provides the necessary detailed background to the study, using the published literature to establish a global and local context for the data outlined in the rest of the thesis. This is then followed by three data chapters, each representing either a published peer-reviewed publication, or a manuscript formatted ready for submission.

Chapter 3: Witts, J.D., Bowman, V.C., Wignall, P.B., Crame, J.A., Francis, J.E., Newton, R.J. Evolution and extinction of Maastrichtian (Late Cretaceous) cephalopods from the López de Bertodano Formation, Seymour Island, Antarctica. **Published** – *Palaeogeography, Palaeoclimatology, Palaeoecology*. 418 (January 2015), 193-212.

This chapter examines the fate of the ammonoid and nautiloid cephalopod fauna of the López de Bertodano Formation using well-constrained data from two measured sections across southern Seymour Island. Following taxonomic identification of a collection of 700 + macrofossils, stratigraphic range and occurrence data are used to examine diversity (measured as species richness) in a composite section through the Maastrichtian, and compare this to evidence for environmental changes (e.g. sea level, palaeotemperature changes) prior to the K–Pg extinction.

To place the record from Seymour Island in context, an examination is also made of the longer-term Late Cretaceous record of diversity changes in ammonoid and nautiloid cephalopods compared to other groups (inoceramid bivalves, belemnites), as well as evidence for long-term environmental change through the entire Coniacian–Maastrichtian interval of the James Ross Basin (e.g. Crame et al., 1996; Crame and Luther, 1997; Olivero, 2012).

Interpretation of the ammonite record at the K–Pg boundary in Antarctica is made using data collected for this thesis, and integration with published information (Zinsmeister, 1998). An attempt is also made to estimate the Signor-Lipps effect prior to the K–Pg boundary for cephalopods in the British

4

Antarctic Survey (BAS) sedimentary sections using stratigraphic confidence intervals (Marshall, 2010), and stratigraphic abundance data (Meldahl, 1990).

Chapter 4: Witts, J.D., Whittle, R.J., Wignall, P.B., Crame, J.A., Francis, J.E., Newton, R.J., Bowman, V.C. Macrofossil evidence for a rapid and severe Cretaceous–Paleogene (K–Pg) mass extinction event in Antarctica. **Published** – *Nature Communications.* 7 (May 2016), March 2016.

This chapter builds on the results of Chapter 3, but focuses primarily on the record of benthic molluscs (bivalves and gastropods) from the López de Bertodano Formation. Updated taxonomic information (Beu, 2009; Crame et al., 2014) is used to re-assess the identifications of a number of benthic molluscan taxa (e.g. Zinsmeister and Macellari, 1988; Stilwell et al., 2004), and stratigraphic range data based on first and last occurrence is again used to examine diversity (measured as species richness), as well as estimates of (local) extinction and origination rates through time (Foote, 2000).

This chapter includes data from an additional sedimentary section from Seymour Island, thus updating information presented in **Chapter 3** and presents a synthetic view of the K–Pg extinction record from the López de Bertodano Formation which can be directly compared with existing hypotheses concerning the rate and timing of the extinction event in Antarctica (Zinsmeister et al., 1989; Zinsmeister, 1998; Tobin et al., 2012).

As well as comparison of benthic diversity with palaeotemperature and sea level changes, new data is also presented based on sedimentary microfacies analysis of a suite of bulk sediment samples. This allows an examination of benthic redox fluctuations using pyrite framboids and pyrite petrography (Wilkin et al., 1996; Bond and Wignall, 2010), and suggests that contrary to previous studies, these may have had some effect on diversity during the Maastrichtian–Paleocene interval in Antarctica.

Chapter 5: Witts, J.D., Newton, R.J., Wignall, P.B., Bottrell, S.H., Hall, J.L.O., Francis, J.E., Crame, J.A. A biogenic and sedimentary sulphur isotope record across the Cretaceous–Paleogene (K–Pg) boundary in Antarctica: relationship

to environmental change, mass extinction and recovery. **Formatted for submission** – *Geochemica Cosmochemica Acta*.

The focus of this chapter is the generation of a high-resolution seawater sulphur isotope record through the López de Bertodano Formation, primarily based on the Carbonate Associated Sulphate (CAS) proxy from well-preserved fossil bivalve shells. This represents the first detailed record of seawater sulphate across the K–Pg boundary, with additional datasets derived from sedimentary sulphide (pyrite) and an assessment of sedimentary geochemistry (total organic carbon, total sulphur). The new seawater sulphate record reveals several interesting features which could be related to Maastrichtian environmental change before the K–Pg extinction, as well as the immediate after-effects of the extinction event – principally the hypothesised collapse in marine productivity.

Using the isotopic difference ($\Delta^{34}S$) between CAS and sedimentary pyrite, an estimate is made of seawater sulphate concentration during the Maastrichtian. An additional discussion highlights local effects (sedimentation rate, local sedimentary biogeochemistry related to anaerobic oxidation of methane (AOM), which preclude the estimation of concentration data over the K–Pg boundary itself.

Chapter 6 discusses how the preceding chapters/papers both form a coherent body of work, and how they have answered the research questions outlined above. A summary of the main conclusions and implications of the work is provided, together with some suggestions for areas of ongoing research.

Supplementary Information for the three primary data chapters/papers is included as **Appendices A–C**, either in the main body of the thesis, or on an accompanying CD.

Appendices D and **E** are copies of two additional relevant manuscripts appended to the thesis, or on the accompanying CD. These include data contributed by the candidate, (which is also presented in other parts of the thesis), but are not manuscripts where the candidate is lead or corresponding author.

Appendix D: Little, C.T.S., Birgel, D., Boyce, A.J., Crame, J.A., Francis, J.E., Kiel, S., Peckmann, J., Pirrie, D., Rollinson, G.K., **Witts, J.D.,** Late Cretaceous (Maastrichtian) shallow water hydrocarbon seeps from Snow Hill and Seymour Islands, James Ross Basin, Antarctica. **Published -** *Palaeogeography, Palaeoclimatology, Palaeoecology*, 418 (January 2015), 213-228.

This appendix is included on the accompanying CD.

Appendix E: Hall, J.L.O., Newton, R.J., **Witts, J.D**., Francis, J.E., Harper, E.M., Crame, J.A., Haywood, A.M., Hunter, S.J. Sedimentary carbon cycling in a low sulfate ocean: Evidence of episodic seasonal methane oxidation in the Cretaceous Antarctic. **In preparation for submission** - *Proceedings of the National Academy of Science.*

This appendix is included in the main body of the thesis.

1.4 References

Alroy, J., 1998. Cope's rule and the dynamics of body mass evolution in North American fossil mammals. *Science* **280**, 731–734.

Alvarez, L.W., Alvarez, W., Asaro, F., Michel, H.V., 1980. Extraterrestrial cause for the Cretaceous-Tertiary Extinction. *Science* **208**, 1095–1108.

Archibald, J.D., Clemens, W.A., Padian, K., Rowe, T., MacLeod, N., Barrett, P.M., Gale, A., Holroyd, P., Sues, H.-D., Arens, N.C., Horner, J.R., Wilson, G.P., Goodwin, M.B., Brochu, C.A., Lofgren, D.L., Hurlbert, S.H., Hartman, J.H., Eberth, D.A., Wignall, P.B., Currie, P.J., Weil, A., Prasad, G.V.R., Dingus, L., Courtillot, V., Milner, A., Milner, A., Bajpai, S., Ward, D.J., Sahni, A., 2010. Cretaceous extinctions: multiple causes. *Science* **328**, 973.

Arenillas, I., Arz, J.A., Grajales-Nishimura, J.M., Murillo-Muňetón, G., Alvarez, W., Carmargo-Zanoguera, A., Molina, E., Rosales-Domínguez, C., 2006. Chicxulub impact event is Cretaceous/Paleogene boundary in age: new micropaleontological evidence. *Earth and Planetary Science Letters* **249**, 241–257.

Bambach, R.K., 2006. Phanerozoic biodiversity mass extinctions. *Annual Reviews of Earth and Planetary Science* **34**, 127–155.

Barreda, V.D., Cúneo,N.R., Wilf, P., Currano, E.D., Scasso, R.A., Brinkhuis, H., 2012. Cretaceous/Paleogene floral turnover in Patagonia: drop in diversity, low extinction, and a *Classopollis* spike. PLoS ONE **7**, e52455. http://dx.doi.org/10.1371/journal.pone.0052455 .

Beu, A. G., 2009. Before the ice: biogeography of Antarctic Paleogene molluscan faunas. *Palaeogeography Palaeoclimatology Palaeoecology* **284**, 191–226.

Bond, D.P.G., Wignall, P.B., 2010. Pyrite framboid study of marine Permian-Triassic boundary sections: a complex anoxic event and its relationship to contemporaneous mass extinction. *Geological Society of America Bulletin* **122**, 1265–1279.

Brusatte, S.L., Butler, R.J., Barrett, P.M., Carrano, M.T., Evans, D.C., Lloyd, G.T., Mannion, P.D., Norell, M.A., Peppe, D.J., Upchurch, P., Williamson, T.E. 2015. The Extinction of the Dinosaurs. *Biological Reviews* **90**, 628–642.

Courtillot, V., Fluteau, F., 2010. Cretaceous extinctions: the volcanic hypothesis. *Science* **328**, 973–974.

Crame, J.A., Luther, A., 1997. The last inoceramid bivalves in Antarctica. *Cretaceous Research* **18**, 179–195.

Crame, J.A., Lomas, S.A., Pirrie, D., Luther, A., 1996. Late Cretaceous extinction patterns in Antarctica. *Journal of the Geological Society of London.* **153**, 503–506.

Crame, J. A., Beu, A. G., Ineson, J. R., Francis, J. E., Whittle, R. J. & Bowman, V. C., 2014. The early origins of the Antarctic marine fauna and its evolutionary implications. *PLoS ONE* **9**, e114732.

Foote, M., 2000. Origination and extinction components of taxonomic diversity: general problems. *Paleobiology* **26**, 74–102.

Hallam, A. and Wignall, P.B. *Mass extinctions and their aftermath*. Oxford, Oxford University Press, 330pp.

Hart, M.B., Yancey, T.E., Leighton, A.D., Miller, B., Liu, C., Smart, C.W., Twitchett, R., 2012. The Cretaceous-Paleogene boundary on the Brazos River, Texas: New stratigraphic sections and revised interpretations. Gulf Coast Association of Geological Sciences Journal **1**, 69–80.

Hildebrand, A.R., Penfield, G.T., Kring, D.A., Pilkington, M., Camargo Z, A., Jacobsen, S.B., Boynton, W.V., 1991. Chicxulub crater: A possible Cretaceous/Tertiary boundary impact crater on the Yucatán Peninsula, Mexico. *Geology* **19**, 867–871.

Jiang, S., Bralower, T. J., Patzkowsky, M. E., Kump, L. R., Schueth, J. D., 2010. Geographic controls on nannoplankton extinction across the Cretaceous/Paleogene boundary. *Nature Geoscience* **3**, 280–285.

Keller, G., Adatte, T., Pardo, A., Bajpai, S., Khosla, A., Samant, B., 2010. Cretaceous extinctions: evidence overlooked. *Science* **328**, 974–975.

Krug, A.Z., Jablonski, D., Valentine, J.W., 2009. Signature of the end-Cretaceous mass extinction in the modern biota. *Science* **323**, 767–771.

Landman N.H., Goolaerts S., Jagt J.W.M., Jagt-Yazykova E.A., Machalski M., 2015. Ammonites on the Brink of Extinction: Diversity, Abundance, and Ecology of the Order Ammonoidea at the Cretaceous/Paleogene (K–Pg) Boundary. In: Klug C, Korn D, Baets KD, Kruta I, Mapes RH, (Eds.), *Ammonoid Paleobiology: From macroevolution to paleogeography*. Springer Netherlands; 2015. pp. 497–553.

MacLeod, N., Rawson, P.F., Forey, P.L., Banner, F.T., Boudagher-Fadel, M.K., Bown, P.R., Burnett, J.A., Chambers, P., Culver, S., Evans, S.E., Jeffrey, C., Kaminski, M.A., Lord, A.R., Milner, A.C., Milner, A.R., Morris, N., Owen, E., Rosen, B.R., Smith, A.B., Taylor, P.D., Urquhart, E., Young, J.R., 1997. The Cretaceous-Tertiary biotic transition. *Journal of the Geological Society of London* **154**, 265–292.

Marshall, C. R., 2010. in: *Quantitative methods in paleobiology.* (eds Alroy, J. and Hunt, G.) The Palentological Society Papers **16**, 291–316.

Meldahl, K.H., 1990. Sampling, species abundance, and the stratigraphic signature, of mass extinction: a test using Holocene tidal flat molluscs. *Geology* **18**, 890–893.

Ocampo A., Vajda, V., Buffetaut, E., 2006. Unravelling the Cretaceous–Paleogene (KT) turnover, evidence from flora, fauna and geology. In: Cockell, C., Gilmour, I., Koeberl, C., (Eds.), *Biological Processes Associated with impact events*, Springer, Berlin Heidelberg (2006). 197–219.

Olivero, E.B., 2012. Sedimentary cycles, ammonite diversity and palaeoenvironmental changes in the Upper Cretaceous Marambio Group, Antarctica. *Cretaceous Research* **34**, 348–366.

Raup, D.M., Sepkoski, J.J. 1982. Mass extinctions in the marine fossil record. *Science* **215**, 1501–1503.

Renne, P. R., Deino, A.L., Hilgen, F.J., Kuiper, K.F., Mark, D.F., Mitchell, W.S.III., Morgan, L.E., Mundil, R., Smit, J., 2013. Time scales of critical events around the Cretaceous–Paleogene boundary. *Science* **339**, 684–687 (2013).

Renne, P.R., Sprain, C.J., Richards, M.A., Self, S., Vanderkluysen, L., Pande, K., 2015. State shift in Deccan volcanism at the Cretaceous–Paleogene boundary, possibly induced by impact. *Science* **350**, 76–78.

Richards, M. A., Alvarez, W., Self, S., Karlstrom, L., Renne, P.R., Manga, M., Sprain, C.J., Smit, J., Vanderkluysen, L., Gibson, S.A., 2015. Triggering of the largest Deccan eruptions by the Chicxulub impact. *Geological Society of America Bulletin* **127**, 1507–1520.

Schulte, P.D., Alegret, L., Arenillas, I., Arz, J.A., Barton, P.J., Bown, P.R., Bralower, T.J., Chisteson, G.L., Claeys, P., Cockell, C.S., Collins, G.S., Deutsch, A., Goldin, T.J., Goto, K., Grajales-Nishimura, J.M., Grieve, R.A.F., Gulick, S.P.S., Johnson, K.R., Kiessling, W., Koeberl, C., Kring, D.A., MacLeod, K.G., Matsui, T., Melosh, J., Montanari, A., Morgan, J.V., Neal, C.R., Nichols, D.J., Norris, R.D., Pierazzo, E., Ravizza, G., Rebolledo-Vieyra, M., Reimold, W.U., Robin, E., Salge, T., Speijer, R.P., Sweet, A.R., Urrutia-Fucugauchi, J., Vajda, V., Whalen, M.T., Willumsen, P.S., 2010. The

Chicxulub asteroid impact and mass extinction at the Cretaceous-Paleogene boundary. *Science* **327**, 1214–1218.

Sepúlveda J., Wendler, J.E., Summons, R.E., Hinrichs, K.U., 2009. Rapid resurgence of marine productivity after the Cretaceous-Paleogene mass extinction. *Science* **326**, 129–132.

Stilwell, J. D., Zinsmeister, W. J., Oleinik, A. E., 2004. Early Paleocene mollusks of Antarctica: systematics, paleoecology and paleogeographic significance. *Bulletins of American Paleontology* **367**, 1–89.

Tobin, T. S., Ward, P.D., Steig, E.J., Olivero, E.B., Hilburn, I.A., Mitchell, R.N., Diamond, M.R., Raub, T.D., Kirschvink, J.L., 2012. Extinction patterns, $\delta^{18}O$ trends, and magnetostratigraphy from a southern high-latitude Cretaceous–Paleogene section: links with Deccan volcanism. *Palaeogeography Palaeoclimatology Palaeoecology* **350–352**, 180–188.

Vilhena, D.A., Harris, E.B., Bergstrom, C.T., Maliska, M.E., Ward, P.D., Sidor, C.A., Stromberg, C.A.E., and Wilson, G.P., 2013. Bivalve network reveals latitudinal selectivity gradient at the end-Cretaceous mass extinction. *Scientific Reports* **3**, http://dx.doi.org/10.1038/srep01790 .

Wilkin, R. T., Barnes, H. L. & Brantley, S. L., 1996. The size distribution of framboidal pyrite in modern sediments: an indicator of redox conditions. *Geochimica et Cosmochimica Acta* **60**, 3897–3912.

Zinsmeister, W.J., 1998. Discovery of fish mortality horizon at the K–T boundary on Seymour Island: re-evaluation of events at the end of the Cretaceous. *Journal of Paleontology* **72**, 556–571.

Zinsmeister W.J., Macellari, C.E.,1988. Bivalvia (Mollusca) from Seymour Island, Antarctic Peninsula. In: Feldmann, R.M., Woodburne, M.O. (Eds.), *Geology and Paleontology of Seymour Island, Antarctic Peninsula*. Geological Society of America, Memoirs **169**, 253–284.

Zinsmeister, W. J., Feldmann, R. M., Woodburne, M. O., Elliot, D. H., 1989. Latest Cretaceous/earliest Tertiary transition on Seymour Island, Antarctica. *Journal of Palaeontology* **63**, 731–738.

Chapter 2 : Background and literature review

2.1 Mass extinction events: background

A constant background level of extinction occurs naturally on Earth, meaning that existing species disappear and new species arise continually over time. Compilations of taxonomic diversity taken directly from analysis of the fossil record (e.g. Sepkoski, 2002) indicate that during the Phanerozoic Eon (541.0 Ma to present), there have been a number of time intervals where the rate of extinction is significantly elevated relative to this natural background, leading to a large proportion of biodiversity loss over geologically short periods of time (e.g. Raup and Sepkoski, 1982; Alroy et al., 2008). These events are commonly identified as mass extinction events, and it is now well understood that they have played a key role in shaping the course and trajectory of life on Earth throughout the Phanerozoic (Raup and Sepkoski, 1982; Sepkoski, 1986; Hallam and Wignall, 1996; Bambach, 2004; 2006; Jablonski, 2005; Alroy et al., 2008). Mass extinction events are not only responsible for global depletions in biodiversity, but are also drivers of macroevolutionary change; leading to the construction of entirely new ecosystems in their aftermath, as well as sparking changes and new innovations in morphology and ecology (Jablonski, 2005; Twitchett, 2006; Hull and Darroch, 2013).

Despite their importance, no clear definition of what classes a 'mass extinction' is agreed upon in the literature, nor is their complete agreement over exactly how many of the episodes of apparent accelerated biodiversity loss in the Phanerozoic truly qualify as mass extinction events (see reviews by Bambach, 2004; 2006; Hull and Darroch, 2013). One commonly used definition is that of Sepkoski (1986);

 "*A mass extinction is any substantial increase in the amount of extinction (i.e., lineage termination) suffered by more than one geographically wide-spread higher taxon during a relatively short interval of geologic time, resulting in an at least temporary decline in their standing diversity*" (Quoted in Hallam and Wignall (1996).

As noted by Bambach (2006), this definition is sufficiently flexible to cover a variety of events in the Phanerozoic, each of which exhibit differing properties; either in the rate or magnitude of the biodiversity loss, or in the likely driving mechanism behind the extinction event.

Up to twenty distinct periods of elevated extinction throughout the Phanerozoic have been put forward as candidates for the term 'mass extinction' (Hallam and Wignall, 1996; Bambach, 2006), with five such events often suggested as forming a separate, higher category (the 'Big Five') (Figure 2.1); end-Ordovician (e-O), Frasnian–Fammenian (Late Devonian) (F–F), Permian–Triassic (P–T), Triassic–Jurassic (T–J), and Cretaceous–Paleogene (K–Pg) (Raup and Sepkoski, 1982; Hallam and Wignall, 1996; Bambach, 2004; 2006; Twitchett, 2006). Analyses suggest that in fact, only three of these events (e-O, P–T, and K–Pg) form a statistically separate class of event based on magnitude alone (Bambach, 2004).
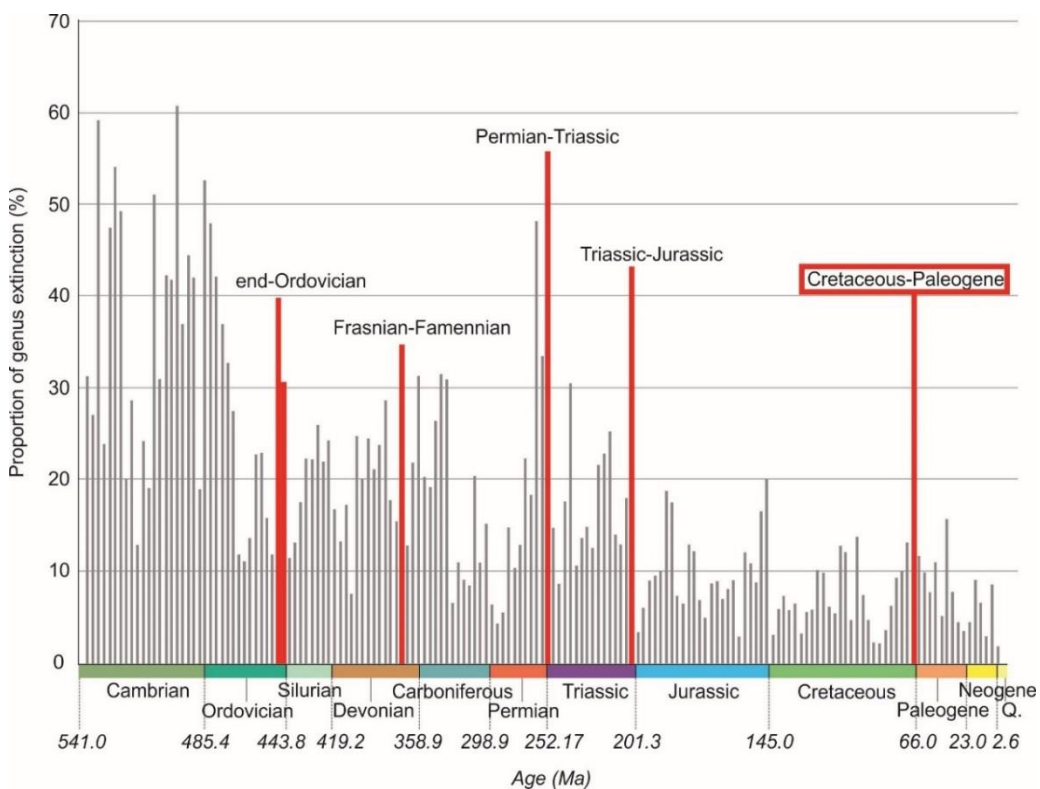
Figure 2.1: Taxonomic severity of the major Phanerozoic mass extinction events according to Bambach (2006). The 'Big Five' mass extinction events are highlighted in red, with the K–Pg event additionally highlighted with the red box. Taxonomic severity is expressed as proportion of genus extinction at the substage level (%).

Although extinction events are traditionally classified according to the magnitude of biodiversity loss (expressed typically as a percentage extinction), an additional and alternative measure of the severity of a biodiversity crisis is to examine the ecological severity of such an event, which often appears decoupled from the taxonomic impact (e.g. McGhee et al., 2004; 2013). Mass extinctions can lead to fundamental changes in the different organismal groups that dominate marine and terrestrial communities in the aftermath of mass extinctions (e.g. the classic view of dinosaur extinction followed by rapid mammalian evolution and rise to dominance in terrestrial communities after the K–Pg extinction (Alroy, 1998)).

Many mass extinction events are also associated with significant perturbations to global biogeochemical cycles, typically manifest as prominent and apparently rapid excursions in stable isotope records of common elements such as carbon and sulphur (e.g. Hsü and Mackenzie, 1985; Kump, 1991; Newton et al., 2004; Payne et al., 2004; Whiteside and Ward, 2009). These perturbations are often thought to be key to understanding the potential driving mechanisms behind these events, as a variety of hypothesised causal mechanisms for mass extinction (e.g. bolide impact, marine anoxia, LIP volcanism, sea level change) will leave distinctly different signatures on a variety of stable isotope systems.

One school of thought suggests that caution is required when taking a literal view of biodiversity loss and links to 'catastrophic' rapid environmental change in the fossil record, primarily due to the vagaries of preservation and subsequent controls on sampling (e.g. Benton et al., 2013). Related to this, attention is often payed to the role that sea level and associated facies changes play in controlling the quality and completeness of the marine fossil record (the so-called 'taphonomic megabias' problem) (Smith et al., 2001; Holland and Patzkowsky, 2015). A recent review suggests that concentrations of fossil disappearances at sequence stratigraphic boundaries, and coincident evidence for sea level and facies changes appear to be common features of the rock record coincident with many extinction events throughout the Phanerozoic (Holland and Patzkowsky, 2015). Any data pertaining to answer

questions concerning environmental and biotic change at times of mass extinction must be carefully placed in a stable and rigorous stratigraphic and sedimentological framework. Crucially, this study found that the stratigraphic record of the K–Pg extinction appeared to be the least affected by complications due to sea level or facies changes (Holland and Patzkowsky, 2015) although local conditions obviously control this at an outcrop scale.

Sampling and rarity of fossil taxa still exerts a considerable control on stratigraphic distribution of fossils relative to extinction horizons (the 'Signor-Lipps' effect (Signor and Lipps, 1982)). The rarer a fossil is in any given stratigraphic section, the less likely its last appearance is to record its extinction level. A variety of techniques have been developed to deal with this problem, including calculating confidence intervals on stratigraphic ranges at varying scales (Marshall, 2010), or assessing stratigraphic abundance (Meldahl, 1990; Song et al., 2012).

Perhaps because of these difficulties, there remains considerable debate as to whether there is a common cause and driving mechanism behind mass extinction events. Since the publication of Alvarez et al. (1980), two principal hypotheses have developed as to the ultimate drivers of mass extinctions; the environmental consequences of extraterrestrial impact events (principally thought to involve food chain collapse related to the blocking of sunlight by dust and debris in the atmosphere, leading to productivity collapse, rapid ocean acidification and anoxia). And/or climate changes, in many cases driven by Large Igneous Province (LIP) volcanism (volatile release leading to climate warming (and short-term cooling), increased continental weathering patterns and runoff, increased productivity in the oceans, slow-down in ocean and atmospheric circulation, increase in shallow water anoxia, potential release of gas hydrate deposits causing further warming) (e.g. Schulte et al., 2010; Bond and Wignall, 2014; Wignall, 2015).

The temporal coincidence between LIPs, bolide impact and mass extinction during the Phanerozoic is explored in Figure 2.2. A good coincidence has been demonstrated between LIP eruptions and several mass extinctions (Late Permian, Triassic–Jurassic, early Jurassic) (Wignall, 2001; Bond and Wignall,

2014). Note the coincidence between the Deccan Traps, the largest LIP in the last 300 myrs, the Chicxulub crater, the largest recorded impact event in the Phanerozoic, and the K–Pg extinction (to within 1 million years). Several authors have proposed the so-called 'Press-Pulse' extinction theory based on this coincidence (White and Saunders, 2005; Arens and West, 2008; Arens and Thompson, 2014), whereby a combination of LIP volcanism and bolide impact could conspire to cause a mass extinction. In this scenario, applied most commonly to the K–Pg extinction, volcanism (or rapid climate change (Renne et al., 2013)) causes a destabilisation of global communities, making them more susceptible to sudden extinction following a bolide impact event.
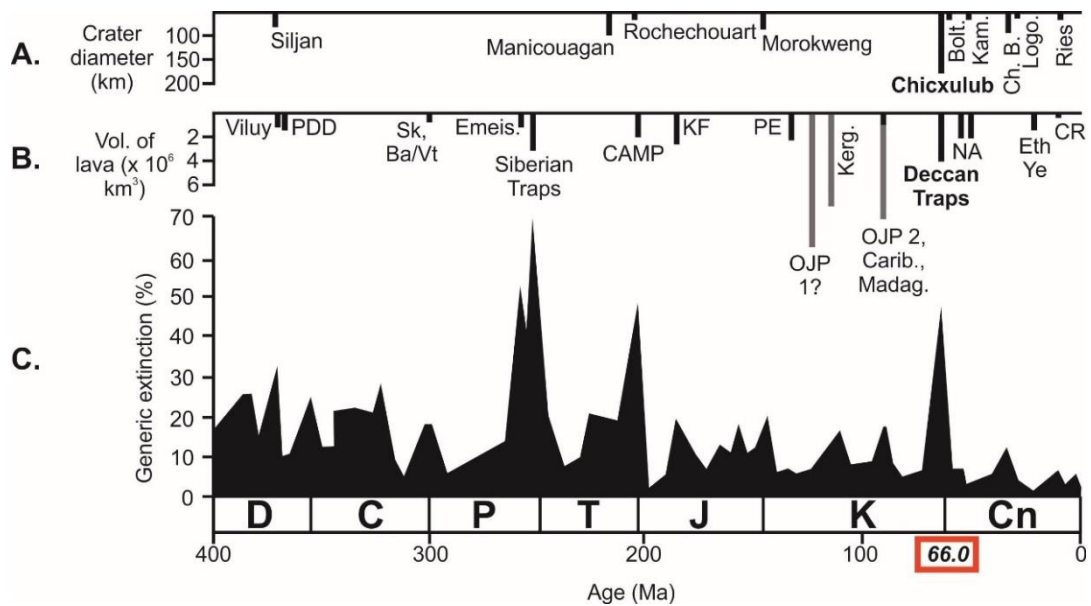
Figure 2.2: Exploring the temporal coincidence between bolide impact events (A. –Diameter of significant impact craters in km), LIP volcanism (B. – volume of lava erupted in km³, black bars = continental LIP's, grey bars = oceanic LIP's), and mass extinction (C. – % genus extinction, black shaded areas) for the last 400 myrs of the Phanerozoic. D, Devonian, C, Carboniferous, P, Permian, T, Triassic, J, Jurassic, K, Cretaceous, Cn, Cenozoic. Modified from Bond and Wignall (2014) with crater diameters and ages from Jourdan et al. (2012). Generic extinction in this case based on Sepkoski (1996; 2002). Crater abbreviations; Bolt., Boltysh; Kam., Kamensk; Ch. B., Chesapeake Bay; Logo., Logoisk. LIP abbreviations: PDD, Pripyat-Dnieper-Donets; Sk, Ba/Vt, Skagerrak, Barguzin/Vitim; Emeis., Emeishan Traps; CAMP, Central Atlantic Magmatic Province; KF, Karoo-Ferrar; PE, Parana Etendeka; OJP 1 and 2, Ontong-Java Plateau; Kerg., Kerguelen Plateau; Carib., Madag., Carribean, Madagascar; NA, North Atlantic; Eth Ye, Ethiopia Yemen; CR, Columbia River.

To test the 'Press-Pulse' model requires a rigorous examination of a suitably high resolution fossil record, and detailed knowledge of the relative timings of the 'press' and 'pulse' events, as well as background environmental conditions. In reality, the search for generalised drivers of mass extinction events has revealed many of these events to have unique characteristics, although it is worth noting that the K–Pg extinction remains the only one of the 'Big Five' convincingly linked to a bolide impact.

2.2 The K–Pg mass extinction

The Cretaceous–Paleogene (K–Pg) mass extinction is defined as occurring precisely at the boundary between the Maastrichtian (72.1–66.0 Ma) and Danian (66.0–61.6 Ma) stages (Molina et al., 2006; Gradstein et al., 2012). Current estimates of taxonomic loss suggest that up to 76% of species and ~40–45% of genera worldwide went extinct during the K–Pg crisis (Raup and Sepkoski, 1982; Bambach, 2006) (Figure 2.1), thus firmly identifying it as one of the most severe of the 'Big Five' Phanerozoic mass extinction events.

In terrestrial ecosystems the K–Pg is characterised by the complete collapse and disappearance of dinosaur-dominated ecosystems which first appeared some 165 million years earlier in the Late Triassic, following the P–T extinction (Benton et al., 2014). After the K–Pg event, terrestrial ecosystems in the Cenozoic were rapidly dominated by newly evolved mammals (Alroy, 1998). Considerable debate has surrounded the fate of the dinosaurs at the K–Pg boundary (Sheehan et al., 2000; Brusatte et al., 2014), although the only stratigraphically well-constrained record of their demise, and the fate of terrestrial ecosystems at the K–Pg boundary itself is located in the Hell Creek Formation of Western North America, a region with complex local stratigraphy (Fastovsky and Bercovici, 2015). Sections in Europe do contain evidence for Maastrichtian dinosaur faunas (Vila et al., 2016), but the stratigraphic and temporal coverage is insufficient to match the North American record.

Although typically overshadowed by the loss of the dinosaurs, other groups of terrestrial animals in the Hell Creek Formation suffered large-scale biodiversity loss during the K–Pg extinction, including many groups that survived and recovered to successfully dominate modern ecosystems. Thus the mammal fossil record from North America shows a 75–93% extinction (Wilson, 2014a; Longrich et al., In Press), archaic bird groups, lizards and snakes also show locally high species-level extirpation rates of up to 83% (Longrich et al., 2012), while the record from lissamphibians is lower at 22% species loss (Wilson et al., 2014b). The plant fossil record also shows dramatic change at the K–Pg boundary (see review by Nichols and Johnson, 2008), with extinctions of many

megafossil and pollen morphotypes, and a dramatic increase in the abundance of fern spores signifying a sudden die-back in vegetation (Tschudy et al., 1984). The extent to which these results are local to North America is not clear and must await the discovery of other well-constrained terrestrial K–Pg boundary sections. Crucially, the 'fern spike' has been confirmed in the Southern Hemisphere (Vajda et al., 2001), suggesting a global disruption to terrestrial ecosystems.

In the oceans, the K–Pg extinction triggered fundamental changes to the structure of oceanic ecosystems on a global scale, with the permanent loss of at least some groups (100% extinction of marine reptiles, ammonites, rudist bivalves) (Steuber, 2002; Polcyn et al., 2014; Landman et al., 2014), and the near total extirpation but subsequent recovery of others (>80% extinction of various groups of marine plankton) (Bown, 2005; Molina et al., 2015). Other groups such as benthic molluscs (bivalves and gastropods), benthic foraminifera, dinoflagellates, echinoids, fish and sharks, show variable extinction rates (Raup and Jablonski, 1993; Brinkhuis et al., 1998; Jeffery, 2001; Aberhan et al., 2007; Alegret and Thomas, 2007; Friedmann and Sallan, 2012) and similarly varying recovery times.

This is partly due to a degree of heterogeneity seen in palaeontological records from different ocean basins (Hull and Norris, 2011; Sibert et al., 2014), and potentially different latitudes (Zinsmeister et al., 1989; Keller, 1993; Jiang et al., 2010; Barreda et al., 2012, but see also Huber et al., 1994). This suggests that while the effects of this extinction were global, they may not have been uniform around the globe.

2.2.1 Bolide impact hypothesis, evidence, and potential kill-mechanisms

Modern research into the K–Pg extinction began with the study of Alvarez et al. (1980), who suggested the cause of the widespread extinctions seen in the rock record at the K–Pg boundary were the result of a catastrophic bolide impact. The original hypothesis was based on the discovery of a thin clay layer significantly enriched in the rare earth element iridium (Ir) coincident with the

sudden and catastrophic mass extinction in planktonic foraminifera in multiple sections worldwide (Smit and Hertogen, 1980). Subsequent discoveries of shocked minerals (Bohor et al., 1987), and Ni-rich spinels contained with small spherules, characteristic of deposition from molten material (Kyte and Smit, 1984), in K–Pg boundary layers worldwide bolstered the hypothesis (Figure 2.3). The discovery of the >170 km-wide Chicxulub crater buried beneath the Yucatan Peninsula, Gulf of Mexico (Hildebrand et al., 1991) and accurately dated to within 31 kyrs of the boundary layer and mass extinction (Arenillas et al., 2006; Renne et al., 2013) cemented the idea as the leading hypothesis for the cause of the mass extinction. Exhaustive study has confirmed similar geochemical, stratigraphic, and palaeontological signatures at K–Pg boundary sites worldwide (Schulte et al., 2010) (Figure 2.4).
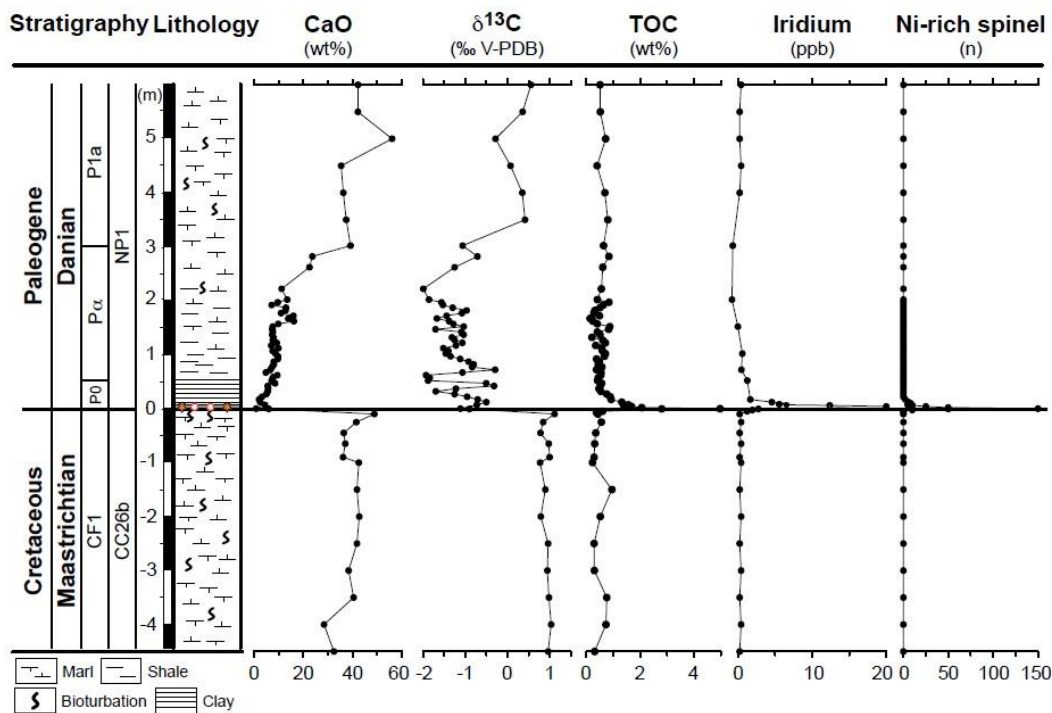
Figure 2.3: Integrated stratigraphy and geochemistry of the El Kef site; the GSSP for the K–Pg boundary. Note impact debris (spinels, microtektites) precisely at the biostratigraphic K–Pg boundary (coloured symbols in Lithology column at the base of the clay layer and P0 biozone). This level is also coincident with sharp negative excursion in bulk δ¹³C, and sudden extinction of 91% of planktonic foraminifera (Arenillas et al., 2000; Molina, 2015).

A general pattern of increasing thickness of K–Pg boundary deposits with closer proximity to the Chicxulub crater has also been observed (Figure 2.4). Many of the most proximal sites contain evidence for apparently chaotic sedimentation, extensive reworking, and complicated stratigraphy – perhaps related to deposition from mega-tsunami waves emanating from the impact site. These sections have proved difficult and controversial to interpret (e.g. Arenillas et al., 2006; Keller et al., 2007; Schulte et al., 2008; Hart et al., 2012).
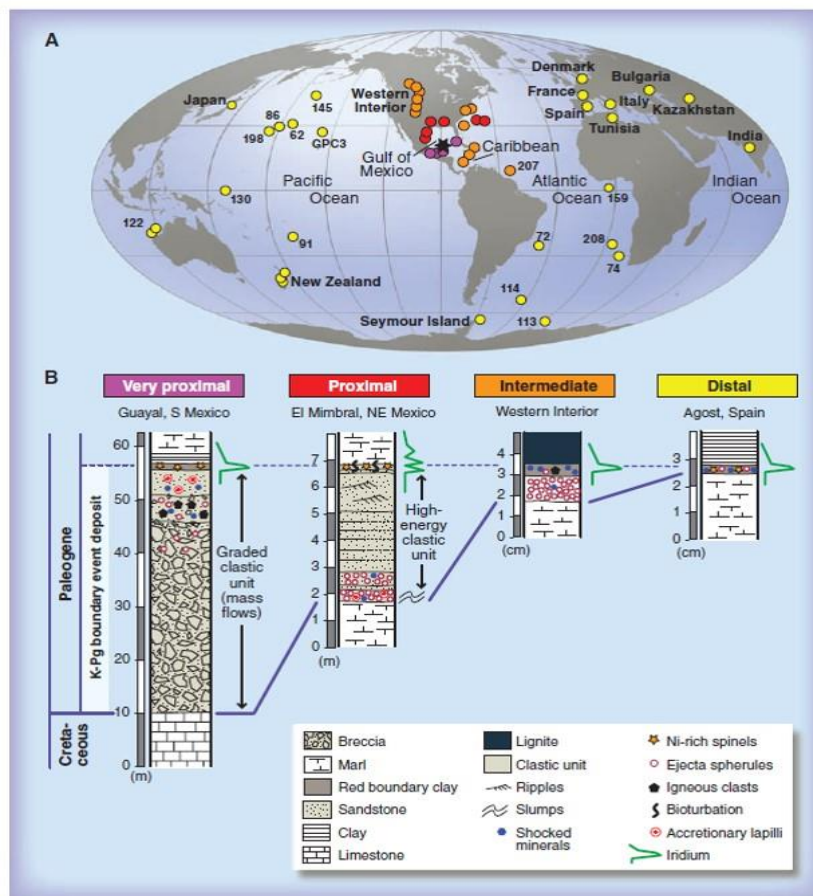
Figure 2.4: A: Global distribution of K–Pg boundary locations. Deep-sea sites are referred to using Ocean Drilling Program or Deep Sea Drilling Program numbers. Asterisk marks location of Chicxulub crater. Coloured dots mark the four different types (Very proximal-distal) of K–Pg boundary deposit with increasing distance from the Gulf of Mexico. B: Schematic lithological columns of the four types of site and key. Highlighting 'chaotic' nature of sites proximal to the Chicxulub crater, and the depositional sequence of different materials that are hypothesised to originate from a single event. Taken from Schulte et al. (2010).

In the bolide impact hypothesis, the extinctions occurred catastrophically, with the kill mechanisms a cascade of secondary effects from the impact (e.g. Kring, 2007; Pierazzo and Artemieva, 2012; Robertson et al., 2013a; Robertson et al., 2013b). Impact models suggest an initial phase of large earthquakes, generation of tsunamis and mass wasting of continental margins (Klaus et al., 2000) close to the impact site, and a globally distributed 'heat pulse' as ballistic ejecta falls back through the atmosphere (Robertson et al., 2013a). This is followed by an 'impact winter' as dust, and sulphate aerosols from the Chicxulub basement rocks (limestone platform carbonates and evaporites - Brett, 1992) remain in the atmosphere and supress light levels. Models indicate the potential for a general cooling of the surface ocean by several degrees (Pierazzo and Artemieva, 2012), supported by high-resolution temperature (Vellekoop et al., 2014; Vellekoop et al., 2016) and faunal data (Vellekoop et al., 2015) from successions in the Gulf of Mexico, Atlantic Coastal Plain USA, and former Tethys ocean (Tunisia). A short-lived period of transient ocean acidification from generation of a sulphur-rich vapour plume has also been proposed (Ohno et al., 2014) based on high extinction rates in calcareous surface water organism (Alegret et al., 2012). However, geochemical models do not provide much support for this (Tyrrel et al., 2015). Disruption to the carbon cycle may actually have caused a shallowing of the carbonate compensation depth and short term alkalinity increase after the boundary, buffering the oceans from the effects of any acidification (Henehan et al., 2016).

In the original impact hypothesis Alvarez et al. (1980) suggested that an impact event of a ~10 km bolide would trigger suppression of light levels sufficient enough to collapse photosynthesis and food chains globally. Although the amount of dust generated by the impact may not have been sufficient to generate substantial periods of global darkness (Pope, 2002), the huge extinctions seen in primary producers globally (calcareous microplankton and nannoplankton) at the boundary (Coxall et al., 2006), and disappearance of organisms higher in the food chain (marine reptiles, ammonites) supports the food chain collapse theory. Further evidence comes from the behaviour of

the carbon cycle at the K–Pg boundary. A prominent negative excursion (Figure 2.3) is seen in bulk rock records, along with a collapse in the isotopic difference between benthic and planktonic foraminifera in the aftermath of the extinction (Zachos and Arthur, 1989; Birch et al., 2016). This represents a generalised decrease in the sinking of organic material to the deep sea floor, lasting >1 Myr (D'Hondt, 2005; Birch et al., 2016). Overall evidence points to a period of supressed productivity in the oceans (Esmeray-Senlet et al., 2015) and on land (Beerling et al., 2001) lasting decades (terrestrial) to several 100 kyrs (marine) after the impact event. A generalised model of enhanced survivorship for detritus feeding organisms around the globe (Hansen et al., 1993; Aberhan et al., 2007), also lends some support to this hypothesis.

2.2.2 Deccan Traps and LIP volcanism; hypothesis, evidence and potential kill mechanisms

The most prominent alternative theory for the cause of the K–Pg extinction event remains the temporal coincidence of the extinction with the eruption of the Deccan Traps LIP in continental India (Courtillot and Flueteau, 2010; Schoene et al., 2015; Font et al., 2016). As previously mentioned, strong links exist between LIP eruptions and other mass extinction events in the Phanerozoic (Wignall, 2001; Bond and Wignall, 2014; Wignall, 2015). LIPs have the potential to alter global environments primarily through volatile release from magmas or magma-sediment interactions, leading to alteration of atmospheric chemistry and global climate warming or cooling (Self et al., 2014). Associated changes to the Earth system as a result of LIP-driven climate change could include weathering rate variations, the expansion of ocean anoxia, metal poisoning and ocean acidification (Wignall, 2005; 2015 Bond and Wignall, 2014; Self et al., 2014). The extent to which this occurs appears to vary according to the tectonic, geological, and geographic setting of any given LIP (Bond and Wignall, 2014; Self et al., 2014; Glaze et al., In Press).

The Deccan Traps covers approximately 512,000 km^2, with the original volume prior to erosion probably close to 1.5 million km^3 (Keller et al., 2012). Although establishing a simple stratigraphy through the lava pile is

challenging, the main body of the traps is made up of three main groups, and attains a thickness of ~3500m (Chenet et al., 2009). Traditional models for Deccan emplacement involved three main 'phases' of eruption (Chenet et al., 2009; Keller et al., 2012); an initial pulse of minor activity occurring an estimated one million years prior to the K–Pg boundary (Chenet et al., 2009; Keller et al., 2016), followed by a main phase of eruptions correlated to magnetochron C29R that straddles the K–Pg boundary, with the final phase in the early Danian (Chenet et al., 2009; Schoene et al., 2015; Keller et al., 2016). Magnetostratigraphy and recent high-precision dating analyses suggest the main phase accounts for ~80% of the total volume of erupted material (Figure 2.5), temporally overlapped with the K–Pg boundary, and was probably characterised by higher eruption rates and frequencies (Renne et al., 2015), although the precise location of the boundary in the lava pile is unknown.
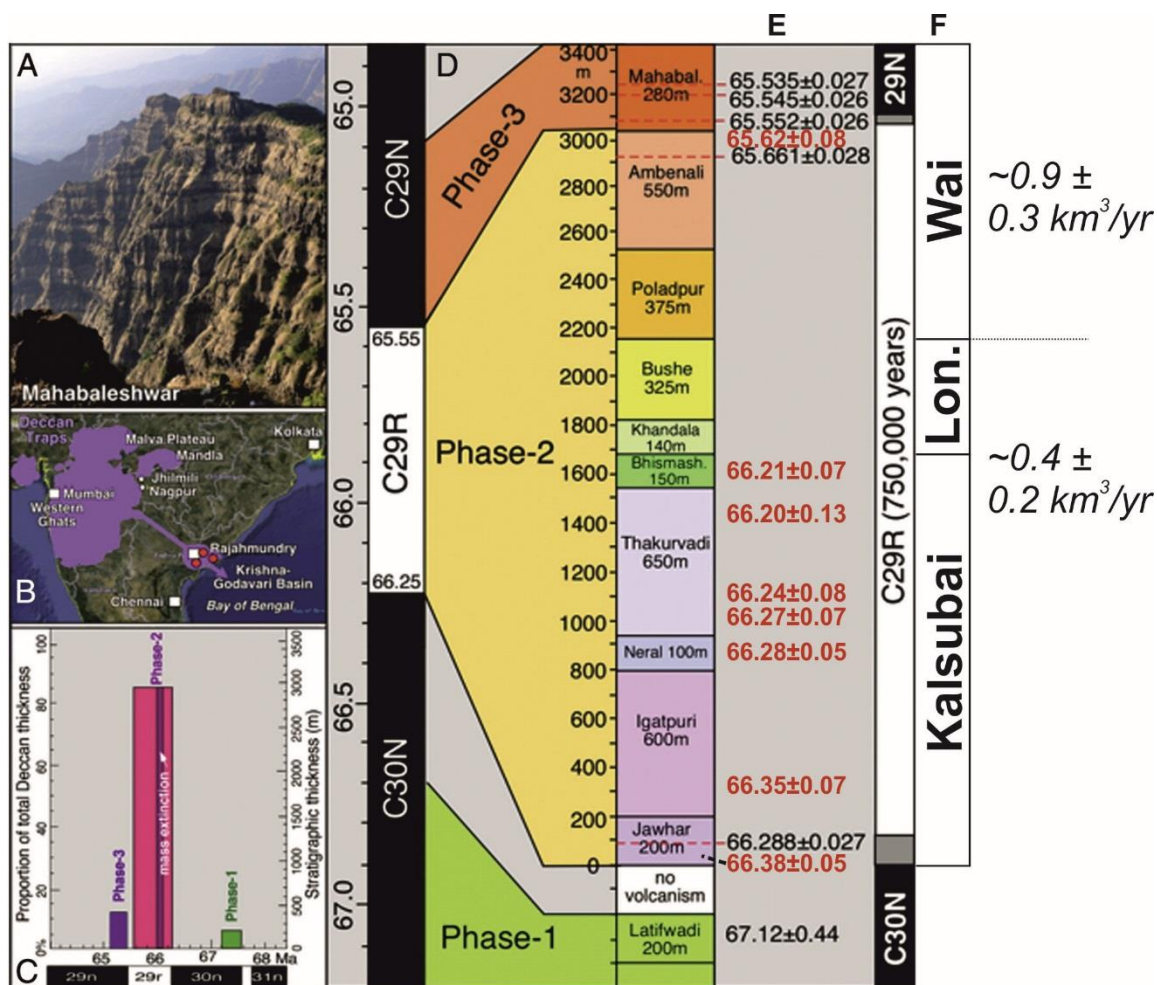
Figure 2.5 (previous page): Geography and stratigraphy of the Deccan Traps: A, Deccan Traps near Mahalabeshwar, Western Ghats. B, Geography of India showing the current extent of Deccan volcanic rocks (purple) with long lava flows to Rajahmundry and Krishna-Godavari Basin. C, Ages of the three phases of Deccan volcanism and estimated lava eruptions by percent of total volume. D, Composite stratigraphic section of the Deccan Traps in the Western Ghats, with approximate formation thicknesses. E, Absolute ages based on U–Pb geochronology (black text) (Schoene et al., 2015) and $^{40}Ar/^{39}Ar$ (red text) (Renne et al., 2015). F, Palaeomagnetic timescale for Deccan Traps, with grey areas corresponding to uncertainty in location of magnetic reversals. Large-scale Deccan stratigraphy and eruption rates based on Renne et al. (2015). Lon = Lonavalla. Figure is modified from Keller et al. (2016) with additional data from Renne et al. (2015).

An estimated $>1.3 \times 10^6$ km^3 of lava was erupted from the Deccan Traps, although using thickness of individual lava flows and formations as a proxy for volume and estimates of volatile release is problematic. Nevertheless, total volatile emissions from the Deccan are generally thought to be high compared to other LIPs (totals of 3.5-6.5 x 10^6 Mt (SO_2), 1.4 x 10^7 Mt (CO_2), and 1 x 10^6 Mt (Cl) respectively) (Self et al., 2014). Individual eruptions probably occurred as short-lived pulses over years, decades, or centuries (Callegaro et al., 2014). The potential for environmental change resulting from release of volatiles during these individual eruptions is still debated (Schmidt et al., 2016; Tobin et al., in press).

Deccan lavas had a high sulphur content (Self et al., 2008; Callegaro et al., 2014), which could lead to transient global cooling and acid rain deposition. Models suggest this would only be the case if the volatile-laden eruption plumes reached sufficient heights in the stratosphere (Wignall, 2001; Glaze et al., In Press), and if eruption frequencies and lava discharge rate were high (Schmidt et al., 2015). CO_2 release leading to climate warming seems a more plausible explanation for Deccan-induced environmental change (Wignall, 2005; Tobin et al., in press), with a pronounced and apparently global warming event recorded in chron C29R prior to the K–Pg boundary (see below). Mercury anomalies in marine sediments have recently emerged as a promising proxy for tracing LIP activity (e.g. Grasby et al., 2016; Thibodeau et al., 2016), representing emissions of this toxic element during large scale

volcanism. Such emissions may even play a role as a kill mechanism through metal poisoning. Mercury anomalies are present in a number of Maastrichtian–Danian successions and are suggestive of a link with Deccan volcanism (Font et al., 2016; Sial et al., 2016). However, it is important to note that these anomalies do not occur consistently in any one stratigraphic interval – but are spaced out over several 100 kyrs depending on location (Sial et al., 2016).

The onset of the main phase of Deccan volcanism is recorded in land-based and deep-sea marine sections by a decline in osmium (Os) isotope values, representing weathering of unradiogenic Os from freshly erupted lavas (Robinson et al., 2009). This decline commences close to the C30N/29R magnetic reversal, and is followed by evidence for a transient warming event of 2–3°C recorded in both geochemical and palaeoecological data at all latitudes (Li and Keller, 1998; Tobin et al., 2012; Thibault and Gardin, 2012) (

Figure 2.6). Terrestrial warming of 5°C recorded is in North America (Wilf et al., 2003; Tobin et al., 2013), suggesting marine records may underestimate the magnitude of the change. Biotic events associated with this warming event include dwarfing in some species of foraminifera (Abramovich and Keller, 2003), and assemblage changes and apparent latitudinal migrations in planktonic foraminifera (Olsson et al., 2001; Abramovich et al., 2010) and calcareous nannofossils (Thibault and Gardin, 2012; Thibault and Husson, 2016), some of which also show a drop in diversity. In deep sea sections, an increase in foraminiferal fragmentation indices and decrease in bulk rock weight percent carbonate values provide evidence for a transient ocean acidification episode in surface waters and shoaling of the lysocline (Henehan et al., 2016). Again, it is important to note that species richness and fragmentation indices appear in some cases to recover to pre-warming values prior to the K–Pg boundary (Figure 2.6) (Henehan et al., 2016).
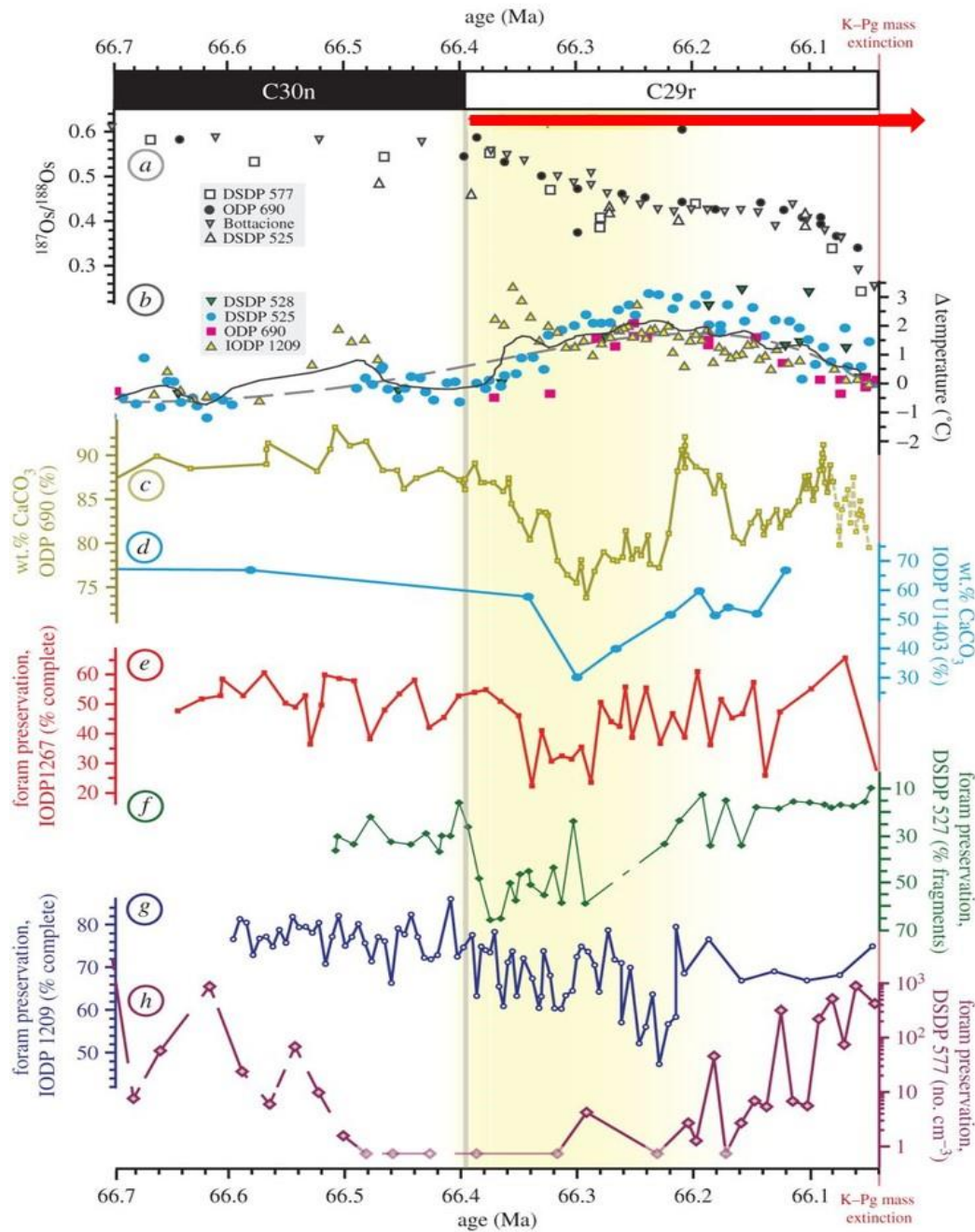
Figure 2.6: Evidence for environmental change linked to Deccan volcanism, prior to the K–Pg boundary and mass extinction. a, global Os isotope (187Os/186Os) decline related to the onset of main phase Deccan volcanism (red arrow). b, deep-sea ocean temperature records of transient late Maastrichtian warming event at all latitudes. c–h, wt% CaCO$_3$ and foraminiferal fragmentation indices from ODP and DSDP sites, showing evidence for transient acidification/shoaling of the CCD related to the warming event. Note decline in temperature and ~recovery of foraminiferal preservation prior to the K–Pg boundary. Modified from Henehan et al. (2016).

27

These various data provide a good argument for a Deccan-induced climate warming event coincident with the onset of the main phase of LIP emplacement with apparently global effects. However, evidence for significant diversity declines and extinctions in key macrofossil and microfossil groups which can be linked with this event are still difficult to recognise (e.g. Hansen and Surlyk, 2014; Thibault and Husson, 2016), especially as in many locations the warming event is stratigraphically very close to the K–Pg boundary and associated faunal change which can be linked to the Chicxulub impact event. Tobin et al. (2012) suggested that high latitude Deccan warming led to a 'precursor' extinction event in the molluscan fauna of high latitude sections on Seymour Island, Antarctica ~300 kyrs prior to the K–Pg boundary and separate, Chicxulub-induced extinction event (Figure 2.7). This hypothesis will be examined further in the rest of this thesis.

Elsewhere, Wilson et al. (2014a; 2014b) have argued that assemblage changes and apparent early extinctions in North American mammal and amphibian faunas from the Hell Creek Formation are evidence of pre-boundary Deccan-induced stress. Local temperature changes (warming and cooling of ~5°C (Wilf et al., 2003; Tobin et al., 2013)) do appear associated with this interval. Further disappearances of groups like ammonites (Goolaerts et al., 2004; Stinnesbeck et al., 2012) and even dinosaurs (e.g. Archibald, 1996; Sheehan et al., 2000) in different sections, have been linked to environmental deterioration prior to the K–Pg boundary – often in the context of a 'Press-Pulse' scenario with Deccan-induced climate change acting as the 'press', leading to a weakening of community structure and/or diversity decline prior to the 'pulse' event – the Chicxulub impact – and mass extinction (Arens and West, 2008; Arens et al., 2014).

Recent high-precision dating of Deccan has not only led to an increase in understanding of the short-term nature of the volcanism, but also the provocative suggestion of a temporal link between the most voluminous eruptions and the Chicxulub impact itself. In this scenario, impact-induced seismic activity may have caused an increase in volcanic activity recorded in an apparent increase in eruption rates of the Wai supergroup in the upper

portion of the Deccan lava pile (Richards et al., 2015; Renne et al., 2015)
(Figure 2.7). Ultimately the precise temporal link between volcanism, climate
change, the Chicxulub impact event and extinction, relies on high resolution
fossil record tied to accurate age models; something this thesis aims to help
achieve for a southern high latitude succession in Antarctica.
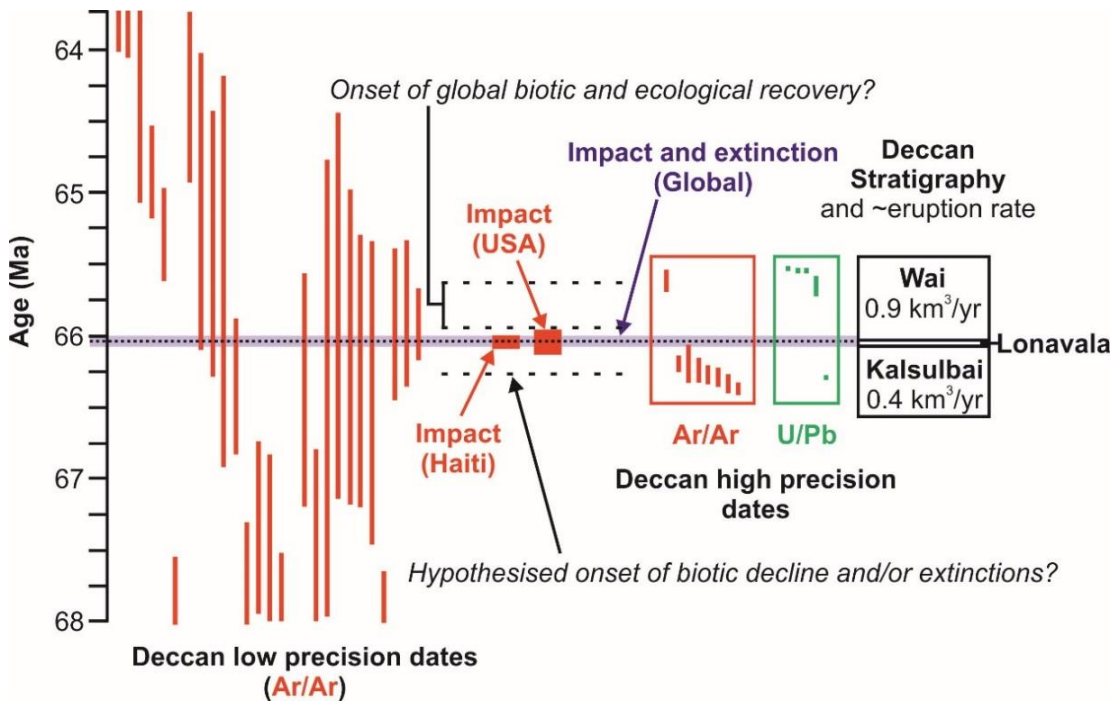
**Figure 2.7: Summary of current dating evidence for impact and LIP
volcanism at the time of the K–Pg extinction. Red text and bars
indicates evidence based on Ar/Ar dating methods, green based on
U/Pb, and blue and black (italicised) sedimentological, geochemical
and palaeontological datasets. Impact age estimates come from
melt glass (Haiti) and tephra layers interbedded with the K–Pg
boundary clay in the Western Interior (USA). Blue box represents
interval of K–Pg boundary clay deposition and microfossil
extinction. Dashed black lines represent hypothesised intervals of
biotic decline before the K–Pg boundary, and step-wise recovery in
marine and terrestrial environments after the extinction. New high
precision Deccan age estimates (Ar/Ar and U/Pb) and Deccan
stratigraphy (main Groups within the lava pile) with updated mean
eruption rates also shown. Based on data from Arenillas et al.
(2006), Tobin et al. (2012), Renne et al. (2013), Richards et al. (2015),
Schoene et al. (2015), Renne et al. (2015), Keller et al. (2016).**

2.3 The K–Pg world: Maastrichtian–Danian palaeoenvironmental, palaeoclimatic and palaeoceanographic change

Much of the environmental changes described in the preceding section occurred relatively close to (±500 kyrs) the K–Pg boundary itself. To understand the longer term context of the extinction, data must be placed in an appropriate longer term framework with an understanding of climate, tectonics, and sea level (Figure 2.8). Palaeoclimate or palaeoenvironmental changes during the latest Cretaceous but unrelated to either the Chicxulub impact or Deccan volcanism have also been proposed as drivers of the K–Pg extinction (e.g. Hallam and Wignall, 1996; Zinsmeister and Feldmann, 1996; Renne et al., 2013), either directly or through a modified 'press-pulse' style scenario whereby global ecosystems were stressed or degraded prior to the mass extinction (Arens and West, 2008).
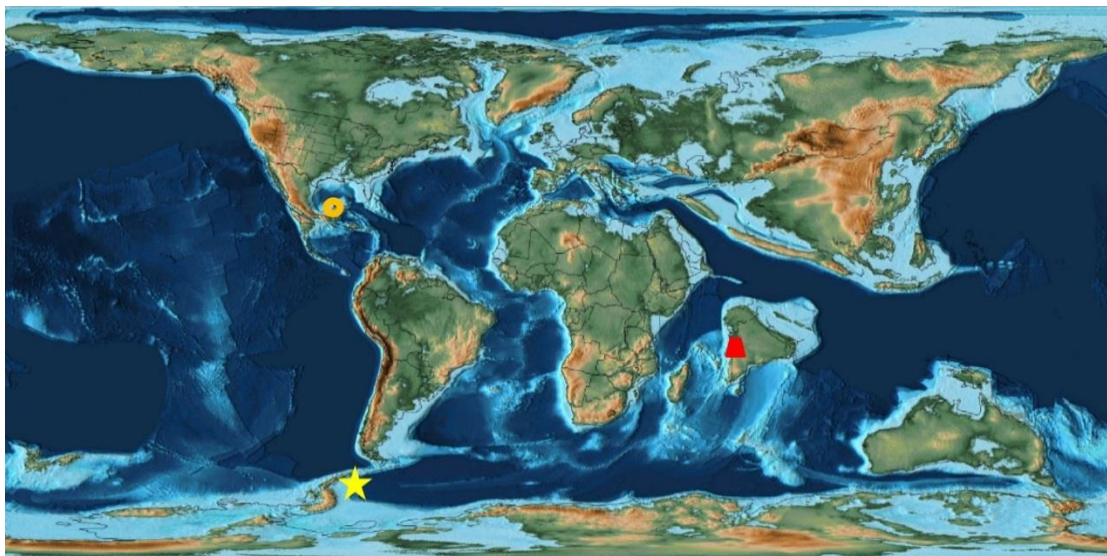
Figure 2.8: Palaeogeographic reconstruction of the Maastrichtian world; with the positions of major ocean basins (dark blue) shallow basins and shelves (light blue), continents (green) and high ground (brown) illustrated. Location of Seymour Island, Antarctica illustrated by yellow star. Orange circle = Chicxulub crater. Red polygon = Deccan LIP. Modified from Scotese (2013).

In parallel to work on the K–Pg extinction event, much research has uncovered abundant evidence to suggest that the climate of the Maastrichtian

was considerably less warm and equable than the preceding mid and Late Cretaceous stages (Barrera and Savin, 1999; Huber et al., 2002; Friedrich et al., 2012). Following a thermal maximum during the Cenomanian–Turonian interval (Cretaceous 'super greenhouse'), proxy records indicate a distinct global cooling trend recorded in both marine and terrestrial sections worldwide (Friedrich et al., 2012; Ando et al., 2013; Linnert et al., 2014). During the Late Campanian–Maastrichtian interval (~73–66 Ma), this cooling trend reached its peak, but was interrupted several times by episodes of geologically rapid global cooling and warming (e.g. Li and Keller, 1998; Barrera and Savin, 1999; Bowman et al., 2013; Thibault, 2016). Many of these climate shifts are associated with small carbon isotope excursions (Figure 2.9A) which may be driven by complicated mixture of orbital forcing, sea-level fluctuations, productivity and associated shifts in the location and nature of carbon burial (e.g. Voigt et al., 2012; Thibault et al., 2015a). CO_2 records are generally low resolution, but do show increases and decreases that have been linked to these environmental changes (e.g. Nordt et al., 2003; Steinthorsdottir et al., 2016).

Climatic shifts are also manifest in the fossil record, in particular in diachronous first and last appearances of marine microplankton between high and low latitude sites, reflecting equator and pole-ward migration events in response to climatic change (Huber and Watkins, 1992; Thibault and Husson, 2016). These diachronous changes and associated pronounced endemism of key micro (planktonic foraminifera, calcareous nannofossil) and macrofossil (ammonites) groups is why a truly global biostratigraphic zonation of the Maastrichtian has proved a challenge for many fossil groups.

A synthetic overview of Maastrichtian carbon cycle, climate and sea-level change is presented in Figure 2.9. Broadly speaking the Maastrichtian carbon isotope curve is characterised by a prominent 1–2‰ negative excursion which begins close to the Campanian–Maastrichtian boundary (CMBE) (Friedrich et al., 2009; Friedrich et al., 2012; Voigt et al., 2012), and lasts ~1.5 myrs. This is followed by a rise in values to a mid-Maastrichtian high, with several rapid oscillations <1‰ superimposed on the overall trend (MME). A gradual decline

through the later Maastrichtian is apparent globally, again with relatively small negative and positive shifts superimposed on the trend (KPgE) (e.g. Husson et al., 2014) prior to the prominent ~2‰ negative shift in bulk carbon values at the K–Pg boundary itself (Esmeray-Senlet et al., 2015; Birch et al., 2016).
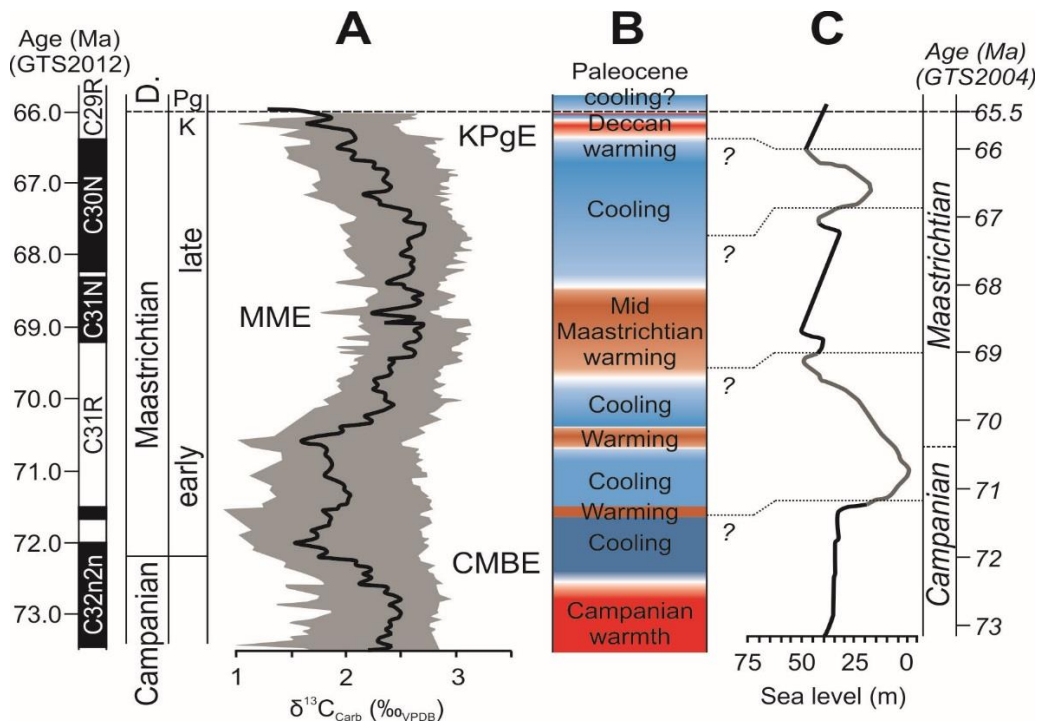
Figure 2.9: Synthetic overview of carbon cycle, climate and sea level change during the latest Campanian and Maastrichtian. A, bulk rock carbon isotope stack modified from global stack presented by Wendler (2013). This is based on a compilation of five curves from different ocean basins (see also Voigt et al. (2012)), with the grey envelope encompassing variability in these different records. The black line represents a running average, visualising shifts in δ^{13}C common to all records. Prominent isotope excursions are named: CMBE= Campanian–Maastrichtian boundary event, MME= Mid-Maastrichtian Event, KPgE= Cretaceous–Paleogene Excursions. B, Maastrichtian climate evolution, based on data presented by Barrera and Savin (1999), Wilf et al. (2003), Bowman et al. (2013) and Thibault (2016). Some of the short term warming events may be regional rather than global. C, global sea level variations as estimated by Miller et al. (2005) and Komintz et al. (2008). Age model for carbon isotope and climate records based on Gradstein et al. (2012). The Miller et al. (2005) sea level curve is calibrated to the Geological Time Scale 2004 (Gradstein et al., 2004). Tentative correlation to GTS2012 timescale is based on Thibault et al. (2015a).

Interbasinal gradients and regional differences in the magnitude of δ^{13}C changes are apparent through much of the Maastrichtian (Frank and Arthur,

1999; Cramer et al., 2009; Voigt et al., 2012) but become less pronounced into the Paleocene, perhaps indicative of a global reorganisation of ocean circulation patterns and establishment of a more 'modern' style of ocean overturning (Cramer et al., 2009). The relationship between ocean overturning and climate during the Late Cretaceous is complex; circulation changes have been invoked as drivers of Maastrichtian climate variability (e.g. for the CMBE and MME) (Barrera and Savin, 1999; Friedrich et al., 2009), with pronounced changes in the locations of deep water formation and water mass conditions related to opening and closing of tectonic gateways around the Southern Ocean and Atlantic (Frank and Arthur, 1999; Jung et al., 2013). The reverse has also been proposed, with climate shifts driving changes to ocean circulation and bottom water formation (e.g. a shift to more vigorous circulation and bottom water formation around Antarctica during the CMBE, terminated by return to a more sluggish style of ocean overturning during MME warming) (Jung et al., 2013).

Neodynium (Nd) isotope data generally support formation of local water bodies in tectonically restricted ocean basins – particularly the north and south Atlantic– during the Maastrichtian (Voigt et al., 2013), with the change to a more modern style of circulation and homogenous ocean interior only occurring during the Paleogene (Voigt et al., 2013; Jung et al., 2013) (Figure 2.10). This may explain local variations to global carbonate carbon isotope records; whereby the magnitude of isotopic shifts is different in differing palaeoenvironmental settings due to basin restriction and dominance of local organic-carbon sources and sinks (Voigt et al., 2012)
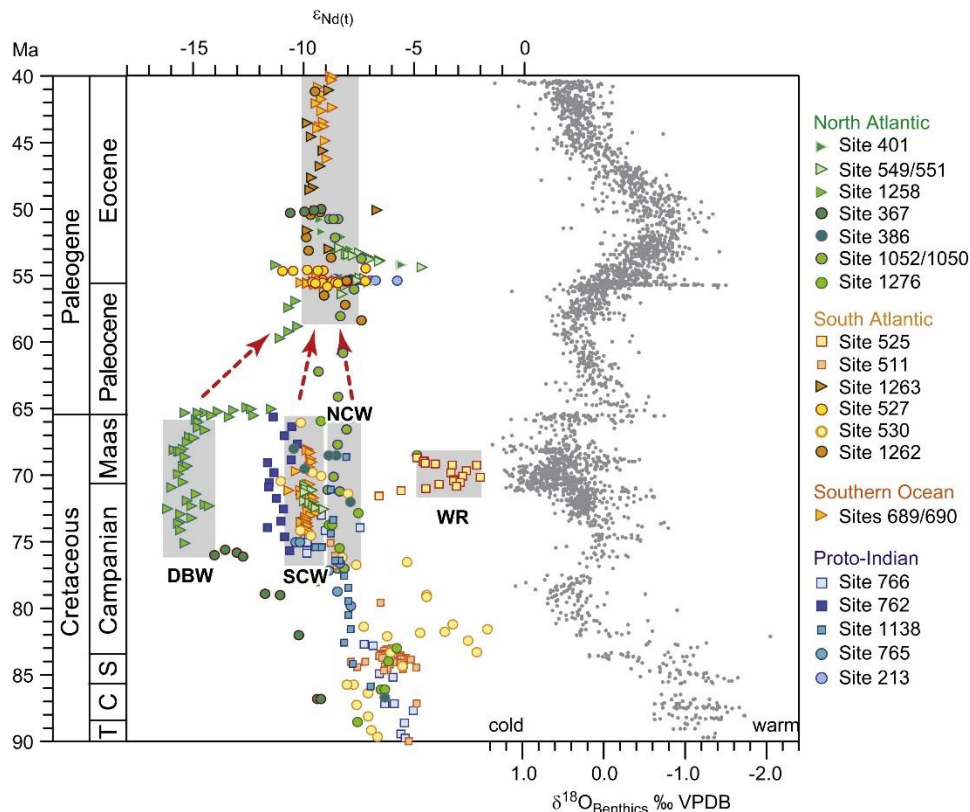
Figure 2.10: Nd (coloured symbols) and oxygen isotope data (grey circles) for the Late Cretaceous–Paleogene taken from the Atlantic, Southern, and Indian oceans. Different water depths are indicated by circles (abyssal, >2000 m), triangles (deep bathyal, 2000–1500 m) and squares (mid- to upper bathyal, <1500 m). The timescale is the GTS04 (Gradstein et al., 2004). Nd data show the dominance of local water masses during most of the Maastrichtian, with a change to more homogenous ocean interior during the Paleogene. DBW=Demerera Bottom Water, SCW=Southern Component Water, NCW=Northern Component Water, WR=Walvis Ridge. Taken from Jung et al. (2013). Oxygen isotope data is from Friedrich et al. (2012).

Large and rapid sea-level changes also occurred during the Maastrichtian (Figure 2.9C) superimposed on an overall long-term fall from a mid-Cretaceous high (e.g. Miller et al., 2005; Komintz et al., 2008; Haq, 2014). Sea level records indicate a pronounced fall over or close to the Campanian–Maastrichtian boundary, followed by a sea level rise during the mid-Maastrichtian, a further fall during chron C30N, before a subsequent rise and gradual fall over the K–Pg boundary (Komintz et al., 2008; Haq, 2014). It has been suggested that some of these sea-level changes are of sufficiently large amplitude and rapidity to suggest a glacioeustatic control (Miller et al., 2005).

Although physical evidence for the growth of significant Antarctic ice sheets at this time is lacking, temperatures may have been low enough during parts of the Maastrichtian for sea ice to form in the Arctic Ocean (Davies et al., 2009) and on the Antarctic margin (Bowman et al., 2013).

Geochemical and faunal proxies suggest the CMBE carbon isotope excursion and sea-level fall is associated with a cooling event, recorded by a 0.5–1‰ shift in oxygen isotopes (Barrera and Savin, 1999; Friedrich et al., 2012; Jung et al., 2012) (Figure 2.9B). Disagreement remains as to the cause of the CMBE; with either ocean circulation changes and deep water formation in the Southern Ocean (Friedrich et al., 2009) and/or glaciation invoked as a driving mechanism (Thibault et al., 2015a). No significant extinctions are associated with the CMBE, but assemblage changes and pole and equator-ward migrations are apparent in plankton assemblages (Huber and Watkins, 1992).

Climate warming occurred during the mid-Maastrichtian (magnetochron C31N) (Li and Keller, 1998; Jung et al., 2013) (MME), associated with a eustatic sea-level rise (Komintz et al., 2008). The MME coincides with the final extinction of the majority of 'true' inoceramid bivalves following a protracted and diachronous loss of diversity which began in the Campanian, and at high latitudes (MacLeod et al., 1996; Crame et al., 1997; Olivero, 2012a). Depletion of rudist bivalve-dominated reef assemblages at all latitudes also occurs at this time (Barrera et al., 1994; Frank et al., 2005; Nifuku et al., 2009), although such assemblages may have persisted to the K–Pg boundary (Steuber et al., 2002), albeit in reduced numbers. Various causes of the MME event have been suggested, such as a reorganisation of ocean circulation associated with breaching of tectonic sills in the south Atlantic, and a weakening of formation and convection of deep water in the high southern latitudes (Barrera and Savin, 1999; Frank et al., 1999; Abramovich et al., 2010; Jung et al., 2013).

Following a return to an overall cooling trend through chron C30N, associated with another fall in sea level, a distinct pulse of warming occurred in the late Maastrichtian close to the base of magnetochron C29R, ~300kyr prior to the K–Pg boundary. Some regional records suggest warming could have started in C30N (Wilf et al., 2003; Bowman et al., 2013). However, the best records of

this event is recorded in proxies from deep sea cores in both surface and deep waters (Li & Keller, 1998; Henehan et al., 2016). As has been mentioned, this warming is linked with the onset of a major pulse of volcanism from the Deccan Traps LIP in India. In many places, temperatures subsequently cool slowly towards a pre-warming average, although further short-term warming events are recorded very close to the K–Pg boundary in a number of the most complete successions (e.g. Elles, Tunisia (Thibault et al., 2015b).

Following the mass extinction, the early Paleocene was likely a period of overall cooler temperatures (e.g. Kemp et al., 2014), supported by evidence for a drop in CO_2 over the K–Pg boundary (Steinthorsdottir et al., 2016).

2.4 Local geological context – the James Ross Basin

The James Ross Basin, Antarctica (Figure 2.11), part of the much larger Larsen Basin (Hathway, 2000), has long been known to contain one of the best sedimentary sequences in the world in which to investigate Late Cretaceous–Paleogene environmental and biotic change (Francis et al., 2006) (see also Zinsmeister (1988) for an early history of scientific exploration). The basin contains a thick (6–7km) sequence of primarily volcaniclastic sedimentary rocks ranging from Jurassic to Neogene in age. These were deposited in an evolving back-arc basin to the east of the Antarctic Peninsula (Elliot, 1988; Hathway, 2000), which during the Late Cretaceous was an active volcanic arc related to subduction of the Pacific Plate beneath the Antarctic Plate to the west. Plate reconstructions indicate that during the Late Cretaceous, the James Ross Basin was located close to its present location of 65°S (Lawver et al., 1992), and was likely one of many similar sedimentary basins which developed along the margins of the tectonic remnants of Gondwana (South America, Antarctica, New Zealand, Australia) following tectonic break-up (Zinsmeister, 1982).

The sedimentary basin-fill of the James Ross Basin can be divided into three main groups; the Aptian–Coniacian Gustav Group (Riding and Crame, 2002; Crame et al., 2006; Kennedy et al., 2007), the latest Coniacian–Paleocene

Marambio Group (Rinaldi, 1978; Crame et al., 1991; McArthur et al., 2000; Olivero, 2012a; Bowman et al., in press), and the Paleocene–Eocene Seymour Island Group (Elliot and Trautman, 1982; Marenssi et al., 1998). These three groups are divided by boundaries (major unconformities) (Figure 2.12) representing periods of change in basin configuration; likely driven by a mixture of tectonic and eustatic change (Pirrie et al., 1991; Olivero et al., 2008; Olivero, 2012a).

One of the considerable challenges in understanding the stratigraphy and palaeoenvironment of the James Ross Basin, in particular that of the Marambio Group, is the isolated nature of the key outcrops on small islands throughout the James Ross Island chain. This, and the homogenous nature of much of the fine-grained sedimentary succession has led to difficulties and disagreements in correlating units across the basin based on either biostratigraphy or sedimentological and lithological features. In detail, it has not always been apparent how the extensive stratigraphic sequences in north-west (NW) James Ross Island, Vega Island and Humps Island, correlated with smaller exposures of south-east (SE) James Ross Island, as well as the important and well-studied sequences on Snow Hill Island and Seymour Island some 80 km to the SE. This has implications for placing records of biotic change from the basin in a robust temporal and stratigraphic framework.
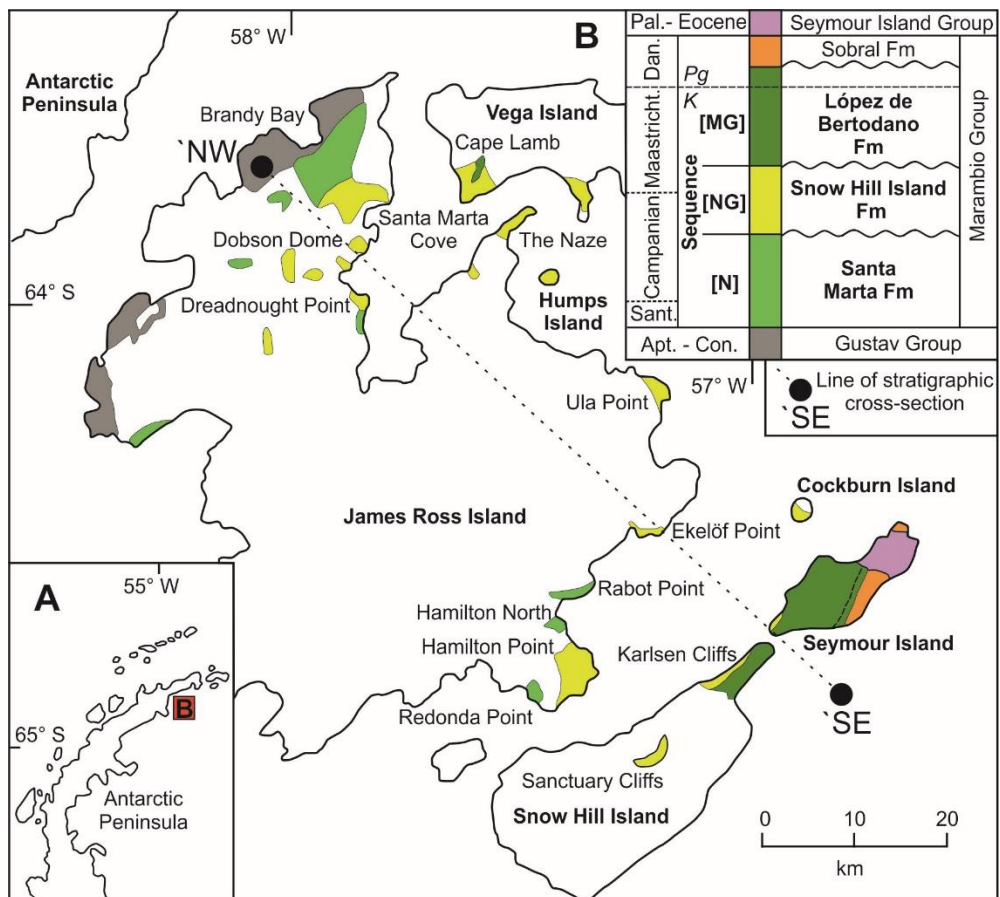
Figure 2.11: Geological setting (A) and map (B) of part of the James Ross Basin showing the principal Cretaceous–Paleogene basin-fill (Gustav, Marambio, Seymour Island Groups). The Marambio Group is sub-divided using the sequence stratigraphic framework of Olivero and Medina (2000) and Olivero (2012a) based on ammonite biostratigraphy. [N] = *Natalites***, [NG] =** *Neograhamites, Gunnarites***, [MG] =** *Maorites, Grossouvrites***. Apt. – Con., Aptian – Coniacian. Sant., Santonian. Dan., Danian. Position of the K–Pg boundary indicated in the upper levels of the López de Bertodano Formation on Seymour Island. Line of stratigraphic cross-section refers to Figure 2.12.**

The key macrofossil group for correlation and biostratigraphy within the Cretaceous portion of the James Ross Basin, in particular the Marambio Group, are the ammonites, as noted by Olivero and Medina (2000), Olivero et al. (2007; 2008), Olivero (2012a; 2012b). Locally, dinoflagellate floras also have good biostratigraphic potential (Pirrie et al., 1997; Riding and Crame, 2002; Bowman et al., 2012), but substantial gaps remain in the stratigraphic coverage of their record.
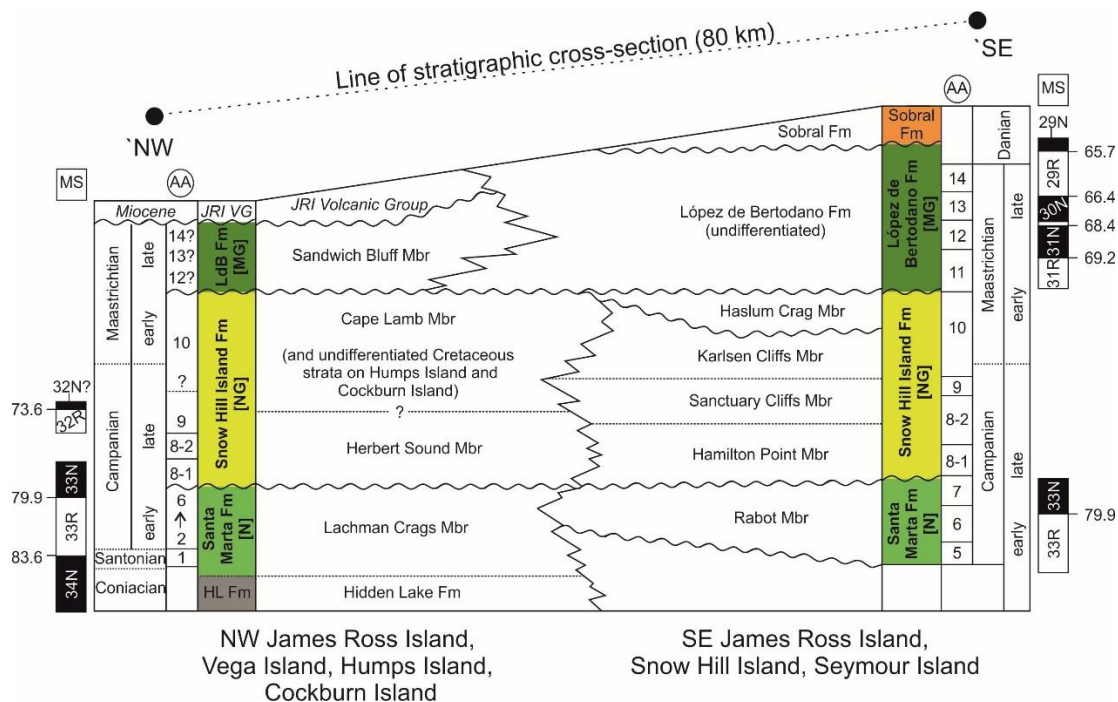
Figure 2.12: Correlation panel based on stratigraphic cross-section line in Figure 2.11, from NW to SE across the James Ross Basin, showing principal lithostratigraphic, biostratigraphic, and magnetostratigraphic correlations within the Marambio Group (N, NG, MG sequences (Olivero, 2012a). MS = magnetostratigraphy with chron reversal ages based on absolute dates in the Geological Timescale 2012 (Gradstein et al., 2012). AA = ammonite assemblages of Olivero and Medina (2000), Olivero (2012a; 2012b). Based on integration of data from multiple publications (Crame et al., 1991; Crame et al., 1996; Pirrie et al., 1997; Olivero and Medina, 2000; Crame et al., 2004; Olivero et al., 2008; Olivero 2012a; 2012b; Bowman et al., 2012; Tobin et al., 2012; Milanese et al., 2013; Milanese et al., 2016; Roberts et al., 2014). Unpublished magnetostratigraphic data for the Santa Marta Formation in NW James Ross Island courtesy of Peter Ward (pers. comm. 2016).

In terms of absolute age control, both strontium isotope chemostratigraphy (McArthur et al., 2000), and more recently magnetostratigraphy (Tobin et al., 2012; Milanese et al., 2013; Milanese et al., 2016) provide some precise age constraints (Figure 2.12).

Olivero and Medina (2000) were the first to fully document 14 distinct and sequential ammonite assemblages, the base of each defined primarily by the first occurrence of particular members of the highly endemic family Kossmaticeratidae, which could be used to correlate Late Cretaceous strata ~80 km across the basin. These assemblages can also be used to define

39

three groups based on ammonite biostratigraphy, which conform to three sedimentary sequences within the Marambio Group, together with several important sequence boundaries marked by regional unconformities which separate them (Figure 2.12), that are likely the product of eustatic and tectonic changes. This updated litho- and biostratigraphic scheme broadly correlates with the existing framework initially set out by Crame et al. (1991) and expanded by subsequent studies (e.g. Pirrie et al., 1991; Pirrie et al., 1997; Crame et al., 2004). Each of the three groups is named after the principal kossmaticeratid ammonite genera which occur therein; N for *Natalites*, NG for *Neograhamites* and *Gunnarites*, and MG for *Maorites* and *Grossouvrites*.
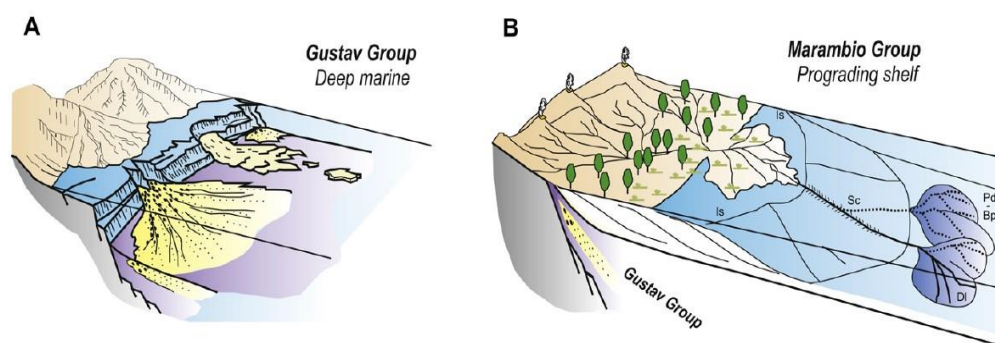
Figure 2.13: Cartoons representing the evolving palaeoenvironmental setting of the James Ross Basin in the Late Cretaceous–Paleogene. A: during deposition of the deep-marine, Aptian–Coniacian Gustav Group (Whitham, 2006). B: corresponding to the deltaic system prevalent during deposition of the Coniacian–Eocene Marambio Group (Macellari, 1988; Scasso et al., 1991; Marenssi et al., 1998). Pd-Bp, prodelta-basin plain settings, DL, depositional lobes, Sc, slope-channel complex, Is, inner shelf settings. Taken from Olivero (2012a).

In terms of palaeoenvironment, rocks of the Marambio Group represent an overall regressive megasequence; overlying the Gustav Group, which was deposited in deep-water settings (Figure 2.13A) (Whitham, 2006). At the base of the Marambio Group is the Santa Marta Formation (N group), which was deposited on the outer margins of a deep-water delta system, shallowing upward to finer grained inner shelf deposits (Scasso et al., 1991; Olivero, 2012a). The Snow Hill, López de Bertodano (NG, MG groups), and Sobral

formations probably represent more upper slope-inner shelf environments (Figure 2.13B) (Macellari, 1988; Pirrie et al., 1997; Crame et al., 2004; Crame et al., 2014; Bowman et al., In Press). On a regional scale, the NW section of the James Ross Basin (represented by the outcrops around Santa Marta Cove, Dreadnought Point, on Vega Island, and Humps Island) (Figure 2.11) records deposition in the proximal portion of the basin during deposition of the N sequence in particular, whereas the SE section (SE James Ross Island around Hamilton, Rabot, and Redonda points, on Snow Hill and Seymour Island) represent deposition in a more distal location (Olivero, 2012a).

The overall position of a shoreline to the NW of the basin-fill is consistent with palaeoflow indicators (Pirrie, 1989) and the hypothesised primary source for sediment input; large river systems draining the Antarctic Peninsula to the North West, during the Cretaceous–Paleogene interval an active and forested volcanic arc (Macellari, 1988; Elliot, 1988; Olivero et al., 2007; 2008; Bowman et al., 2014). During the upper NG and MG sequence, the shoreline appears to have shifted to the SE, as recorded by deposition of more proximal strata indicative of shallow marine settings in the basal López de Bertodano Formation on Snow Hill Island and Seymour Island during the early Maastrichtian (Macellari, 1988; Olivero et al., 2007; 2008), and in the Sandwich Bluff member on Vega Island during the late Maastrichtian (Pirrie et al., 1991; Roberts et al., 2014). Volcanism in the arc appears to have experienced fluctuating periods of activity and quiescence (Elliot, 1988), with a late Campanian–early Maastrichtian low in activity ending with increased evidence for volcanism close to the K–Pg boundary and into the Paleogene (Macellari, 1988).

2.4.1 Geological setting of this study – the López de Bertodano Formation on Seymour Island

This project is based around extensive fossil and sediment collections made from the upper portion of the Marambio Group which contains a record of environmental change in Antarctica across the K–Pg boundary. Samples come from several measured sections made through the 1100 m-thick López

de Bertodano Formation as exposed on southern Seymour Island. These outcrops have been the subject of extensive study over the last 30 years (see Feldman and Woodburne, 1988; Crame et al., 2004; Olivero et al., 2007; 2008; Bowman et al., 2014 for details). Geologically, Seymour Island contains deposits belonging to the upper Marambio Group, and the overlying Seymour Island Group (Montes et al., 2013) (Figure 2.14). Whilst the upper Snow Hill Island, López de Bertodano and Sobral Formations were deposited in a variety of shallow marine environments (Macellari, 1988; Olivero et al., 2007; Olivero et al., 2008), the overlying Cross Valley and La Meseta Formations represent a more complex stratigraphic setting; specifically deposition in large-scale channel structures cut into the underlying shelf deposits (Elliot and Trautman, 1982; Marenssi et al., 1998).
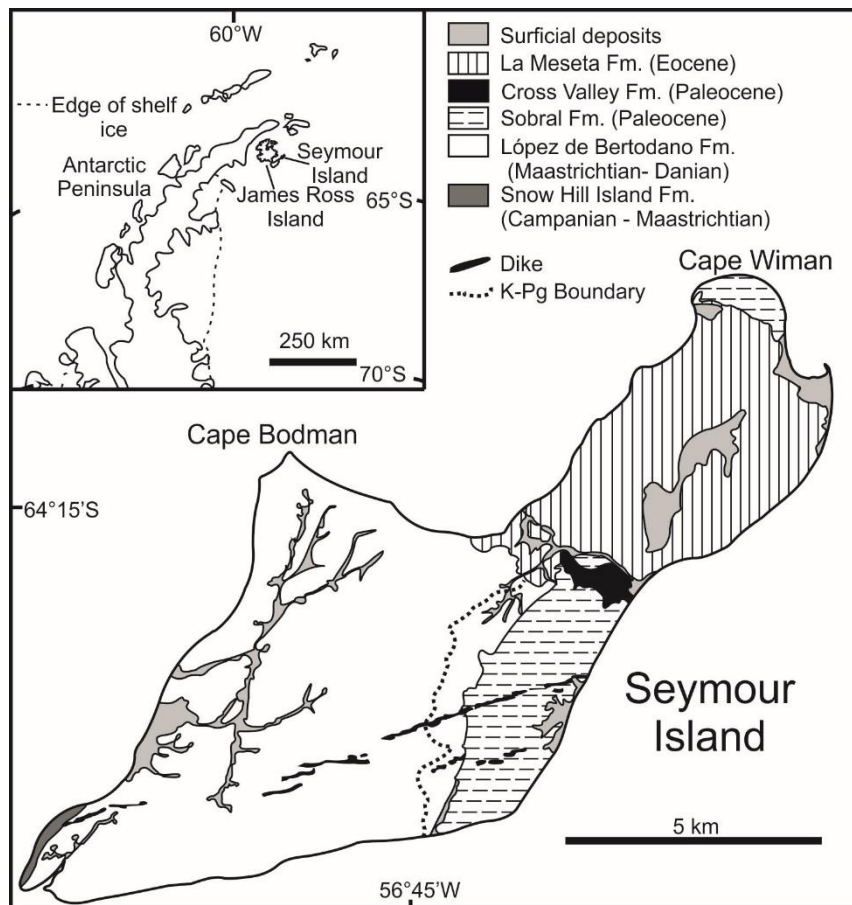
Figure 2.14: Geological map of Seymour Island, showing principal lithostratigraphic division, and the location of the K–Pg boundary in the upper levels of the López de Bertodano Formation. Modified from Montes et al. (2013).

A more detailed description of the geological setting of the samples utilised in this thesis from Seymour Island, as well as the age model for the 1100m-thick López de Bertodano Formation is provided in the succeeding chapters. Broadly speaking, these fine-grained, monotonous deposits which outcrop across southern Seymour Island (Figure 2.14; Figure 2.15) record deposition of a transgressive-regressive cycle driven by a mix of eustatic and tectonic controls (Crame et al., 2004; Olivero et al., 2007; Olivero, 2012). Internal subdivision of the López de Bertodano Formation was attempted by Macellari (1988) who defined 10 mappable units based on their internal facies and fossil content. In practice these are difficult to recognise in the field, and so in this thesis the López de Bertodano Formation remains undifferentiated (Crame et al., 2004; Bowman et al., 2012).
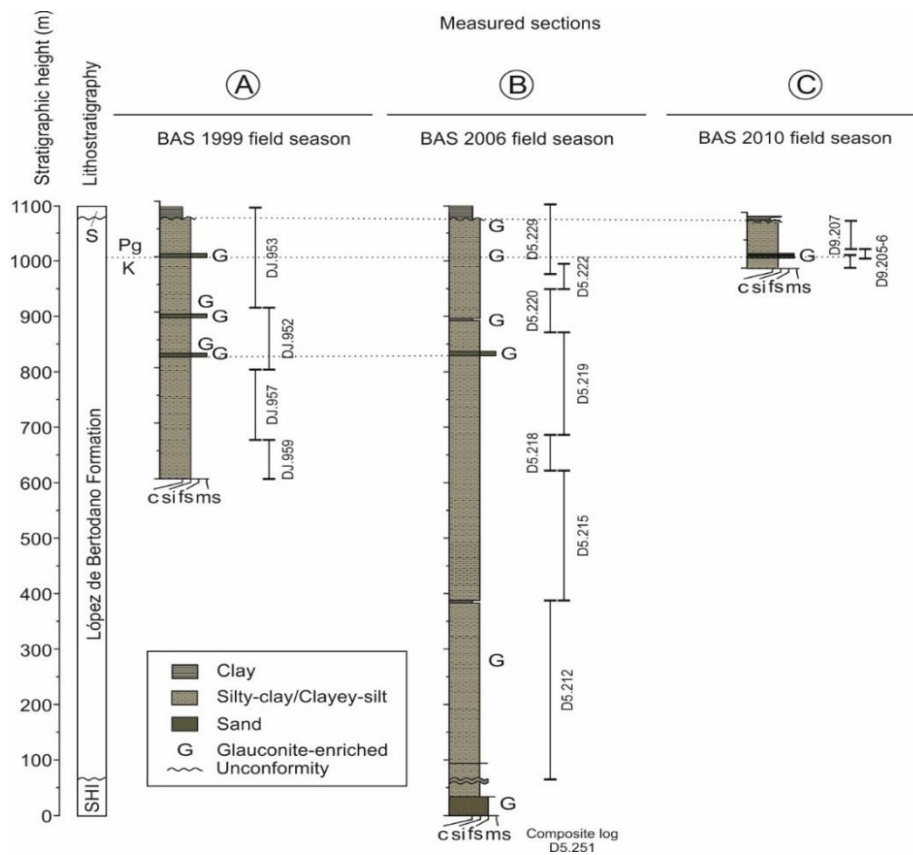
Figure 2.15: Sedimentary logs and section correlations through the López de Bertodano Formation on southern Seymour Island (see Crame et al., 2004; Bowman et al., 2012; Crame et al., 2014; Bowman et al., In Press for further details). Fossil and sediment samples utilised in this thesis were collected from these section lines (see Appendices for raw field data).

The entire sequence on Seymour Island dips towards the south east at 10°, and is predominantly made up of intensely bioturbated, silty clays and clay-rich siltstones (Macellari, 1988; Olivero et al., 2007). The lower portion of the succession contains several large mud-rich intervals with complex internal geometries (Olivero et al., 1998). These are interpreted as shore-parallel sub-tidal channels formed offshore to an estuary or embayment (Olivero et al., 2008). Changes in fossil content, sedimentary architecture and structures, and grain size suggest thick transgressive deposits occur above this interval (Macellari, 1988; Olivero et al., 2007; Olivero et al., 2008; Olivero 2012). The ~300m portion of the succession contains a number of prominent glauconite-rich horizons, possibly representing a period of lower sedimentation rates or laterally variable facies boundaries (Macellari, 1988; Bowman et al., in press). Further sea-level changes are difficult to define, although a distinct shallowing trend is evident in the contemporaneous Sandwich Bluff Member on nearby Vega Island (Pirrie et al., 1991; Roberts et al., 2014).

The abundantly fossiliferous nature of the deposits on Seymour Island, both in terms of microfossils (Askin,1988; Huber, 1988; Harwood, 1988; Bowman et al., 2012; Bowman et al., 2014) and macrofossils (Francis, 1986; Macellari, 1988; Zinsmeister and Macellari, 1988; Crame et al., 2004; Stilwell et al., 2004; Crame et al., 2014) made it an obvious target for scientific exploration (Zinsmeister, 1988). A significant amount of palaeoenvironmental data has been derived from these deposits over the last 30 years (e.g. Feldman and Woodburne, 1988; Bowman et al., 2012; Crame et al., 2014), as well as the development of new age models which confirm the Maastrichtian–Danian age, and highly expanded nature of the succession (Tobin et al., 2012; Bowman et al., 2013).

The K–Pg boundary is located ~1008m above the base of the formation in the base of a glauconite-rich interval, but with apparently continuous sedimentation across this crucial interval (Zinsmeister, 1998). The discovery of an Ir anomaly coincident with the microfossil-defined K–Pg boundary (Elliot et al., 1994; Bowman et al., 2012) confirmed the importance of these deposits for studying the K–Pg extinction event. However, few faunal studies of the

macrofossil record of the full Maastrichtian–Danian interval for all molluscan groups have been completed before this thesis (Zinsmeister et al., 1989; Zinsmeister, 1998; Tobin et al., 2012).

2.5 References

Aberhan, M., Weidemeyer, S., Kiessling, W., Scasso, R.A., Medina, F.A., 2007. Faunal evidence for reduced productivity and uncoordinated recovery in Southern Hemisphere Cretaceous-Paleogene boundary sections. *Geology* **35**, 227-230.

Abramovich, S., Keller, G., 2003. Planktonic foraminiferal response to the latest Maastrichtian abrupt warm event: A case study from South Atlantic DSDP Site 525A. *Marine Micropaleontology* **48**, 225-249.

Abramovich, S., Yovel-Corem, S., Almogi-Labin, A., Benjamini, C., 2010. Global climate change and planktic foraminiferal response in the Maastrichtian. *Paleoceanography* 25.

Alegret, L., Thomas, E., 2009. Food supply to the seafloor in the Pacific Ocean after the Cretaceous/Paleogene boundary event. *Marine Micropalaeontology* **73**, 105–116.

Alegret, L., Thomas, E., Lohmann, K.C., 2012. End-Cretaceous marine mass extinction not caused by productivity collapse. *Proceedings of the National Academy of Science* **109**, 728–732.

Alroy, J., 1998. Cope's rule and the dynamics of body mass evolution in North American fossil mammals. *Science* **280**, 731–734.

Alroy, J., Aberhan, M., Bottjer, D.J., Foote, M., Fürsich, F.T., Harries, P.J., Hendy, A.J.W., Holland, S.M., Ivany, L.C., Kiessling, W., Kosnik, M.A., Marshall, C.R., McGowan, A.J., Miller, A.I., Olszewski, T.D., Patzkowsky, M.E., Peters, S.E., Villier, L., Wagner, P.J., Bonuso, N., Borkow, P.S., Brenneis, B., Clapham, M.E., Fall, L.M., Ferguson, C.A., Hanson, V.L., Krug, A.Z., Layou, K.M., Leckey, E.H., Nürnberg, S., Powers, C.M., Sessa, J.A.,

Simpson, C., Tomašových, A., Visaggi, C.C., 2008. Phanerozoic trends in the global diversity of marine invertebrates. *Science* **321**, 97-100.

Alvarez, L.W., Alvarez, W., Asaro, F., Michel, H.V., 1980. Extraterrestrial cause for the Cretaceous-Tertiary Extinction. *Science* **208**, 1095–1108.

Archibald, J.D., 1996. Fossil evidence for a late cretaceous origin of 'Hoofed' mammals. *Science* **272**, 1150-1153.

Arenillas, I., Arz, J.A., Molina, E., Dupuis, C., 2000. The Cretaceous/Paleogene (K/P) boundary at Aïn Settara, Tunisia: Sudden catastrophic mass extinction in planktic foraminifera. *Journal of Foraminiferal Research* **30**, 202-218.

Arenillas, I., Arz, J.A., Grajales-Nishimura, J.M., Murillo-Muňetón, G., Alvarez, W., Carmargo-Zanoguera, A., Molina, E., Rosales-Domínguez, C., 2006. Chicxulub impact event is Cretaceous/Paleogene boundary in age: new micropaleontological evidence. *Earth and Planetary Science Letters* **249**, 241–257.

Arens, N.C., West, I.D., 2008. Press-pulse: A general theory of mass extinction? *Paleobiology* **34**, 456-471.

Arens, N.C., Thompson, A., Jahren, A.H., 2014. A preliminary test of the press-pulse extinction hypothesis: Palynological indicators of vegetation change preceding the Cretaceous-Paleogene boundary, McCone County, Montana, USA, *Special Paper of the Geological Society of America*, pp. 209-227.

Askin, R.A., 1988. The palynological record across the Cretaceous/Tertiary transition on Seymour Island, Antarctica, In: Feldmann, R.M., Woodburne, M.O. (Eds.), *Geology and Paleontology of Seymour Island, Antarctic Peninsula*. Geological Society of America, Memoirs **169**. 155-162.

Bambach, R.K., 2006. Phanerozoic biodiversity mass extinctions. *Annual Reviews of Earth and Planetary Science* **34**, 127–155.

Bambach, R.K., Knoll, A.H., Wang, S.C., 2004. Origination, extinction, and mass depletions of marine diversity. *Paleobiology* 30, 522-542.

Barreda, V.D., Cúneo, N.R., Wilf, P., Currano, E.D., Scasso, R.A., Brinkhuis, H., 2012. Cretaceous/Paleogene Floral Turnover in Patagonia: Drop in Diversity, Low Extinction, and a Classopollis Spike. *PLoS ONE* **7**.

Barrera, E., 1994. Global environmental changes preceding the Cretaceous-Tertiary boundary: Early–late Maastrichtian transition. *Geology* **22**, 877–880.

Barrera, E., Savin, S.M., 1999. Evolution of late Campanian–Maastrichtian marine climates and oceans. In: *Barrera, E., Johnson, C.C. (Eds.), Evolution of the Cretaceous Ocean- Climate System.* Geological Society of America Special Paper **332**, pp. 245–282.

Beerling, D.J., Lomax, B.H., Upchurch G.R, Jr., Nichols, D.J., Pillmore, C.L., Handley, L.L., Scrimgeour, C.M., 2001. Evidence for the recovery of terrestrial ecosystems ahead of marine primary production following a biotic crisis at the Cretaceous-Tertiary boundary. *Journal of the Geological Society of London* **158**, 737–740.

Benton, M.J., Ruta, M., Dunhill, A.M., Sakamoto, M., 2013. The first half of tetrapod evolution, sampling proxies, and fossil record quality. *Palaeogeography, Palaeoclimatology, Palaeoecology* **372**, 18–41.

Benton, M.J., Forth, J. and Langer, M.C. 2014. Models for the rise of the dinosaurs. *Current Biology* **24**.

Birch, H.S., Coxall, H.K., Pearson, P.N., Kroon, D. and Schmidt, D.N. 2016. Partial collapse of the marine carbon pump after the Cretaceous-Paleogene boundary. *Geology* **44**, 287–290.

Bohor, B.F., Modreski, P.J. and Foord, E.E. 1987. Shocked quartz in the cretaceous-tertiary boundary clays: Evidence for a global distribution. *Science* **236**, 705–709.

Bond, D.P.G., Wignall, P.B., 2014. Large igneous provinces and mass extinctions: An update. In: *Keller, G., Kerr, A.C. (Eds.), Volcanism, Impacts, and Mass Extinctions: Causes and Effects.* Geological Society of America Special Paper **505**, 29–55.

Bowman, V. C., Francis, J. E. & Riding, J. B. 2013. Late Cretaceous winter sea ice in Antarctica? *Geology* **41**, 1227–1230.

Bowman, V.C. *et al.*, In Press. The Paleocene of Antarctica: Dinoflagellate cyst biostratigraphy, chronostratigraphy and implications for the palaeo-Pacific margin of Gondwana. *Gondwana Research* doi:10.1016/j.gr.2015.10.018 .

Bowman, V.C., Francis, J.E., Askin, R.A., Riding, J.B., Swindles, G.T., 2014. Latest Cretaceous–earliest Paleogene vegetation and climate change at the high southern latitudes: palynological evidence from Seymour Island, Antarctic Peninsula. *Palaeogeography Palaeoclimatolology Palaeoecology* **408**, 26–47.

Bowman, V.C., Francis, J.E., Riding, J.B., Hunter, S.J., Haywood, A.M., 2012. A latest Cretaceous to earliest Paleogene dinoflagellate cyst zonation from Antarctica, and implications for phytoprovincialism in the high southern latitudes. *Review of Palaeobotany and Palynology* **171**, 40–56.

Bown, P., 2005. Selective calcareous nannoplankton survivorship at the Cretaceous-Tertiary boundary. *Geology* **33**, 653–656.

Brett, R., 1992. The Cretaceous-Tertiary extinction: A lethal mechanism involving anhydrite target rocks. *Geochimica et Cosmochimica Acta* **56**, 3603-3606.

Brinkhuis, H., Bujak, J.P., Smit, J., Versteegh, G.J.M., Visscher, H., 1998. Dinoflagellate-based sea surface temperature reconstructions across the Cretaceous-Tertiary boundary. *Palaeogeography, Palaeoclimatology, Palaeoecology* **141**, 67-83.

Brusatte, S.L., Butler, R.J., Barrett, P.M., Carrano, M.T., Evans, D.C., Lloyd, G.T., Mannion, P.D., Norell, M.A., Peppe, D.J., Upchurch, P., Williamson, T.E. 2015. The Extinction of the Dinosaurs. *Biological Reviews* **90**, 628–642.

Callegaro, S., Baker, D.R., de Min, A., Marzoli, A., Geraki, K., Bertrand, H., Viti, C., Nestola, F., 2014. Microanalyses link sulfur from large igneous provinces and Mesozoic mass extinctions. *Geology* **42**, 895-898.

Chenet, A.-L., Courtillot, V., Fluteau, F., Gérard, M., Quidelleur, X., Khadri, S.F.R., Subbarao, K.V., Thordarson, T., 2009. Determination of rapid Deccan

eruptions across the Cretaceous-Tertiary boundary using paleomagnetic secular variation: 2. Constraints from analysis of eight new sections and synthesis for a 3500-m-thick composite section. *Journal of Geophysical Research* **114**, B06103. http://dx.doi.org/10.1029/2008JB005644.

Courtillot, V., Fluteau, F., 2010. Cretaceous extinctions: the volcanic hypothesis. *Science* **328**, 973–974.

Coxall, H.K., D'Hondt, S., Zachos, J.C., 2006. Pelagic evolution and environmental recovery after the Cretaceous-Paleogene mass extinction. *Geology* **34,** 297-300.

Crame, J.A., Luther, A., 1997. The last inoceramid bivalves in Antarctica. *Cretaceous Research* **18**, 179–195.

Crame, J.A., Pirrie, D., Riding, J.B., Thomsen, M.R.A., 1991. Campanian-Maastrichtian (Cretaceous) stratigraphy of the James Ross Island area, Antarctica. *Journal of the Geological Society of London.* **148**, 1125–1140.

Crame, J.A., Lomas, S.A., Pirrie, D., Luther, A., 1996. Late Cretaceous extinction patterns in Antarctica. *Journal of the Geological Society of London.* **153**, 503–506.

Crame, J.A., Francis, J.E., Cantrill, D.E., Pirrie, D., 2004. Maastrichtian stratigraphy of Antarctica. *Cretaceous Research* **25**, 411–423.

Crame, J.A., Pirrie, D., Riding, J.B., 2006. Mid-Cretaceous stratigraphy of the James Ross Basin, Antarctica. In: Francis, J.E., Pirrie, D., Crame, J.A. (Eds.), *Cretaceous–Tertiary High-Latitude Palaeoenvironments, James Ross Basin, Antarctica*, Special Publication vol. **258**. Geological Society, London, pp. 7–19.

Crame, J. A., Beu, A. G., Ineson, J. R., Francis, J. E., Whittle, R. J. & Bowman, V. C., 2014. The early origins of the Antarctic marine fauna and its evolutionary implications. *PLoS ONE* **9**, e114732.

Cramer, B.S., Toggweiler, J.R., Wright, J.D., Katz, M.E., Miller, K.G., 2009. Ocean overturning since the late cretaceous: Inferences from a new benthic foraminiferal isotope compilation. *Paleoceanography* **24.**

Davies, A., Kemp, A.E.S., Pike, J., 2009. Late Cretaceous seasonal ocean variability from the Arctic. *Nature* **460**, 254-258.

Elliot, D.H., 1988. Tectonic setting and evolution of the James Ross Basin, northern Antarctic Peninsula. In: Feldmann, R.M., Woodburne, M.O. (Eds.), *Geology and Paleontology of Seymour Island, Antarctic Peninsula*. Geological Society of America, Memoirs **169**. 541-555.

Elliot, D.H., Askin, R.A., Kyte, F.T., Zinsmeister, W.J., 1994. Iridium and dinocysts at the Cretaceous-Tertiary boundary on Seymour Island, Antarctica: implication for the K–T event. *Geology* **22**, 675–678.

Elliot, D.H., Trautman, T.A., 1982. Lower Tertiary strata on Seymour Island, Antarctic Peninsula. *Antarctic geoscience. 3rd symposium on Antarctic geology and geophysics, Madison, August 1977*, 287-297.

Esmeray-Senlet, S., Wright, J.D., Olsson, R.K., Miller, K.G., Browning, J.V., Quan, T.M., 2015. Evidence for reduced export productivity following the Cretaceous/Paleogene mass extinction. *Paleoceanography* **30**, 718-738.

Fastovsky, D.E., Bercovici, A., 2016. The Hell Creek Formation and its contribution to the Cretaceous-Paleogene extinction: A short primer. Cretaceous Research **57**, 368-390.

Feldmann R. M., Woodburne M. O.*, eds (1988) Geology and Paleontology of Seymour Island, Antarctic Peninsula 169:*Memoir, Geological Society of America*.

Font, E., Adatte, T., Keller, G., Abrajevitch, A., Sial, A.N., De Lacerda, L.D. and Punekar, J. 2016. Mercury anomaly, Deccan volcanism and the end-Cretaceous Mass Extinction. *Geology* **44** pe382.

Francis, J.E., 1986. Growth rings in Cretaceous and Tertiary wood from Antarctica and their palaeoclimatic implications. *Palaeontology* **29**, 665–684.

Francis, J.E., Crame, J.A. and Pirrie, D. 2006. Cretaceous-Tertiary high-latitude palaeoenvironments, James Ross Basin, Antarctica: Introduction. *Geological Society Special Publication* **258**, 1-5.

Frank, T.D. and Arthur, M.A. 1999. Tectonic forcings of Maastrichtian ocean-climate evolution. *Paleoceanography* **14**, 103-117.

Frank, T.D., Thomas, D.J., Leckie, R.M., Arthur, M.A., Brown, P.R., Jones, K. and Lees, J.A. 2005. The Maastrichtian record from Shatsky Rise (northwest Pacific): A tropical perspective on global ecological and oceanographic changes. *Paleoceanography* **20,** 1-14.

Friedman, M. and Sallan, L.C. 2012. Five hundred million years of extinction and recovery: A phanerozoic survey of large-scale diversity patterns in fishes. *Palaeontology* **55**, 707-742.

Friedrich, O., Herrle, J.O., Wilson, P.A., Cooper, M.J., Erbacher, J. and Hemleben, C. 2009. Early Maastrichtian carbon cycle perturbation and cooling event: Implications from the South Atlantic Ocean. *Paleoceanography* **24**.

Friedrich, O., Norris, R.D., Erbacher, J., 2012. Evolution of middle to Late Cretaceous oceans—a 55 m.y. record of Earth's temperature and carbon cycle. *Geology* **40**, 107–110.

Glaze, L.S., Self, S., Schmidt, A., Hunter, S.J., In Press. Assessing eruption column height in ancient flood basalt eruptions. *Earth and Planetary Science Letters*, Available online 6th August 2015. doi:10.1016/j.epsl.2014.07.043

Goolaerts, S., Kennedy, W.J., Dupuis, C., Steurbaut, E., 2004. Terminal Maastrichtian ammonites from the Cretaceous–Paleogene Global Stratotype Section and Point, El Kef, Tunisia. *Cretaceous Research* **25**, 313–328.

Gradstein, F. M., Ogg, J. G., Smith, A.G., 2004. *A Geologic Time Scale 2004* Cambridge University Press, Cambridge, 589p.

Gradstein, F. M., Ogg, J. G., Schmitz, M. & Ogg, G., 2012. *The Geological Time Scale 2012* Elsevier Science Ltd: Boston.

Grasby S.E., Beauchamp, B., Bond, D.P.G., Wignall, P.B., Sanei, H., 2016. Mercury anomalies associated with three extinction events (Capitanian Crisis, Latest Permian Extinction and the Smithian/Spathian Extinction) in NW Pangea. *Geological Magazine* **153**, 285–297.

Hallam, A. and Wignall, P.B. 1996 *Mass extinctions and their aftermath*. Oxford, Oxford University Press, 330pp.

Hansen, T. A., Farrell, B. R. & Upshaw, B III., 1993. The first 2 million years after the Cretaceous–Tertiary boundary in east Texas: rate and paleoecology of the molluscan recovery. *Paleobiology* **19**, 251–265.

Hansen, T., Surlyk, F., 2014. Marine macrofossil communities in the uppermost Maastrichtian chalk of Stevns Klint, Denmark. *Palaeogeography, Palaeoclimatology, Palaeoecology* **399**, 332–344.

Haq, B.U., 2014. Cretaceous eustasy revisited. *Global and Planetary Change* **113**, 44–58.

Hart, M.B., Yancey, T.E., Leighton, A.D., Miller, B., Liu, C., Smart, C.W., Twitchett, R., 2012. The Cretaceous-Paleogene boundary on the Brazos River, Texas: New stratigraphic sections and revised interpretations. *Gulf Coast Association of Geological Sciences Journal* **1**, 69–80.

Harwood, D. M., 1988. Upper Cretaceous and lower Paleocene diatom and silicoflagellate biostratigraphy of Seymour Island, eastern Antarctic Peninsula. In: Feldmann, R.M., Woodburne, M.O. (Eds.), *Geology and Paleontology of Seymour Island, Antarctic Peninsula*. Geological Society of America, Memoirs **169,** 55–130.

Hathway, B., 2000. Continental rift to back-arc basin: Jurassic–Cretaceous stratigraphical and structural evolution of the Larsen Basin, Antarctic Peninsula. *Journal of the Geological Society of London*. **157**, 417–432.

Henehan, M.J., Hull, P.M., Penman, D.E., Rae, J.W.B. and Schmidt, D.N. 2016. Biogeochemical significance of pelagic ecosystem function: An end-cretaceous case study. *Philosophical Transactions of the Royal Society B: Biological Sciences* **371**.

Hildebrand, A.R., Penfield, G.T., Kring, D.A., Pilkington, M., Camargo Z, A., Jacobsen, S.B., Boynton, W.V., 1991. Chicxulub crater: A possible Cretaceous/Tertiary boundary impact crater on the Yucatán Peninsula, Mexico. *Geology* **19**, 867–871.

Holland, S.M. and Patzkowsky, M.E. 2015. The stratigraphy of mass extinction. *Palaeontology* **58**, 903-924.

Hsü, K.J., McKenzie, J.A., 1985. A "Strangelove" ocean in the earliest Tertiary. In: Sunquist, E.T., Broecker,W.S. (Eds.), *The Carbon Cycle and Atmospheric CO₂: Natural Variations Archaean to Presen*t. American Geophysical Union, Washington D.C., pp. 487–492.

Huber, B. T., 1988. Upper Campanian–Paleocene foraminfera from the James Ross Island region, Antarctic Peninsula. In: Feldmann, R.M., Woodburne, M.O. (Eds.), *Geology and Paleontology of Seymour Island, Antarctic Peninsula*. Geological Society of America, Memoirs **169,** 163–252.

Huber, B.T., Watkins, D.K., 1992. Biogeography of Campanian–Maastrichtian calcareous plankton in the region of the Southern Ocean: palaeogeographic and palaeoclimatic implications. In: Kennett, J.P.,Warnke, D.A. (Eds.), *The Antarctic Palaeoenvironment: A Perspective on Global Change*. AGU Antarctic Research Series **56**, pp. 31–60.

Huber, B.T., Liu, C., Olsson, R.K., Berggren, W.A., 1994. Comment on "The Cretaceous-Tertiary boundary transition in the Antarctic Ocean and its global implications" by G. Keller. Marine Micropalaeontology **24**, 91–99.

Huber, B.T., Norris, R.D. and MacLeod, K.G. 2002. Deep-sea paleotemperature record of extreme warmth during the Cretaceous. *Geology* **30**, 123-126.

Hull, P.M., Norris, R.D., 2011. Diverse patterns of ocean export productivity change across the Cretaceous-Paleogene boundary: new insights frombiogenic barium. *Paleoceanography* **26**, 1–10.

Hull, P.M. and Darroch, S.A. 2013. Mass extinctions and the structure and function of ecosystems. *Ecosystem Paleobiology and Geobiology, The Paleontological Society Papers* **19**, 1-42.

Jablonski, D. 2005. Mass extinctions and macroevolution. *Paleobiology* **31**, 192-210.

Jeffery, C.H. 2001. Heart urchins at the Cretaceous/Tertiary boundary: A tale of two clades. *Paleobiology* **27**, 140-158.

Jiang, S., Bralower, T. J., Patzkowsky, M. E., Kump, L. R., Schueth, J. D., 2010. Geographic controls on nannoplankton extinction across the Cretaceous/Paleogene boundary. *Nature Geoscience* **3**, 280–285.

Jourdan, F., Reimold, W.U. and Deutsch, A. 2012. Dating terrestrial impact structures. *Elements* **8**, 49-53.

Jung, C., Voigt, S. and Friedrich, O. 2012. High-resolution carbon-isotope stratigraphy across the Campanian-Maastrichtian boundary at Shatsky Rise (tropical Pacific). *Cretaceous Research* **37**, 177-185.

Jung, C., Voigt, S., Friedrich, O., Koch, M.C., Frank, M., 2013. Campanian-Maastrichtian ocean circulation in the tropical Pacific*. Paleoceanography* **28**, 562–573. http://dx.doi.org/10.1002/palo.20051 .

Keller, G., Adatte, T., Bhowmick, P.K., Upadhyay, H., Dave, A., Reddy, A.N., Jaiprakash, B.C., 2012. Nature and timing of extinctions in the Cretaceous–Tertiary planktic foraminifera preserved in Deccan intertrappen sediments of the Krishna-Godavari Basin, India. *Earth and Planetary Science Letters* **341**–**344**, 211–221.

Keller, G., Adatte, T., Pardo, A., Bajpai, S., Khosla, A., Samant, B., 2010. Cretaceous extinctions: evidence overlooked. *Science* **328**, 974–975.

Keller, G., Adatte, T., Tantawy, A.A., Berner, Z., Stinnesbeck, W., Steuben, D., Leanza, H.A., 2007. High stress late Maastrichtian–early Danian palaeoenvironments in the Neuquén Basin, Argentina. *Cretaceous Research* **28**, 939–960.

Keller, G., Punekar, J., Mateo, P., 2016. Upheavals during the Late Maastrichtian: Volcanism, climate and faunal events preceding the end-Cretaceous mass extinction. *Palaeogeography, Palaeoclimatology, Palaeoecology* **441**, 137–151.

Keller, G., 1993. The Cretaceous-Tertiary boundary transition in the Antarctic Ocean and its global implications. *Marine Micropalaeontology* **21**, 1–45.

Kemp, D.B., Robinson, S.A., Crame, J.A., Francis, J.E., Ineson, J., Whittle, R.J., Bowman, V.C., O'Brien, C., 2014. A cool temperate climate on the Antarctic Peninsula through the latest Cretaceous to early Paleogene. *Geology* **42**, 583–586.

Kennedy, W.J., Crame, J.A., Bengston, P., Thompson, M.R.A., 2007. Coniacian ammonites from the James Ross Island, Antarctica. *Cretaceous Research* **28**, 509–531.

Klaus, A., Norris, R.D., Kroon, D., Smit, J., 2000. Impact-induced mass wasting at the K-T boundary: Blake Nose, western North Atlantic. *Geology* **28**, 319–322.

Komintz, M.A., Browning, J.V., Miller, K.G., Sugarman, P.J., Misintseva, S., Scotese, C.R., 2008. Late Cretaceous to Miocene sea-level estimates from the New Jersey and Delaware coastal plain coreholes: an error analysis. *Basin Research* **20**, 211–226.

Kring, D.A. 2007. The Chicxulub impact event and its environmental consequences at the Cretaceous–Tertiary boundary. *Palaeogeography, Palaeoclimatology, Palaeoecology* **255**, 4-21.

Kump, L.R. 1991. Interpreting carbon-isotope excursions: Strangelove oceans. *Geology* **19**, 299-302.

Kyte, F.T., Smit, J., 1984. Regional variations in spinel compositions: an important key to the Cretaceous/Tertiary event. *Geology* **14**, 485–487.

Landman, N.H., Goolaerts, S., Jagt, J.W.M., Jagt-Yazykova, E.A., Machalski, M., Yacobucci, M.M., 2014. Ammonite extinction and nautilid survival at the end of the Cretaceous. *Geology* **42**, 707–710.

Lawver, L.A., Gahagan, L.M., Coffin, M.F., 1992. The development of paleoseaways around Antarctica. In: Kennett, J.P., Warnke, D.A. (Eds.), *Antarctic Research Series* **56**, pp. 7–30.

Li, L., Keller, G., 1998. Abrupt deep-sea warming at the end of the Cretaceous. *Geology* **26**, 995–998.

Linnert, C., Robinson, S.A., Lees, J.A., Bown, P.R., Pérez-Rodríguez, I., Falzoni, F., Littler, K., Arz, J.A., Russell, E.R., 2014. Evidence for global cooling in the Late Cretaceous. *Nature Communications* **5**. http://dx.doi.org/10.1038/ncomms5194 (Article number 4194).

Longrich, N.R., Scriberas, J., Wills, M.A., In Press. Severe extinction and rapid recovery of mammals across the Cretaceous–Paleogene boundary, and the effects of rarity on patterns of extinction and recovery. *Journal of Evolutionary Biology*. doi: 10.1111/jeb.12882

Longrich, N.R., Bhullar, B.A.S. and Gauthier, J.A. 2012. A transitional snake from the Late Cretaceous period of North America. *Nature* **488**, 205-208.

Macellari, C.E., 1988. Stratigraphy, sedimentology and paleoecology of Upper Cretaceous/Paleocene shelf-deltaic sediments of Seymour Island (Antarctic Peninsula). In: Feldmann, R.M., Woodburne, M.O. (Eds.), *Geology and Paleontology of Seymour Island, Antarctic Peninsula*. Geological Society of America, Memoirs **169**, pp. 25–53.

MacLeod, K.G., Huber, B.T., Ward, P.D., 1996. The biostratigraphy and paleobiogeography of Maastrichtian inoceramids. In: Ryder, G., Fastovsky, D., Gartner, S. (Eds.), *The Cretaceous-Tertiary Event and Other Catastrophes in Earth History*. Geological Society of America Special Paper **307**, pp. 361–373.

Marenssi S.A., Santillana S.N., Rinaldi C.A., 1998. Stratigraphy of the La Meseta Formation (Eocene), Marambio (Seymour Island), Antarctica. *Asoc. Pal. Arg. Pub. Espec.*, **5**, 137–146.

Marshall, C. R., 2010. in: *Quantitative methods in paleobiology.* (eds Alroy, J. and Hunt, G.) The Palentological Society Papers **16**, 291–316.

Marshall, C.R., Ward, P.D., 1996. Sudden and gradual molluscan extinctions in the Latest Cretaceous of Western European Tethys. *Science* **274**, 1360–1363.

McArthur, J.M., Crame, J.A., Thirlwall, M.F., 2000. Definition of Late Cretaceous stage boundaries in Antarctica using strontium isotope stratigraphy. *Journal of Geology* **108**, 623–640.

McGhee Jr, G.R., Sheehan, P.M., Bottjer, D.J. and Droser, M.L. 2004. Ecological ranking of Phanerozoic biodiversity crises: Ecological and taxonomic severities are decoupled. *Palaeogeography, Palaeoclimatology, Palaeoecology* **211**, 289-297.

McGhee, G.R., Clapham, M.E., Sheehan, P.M., Bottjer, D.J., Droser, M.L., 2013. A new ecological severity ranking of major Phanerozoic biodiversity crises. *Palaeogeography Palaeoclimatolology Palaeoecology* **283**, 260–270.

Meldahl, K.H., 1990. Sampling, species abundance, and the stratigraphic signature, of mass extinction: a test using Holocene tidal flat molluscs. *Geology* **18**, 890–893.

Milanese, F., Kirschvink, J., Olivero, E., Rapalini, A., 2013. Magnetostratigraphy of an Upper Cretaceous Section of James Ross Basin, Antarctica. *Latinmag Letters* **3**, 1–9.

Milanese, F., Olivero, E., Kirschvink, J., Rapalini, A., 2016. C34/C33 limit in proximal marine Santa Marta formation and its correlation with distal rabot formation in James Ross basin, Antarctica*. Latinmag Letters* **6**, Special Issue (2016), B21, 1-4.

Miller, K.G., Kominz, M.A., Browning, J.V., Wright, J.D., Mountain, G.S., Katz, M.E., Sugarman, P.J., Cramer, B.S., Christie-Blick, N., Pekar, S.F., 2005. The Phanerozoic record of global sea-level change. *Science* **310**, 1293-1298.

Molina, E., 2015. Evidence and causes of the main extinction events in the Paleogene based on extinction and survival patterns of foraminifera. *Earth-Science Reviews* **140**, 166-181.

Molina, E., Alegret, L., Arenillas, I., Arz, J.A., Gallala, N., Hardenbol, J., von Salis, K., Steurbaut, E., Vandenberghe, N., Zaghbib-Turki, D., 2006. The global boundary stratotype section and point for the base of the Danian stage (Paleocene, Paleogene, "Tertiary", Cenozoic) at El Kef, Tunisia – original definition and revision. *Episodes* **29**, 263–273.

Montes, N., Nozal, F., Santillana, S., Marenssi, S. A., Olivero, E. B., 2010. Mapa geológioco de la Isla Marambio (Seymour). Escala 1:20,000. *Inst. Ant. Arg. & Inst. Geol. Min. España.*

Newton, R.J., Pevitt, E.L., Wignall, P.B., Bottrell, S.H., 2004. Large shifts in the isotopic composition of seawater sulphate across the Permo-Triassic boundary in northern Italy. *Earth and Planetary Science Letters* **218**, 331-345.

Nichols, D.J. and Johnson, K.R., 2008. *Plants and the KT Boundary*. Cambridge University Press.

Nifuku, K., Kodama, K., Shigeta, Y. and Naruse, H., 2009. Faunal turnover at the end of the Cretaceous in the North Pacific region: Implications from combined magnetostratigraphy and biostratigraphy of the Maastrichtian Senpohshi Formation in the eastern Hokkaido Island, northern Japan. *Palaeogeography, Palaeoclimatology, Palaeoecology*, **271,** 84-95.

Nordt, L., Atchley, S. and Dworkin, S., 2003. Terrestrial evidence for two greenhouse events in the latest Cretaceous. *GSA Today*, **13**, 4-9.

Ohno, S., Kadono, T., Kurosawa, K., Hamura, T., Sakaiya, T., Shigemori, K., Hironaka, Y., Sano, T., Watari, T., Otani, K. and Matsui, T., 2014. Production of sulphate-rich vapour during the Chicxulub impact and implications for ocean acidification. *Nature Geoscience*, **7**, 279-282.

Olivero, E.B., 1998. Large mud-filled channels in the Maastrichtian of the López de Bertodano Formation (Seymour Island, Antarctica): stratigraphical implications. *Revista de la Asociación Geológica Argentina* **53**, 553–556.

Olivero, E.B., 2012a. Sedimentary cycles, ammonite diversity and palaeoenvironmental changes in the Upper Cretaceous Marambio Group, Antarctica. *Cretaceous Research* **34**, 348–366.

Olivero, E.B., 2012b. New Campanian kossmaticeratid ammonites from the James Ross Basin, Antarctica, and their possible relationships with *Jimboiceras*? *antarcticum* Riccardi. *Revue de Paléobiologie*, Genève Volume spécial **11**, pp. 133–149.

Olivero, E.B., Medina, F.A., 2000. Patterns of Late Cretaceous ammonite biogeography in the southern high latitudes: the family Kossmaticeratidae in Antarctica. *Cretaceous Research* **21**, 269–279.

Olivero, E.B., Ponce, J.J., Marsicano, C.A., Martinioni, D.R., 2007. Depositional settings of the basal López de Bertodano Formation, Maastrichtian, Antarctica. *Revista de la Asociación Geológica Argentina*. **62**, 521–529.

Olivero, E.B., Ponce, J.J., Martinioni, D.R., 2008. Sedimentology and architecture of sharp based tidal sandstones in the Upper Marambio Group, Maastrichtian of Antarctica. *Sedimentary Geology* **210**, 11–26.

Olsson, R.K., Wright, J.D., Miller, K.G., 2001. Paleobiogeography of *Pseudotextularia elegans* during the latest Maastrichtian global warming event. *Journal of Foraminiferal Research* **31**, 275–282.

Payne, J.L., Lehrmann, D.J., Wei, J., Orchard, M.J., Schrag, D.P., Knoll, A.H., 2004. Large perturbations of the carbon cycle during recovery from the End-Permian extinction. *Science* **305**, 506–509.

Pierazzo, E. and Artemieva, N., 2012. Local and global environmental effects of impacts on earth. *Elements* **8,** 55-60.

Pirrie, D., 1989. Shallow marine sedimentation within an active margin basin, James Ross Island, Antarctica. *Sedimentary Geology* **63,** 61-82.

Pirrie, D., Crame, J.A., Riding, J.B., 1991. Late Cretaceous stratigraphy and sedimentology of Cape Lamb, Vega Island, Antarctica. *Cretaceous Research* **12**, 227–258.

Pirrie, D., Crame, J.A., Lomas, S.A., Riding, J.B., 1997. Late Cretaceous stratigraphy of the Admiralty Sound region, James Ross Basin, Antarctica. *Cretaceous Research* **18**, 109–137.

Polcyn, M.J., Jacobs, L.L., Araújo, R., Schulp, A.S. and Mateus, O., 2014. Physical drivers of mosasaur evolution. *Palaeogeography, Palaeoclimatology, Palaeoecology* **400**, 17-27.

Pope, K.O., 2002. Impact dust not the cause of the Cretaceous-Tertiary mass extinction. *Geology* **30,** 99-102.

Raup, D.M., Sepkoski, J.J. 1982. Mass extinctions in the marine fossil record. *Science* **215**, 1501–1503.

Raup, D. M., Jablonski, D., 1993. Geography of end-Cretaceous marine bivalve extinctions. *Science* **260**, 971–973.

Renne, P. R., Deino, A.L., Hilgen, F.J., Kuiper, K.F., Mark, D.F., Mitchell, W.S.III., Morgan, L.E., Mundil, R., Smit, J., 2013. Time scales of critical events around the Cretaceous–Paleogene boundary. *Science* **339**, 684–687 (2013).

Renne, P.R., Sprain, C.J., Richards, M.A., Self, S., Vanderkluysen, L., Pande, K., 2015. State shift in Deccan volcanism at the Cretaceous–Paleogene boundary, possibly induced by impact. *Science* **350**, 76–78.

Richards, M. A., Alvarez, W., Self, S., Karlstrom, L., Renne, P.R., Manga, M., Sprain, C.J., Smit, J., Vanderkluysen, L., Gibson, S.A., 2015. Triggering of the largest Deccan eruptions by the Chicxulub impact. *Geological Society of America Bulletin* **127**, 1507–1520.

Riding, J.B. and Crame, J.A., 2002. Aptian to Coniacian (Early–Late Cretaceous) palynostratigraphy of the Gustav Group, James Ross Basin, Antarctica. *Cretaceous Research* **23**, 739-760.

Rinaldi, C.A., Massabie, A., Morelli, J., Rosenman, H.L. and Del Valle, R., 1978. Geologia de la isla Vicecomodoro Marambio. *Contribución del Instituto Antártico Argentino* **217**, 1-37.

Roberts, E.M., Lamanna, M.C., Clarke, J.A., Meng, J., Gorsack, E., Sertich, J.J.W., O'Connor, P.M., Claeson, K.M., MacPhee, R.D.E., 2014. Stratigraphy and vertebrate paleoecology of Upper Cretaceous–?lowest Paleogene strata on Vega Island, Antarctica. *Palaeogeography, Palaeoclimatology, Palaeoecology* **402**, 55–72.

Robertson, D.S., Lewis, W.M., Sheehan, P.M., Toon, O.B., 2013a. K–Pg extinction patterns in marine and freshwater environments: the impact winter model. *Journal of Geophysical Research: Biogeosciences* **118**, 1–9.

Robertson, D.S., Lewis, W.M., Sheehan, P.M. and Toon, O.B., 2013b. K-Pg extinction: Reevaluation of the heat-fire hypothesis. *Journal of Geophysical Research: Biogeosciences* **118,** 329-336.

Robinson, N., Ravizza, G., Coccioni, R., Peucker-Ehrenbrink, B., Norris, R.D., 2009. A high resolution marine ^{187}Os/^{188}Os record for the late Maastrichian: distinguishing the chemical fingerprints of Deccan volcanism and the KP impact event. *Earth and Planetary Science Letters* **281**, 159–168.

Scasso, R.A., Olivero, E.B., Buatois, L.A., 1991. Lithofacies, biofacies, and ichnoassemblage evolution of a shallow submarine volcaniclastic fan-shelf depositional system (Upper Cretaceous, James Ross Island, Antarctica). *Journal of South American Earth Science* **4**, 239–260.

Schmidt, A., Skeffington, R.A., Thordarson, T., Self, S., Forster, P.M., Rap, A., Ridgwell, A., Fowler, D., Wilson, M., Mann, G.W., Wignall, P.B., Carslaw, K.S., 2016. Selective environmental stress from sulphur emitted by continental flood basalt eruptions. *Nature Geoscience* **9**. 77–82 (2016).

Schoene, B., Samperton, K.M., Eddy, M.P., Keller, G., Adatte, T., Bowring, S.A., Khadri, S.F. and Gertsch, B., 2015. U-Pb geochronology of the Deccan Traps and relation to the end-Cretaceous mass extinction. *Science* **347,** 182-184.

Schulte, P., Speijer, R.P., Brinkhuis, H., Kontny, A., Claeys, P., Galeotti, S., Smit, J., 2008. Comment on the paper "Chicxulub impact predates K-T boundary: New evidence from Brazos, Texas" by Keller et al. (2007). *Earth and Planetary Science Letters* **269**, 613-619.

Schulte, P.D., Alegret, L., Arenillas, I., Arz, J.A., Barton, P.J., Bown, P.R., Bralower, T.J., Chisteson, G.L., Claeys, P., Cockell, C.S., Collins, G.S., Deutsch, A., Goldin, T.J., Goto, K., Grajales-Nishimura, J.M., Grieve, R.A.F., Gulick, S.P.S., Johnson, K.R., Kiessling, W., Koeberl, C., Kring, D.A., MacLeod, K.G., Matsui, T., Melosh, J., Montanari, A., Morgan, J.V., Neal, C.R., Nichols, D.J., Norris, R.D., Pierazzo, E., Ravizza, G., Rebolledo-Vieyra, M., Reimold, W.U., Robin, E., Salge, T., Speijer, R.P., Sweet, A.R., Urrutia-Fucugauchi, J., Vajda, V., Whalen, M.T., Willumsen, P.S., 2010. The

Chicxulub asteroid impact and mass extinction at the Cretaceous-Paleogene boundary. *Science* **327**, 1214–1218.

Self, S., Blake, S., Sharma, K., Widdowson, M. and Sephton, S., 2008. Sulfur and chlorine in Late Cretaceous Deccan magmas and eruptive gas release. *Science* **319**, 1654-1657.

Self, S., Schmidt, A. and Mather, T.A., 2014. Emplacement characteristics, time scales, and volcanic gas release rates of continental flood basalt eruptions on Earth. In: *Keller, G., Kerr, A.C. (Eds.), Volcanism, Impacts, and Mass Extinctions: Causes and Effects*. Geological Society of America Special Paper **505**

Sepkoski Jr, J.J., 1986. Phanerozoic overview of mass extinction. In *Patterns and Processes in the History of Life* (pp. 277-295). Springer Berlin Heidelberg.

Sepkoski, J.J., 2002. A compendium of fossil marine genera. *Bulletins of American Paleontology* **363**, 2002. 1–563.

Sheehan, P.M., Fastovsky, D.E., Barreto, C. and Hoffmann, R.G., 2000. Dinosaur abundance was not declining in a "3 m gap" at the top of the Hell Creek Formation, Montana and North Dakota. *Geology* **28**, 523-526.

Sial, A.N., Chen, J., Lacerda, L.D., Frei, R., Tewari, V.C., Pandit, M.K., Gaucher, C., Ferreira, V.P., Cirilli, S., Peralta, S. and Korte, C., 2016. Mercury enrichments and Hg isotopes in Cretaceous–Paleogene boundary successions: Links to volcanism and palaeoenvironmental impacts. *Cretaceous Research* **66**, 60–81.

Sibert, E.C., Hull, P.M. and Norris, R.D., 2014. Resilience of Pacific pelagic fish across the Cretaceous/Palaeogene mass extinction. *Nature Geoscience* **7**, 667-670.

Signor, P.W., Lipps, J.H., 1982. Sampling bias, gradual extinction patterns, and catastrophes in the fossil record. In: Silver, L.T., Schulz, P.H. (Eds.), *Geological Implications of Large Asteroids and Comets on the Earth*. Geol. Soc. Am. Spec. Publ. **190**, pp. 291–296.

Smit, J. and Hertogen, J., 1980. An extraterrestrial event at the Cretaceous–Tertiary boundary. *Nature* **285**, 198-200.

Smit, J. and Kyte, F.T. 1984. Siderophile-rich magnetic spheroids from the Cretaceous-Tertiary Boundary in Umbria, Italy. *Nature* **310**, 403-405.

Smith, A.B., Gale, A.S. and Monks, N.E., 2001. Sea-level change and rock-record bias in the Cretaceous: a problem for extinction and biodiversity studies. *Paleobiology* **27**,241-253.

Song, H., Wignall, P. B., Tong, J. Yin, H., 2012. Two pulses of extinction during the Permian–Triassic crisis. *Nature Geoscience* **6**, 52–56.

Steinthorsdottir, M., Vajda, V., Pole. M, In Press. Global trends of pCO_2 across the Cretaceous–Paleogene boundary supported by the first Southern Hemisphere stomatal proxy-based pCO_2 reconstruction. *Palaeogeography, Palaeoclimatology, Palaeoecology.* doi:10.1016/j.palaeo.2016.04.033

Steuber, T., Mitchell, S.F., Buhl, D., Gunter, G. and Kasper, H.U., 2002. Catastrophic extinction of Caribbean rudist bivalves at the Cretaceous-Tertiary boundary. *Geology* **30**, 999-1002.

Stilwell, J.D., Zinsmeister, J.D., Oleinik, A.E., 2004. Early Paleocene mollusks of Antarctica: systematics, palaeoecology and palaeobiogeographic significance. *Bulletins of American Paleontology* **367**, 1–89.

Stinnesbeck, W., Ifrim, C., Salazar, C., 2012. The last Cretaceous ammonites in Latin America. *Acta Palaeontologica Polonica* **57**, 717–728.

Thibault, N., 2016. Calcareous nannofossil biostratigraphy and turnover dynamics in the late Campanian–Maastrichtian of the tropical South Atlantic. *Revue de Micropaléontologie* **59**, 57-69.

Thibault, N. & Husson, D., 2016. Climatic fluctuations and sea-surface water circulation patterns at the end of the Cretaceous era: Calcareous nannofossil response. *Palaeogeography Palaeoclimatology Palaeoecology* **441**, 152–164.

Thibault, N., Gardin, S. 2010. The nannofossil response to the end-Cretaceous warm event in the tropical Pacific. *Palaeogeography Palaeoclimatology Palaeoecology* **291**. 239–252.

Thibault, N., Harlou, R., Schovsbo, N.H., Stemmerik, L. and Surlyk, F., 2015a. Late Cretaceous (Late Campanian–Maastrichtian) sea surface temperature record of the Boreal Chalk Sea. *Climate of the Past Discussions* **11**, 5049-5071.

Thibault, N., Galbrun, B., Gardin, S., Minoletti, F., Le Callonnec, L., 2015b. The end-Cretaceous in the southwestern Tethys (Elles, Tunisia): orbital calibration of paleoenvironmental events before the mass extinction. *International Journal of Earth Science* **105**, 771–795.

Thibodeau, A.M., Ritterbush, K., Yager, J.A., West, A.J., Ibarra, Y., Bottjer, D.J., Berelson, W.M., Bergquist, B.A. and Corsetti, F.A., 2016. Mercury anomalies and the timing of biotic recovery following the end-Triassic mass extinction. *Nature Communications*, **7.**

Tobin, T.S., Bitz, C.M., Archer, D., In Press. Modeling climatic effects of carbon dioxide emissions from the Deccan Traps Volcanic Eruptions around the Cretaceous–Paleogene boundary. *Palaeogeograpgy, Palaeoclimatology, Palaeoecology*. doi:10.1016/j.palaeo.2016.05.028

Tobin, T.S.,Ward, P.D., Steig, E.J., Olivero, E.B., Hilburn, I.A.,Mitchell, R.N., Diamond,M.R.,Raub, T.D., Kirschvink, J.L., 2012. Extinction patterns, $\delta_{18}O$ trends, and magnetostratigraphy from a southern high-latitude Cretaceous-Paleogene section: links with Deccan volcanism. *Palaeogeography Palaeoclimatolology Palaeoecology* **350–352**, 180–188.

Tobin, T.S., Wilson, G.P., Eiler, J.M. and Hartman, J.H., 2014. Environmental change across a terrestrial Cretaceous-Paleogene boundary section in eastern Montana, USA, constrained by carbonate clumped isotope paleothermometry. *Geology* **42**, 351-354.

Tschudy, R.H., Pillmore, C.L., Orth, C.J., Gilmore, J.S. and Knight, J.D., 1984. Disruption of the terrestrial plant ecosystem at the Cretaceous-Tertiary boundary, Western Interior. *Science* **225**,1030-1032.

Twitchett, R.J., 2006. The palaeoclimatology, palaeoecology and palaeoenvironmental analysis of mass extinction events. *Palaeogeography, Palaeoclimatology, Palaeoecology* **232**,190-213.

Tyrrell, T., Merico, A. and McKay, D.I.A., 2015. Severity of ocean acidification following the end-Cretaceous asteroid impact. *Proceedings of the National Academy of Sciences* **112**, 6556-6561.

Vajda, V., Raine, J.I. and Hollis, C.J., 2001. Indication of global deforestation at the Cretaceous-Tertiary boundary by New Zealand fern spike. *Science* **294**, 1700-1702.

Vellekoop, J., Sluijs, A., Smit, J., Schouten, S., Weijers, J.W., Damsté, J.S.S. and Brinkhuis, H., 2014. Rapid short-term cooling following the Chicxulub impact at the Cretaceous–Paleogene boundary. *Proceedings of the National Academy of Sciences* **111**, 7537-7541.

Vellekoop, J., Smit, J., van de Schootbrugge, B., Weijers, J.W., Galeotti, S., Damsté, J.S.S. and Brinkhuis, H., 2015. Palynological evidence for prolonged cooling along the Tunisian continental shelf following the K–Pg boundary impact. *Palaeogeography, Palaeoclimatology, Palaeoecology* **426**, 216-228.

Vellekoop, J., Esmeray-Senlet, S., Miller, K.G., Browning, J.V., Sluijs, A., van der Schootbrugge, B., Sinninghe Damsté, J.S., Brinkhuis, H., 2016. Evidence for Cretaceous–Palegoene boundary bolide "impact winter" conditions from New Jersey, USA. *Geology*, doi: 10.1130/G37961.1

Vila, B., Sellés, A.G., Brusatte, S.L., 2016. Diversity and faunal changes in the latest Cretaceous dinosaur communities of southwestern Europe. *Cretaceous Research* **57**, 552–564.

Voigt, S., Gale, A.S., Jung, C., Jenkyns, H.C., 2012. Global correlation of upper Campanian–Maastrichtian successions using carbon-isotope stratigraphy: development of a new Maastrichtian timescale. *Newsletters on Stratigraphy* **45**, 25–53.

Voigt, S., Jung, C., Friedrich, O., Frank, M., Teschner, C., Hoffman, J., 2013. Tectonically restricted deep-ocean circulation at the end of the Cretaceous. *Earth and Planetary Science Letters* **369–370**, 169–177.

White, R.V. and Saunders, A.D., 2005. Volcanism, impact and mass extinctions: incredible or credible coincidences? *Lithos* **79**, 299-316.

Whiteside, J.H.,Ward, P.D., 2009. Ammonoid diversity and disparity track episodes of chaotic carbon cycling during the early Mesozoic. *Geology* **39**, 99–102.

Whitham, A.G., Ineson, J.R. and Pirrie, D., 2006. Marine volcaniclastics of the Hidden Lake Formation (Coniacian) of James Ross Island, Antarctica: an enigmatic element in the history of a back-arc basin. *Geological Society, London, Special Publications* **258**, 21-47.

Wignall, P.B., 2005. The link between large igneous province eruptions and mass extinctions. *Elements* **1**, 293-297.

Wignall, P.B., 2001. Large igneous provinces and mass extinctions. *Earth-Science Reviews* **53**, 1-33.

Wignall, P.B., 2015. The Worst of Times: How Life on Earth Survived Eighty Million Years of Extinctions. Princeton University Press. 199 pp.

Wilf, P., Johnson, K., Huber, B.T., 2003. Correlated terrestrial andmarine evidence for global climate change before mass extinction at the Cretaceous-Paleogene boundary. *Proceedings of the National Acadamey of Science* **100**, 599–604.

Wilson, G.P., 2014a. Mammalian extinction, survival, and recovery dynamics across the Cretaceous-Paleogene boundary in northeastern Montana, USA. *Geological Society of America Special Papers* **503**, 365-392.

Wilson, G.P., DeMar, D.G. and Carter, G., 2014b. Extinction and survival of salamander and salamander-like amphibians across the Cretaceous-Paleogene boundary in northeastern Montana, USA. *Geological Society of America Special Papers* **503**, 271-297.

Zachos, J. C.*, and* M. A. Arthur *(*1986*),* Paleoceanography of the Cretaceous-Tertiary boundary event: Inferences from stable isotopic and other data. *Paleoceanography* **1***,* 5–26*.*

Zinsmeister, W. J. & Macellari, C. E., 1988. Bivalvia (Mollusca) from Seymour Island, Antarctic Peninsula. *Geological Society of America Memoirs* **169,** 25–53.

Zinsmeister, W. J., Feldmann, R. M., Woodburne, M. O., Elliot, D. H., 1989. Latest Cretaceous/earliest Tertiary transition on Seymour Island, Antarctica. *Journal of Palaeontology* **63**, 731–738.

Zinsmeister, W.J., 1982. Late Cretaceous-early Tertiary molluscan biogeography of the southern circum-Pacific. *Journal of Paleontology*, 84-102.

Zinsmeister, W.J., 1988. Early geological exploration of Seymour Island, Antarctica. In: Feldmann, R.M., Woodburne, M.O. (Eds.), *Geology and Paleontology of Seymour Island, Antarctic Peninsula*. Geological Society of America, Memoirs **169**, pp. 1–16.

Zinsmeister,W.J., Feldmann, R.M., 1996. Late Cretaceous faunal changes in the high southern latitudes: a harbinger of global biotic catastrophe? In: Macleod, N., Keller, G. (Eds.), *Cretaceous–Tertiary Mass Extinctions: Biotic and Environmental Changes*. W.W. Norton, New York, pp. 303–325.

Chapter 3 : Evolution and extinction of Maastrichtian (Late Cretaceous) cephalopods from the López de Bertodano Formation, Seymour Island, Antarctic

This chapter has been published as;

3.1 Abstract

One of the most expanded records to contain the final fortunes of ammonoid cephalopods is within the López de Bertodano Formation of Seymour Island, James Ross Basin, Antarctica. Located at ~65° South now, and during the Cretaceous, this sequence is the highest southern latitude onshore outcrop containing the Cretaceous-Paleogene (K–Pg) transition. We present comprehensive new biostratigraphic range data for 14 ammonite and one nautiloid species based on a collection of >700 macrofossils from high-resolution sampling of parallel sedimentary sections, dated Maastrichtian to earliest Danian in age, across southern Seymour Island. We find evidence for only a single, abrupt pulse of cephalopod extinction at the end of the Cretaceous when the final seven ammonite species disappeared, consistent with most evidence globally. In the lead up to the K–Pg extinction in the James Ross Basin, starting during the Campanian, ammonite diversity decreased overall, but the number of endemic taxa belonging to the family Kossmaticeratidae actually increased. This pattern continued into the Maastrichtian and may be facies controlled, linked to changes in sea level and seawater temperature. During the early Maastrichtian, ammonite diversity dropped significantly with only two species recorded from the basal López de Bertodano Formation on Seymour Island. The subsequent diversification of endemic taxa and reappearance of long-ranging, widespread species into the

basin resulted in an increase in ammonite diversity and abundance during the mid-Maastrichtian. This was coincident with an apparent period of warming temperatures and sea level rise interpreted from palynology and sedimentology, perhaps reflecting a high latitude expression of the Mid-Maastrichtian Event. Late Maastrichtian diversity levels remained stable despite reported climatic and environmental variation. Ammonite diversity patterns during the Maastrichtian parallel those of microfossil species such as nannofossil and planktonic foraminifera, suggesting that dynamic climatic and environmental changes affected many planktonic and nektonic organisms during the latest Cretaceous. However, we suggest that these perturbations had a minimal effect on overall diversity prior to the catastrophic extinction event at the K–Pg boundary.

3.2 Introduction

The final demise of the ammonoid cephalopods at the end of the Cretaceous is a key component of the ongoing debate about the nature of the Cretaceous–Paleogene (K–Pg) boundary mass extinction event of 66 Ma (Gallagher, 1991; Ward et al., 1991; Marshall and Ward, 1996). Whether this event was caused by the devastating impact of an extraterrestrial object (Alvarez et al., 1980; Schulte et al., 2010; Renne et al., 2013), or was drawn out through the final few million years of the Cretaceous, with other factors such as climate and sea level changes or the environmental effects of large scale flood basalt volcanism playing a primary role (Archibald et al., 2010; Courtillot and Fluteau, 2010; Keller et al., 2010).

Latest Cretaceous (Maastrichtian, 72–66 Ma) cephalopod faunas are known from every continent and palaeolatitude, although these faunas have traditionally been difficult to correlate to the international timescale due to lack of a global biostratigraphic framework (e.g. Ward, 1990; Landman et al., 2014). This has led to debate about the timing of ammonoid extinction associated with the K–Pg transition, as well as diversity changes throughout the Maastrichtian (e.g. Kennedy, 1989; Marshall and Ward, 1996; Stinnesbeck et al., 2012), a geological age with well-studied climatic and oceanographic

changes (e.g. Barrera, 1994; Barrera and Savin, 1999; Miller et al., 2003; Thibault et al., 2010; Voigt et al., 2012).
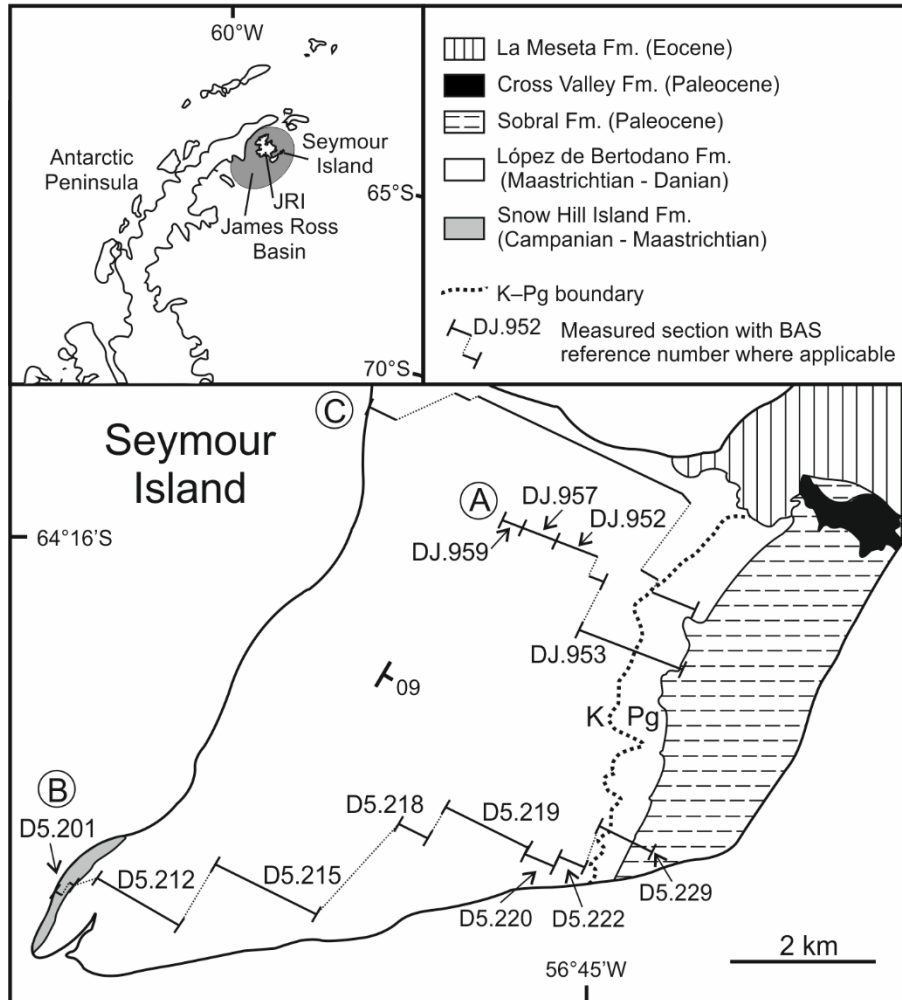
Figure 3.1: Locality and geology map of Seymour Island, James Ross Basin, Antarctic Peninsula. The maps show modern geography. JRI, James Ross Island; BAS, British Antarctic Survey; K, Cretaceous; Pg, Paleogene. The K–Pg boundary is shown by a dotted line and crops out within the uppermost López de Bertodano Formation. A–B, measured sections discussed in this paper. A, BAS 1999 field season, sections DJ.959, DJ.957, DJ.952 and DJ.953 are stratigraphically continuous (Crame et al., 2004). B, BAS 2006 field season, sub-sections D5.201, D5.212, D5.215, D5.218, D5.219, D5.220, D5.222 and D5.229 comprise composite section D5.251 (Bowman et al., 2012, 2013a, 2014). C, Measured section trace from Tobin et al. (2012) based on GPS coordinates taken from that study. Map after Montes et al (2010).

Despite being prominent victims of the end-Cretaceous catastrophe, the actual cause of ammonite extinction remains largely unclear. With a planktonic larval stage (Shigeta, 1993; Landman et al., 1996; Tajika and Wani, 2011), and probable reliance of some groups on plankton as a primary food source (Kruta et al., 2011; Tanabe, 2011), ammonites may have been victims of a mass extinction of marine calcifying organisms and associated productivity or food chain collapse related to the impact event (Hsü and McKenzie, 1985; D'Hondt, 2005; Schulte et al., 2010; Robertson et al., 2013). However, some doubt has recently been cast upon the general model of catastrophic productivity collapse at the K–Pg (Sepulveda et al., 2009; Alegret et al., 2011; Hull and Norris, 2011; Sogot et al., 2013). Other extinction scenarios focus on an alleged long-term decline in ammonite diversity through the Late Cretaceous (Wiedmann and Kullman, 1996; Zinsmeister and Feldmann, 1996; Stinnesbeck et al., 2012) and the subsequent effects of Maastrichtian sea level, climate, and oceanographic changes on an already diminished group (Stinnesbeck et al., 2012). In support of this argument, ammonites appear to have been particularly sensitive to environmental change throughout their long evolutionary history (e.g. House, 1989; O'Dogherty et al., 2000; Whiteside and Ward, 2009; Korn and Klug, 2012). Ultimately only high-resolution stratigraphic data from well dated K–Pg boundary successions can provide insights into the fate of the group during the last few million years of the Cretaceous.

The López de Bertodano Formation, which crops out on Seymour Island, James Ross Basin, Antarctica (Figure 3.1) is a key unit for assessing biotic change at this time, primarily because it is the highest latitude onshore record available in the Southern Hemisphere (~65°S presently and during the Late Cretaceous; Lawver et al., 1992; Hathway, 2000). Further, the expanded nature of the sedimentary sequence provides excellent temporal resolution (Crame et al., 1999; Crame et al., 2004; Olivero, 2012a). In this paper we present new data based on collections of Maastrichtian cephalopods (ammonites and nautiloids) from measured sections through the López de Bertodano Formation on Seymour Island (Figure 3.2). We provide a detailed

assessment of high latitude ammonoid diversity throughout the Maastrichtian from Seymour Island, discuss diversity trends and extinction patterns with an emphasis on the K–Pg boundary, and assess our record within the longer term context of other changes taking place during the Late Cretaceous in the James Ross Basin.
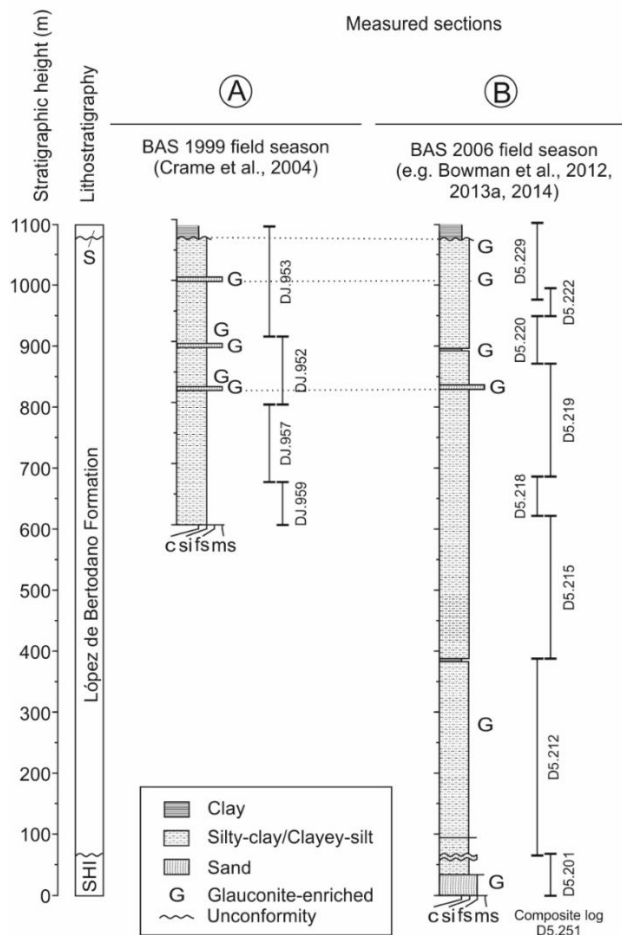
Figure 3.2: Lithostratigraphy, sedimentology and correlation of measured sections as located in Fig. 3.1 (A–B), southern Seymour Island, Antarctic Peninsula. BAS, British Antarctic Survey; K, Cretaceous; Pg, Paleogene. The K–Pg boundary horizon is identifiable using dinoflagellate cyst biostratigraphy (Elliot et al., 1994; Askin and Jacobsen, 1996; Bowman et al., 2012), sedimentology (the base of a prominent glauconite-rich bed, Zinsmeister, 1998) and the disappearance of ammonite macrofossils. The age model is presented in Fig. 3.3. The López de Bertodano Formation consists predominantly of hundreds of metres of clayey-silts and silty-clays. In section B, the sub-section overlap between D5.222 and D5.229 has been taken into account when interpreting the macrofossil data.

The López de Bertodano Formation has become an important section for calibrating ammonite extinction through the use of statistical methods (e.g. Marshall, 1995; Wang and Marshall, 2004) based on early ammonite range data (Macellari, 1986). However, these data came from collections made before the precise location of the K–Pg boundary on Seymour Island was known (Elliot et al., 1994). Whilst previous studies (e.g. Macellari, 1986; Zinsmeister, 1998; Zinsmeister, 2001) have also illustrated cephalopod range data from this succession, our study involves systematic high-resolution sampling tied to measured sedimentary sections in the field, allowing for accurate stratigraphic location of individual fossils.

In addition, we have undertaken a taxonomic review of the fauna (see Section 3.9) and compared our data to newly developed age models (e.g. Tobin et al., 2012; Bowman et al., 2013a), which enable us to accurately place this important record in a global context for the first time. The new data also allow the terminal ammonite extinction to be considered in the context of their Late Cretaceous record in the region and the controls on diversity to be assessed.

3.3 Geological Setting

During the Late Cretaceous the James Ross Basin was located adjacent to an active volcanic island arc (Figure 3.1), now represented by the Antarctic Peninsula (Hathway, 2000; Crame et al., 2004; Olivero et al., 2008; Olivero, 2012a). The principal basin fill is subdivided into three lithostratigraphic groups: Gustav Group (Aptian–Coniacian), Marambio Group (Santonian–Danian), and Seymour Island Group (Paleocene–Eocene) (Crame et al., 1991; Scasso et al., 1991; Pirrie et al., 1997; Crame et al., 2004; Crame et al., 2006; Olivero, 2012a). Samples used in this study were collected from the López de Bertodano Formation, which forms the upper part of the ~3000 m thick Marambio Group (Olivero, 2012a) and crops out over ~70 km^2 of southern Seymour Island and neighbouring Snow Hill Island (Fig. 1; Pirrie et al., 1997; Crame et al., 2004; Olivero et al., 2007, 2008; Bowman et al., 2012).

The lithostratigraphy and sedimentology of the López de Bertodano Formation have been described by a number of authors (Macellari, 1988; Crame et al.,

1991; Pirrie et al., 1997; Crame et al., 2004; Olivero et al., 2007, 2008; Olivero, 2012a). The dominant lithology of the ~1100 m thick succession exposed on Seymour Island is a mix of fine grained clayey-silts and silty-clays with occasional clay-rich layers and sand, demonstrating little lithological variation (Figure 3.2) (Macellari, 1988; Crame et al., 2004; Olivero et al., 2007, 2008). Although largely homogeneous, the succession also contains occasional sandstone beds interspersed with the dominant finer-grained lithologies, as well as many discrete layers of early diagenetic concretions — some containing well-preserved mollusc and crustacean fossils. Regional dip is 8 to 10° to the southeast, and varies little throughout the sequence.

Differing palaeoenvironmental interpretations have been proposed for the López de Bertodano Formation. Macellari (1988) favoured deposition in a shallow water, near shore setting for the basal portion (~300 m), an interpretation elaborated upon by Olivero (1998) and Olivero et al. (2007, 2008), who suggested that large, shore-parallel channels at this level formed within a large estuary or embayment. In contrast, Crame et al. (2004) suggested that a slight decrease in grain size above the underlying Haslum Crag member of the Snow Hill Island Formation (also noted by Pirrie et al., 1997), together with the poorly fossiliferous nature of this portion of the succession, represented deep water shelf conditions. Stratigraphically higher, the mid-upper portion of the formation represents overall transgression and the establishment of mid-outer shelf environments (Macellari, 1988; Crame et al., 2004; Olivero et al., 2008; Olivero, 2012a). In the uppermost 300 m of the sequence on Seymour Island the monotonous bioturbated siltstones also contain a succession of glauconite-rich horizons, often topped with fossiliferous 'lags' containing many molluscs and other fossils. These layers suggest periods of sediment starvation (Crame et al., 2004). Previous authors have suggested that this upper portion of the succession across the K–Pg boundary represents a regressive phase and loss of accommodation space (Macellari, 1988; Crame et al., 2004; Olivero, 2012a). The base of a prominent series of glauconite horizons ~1000 m above the base of the sequence coincides with a distinct change in both macro and microfossil faunas and

74

floras (Elliot et al., 1994; Zinsmeister, 1998; Crame et al., 2004; Stilwell et al., 2004; Bowman et al., 2012), and is interpreted as being equivalent to the 'K–T glauconite' succession of Zinsmeister (1998) (Figure 3.2). The base of this glauconite-rich interval contains a small iridium (Ir) spike and the first appearance (FA) and acme of the dinoflagellate cyst *Senegalinium obscurum*, markers used by previous authors to locate the K–Pg boundary on Seymour Island (Elliot et al., 1994; Crame et al., 2004; Bowman et al., 2012). This horizon is also the contact between informal mapping units 'Klb9' and 'Klb10' of Macellari (1988) and Sadler (1988). Above this the 50–70m thick unit 'Klb10' is made up of brown-grey mudstones and siltstones with scattered concretions and a distinctive macrofossil fauna dominated by the large bivalve *Lahillia* and the gastropod *Struthiochenopus* (Macellari, 1988; Crame et al., 2004; Montes et al., 2010).

There is no sedimentological or palaeontological evidence for any major hiatuses in the López de Bertodano Formation on Seymour Island and most estimates of the rate of sediment accumulation are high at 10–30 cm ka−1 (McArthur et al., 1998; Crame et al., 1999; McArthur et al., 2000; Dutton et al., 2007; Tobin et al., 2012).

3.4 Age Model

Recent work has allowed the construction of an integrated age model for the López de Bertodano Formation (Figure 3.3) based on strontium isotope stratigraphy (McArthur et al., 1998; Crame et al., 2004), ammonite and dinoflagellate cyst biostratigraphy (Bowman et al., 2012; Olivero, 2012a; Bowman et al., 2013a) and magnetostratigraphy (Tobin et al., 2012). Tobin et al. (2012) identified chrons C31R through to C29N on Seymour Island, indicating an early Maastrichtian–Danian age for the sequence, which agrees with strontium isotope data from macrofossil shell material (McArthur et al., 1998; Crame et al., 2004), the presence of an Ir anomaly marking the K–Pg boundary (Elliot et al., 1994) and dinoflagellate cyst biostratigraphy (Elliot et al., 1994; Bowman et al., 2012).
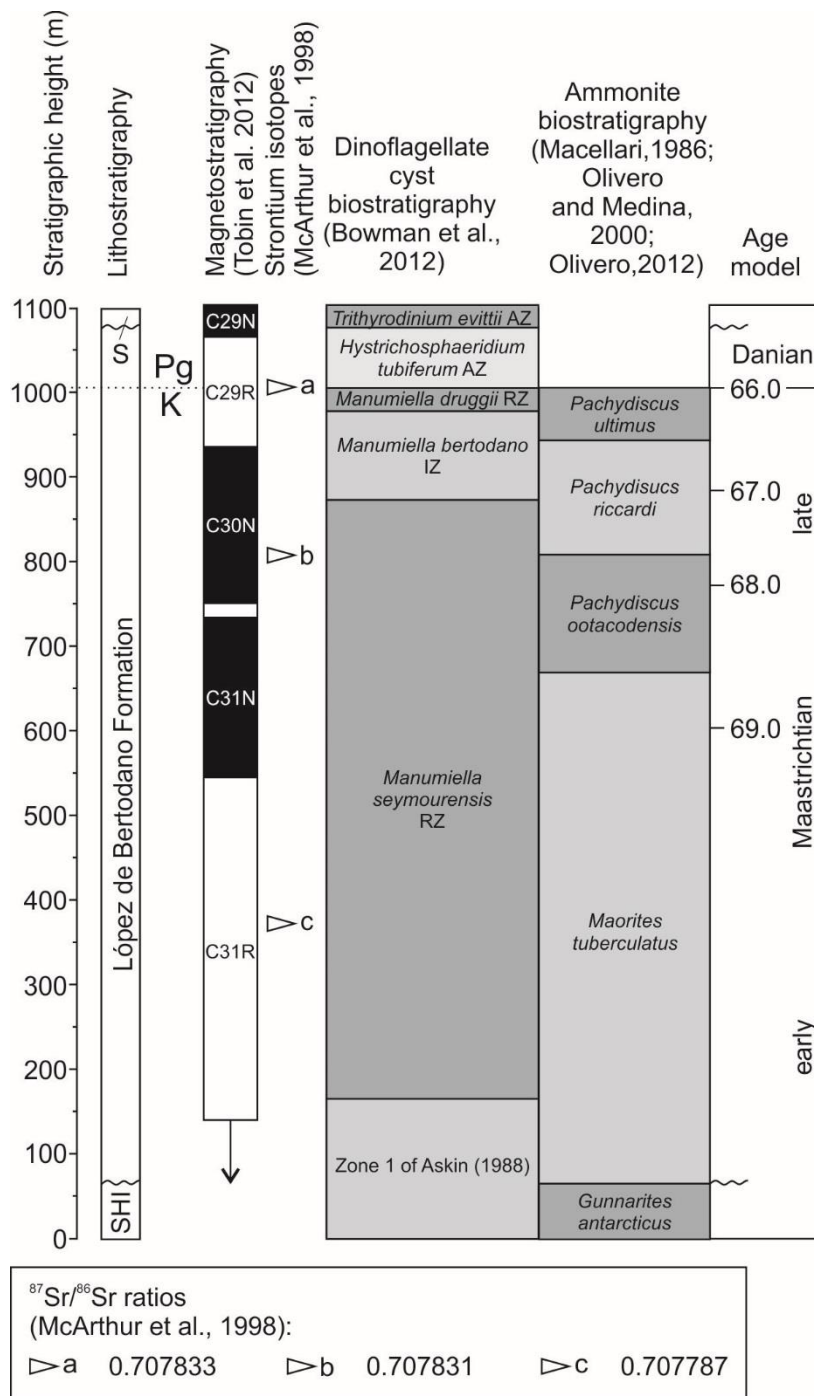
Figure 3.3: Age model for the López de Bertodano Formation, southern Seymour Island, Antarctic Peninsula. This sequence has been dated using biostratigraphy (palynology, micro- and macro-fossil, e.g. Macellari, 1988; Elliot et al., 1994; Bowman et al., 2012; Olivero, 2012a; Bowman et al., 2013a), magnetostratigraphy (Tobin et al., 2012) and strontium isotope stratigraphy (McArthur et al., 1998), calibrated to Gradstein et al. (2012). SHI = Snow Hill Island Formation, S = Sobral Formation.

Correlation of the magnetostratigraphy of Tobin et al. (2012) to our composite section was achieved using GPS coordinates provided in that study, and the location of our measured section lines accurately plotted using field GPS data and the published topographic map of Seymour Island (Figure 3.1; Brecher and Tope, 1988). The timescale of Gradstein et al. (2012) has been added to the age model using linear interpolation between the known ages of chron reversal boundaries. Published ammonite biostratigraphy is useful for correlation within the James Ross Basin but is of limited use for dating purposes due to the presence of primarily endemic taxa (Figure 3.3; Macellari, 1986; Olivero and Medina, 2000; Crame et al., 2004; Olivero, 2012a). In addition, strontium isotope stratigraphy applied to other Maastrichtian successions supports this age model when compared to existing data (Vonhof et al., 2011).

Recent updates to the astronomical (Husson et al., 2011; Batenburg et al., 2014) and geochronological (Gradstein et al., 2012; Voigt et al., 2012; Renne et al., 2013) calibrations of the Maastrichtian timescale suggest that the C31R–C31N chron reversal can be dated at 69.2 Ma, with the Campanian–Maastrichtian boundary at 72.2 Ma and the K–Pg boundary at ~66 Ma. A large portion of the succession can thus be considered late Maastrichtian in age, which is in agreement with dinoflagellate biostratigraphy (Bowman et al., 2012). Previous workers placed the Campanian–Maastrichtian boundary in Antarctica in the lowermost Cape Lamb Member of the Snow Hill Island Formation as exposed on nearby Vega Island, stratigraphically ~200 m below the base of the succession described here (McArthur et al., 1998; Crame et al., 1999; McArthur et al., 2000; Olivero, 2012a).

3.5 Material and Methods

3.5.1 Macrofossil range data

More than 700 cephalopod macrofossils were collected and examined during this study, with over 550 identified to species level (See Appendix A and B for range charts and supplementary data tables). Collection occurred as part of a

multi-field season stratigraphic study of the López de Bertodano Formation on Seymour Island (Crame et al., 2004; Bowman et al., 2012; Bowman et al., 2013a; Bowman et al., 2014). The fossils are stored and curated at the British Antarctic Survey (BAS), Cambridge, UK. All fossils are precisely located on two composite measured sections across the southern part of the island (Figure 3.1). The first is 470 m thick and comprises sub-sections DJ.959, 957, 952, and 953 (Crame et al., 2004). This section encompasses the mid to upper portion of the López de Bertodano Formation extending to the contact with the overlying Sobral Formation. The second section (composite section D5.251) is along strike to the south and is ~1100 m thick comprising sub-sections D5.212, D5.215, D5.218, D5.219, D5.220, D5.222, and D5.229. This extends through the Haslum Crag Member of the Snow Hill Island Formation and the entire López de Bertodano Formation, terminating in the lowermost Sobral Formation (Thorn et al., 2007; Bowman et al., 2012; Bowman et al., 2013a, 2014).

Sedimentary sections were measured using traditional field methods (Jacob's staff and abney level, with some intervals then subdivided using a tape measure), which yielded a high-resolution stratigraphy (e.g. Crame et al., 1991; Pirrie et al., 1997; Crame et al., 2004). Correlation between the two composite sections was made using stratigraphic tie-points, including the K–Pg boundary, the unconformity between the López de Bertodano and Sobral formations, and a prominent glauconite horizon 174m below the K–Pg that can be traced laterally across the island (Figure 3.2). Based on our field knowledge we have assumed planar bedding along strike and no significant hiatuses. Although identification of tie points in the lower portion of the sequence is challenging, our section lines show little lateral facies or structural variation in the field that would impede the use of one main composite section for biostratigraphic purposes. This is particularly evident when the first and last appearances of different macrofossil species are compared across section lines because in many cases these occur at approximately (within ~10 m) the same stratigraphic height (e.g. the last appearance (LA) of *Maorites* cf.

78

weddelliensis and the first appearance (FA) *Grossouvrites joharae*) (Figure 3.4).

Macrofossil collections were made either every metre or in binned intervals several metres thick and of considerable lateral extent along strike (binned intervals were on average 10 m thick in sections DJ.959–953 and 5m thick in D5.251). In such thick stratigraphic sections and with a high sedimentation rate (e.g. McArthur et al., 1998, 2000; Crame et al., 1999; Dutton et al., 2007; Tobin et al., 2012) these are high resolution collections for assessing key biostratigraphic patterns. Effort was also made to ensure that all section lines were collected uniformly with a similar amount of time spent collecting within each binned interval and no increase in sampling intensity close to the K–Pg boundary.

Taxonomic analysis of the Antarctic ammonite fauna was conducted using the monograph of Macellari (1986), supplemented by earlier works such as those of Kilian and Reboul (1909), Spath (1953) and Howarth (1958, 1966) as well as studies of other Maastrichtian faunas (e.g. Henderson and McNamara, 1985; Kennedy and Henderson, 1992a; Klinger and Kennedy, 2003; Ifrim et al., 2004; Salazar et al., 2010). Nautiloid taxonomic analysis used the work of Cichowolski et al. (2005) and Nielsen and Salazar (2011). Systematic nomenclature of Maastrichtian ammonoids follows the Treatise of Invertebrate Paleontology (Wright et al., 1996) to sub-generic level. Taxonomic comments on the cephalopod fauna can be found in Section 3.9. Representative ammonite taxa from the López de Bertodano Formation are illustrated in Figure 3.5 and Figure 3.6.

Following taxonomic identification (Section 3.9), stratigraphic ranges were compiled for each composite section using data from all sub-sections and amalgamated into a single range chart (Figure 3.4), with care taken to ensure that repetition of fossil bearing horizons was avoided. For illustration purposes, each fossil occurrence is placed at the mid-point of the binned interval in which it was collected. Species diversity indices are illustrated in Figure 3.7. Raw species richness is the number of species present at any given horizon,

and standing species richness is the number of species that first appear or last appear at any given horizon, plus those that range through the horizon.

3.5.2 Statistical analysis

To assess the 'Signor-Lipps effect' (i.e. that the final stratigraphic occurrence of any given taxon in a particular stratigraphic succession is unlikely to be the true final occurrence of that taxon in the basin) (Signor and Lipps, 1982) within our dataset, we have applied the stratigraphic abundance method of Meldahl (1990). The last occurrence of a taxon is plotted against their stratigraphic abundance (the percent of stratigraphic sample intervals in which the species occurs, S) (Figure 3.8). Only species with an S value greater than 15% are generally considered reliable indicators of a true extinction horizon (species occurring in more than 15% of all stratigraphic horizons, Meldahl, 1990; Rampino and Adler, 1998; Song et al., 2013).

We also calculated 50% confidence intervals for all taxa, based on the stratigraphic distribution and the number of occurrences of each taxon in the composite section. These are illustrated as range extensions on the composite range chart using the method of Marshall (1995) (Figure 3.4). Range extensions were calculated for all taxa with >1 fossil occurrence in the composite section.

3.6 Results

3.6.1 Antarctic macrofossil range data

In total, fourteen ammonite species assigned to eight genera were identified from our samples, as well as a single species of nautiloid. Four species remain in open nomenclature or are unnamed (Figure 3.5, Figure 3.6, Section 3.9). In terms of taxonomic composition, the fauna is numerically dominated by individuals belonging to members of the family Kossmaticeratidae (the genera *Maorites* and *Grossouvrites*), as well as Desmoceratidae (*Kitchinites*), alongside rarer examples of the Lytoceratidae (*Zelandites*, *Anagaudryceras*, *Pseudophyllites*), Pachydiscidae (*Pachydiscus* (*Pachydiscus*)), and a single species of Diplomoceratidae (*Diplomoceras*).

The basal portion of the López de Bertodano Formation is poorly fossiliferous (Figure 3.4, Figure 3.7). The first appearance of ammonites in our composite section is represented by examples of the large heteromorph *Diplomoceras cylindrace*um (DeFrance) (Figure 3.5G) at 95 m in our composite section D5.251, followed by small fragmentary specimens of *Maorites tuberculatus* (Howarth) (Figure 3.6C) which appear at 235 m, and similarly poorly preserved examples of *Pseudophyllites* cf. *loryi* (Killian and Reboul) (Figure 3.5C) at 330 m.
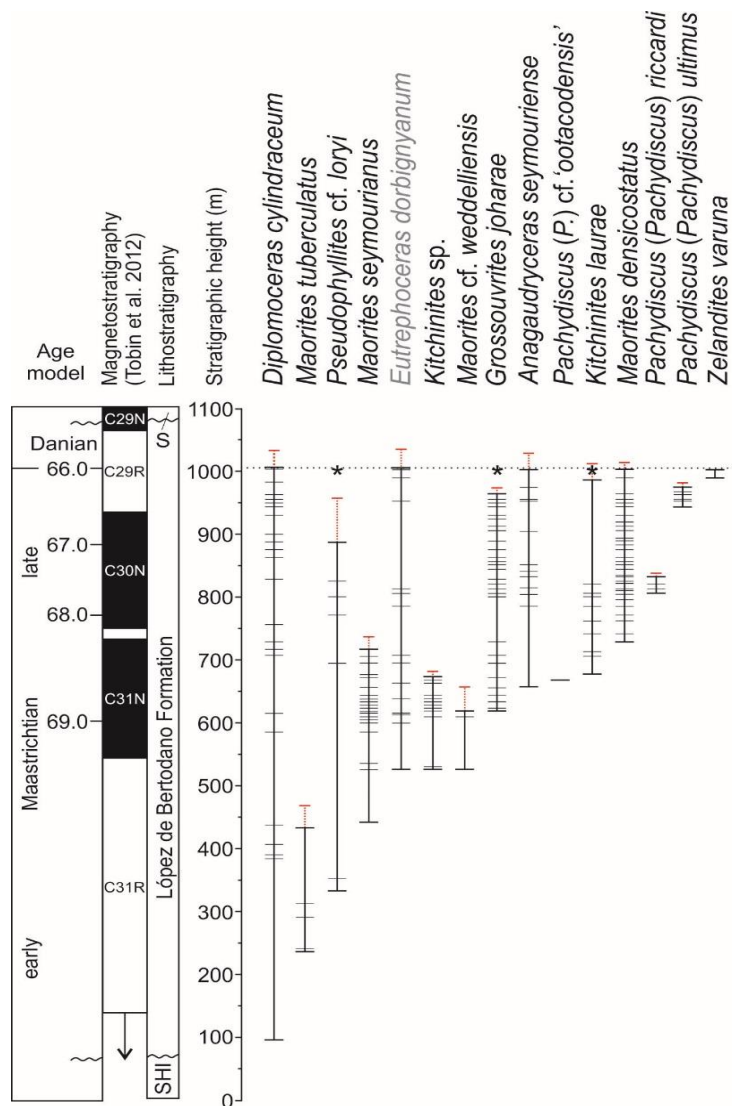
Figure 3.4: Composite range chart of cephalopod (ammonite and nautiloid) taxa from the López de Bertodano Formation, southern Seymour Island, Antarctic Peninsula. Fossil occurrences have been amalgamated from the DJ sections and section D5.251 to show the entire recorded range of each taxon. Section correlation and the age model are illustrated in Figure 3.2 and Figure 3.3, and discussed in the text. Taxa are ordered by first appearance with 50% confidence intervals on ammonite ranges shown as dashed red lines. Although ammonite confidence intervals span the K–Pg boundary, we believe none survived into the Danian. Rare specimens collected above the boundary are not plotted as they are considered reworked and their stratigraphic position probably the result of more recent glacial drift. Tick marks are taxon occurrences plotted at the stratigraphic mid-point of sampling bins. Larger marks correspond to first/last occurrences. Refer to Section 3.9 for taxonomic notes. Ammonite species names in black, nautiloid species name in grey; SHI, Snow Hill Island Formation; S, Sobral Formation; *, last appearance of taxa found beneath K–Pg boundary by Zinsmeister (1998).

A relatively sparse and poorly preserved benthic macrofossil assemblage is also present at these levels (Macellari, 1988; Crame et al., 2004; Olivero et al., 2007). Although not found in either of our section lines, a single horizon containing specimens of the belemnite *Dimitobelus* (*Dimitocamax*) *seymouriensis* (Doyle and Zinsmeister) was located 636 m below the K–Pg boundary (~370 m) (McArthur et al.,1998; Crame et al., 2004). No ammonites were found associated with the belemnites. There appears to be no change in the benthic fauna, which is dominated by serpulid worm tubes (*Rotularia*) and echinoid spines at this level (Doyle and Zinsmeister, 1988; Dutton et al., 2007).

M. tuberculatus has its last appearance datum (LAD) at 431 m and fragmentary specimens of the larger, coarse-ribbed *Maorites seymourianus* (Kilian and Reboul) (Figure 3.6D) were found at 437 m. A distinct change in the fauna is evident at 525 m above the base of the section (Figure 3.4; Figure 3.7); specimens of *Kitchinites* sp. (Figure 3.6E) appear, alongside examples of another coarse-ribbed kossmaticeratid species: *Maorites* cf. *weddelliensis* (Macellari) (Figure 3.6A). This horizon also contains the first example of the nautiloid *Eutrephoceras dorbignyanum* (Forbes (1846b)) (Figure 3.6D).

The base of sub-sections DJ.959 and D5.218 at ~615 m sees an increase in the abundance of large specimens of *M. seymourianus* and *Kitchinites* sp., along with several well-preserved examples of *E. dorbignyanum*. The LAD of *Maorites* cf. *weddelliensis* occurs within a short stratigraphic interval several metres thick at this level, which correlates well across the two section lines. This level also contains the FAD of representatives of the kossmaticeratid *G. joharae* (Salazar) (Fig. 1.7E).
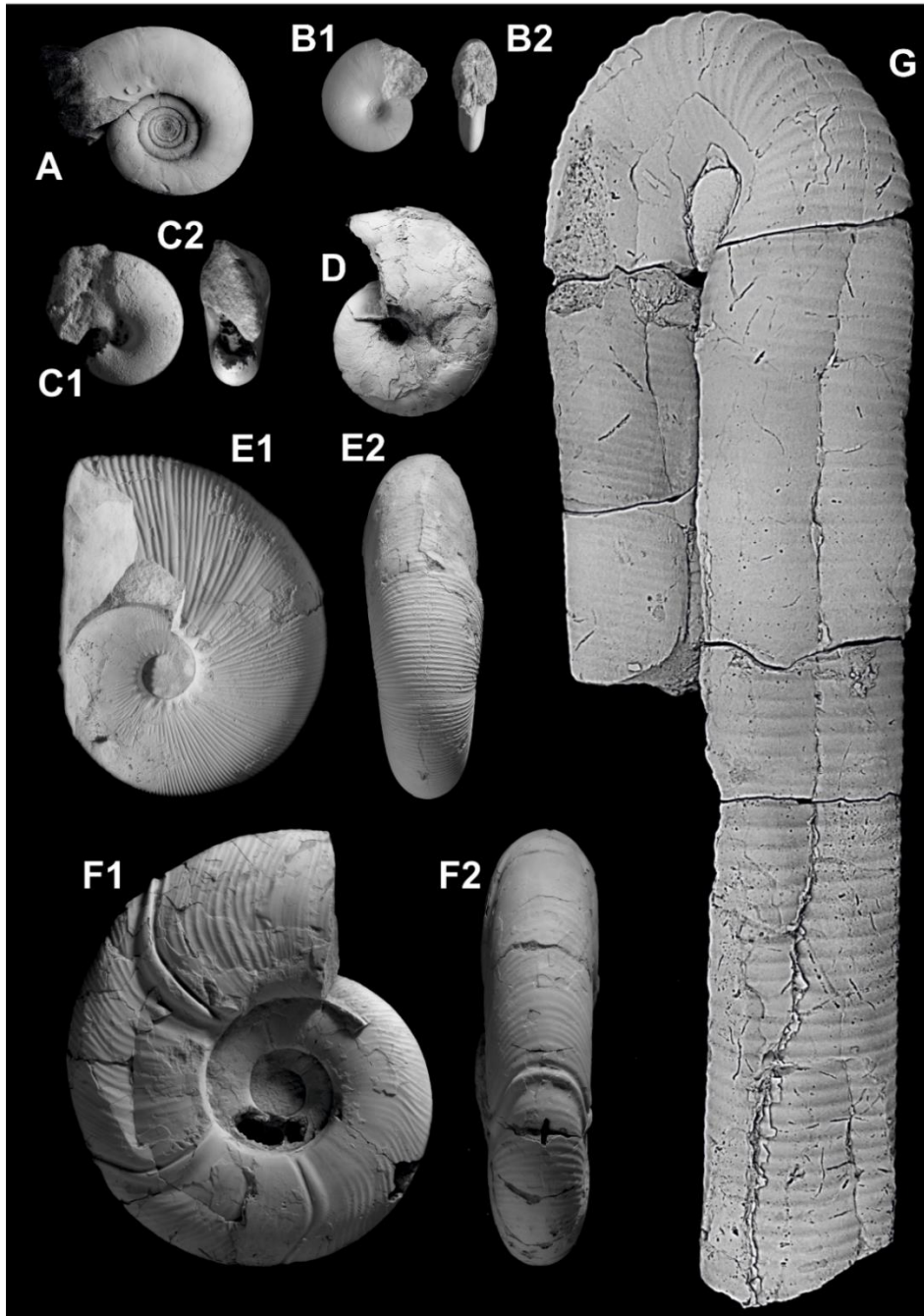
Figure 3.5: A, *Anagaudryceras seymouriense* **Macellari, 1986 (DJ.953.438); B,** *Zelandites varuna* **(Forbes, 1846a) (DJ.953.684), B1—lateral view, B2—apertural view; C,** *Pseudophyllites* **cf.** *loryi* **(Kilian and Reboul, 1909) (DJ.957.189), C1 — lateral view, C2 — apertural view; D,** *Eutrephoceras dorbignyanum* **(Forbes in Darwin 1846) (D5.1011.2); E,** *Grossouvrites joharae* **Salazar et al., 2010 (DJ.952.756), E1 — lateral view, E2 — ventral view; F,** *Kitchinites laurae* **Macellari, 1986 (DJ.952.188), F1 — lateral view, F2 — ventral view; G,** *Diplomoceras cylindraceum* **(Defrance, 1816) (D5.955.2). All figures are ×0.5 except B and C which are ×2. Specimens were coated with ammonium chloride prior to photography.**

84
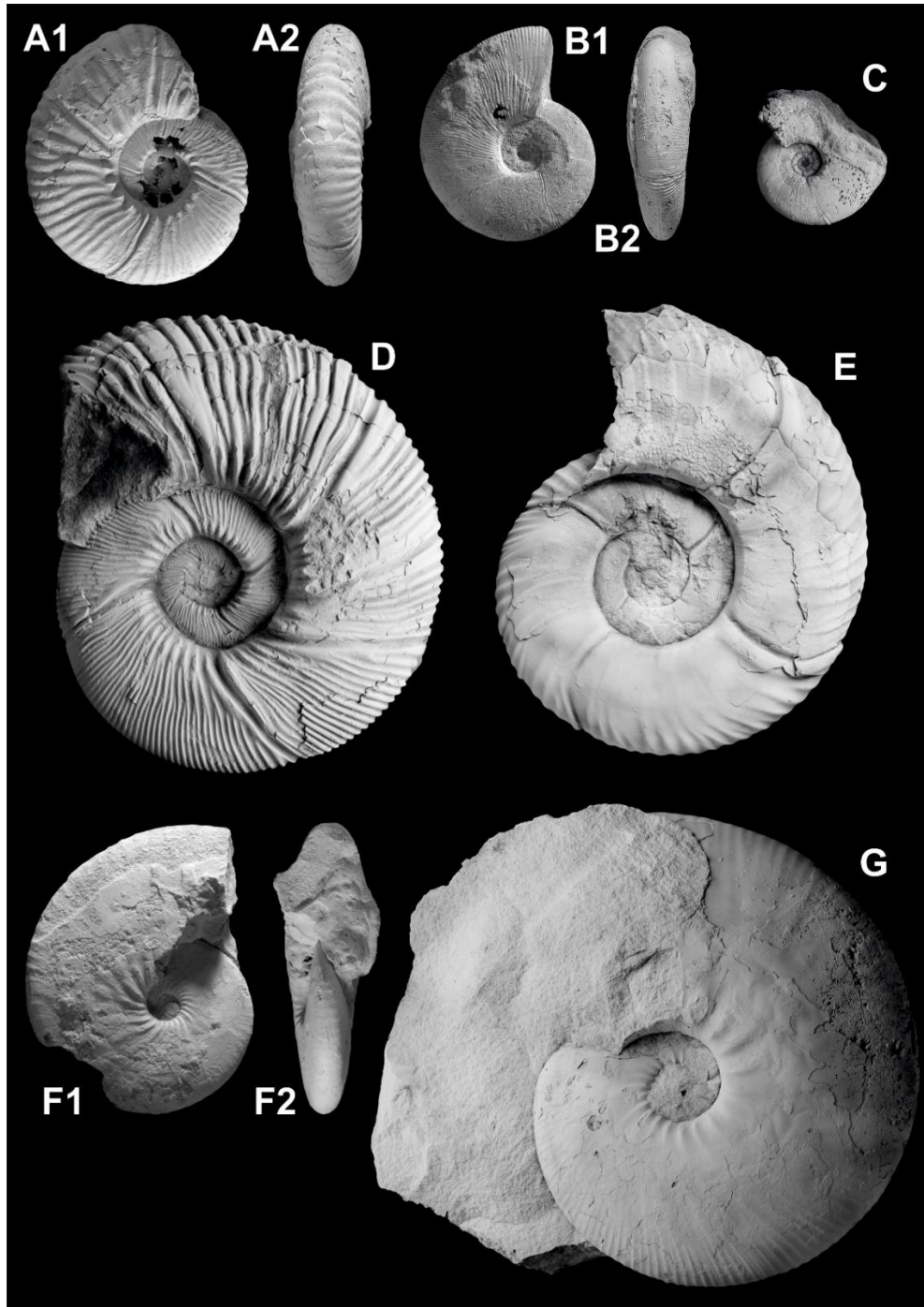
Figure 3.6: A, *Maorites* cf. *weddelliensis* **Macellari, 1986 (D5.691.2), A1 —
lateral view, A2— ventral view; B,** *Maorites densicostatus* **(Kilian
and Reboul, 1909) (DJ.953.379), B1— lateral view, B2— ventral view;
C,** *Maorites tuberculatus* **Howarth, 1958 (D5.955.2); D,** *Maorites
seymourianus* **(Kilian and Reboul, 1909) (D5.1021.2); E,** *Kitchinites*
sp. (D5.1027.2); F, *Pachydiscus* **(***Pachydiscus***)** *ultimus* **Macellari,
1986 (DJ.953.404), F1 — lateral view, F2 — apertural view; G,**
Pachydiscus **(***Pachydiscus***)** *riccardi* **Macellari, 1986 (D5.251 —
unlabelled). All figures are ×0.5. Specimens were coated with
ammonium chloride prior to photography.**

Overall, a steady increase in the diversity of the fauna is notable through the mid portion of the section (Figure 3.7). The lytoceratid *Anagaudryceras seymouriense* (Macellari) (Figure 3.5A) appears at 659 m, followed by an occurrence of a single, poorly preserved pachydiscid resembling *Pachydiscus* (*Pachydiscus*) cf. '*ootacodensis*' (Stoliczka) as also identified by Macellari (1986) at 669 m. Several desmoceratid and kossmaticeratid taxa also exhibit turnover through this interval. Thus, *Kitchinites* sp. disappears at ~674 m and is replaced by *Kitchinites laurae* (Macellari) (Figure 3.5F), and similarly *M. seymourianus* is replaced by the finer-ribbed, more compressed *Maorites densicostatus* (Killian and Reboul) (Figure 3.6B). Macellari (1986) described three morphotypes of this species, but their stratigraphic and morphological ranges overlap and they are considered here as a single rather variable species (Section 3.9).

The upper portion of the succession is dominated by species belonging to long-ranging genera (*Pseudophyllites*, *Anagaudryceras*, and *Diplomoceras*) and kossmaticeratids (*G. joharae, M. densicostatus*) (Figure 3.4). *K. laurae* also occurs sporadically, along with examples of *E. dorbignyanum*. At 809 m the large pachydiscid *Pachydiscus* (*Pachydiscus*) *riccardi* (Macellari) (Figure 3.6G) appears abruptly and remains abundant for around 20 m before a return to the *Maorites–Grossouvrites–Anagaudryceras* fauna. A further influx of large pachydiscids occurs at 942 m (identified as *Pachydiscus* (*Pachydiscus*) *ultimus* (Macellari)) Figure 3.6F) and, like *Pachydiscus* (*Pachydiscus*) *riccardii* they remain abundant for only a short stratigraphic interval until their disappearance at 976 m.

Four ammonite species are present in the five metres beneath the K–Pg boundary in our sections (Figure 3.4, Figure 3.7). Specimens of *D. cylindraceum* and *M. densicostatus* remain common, along with rare *A. seymouriense* until just below the base of the 'K–T glauconite'. There are also several small ammonites similar to those identified by Macellari (1986) as *Zelandites varuna* (Forbes, 1846a) (Figure 3.5B) in this interval. A number of large examples of the nautiloid *E. dorbignyanum* were also found directly below the boundary. Other common taxa in the upper portion of the López de

Bertodano Formation (e.g. *G. joharae, K. laurae*) have LADs in the 40 m below the boundary in all of our section lines (Figure 3.4).

No definitively in situ cephalopod fossils were found above the K–Pg boundary, although poorly preserved ammonites have been previously reported from this interval on Seymour Island (Sadler, 1988; Zinsmeister et al., 1989). Zinsmeister (1998) considered these to be the result of local inliers of Cretaceous-aged sediment in the broad dip-slopes of the Paleocene unit 'Klb10' but our recent observations indicate that their positions may be the result of recent transport due to glacial action, and they are therefore considered reworked.

Composite results suggest that six taxa (*Kitchinites* sp., *M. seymourianus*, *G. joharae, M. densicostatus, E. dorbignyanum*, and *D. cylindraceum*) have a stratigraphic abundance (S) greater than/equal to 15% and should therefore give an accurate record of their true extinction horizon (e.g. Meldahl, 1990). A plot of LAD against stratigraphic height (Figure 3.8) shows a cluster of last appearances close to the K–Pg boundary for three of these taxa (*D. cylindraceum, M. densicostatus, E. dorbignyanum*) along with *A. seymouriense* (S value of 12), with *G. joharae* disappearing some 40 m below in both section lines.

Analysis of 50% confidence intervals shows that ranges are generally well sampled with the larger range extensions clearly being due to rare occurrences (Figure 3.4). Five 50% range extensions extend above the K–Pg boundary, four of which belong to taxa with high stratigraphic abundance (S values ~/>15% *D. cylindraceum, M. densicostatus, A. seymouriense, E. dorbignyanum*). Confidence intervals for the remaining eight taxa all terminate within the Maastrichtian, below the K–Pg interval.

3.7 Discussion

The recently published magnetostratigraphy (Tobin et al., 2012) and updated palynological biostratigraphy (Bowman et al., 2012, 2013a, 2014) allow us to accurately place the Maastrichtian ammonite record from Seymour Island in a

global context for the first time. It is clear that revisions are required to the age models used in previous studies of the Antarctic Maastrichtian successions (e.g. Macellari, 1986; Zinsmeister, 2001) and subsequent comparisons to global events.

3.7.1 K–Pg mass extinction in Antarctica

Previous studies of extinction patterns in the upper part of the López de Bertodano Formation have suggested that the K–Pg mass extinction may have been either a gradual or step-wise event in the southern high latitudes (Zinsmeister et al., 1989; Zinsmeister, 1998; Tobin et al., 2012), with extinction events in the late Maastrichtian preceding the K–Pg extinction event itself (Tobin et al., 2012). However, previous studies using statistical analysis of existing ammonite fossil range data (Macellari, 1986) were unable to rule out the possibility of a sudden extinction at the K–Pg boundary distorted by the Signor–Lipps effect (Marshall, 1995; Marshall and Ward, 1996).

Our new data add support to the hypothesis of a sudden extinction event for ammonites associated with the K–Pg boundary. The largest concentration of last appearances in our composite section occurs between 1 and 5 m below the base of the glauconitic interval containing the K–Pg boundary (Figure 3.4, Figure 3.7). The extinction level is not associated with any major changes in sedimentology but coincides with benthic losses (Macellari, 1988; Crame et al., 2004; Stilwell et al., 2004), the disappearance of marine reptiles (Martin, 2006; Martin and Crame, 2006) and turnover in the palynological record (Elliot et al., 1994; Bowman et al., 2012).

Zinsmeister (1998) reported six ammonite species as having their final occurrence <2 m below the K–Pg boundary on Seymour Island. His records of *M. densicostatus* and *D. cylindraceum* are consistent with our data, as is the restricted occurrence of *Z. varuna*, (Fig. 3.7) but Zinsmeister also reported the presence of *K. laurae*, *Pseudophyllites loryi* and *Grossouvrites gemmatus* (probably *G. joharae* — see Section 3.9 and Salazar et al., 2010), which were not found during our study. In Zinsmeister's (1998) range data the final occurrences of *K. laurae* and *P. loryi* are also the only records of these

species in a 16m interval beneath the boundary. Similarly, examples of *Grossouvrites* only occur twice in the same interval. This suggests that, in addition to four common species, several rare species were present in the latest Maastrichtian. In support of this hypothesis several small external moulds of *A. seymouriense* were discovered ~5m below the K–Pg in one of our section lines, a species not previously recorded from this interval.
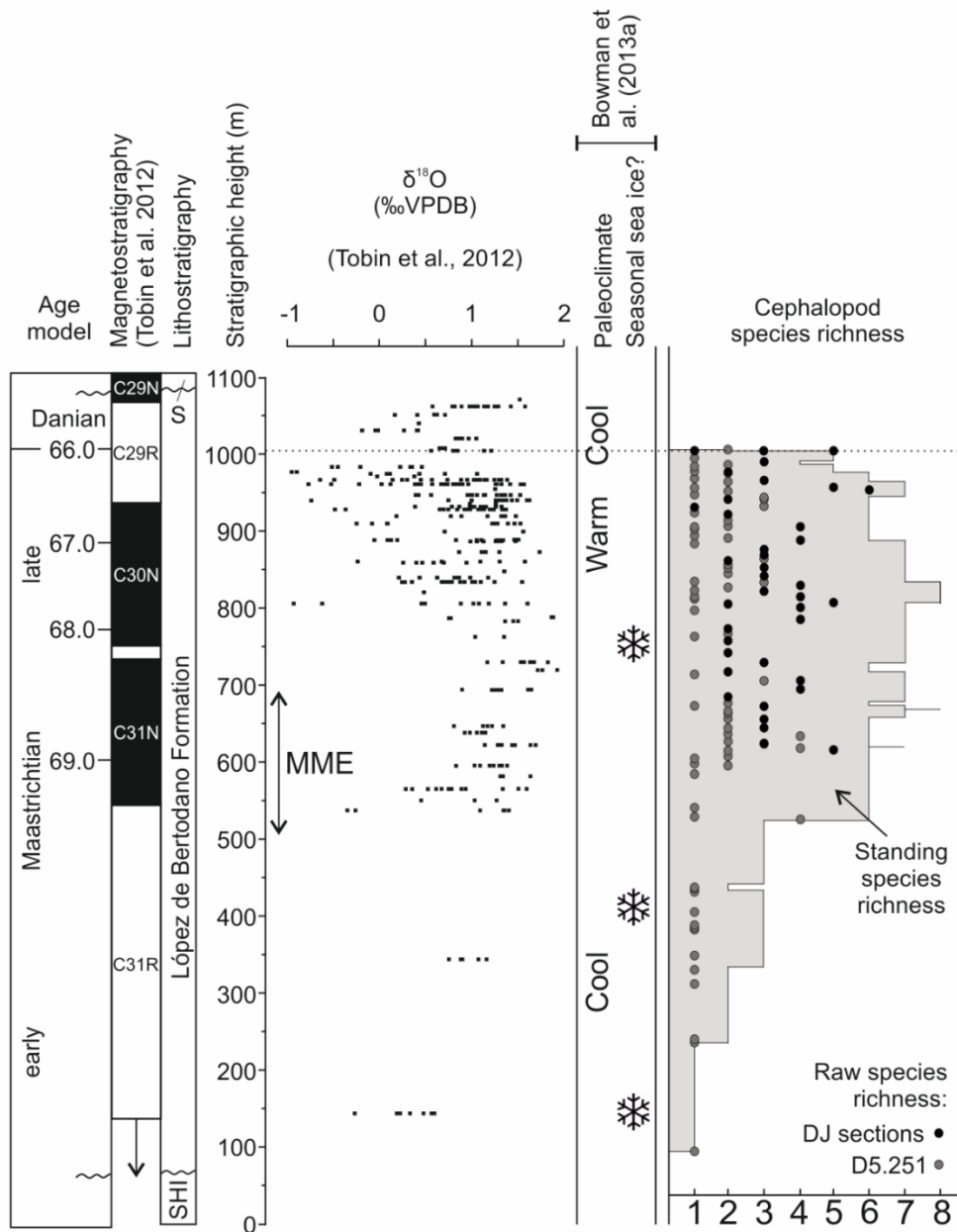
Figure 3.7: Composite cephalopod diversity from the López de Bertodano Formation (southern Seymour Island, Antarctic Peninsula) plotted against molluscan macrofossil oxygen isotope data (Dutton et al., 2007; Tobin et al., 2012) and regional palaeoclimate (Bowman et al., 2013a, 2014). Section correlation and the age model are illustrated in Figure 3.2 and Figure 3.3, and discussed in the text. Snowflake symbols indicate the possible occurrence of seasonal sea ice based on palynological data (Bowman et al., 2013a,b). Cephalopod diversity is represented as: (1) raw species richness (number of species within sampling bin), circles; (2) Standing species richness: (includes taxa that range through). See text for details of these indices and overall sampling strategy. MME, Mid-Maastrichtian Event (e.g. Jung et al., 2013).

Including Zinsmeister's (1998) records with those from this study, a total of seven ammonite species have now been reported from the 5 m interval directly beneath the K–Pg boundary on Seymour Island (Figure 3.4, Figure 3.7) (*M. densicostatus*, *D. cylindraceum*, *Z. varuna*, *G. joharae*, *K. laurae*, *P. loryi*, *A. seymouriense*). Using the age model described herein and published sedimentation rates for the López de Bertodano Formation, a conservative estimate would suggest that this 5m interval could represent as little as ~15 kyr, or as much as ~50 kyr (McArthur et al., 1998, 2000; Crame et al., 1999; Tobin et al., 2012). The highest ammonite occurrence is less than 50 cm below the base of the glauconite sandstone containing the iridium anomaly and K–Pg boundary (Zinsmeister, 1998).

The seven species present in this interval represent three of the four suborders of post-Triassic ammonites (Wright et al., 1996) and are a mixture of taxa endemic to the southern high latitudes (presumably cool-temperate Austral specialists, e.g. kossmaticeratids *Maorites* and *Grossouvrites*, *K. laurae*) and long-ranging cosmopolitan taxa (e.g. *Diplomoceras*, *Pseudophyllites*, *Anagaudryceras*, *Zelandites*). We suggest that these ammonites persisted through the late Maastrichtian but became extinct in a sudden extinction event at the K–Pg boundary. The remaining seven species present in the López de Bertodano Formation are therefore likely victims of background turnover during the Maastrichtian rather than of any sudden event at or before the K–Pg boundary. The high stratigraphic abundance values for two of these species (*M. seymourianus* and *Kitchinites sp.*) and lack of distinct clusters of LAD at any other portion of the section besides the K–Pg interval provide supportive evidence (Figure 3.8). In addition, the nautiloid *E. dorbignyanum* disappears from Antarctica at the K–Pg boundary, raising the total number of cephalopod taxa lost in this interval to eight. This genus exhibits a global distribution in the Maastrichtian (Landman et al., 2014), and although Paleogene representatives are known from lower latitude locations (e.g. Teichert and Glenister, 1952; Stilwell and Grebneff, 1996; Darragh, 1997; Casadío et al., 1999), it failed to recolonize Antarctica.
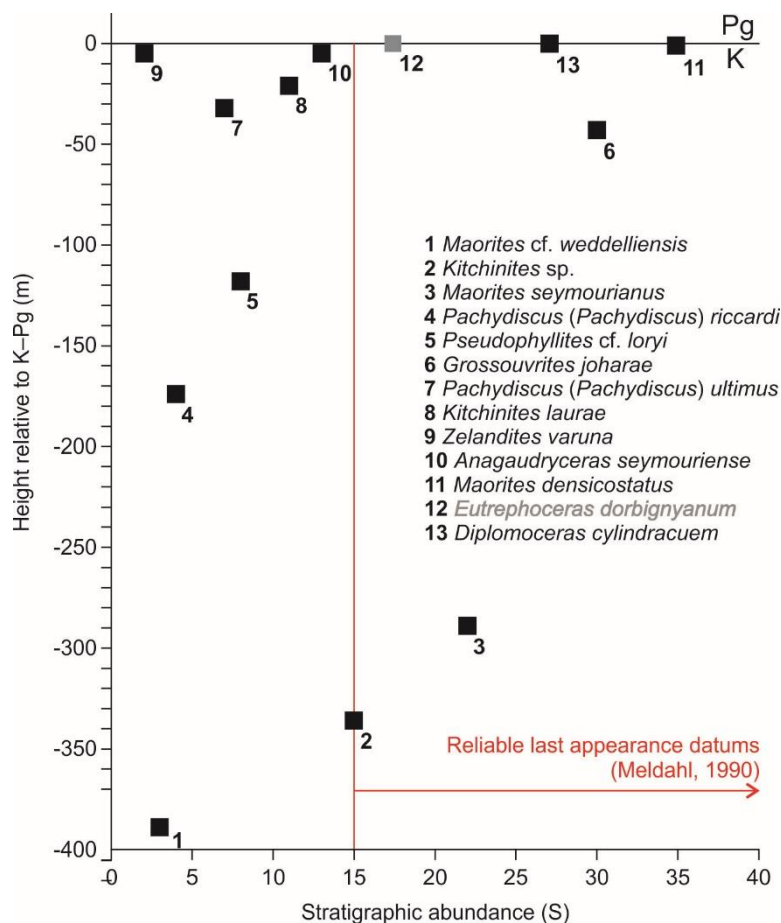
Figure 3.8: Composite stratigraphic abundance of uppermost Maastrichtian cephalopod taxa, López de Bertodano Formation, southern Seymour Island, Antarctic Peninsula. Numbered squares correspond to last appearance datum of taxa ordered stratigraphically. Red line indicates stratigraphic abundance value of 15%, above which indicates a reliable last occurrence (Meldahl, 1990).

3.7.2 Comparison to lower latitude extinction records

Having established the sudden nature of the ammonite extinction event, it is also important to compare the record of ammonite extinction from Antarctica with lower latitudes. Extensive study of Maastrichtian sedimentary successions worldwide suggests that although many macrofossil-bearing shallow water K–Pg successions often contain a hiatus between the upper Maastrichtian and Danian (e.g. Machalski, 2005), a conservative estimate suggests that 30–35 species of ammonite and 31 genera were present in the

final few 100 kyr prior to the K–Pg boundary at a variety of sites around the globe (Landman et al., 2007; Landman et al., 2014). In the most complete successions, ammonites extend to within a few cm of the boundary (as defined by impact debris and/or microfossil turnover, e.g. Birkelund, 1993; Ward and Kennedy, 1993; Landman et al., 2004a,b; Machalski, 2005; Landman et al., 2014). The taxonomic composition of many of these faunas indicates that all four suborders of post-Triassic ammonites (Phylloceratina, Lytoceratina, Ammonitina, and Ancyloceratina) survived into the latest Maastrichtian (Birkelund, 1993; Landman et al., 2007). Below we review the records from several of the most complete K–Pg successions, which also contain palaeoenvironmental information, in order to compare with our new data from Antarctica.

Several localities along the Biscay coast of Spain and France contain complete deep-water (100–500 m) K–Pg successions (Ward et al., 1991; Ward and Kennedy, 1993). A total of 31 species in 19 genera are known from the Maastrichtian, with nine, possibly 10, species belonging to 10 genera ranging to within the final metre beneath the K–Pg boundary (Ward and Kennedy, 1993). The onset of a basin-wide regression is recognised ~20m below the boundary, coinciding with the disappearance of many other ammonite species (Ward and Kennedy, 1993). No ammonite fossils are found in an interval 8–1.5 m below the boundary corresponding to the peak of this regression (Marshall and Ward, 1996). The K–Pg boundary itself is within a period of rising sea level (Pujalte et al., 1998) coincident with the reappearance of ammonites 1.5 m below, and suggesting a strong facies control on ammonite diversity in these sections.

A number of localities in the Danish chalk also contain Maastrichtian successions with little or no hiatus present at the K–Pg boundary (Hart et al., 2005; Hansen and Surlyk, 2014) and with diverse ammonite faunas (Birkelund, 1979, 1993). These faunas are of considerable interest as the only complete Maastrichtian record of ammonites in the Boreal Realm of the Northern Hemisphere (Birkelund, 1993). A total of 19 species belonging to 11 genera were present in the Danish successions during the Maastrichtian, with

seven species in seven genera present directly beneath the K–Pg boundary (Birkelund, 1993; Machalski, 2005; Hansen and Surlyk, 2014). Sea level changes and palaeoenvironmental fluctuations during the Maastrichtian have been recorded from the basin (e.g. Surlyk, 1997; Hart et al., 2005; Hansen and Surlyk, 2014) but cephalopods do not appear to have suffered significant decline prior to the K–Pg boundary (Hansen and Surlyk, 2014). Records of two species indicate that they may even have survived briefly into the early Danian (Surlyk and Nielsen, 1999; Machalski and Heinberg, 2005; Landman et al., 2014).

Elsewhere in Europe, North America, Africa and the Russian Far East, diverse ammonite faunas are also present in the latest Maastrichtian (e.g. Goolaerts et al., 2004; Machalski, 2005; Jagt et al., 2006; Landman et al., 2007; Ifrim et al., 2010; Jagt-Yazykova, 2012), although many of these records are from sites where uncertainties remain about the completeness of the K–Pg interval, or where ammonites are recorded from only part of the succession. Nevertheless, the majority of these low latitude records agree with the evidence from Seymour Island for abrupt ammonite extinction at the K–Pg boundary.

In contrast, Stinnesbeck et al. (2012) concluded that in South America ammonites declined during the Maastrichtian, and disappeared prior to the K–Pg boundary. They suggest a diachronous extinction for the group, beginning in the tropics and expanding towards high latitudes. However, the lack of abundant ammonites in the uppermost Maastrichtian of the Neuquén Basin, Argentina and at Quiriquina Island in Chile, where a diverse Maastrichtian assemblage is present (Salazar et al., 2010), could relate to unfavourable local palaeoenvironmental conditions for cephalopods at these localities where very shallow water environments were developed and possibly stressed by local volcanic activity (Keller et al., 2007).

Although compilations suggest an overall decline in ammonite diversity during the Late Cretaceous in many regions of the globe (Kennedy, 1989; Jagt-Yazykova, 2011; Olivero, 2012a), this may be due to a reduction in the number of short-lived and presumably specialist genera (Yacobucci, 2005).

Many of these genera were likely inhabitants of epeiric or epicratonic seaways, the majority of which were in retreat during the latest Cretaceous (e.g. Kennedy et al., 1998). Data compilations suggest that Maastrichtian faunas were dominated by long-ranging multi-stage taxa (Yacobucci, 2005). Recent work has suggested however, that many ammonite genera that survived to the end of the Maastrichtian were geographically restricted (Landman et al., 2014), perhaps making them more vulnerable to extinction. Despite these observations, that reveal the complex pattern of diversity change during the Late Cretaceous, there is little evidence globally of ammonites becoming seriously impoverished prior to the latest Maastrichtian (but see Section 3.7.3 below for discussion of regional variation). In addition, there does not appear to be evidence of significantly higher extinction rates for the group as a whole when the Maastrichtian record is placed in the context of the entire mid-Late Cretaceous, despite diversity fluctuations (Yacobucci, 2005; Jagt-Yazykova, 2011; Olivero, 2012a). The final extinction of the group therefore appears to have been abrupt and catastrophic, consistent with the idea of a bolide impact as the primary cause.

Ammonite extinction at the K–Pg boundary was probably associated with marine food chain collapse and disruption to surface-water ecosystems resulting from the after-effects of the Chicxulub impact event (Alvarez et al., 1980; Hsü and McKenzie, 1985; D'Hondt, 2005; Schulte et al., 2010), primarily caused by a global dust-cloud that extinguished sunlight and suppressed photosynthesis (Robertson et al., 2013). Suggestion has also been made that a short-lived period of transient ocean acidification may have contributed to the mass extinction of calcifying planktonic organisms across the K–Pg which included embryonic ammonites (Alegret et al., 2011; Arkhipkin and Laptikhovsky, 2012) and their prey (Kruta et al., 2011).

3.7.3 Late Cretaceous faunal diversity and environmental change in Antarctica

Examination of our extended range data (Figure 3.4) reveals patterns in the few million years leading up to the K–Pg extinction that helps to place this event in the context of longer-term changes (Figure 3.9). Olivero and Medina

(2000) identified three major sedimentary cycles in the James Ross Basin during deposition of the Marambio Group, each capped by regional unconformities and containing distinct facies and biota. The N (Santonian–early Campanian), NG (late Campanian–early Maastrichtian), and MG (early Maastrichtian–Danian) sequences are correlated across the basin by means of 14 distinct ammonite assemblages, based on the most common genus of the ammonite family Kossmaticeratidae found within each (N — *Natalites*, NG —*Neograhamites* and *Gunnarites*, MG — *Maorites* and *Grossouvrites*) (Figure 3.9; see also Olivero, 2012a,b).

To examine the picture of ammonite diversity on a longer timescale, ammonite ranges at the generic level through the Coniacian–Maastrichtian (~89–66 Ma) of the James Ross Basin have been plotted (Figure 3.9), based primarily on ammonite assemblage data presented in Olivero (2012a,b), supplemented by information from the Coniacian age Hidden Lake Formation from Kennedy et al. (2007). The generic level diversification through time has been calculated by plotting the difference between the number of generic FAD and LADs in each ammonite assemblage (e.g. O'Dogherty et al., 2000). The K–Pg interval forms the upper boundary of ammonite assemblage 14 and is marked by the disappearance of the final seven genera of ammonites, with one group (Pachydiscidae) disappearing before the boundary, still within assemblage 14. This is the only assemblage for which the accurate position of FADs and LADs within the assemblage is available; all other data are plotted at the mid-point of each assemblage. We have also included range data for belemnites, inoceramid bivalves, and nautilids at the order level based on separate stratigraphic data (see below) (Doyle, 1990; Crame et al., 1996; Crame and Luther, 1997; Cichowolski et al., 2005; Olivero, 2012b).

The low diversity in the López de Bertodano Formation contrasts markedly with the underlying formations (Figure 3.4 and Figure 3.9; Olivero, 1992; Zinsmeister and Feldmann, 1996; Crame et al., 1996; Olivero and Medina, 2000; Olivero, 2012a). Overall, a total of 43 genera were present in the basin during the Coniacian–Maastrichtian interval (Figure 3.9; Zinsmeister and Feldmann, 1996; Kennedy et al., 2007; Olivero, 2012a, b), with the highest

diversities recorded in the Santonian–Campanian Santa Marta Formation, followed by a general decline through the Campanian–Maastrichtian Snow Hill Island Formation (Figure 3.9). The lower portion of the Santa Marta Formation (ammonite assemblages 1–4, Santonian to early Campanian) is an interval where originations and first appearances dominate over extinctions and disappearances, whereas the number of extinctions appear to increase in assemblage 6 of the N sequence towards the top of the formation. This is followed by overall diversity decline within the NG sequence (late Campanian–early Maastrichtian) before a period of stability – at least at generic level – and then a pulse of extinction in assemblage 14 of the MG sequence (i.e. the K–Pg interval within the uppermost López de Bertodano Formation) (Figure 3.9). These patterns are unlikely to be a result of sampling bias, as the key sections within the James Ross Basin have been extensively collected for over 100 years (see reviews in Zinsmeister, 1988; Crame et al., 1991).

Whilst the decline in diversity and disappearance of genera in the Santa Marta Formation could be due to the basin-wide regression at the top of the N sequence, the pattern in the overlying NG sequence in particular does not appear to correlate well with the contemporaneous transgressive–regressive cycle, suggesting that other factors may be responsible for driving diversity changes during this period. In addition, the overall composition of the fauna underwent a series of changes during this interval. Notably, several groups of ammonites disappear from Antarctica during deposition of the N and NG sequences (e.g. scaphitids, baculitids) (Olivero and Medina, 2000; Olivero, 2012a), whilst remaining common components of younger Maastrichtian faunas at lower latitudes. As a result, whereas the Santa Marta Formation contains a mixture of cosmopolitan and endemic genera, faunas from the younger NG and MG sequences are numerically dominated by the largely endemic family Kossmaticeratidae, which shows distinct Austral affinities in its distribution pattern, being found in South America, South Africa, Australia, and New Zealand during the Campanian and Maastrichtian (Henderson, 1970; Henderson and McNamara, 1985; Kennedy and Klinger, 1985; Olivero and Medina, 2000; Salazar et al., 2010).

Other macrofossil groups show similar divergent extinction patterns in the James Ross Basin compared to lower latitudes, in particular inoceramid bivalves and belemnites (Crame et al., 1996; Zinsmeister and Feldmann, 1996). Inoceramid bivalves disappeared from Antarctica during deposition of the upper portion of the Santa Marta Formation (Crame et al., 1996; Crame and Luther, 1997; Olivero and Medina, 2000) in the late Campanian (McArthur et al., 2000) (Figure 3.9) earlier than their mid-Maastrichtian extinction elsewhere (e.g. MacLeod et al., 1996). Belemnites disappeared even earlier, albeit temporarily, in the early Campanian, as recorded in the mid-portion of the Santa Marta Formation on James Ross Island (Doyle, 1990; Crame et al., 1996; McArthur et al., 2000), before a single species reappeared in the basin in the early Maastrichtian of Seymour Island (Figure 3.9; Doyle and Zinsmeister, 1988; Dutton et al., 2007).

(PTO for caption)

99
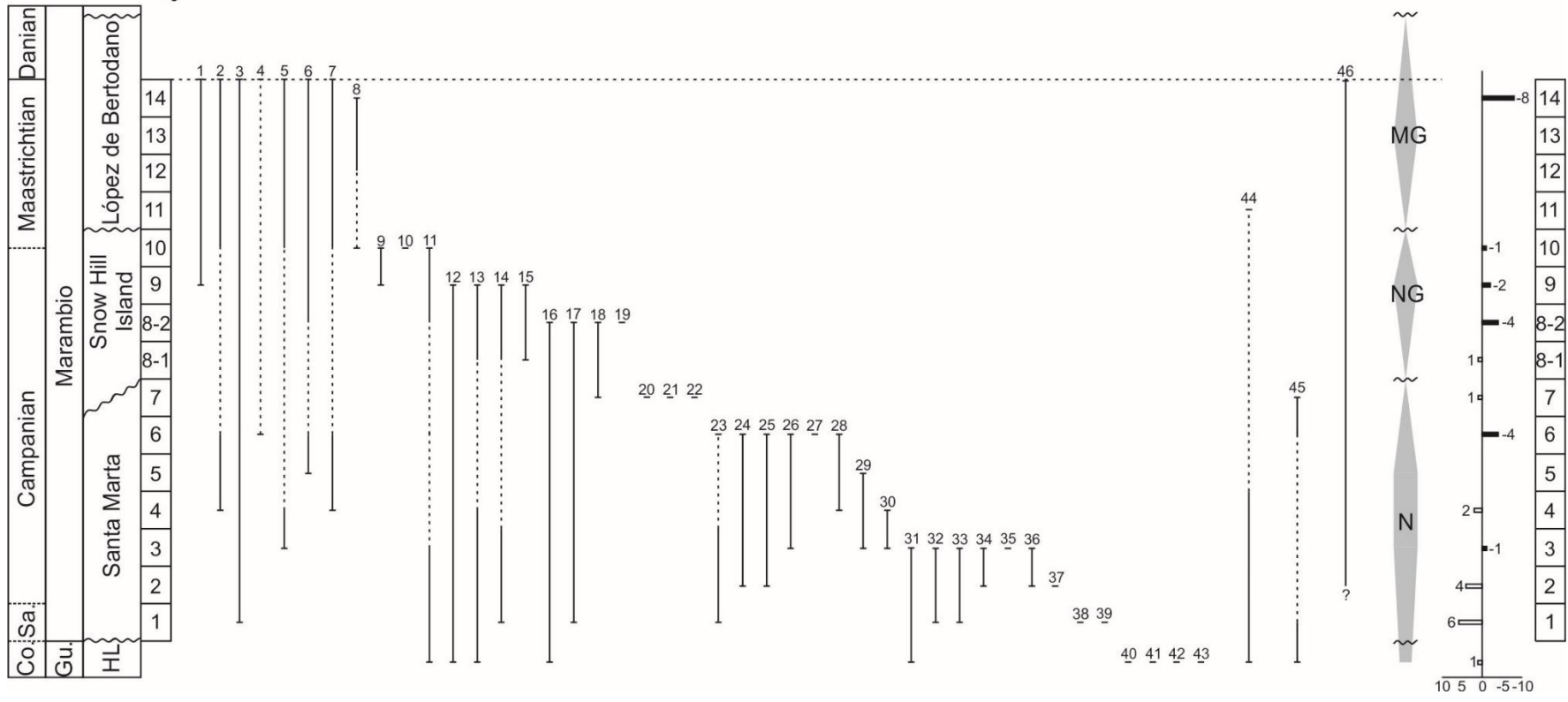
Figure 3.9 (previous page): Stratigraphic distribution and faunal turnover of taxa present in the Late Cretaceous of the James Ross Basin plotted against lithostratigraphy (not to scale) and biostratigraphy (ammonite assemblages 1–14 taken from Olivero and Medina (2000) and Olivero (2012a,b)). Co. = Coniacian, Sa. = Santonian, Gu. = Gustav Group, HL = Hidden Lake Formation. A = composite range chart of taxa. Solid lines correspond to range through data; dashed lines indicate where taxon is not recorded in two or more ammonite assemblages, i.e. temporarily absent from the basin. Horizontal tick marks correspond to the first and last appearances. Numbered ranges correspond to taxa as follows: 1–43 = ammonite genera: 1 = *Diplomoceras*; 2 = *Maorites*; 3 = *Anagaudryceras*; 4 = *Zelandites*; 5 = *Kitchinites* (*Kitchinites*); 6 = *Pseudophyllites*; 7 = *Grossouvrites*; 8 = *Pachydiscus* (*Pachydiscus*); 9 = *Gunnarites*; 10 = *Jacobites*; 11 = *Tetragonites*; 12 = *Gaudryceras* (*Gaudryceras*); 13 = *Eupachydiscus*; 14 = *Anapachydiscus*; 15 = *Neograhamites*; 16 = *Baculites*; 17 = *Polyptychoceras*; 18 = *Astreptoceras*; 19 = *Phyllopachyceras*; 20 = *Neokossmaticeras*; 21 = *Metaplacenticeras*; 22 = *Hoplitoplacenticeras*; 23 = *Neophylloceras*; 24 = *Natalites*; 25 = *Ryugasella*; 26 = *Parasolenoceras*; 27 = *Karapadites*; 28 = *Oiphyllites*; 29 = *Hauriceras*; 30 = *Caledonites*; 31 = *Eubostrychoceras*; 32 = *Yezoites*; 33 = *Hoploscaphites*; 34 = *Ainoceras*; 35 = *Vertebrites*; 36 = *Damesites*; 37 = *Placenticeras*; 38 = *Scaphites*; 39 = *Scalarites*; 40 = *Kossmaticeras* (*Kossmaticeras*); 41 = *Menuites* (*Neopachydiscus*); 42 = *Perinoceras*; and 43 = *Pseudoxybeloceras*. All the first (FADs) and last appearance datums (LADs) plotted at the mid-point of corresponding ammonite assemblage, except for ammonite assemblage 14, where taxa 1–7 extend to the top of the assemblage (i.e. the K–Pg boundary). Genera ordered based on last appearance, data from Kennedy et al. (2007) and Olivero (2012a,b). 44 = dimitobelid belemnites; 45 = inoceramid bivalves; 46 = nautilids (*Eutrephoceras*). Data based on Doyle (1990), Crame et al. (1996), Crame and Luther (1997), Cichowolski et al. (2005), Olivero (2012b). B = Sedimentary cycles and relative sea-level changes identified by Olivero and Medina (2000) and Olivero (2012a,b) (N= Natalites; NG = *Neograhamites–Gunnarites*; MG = *Maorites–Grossouvrites*). C = Faunal diversification data based on ammonite genera 1–43 calculated based on difference between the number of FADs and LADs of ammonite genera in each ammonite assemblage.

These diversity declines and regional extinctions have been linked to a global cooling trend that began during the mid-Campanian (~77 Ma) and culminated around the Campanian–Maastrichtian boundary (Barrera and Savin, 1999; Friedrich et al., 2012; Linnert et al., 2014). It is therefore probable that the diversity decline at the top of the N sequence, which continued into the NG sequence, was at least partly driven by high latitude cooling during the Campanian–Maastrichtian transition (Crame et al., 1996; Olivero and Medina, 2000; Olivero, 2012a), recorded in Antarctica by both marine and terrestrial proxies (e.g. Ditchfield et al., 1994; Francis and Poole, 2002) and synonymous with the trend seen globally. Despite this, ammonites remain locally abundant and reasonably diverse in Antarctica close to the Campanian–Maastrichtian boundary when peak global cooling occurred, as shown by the occurrence of nine genera in the '*Gunnarites antarcticus* fauna' (ammonite assemblage 10) (Crame et al., 1999; Crame et al., 2004; Olivero, 2012a) stratigraphically below the base of the López de Bertodano Formation (Figure 3.9). However, diversity did not return to levels attained during the Campanian.

3.7.4 Maastrichtian faunal diversity and environmental change on Seymour Island

The low diversity in the species-level range data in the lowermost beds of the López de Bertodano Formation on Seymour Island (basal MG sequence of Olivero (2012a)) is striking (Figure 3.4 and Figure 3.7). Only *M. tuberculatus* and *D. cylindraceum* were found despite consistent high-resolution sampling. This diversity minimum is followed by a general increase starting around 500 m above the section base, up until a level ~50 m below the K–Pg boundary.

The main increase in diversity and species richness on Seymour Island appears to occur in several steps during the early–late Maastrichtian, encompassing magnetochrons 31R and 31N (Figure 3.4 and Figure 3.7; Husson et al., 2011; Voigt et al., 2012). This coincides with a global environmental perturbation commonly referred to as the 'Mid-Maastrichtian Event' (MME) (Barrera, 1994; MacLeod, 1994; Barrera and Savin, 1999; MacLeod and Huber, 2001; Voigt et al., 2012; Jung et al., 2013), an interval that saw a eustatic high stand (Hancock, 1993; Dubicka and Peryt, 2012; Haq,

2014) and changes in seawater temperatures and ocean circulation patterns (Thibault and Gardin, 2006; Friedrich et al., 2012; Jung et al., 2013). The sedimentology of the lower portion of the López de Bertodano Formation appears to accord with a eustatic sea level rise prior to the MME high stand (Olivero et al., 2007, 2008; Olivero, 2012a). In addition, palaeotemperature estimates derived from oxygen isotope analysis of molluscan shell material from the lower portion of the López de Bertodano Formation, and correlated to chron C31R, are suggestive of cool ocean temperatures (Figure 3.7; Barrera et al., 1987; Ditchfield et al., 1994; Dutton et al., 2007; Tobin et al., 2012). Abundance peaks of a particular species of dinoflagellate cyst, *Impletosphaeridium clavus* (Wrenn and Hart, 1988), during this interval may even represent the appearance of seasonal sea ice and a stratified water column (Bowman et al., 2013a,b). These same proxies show a warming trend through the middle portion of the sequence (400–600m) coincident with the most prominent diversity increase seen in the cephalopod fauna (Tobin et al., 2012; Bowman et al., 2013a) indicating climate warming, which accords with evidence for global warming during the MME (Figure 3.7; Thibault and Gardin, 2006; Friedrich et al., 2012; Jung et al., 2013).

Most studies of environmental changes during the MME focus on extinction and/or reduction in diversity of groups such as inoceramid bivalves (Macleod, 1994; Macleod et al., 1996) and rudist bivalve dominated tropical reefs (Johnson and Kauffman, 1996), but our data suggest that in Antarctica this event saw an increase in the diversity and abundance of ammonites. A similar mid-Maastrichtian radiation event has been noted for planktonic foraminifera (MacLeod and Huber, 2001). A radiation event for ammonites at this time has also been recorded in the northwest Pacific (Jagt-Yazykova, 2011, 2012) and diversity increases in Mexico (Ifrim et al., 2004; Ifrim et al., 2010) suggest a global event. Ammonites seemed to have flourished during the mid-Maastrichtian, just a few million years before their extinction.

In line with global temperature records (Li and Keller, 1998a; Barrera and Savin, 1999; Thibault and Gardin, 2006; Friedrich et al., 2012), temperature data from both marine and terrestrial proxies (Tobin et al., 2012; Bowman et

102

al., 2013a, 2014; Kemp et al., 2014) in the upper López de Bertodano Formation indicate a renewed period of cooling, before an apparent warming phase in the final two million years of the Maastrichtian (~830–980 m in composite section D5.251) (Figure 3.7) which terminates prior to the K–Pg boundary in a further phase of cooling (Bowman et al., 2013a). This warming phase appears to occur earlier in Antarctica than at lower latitudes, where it is mostly restricted to chron C29R. A eustatic sea level fall just prior to the K–Pg boundary in other regions (Hancock, 1993; Surlyk, 1997; Hallam and Wignall, 1999; Kominz et al., 2008; Haq, 2014) is not clearly manifest in Antarctica, although abundance peaks of the dinoflagellate cyst genus *Manumiella* in the upper portion of the López de Bertodano Formation may record regional water depth changes (Thorn et al., 2009).

Despite the oscillations in temperature and sea level, late Maastrichtian ammonite diversity in Antarctica remained stable (Figure 3.7). Shorter-term environmental changes may, however, be responsible for an intriguing feature in the late Maastrichtian interval on Seymour Island: notably the brief stratigraphic appearance of several ammonite species. Thus, *Pachydiscus* (*Pachydiscus*) *riccardi* occurs in large numbers between 780 and 830 m in our composite section and *Pachydiscus* (*Pachydiscus*) *ultimus* is abundant between 940 and 970 m. In addition, *Pachydiscus* (*Pachydiscus*) cf. '*ootacodensis*' and *Z. varuna* are restricted to short intervals in the middle portion of C31N and directly beneath the K–Pg boundary respectively (Figure 3.4) (Macellari, 1986; Zinsmeister, 2001).

The pachydiscid occurrences could be related to brief warming pulses; the appearance of *Pachydiscus* (*Pachydiscus*) *riccardi* coincides with the onset of climate warming recorded in the upper López de Bertodano Formation (Tobin et al., 2012; Bowman et al., 2013a), whilst *Pachydiscus* (*Pachydiscus*) *ultimus* appears in an interval where Tobin et al. (2012) record their most negative oxygen isotope values from macrofossil shell material, and therefore highest seawater temperatures (Figure 3.7). This warming interval in chron C29R is seen globally (e.g. Stott and Kennett, 1990; Li and Keller, 1998b; Wilf et al., 2003; Thibault et al., 2010; Tobin et al., 2012) and is often linked to the onset

of the main eruptive phase of the Deccan Traps (Olsson et al., 2001; Chenet et al., 2009; Courtillot and Fluteau, 2010; Thibault and Gardin, 2010). *Pachydiscus* (*Pachydiscus*) cf. '*ootacodensis*' is probably closely related to taxa recorded from the Campanian–Maastrichtian of the Pacific northwest (Usher, 1952; Jones, 1963) and its appearance on Seymour Island within chron C31N appears to coincide with evidence from lower latitudes of changes in microfossil faunas and floras, perhaps linked to ocean circulation and/or climatic changes that promoted biotic exchanges between the Indo-Pacific/Tethyan and Austral regions (e.g. Thibault et al., 2010).

In terms of the appearance of *Z. varuna* in the very latest Maastrichtian, taxa assigned to this species also appear just below the K–Pg boundary interval in the northwest Pacific (Jagt-Yazykova, 2011, 2012) and possibly the western Tethys (Ward and Kennedy, 1993), but the significance of these simultaneous occurrences and possible links to environmental change is unclear. A brief period of global cooling is recorded worldwide immediately prior to the K–Pg boundary following the global warming event in chron C29R (Li and Keller, 1998a, b; Wilf et al., 2003) which we suggest could have influenced the distribution pattern of this wide-ranging taxon, considered a cool water specialist (e.g. Ifrim et al., 2004).

3.7.5 Comparison to patterns seen in other faunal groups

The new ammonite diversity data and comparisons with evidence for established Maastrichtian environmental changes show intriguing similarities with patterns exhibited by other faunal groups during the Maastrichtian, which suggest a common cause. Calcareous nannofossil assemblages in the Southern Ocean during the Campanian are largely composed of cosmopolitan taxa with a low degree of endemism (Huber and Watkins, 1992). This pattern changes during the Campanian–Maastrichtian transition with the rise of a distinct Austral Province composed of primarily endemic taxa (Huber and Watkins, 1992), which appears to mirror the rise of the distinctly Austral kossmaticeratid dominated ammonite fauna during the same time interval. This pattern is reversed during the Maastrichtian with a return to assemblages containing mostly cosmopolitan taxa (Huber and Watkins, 1992), perhaps

indicating a response to climate amelioration. Despite this, both nannofossil and planktonic foraminifera exhibit a series of pole- and equator-ward migrations throughout the Maastrichtian, linked to the climate changes described above (Huber and Watkins, 1992; MacLeod and Huber, 2001; Thibault and Gardin, 2006, 2010). Despite these fluctuations, diversity in both groups remains high during the latest Maastrichtian, before a sudden and catastrophic extinction event at the K–Pg boundary (e.g. Arenillas et al., 2000; Bown, 2005).

3.8 Conclusions

New high resolution sampling and stratigraphic range data of ammonoid and nautiloid cephalopods from the highly expanded Maastrichtian López de Bertodano Formation on Seymour Island, Antarctica allow a detailed examination of diversity changes in the few million years before the K–Pg extinction event. Comparison of this data with newly developed age models has also allowed us to place this unique high latitude record in a global context for the first time.

In summary;

1. We confirm that a sudden extinction of ammonites at the K–Pg boundary in Antarctica was coincident with extinctions seen in other macrofossil and microfossil groups. In total seven ammonite species belonging to seven genera range to the final few metres below the boundary, with only a single genus disappearing prior to this in the late Maastrichtian.

2. On Seymour Island there is no evidence for a significant reduction in the diversity of the ammonite fauna prior to a sudden mass extinction at the K–Pg boundary, despite evidence for dynamic environmental fluctuations during this interval. These data from the high southern latitudes are in accordance with those from well-studied lower latitude sections in the Tethyan and Boreal regions, and indicate no evidence of

elevated extinction rates for ammonites globally prior to the sudden K–Pg mass extinction event.

3. On a longer time-scale, ammonite diversity in the James Ross Basin during the Late Cretaceous was controlled by a combination of sea level and temperature change. During the Santonian–early Campanian sea level appears to have been the dominant control, but during the late Campanian–Maastrichtian, data from the Snow Hill Island and López de Bertodano Formations indicate a long-term global cooling trend which began during the Campanian and reached its peak across the Campanian–Maastrichtian boundary, appears to have led to the exclusion of a large number of common cosmopolitan ammonite genera from the James Ross Basin. This faunal change was coincident with the rise to dominance of endemic Austral ammonite taxa, and regional extinction events and temporary disappearances recorded by other molluscan groups such as inoceramid bivalves and belemnites.

4. Ammonites appear to have suffered a crisis in the early Maastrichtian of the James Ross Basin, with a low diversity assemblage in the basal López de Bertodano Formation on Seymour Island comprising just two species, and coincident with evidence for both shallow waters and low temperatures. Diversity increased during the mid-Maastrichtian, a period of climatic warming and sea level rise, which correlates with evidence from lower latitudes for a distinct 'Mid-Maastrichtian Event' at this time. Despite its apparent global nature, the effect of this event appears to vary according to taxonomic group, whereas some (inoceramid and rudist bivalves) suffer extinction, others such as ammonites and planktonic foraminifera appear to radiate and diversify. In Antarctica this event coincides with an influx of cosmopolitan ammonite taxa and proliferation of endemic kossmaticeratids.

5. Short term environmental changes during the late Maastrichtian (chrons C31N–29R) may be responsible for the brief stratigraphic appearances

of a number of ammonite species in the Seymour Island succession prior to the K–Pg extinction event. These fluctuations show intriguing similarities with short-term changes recorded globally by microfossil groups such as calcareous nannofossil and planktonic foraminifera during the Campanian–Maastrichtian, suggesting a common cause — most likely dynamic short-term climate changes which allowed biotic exchange between low and high latitude assemblages. These oscillations do not appear to have had a deleterious effect on the overall diversity of ammonite faunas prior to the K–Pg extinction event.

3.9 Identification and taxonomy of Antarctic Maastrichtian Cephalopoda

3.9.1 Stratigraphic notes

For the 1999 field season each individual specimen received its own unique code number (e.g. DJ.953.100). The first portion of the code refers to the section line itself, whilst the second is a numerical code unique to the individual specimen.

For the 2006 field season sample numbers refer to location and fossil sample number. E.g. D5.1132.2 refers to sample 2 from site D5.1132. Each fossil has a unique number and GPS location record.

Reference is also made to specimens collected by earlier workers from Seymour Island (e.g. Macellari, 1986; Zinsmeister, 2001), currently housed at the Paleontological Research Institute (PRI), Ithaca, NY, USA. Each sample in the PRI database is assigned a unique catalogue number (e.g. 60882). Images of these specimens and associated notes are available online via the PRI Collections Database — www.pricollectionsdatabase.org.

For tabulated raw field data for each section line, reference should be made to Appendix B.

3.9.2 Systematic notes

Order AMMONOIDEA von Zittel, 1884

Suborder LYTOCERATINA Hyatt, 1900

Superfamily TETRAGONITOIDEA Hyatt, 1900

Family GAUDRYCERATIDAE Spath, 1927

Genus ANAGAUDRYCERAS Shimizu, 1934

*Anagaudryceras seymouriens*e Macellari, 1986

Figure 3.5A

Material: 14 specimens

Despite varying degrees of preservation, all specimens in the present study compare favourably with previous descriptions of the genus (e.g. Howarth, 1965; Kennedy and Klinger, 1979; Hoffman, 2010), and specimens assigned to the species *Anagaudryceras seymouriense* from Antarctica by Macellari (1986) (e.g. PRI# 58197, 58222, 60882, 58052, and 58743) and from the NW Pacific by Maeda et al. (2005). A number of internal moulds show ontogenetic change typical for this genus from small evolute juveniles with a depressed whorl section to larger, more involute adults with a slightly more compressed whorl outline. Evolute juveniles show gaudryceratid ornament of very fine ribbing on the flanks, which changes to smoother ornamentation comprising fine flexuous lirae and occasional fold-like ribs or undulations in larger (D N 65 mm) sub-adult and adult examples. Constrictions are apparent on juvenile examples but disappear on specimens greater than ~130mm in diameter (Macellari, 1986). Rare fragments of very large individuals (D N 200mm) containing well-preserved septal lobes and sutures are found associated with glauconite sandstone horizons in the upper López de Bertodano Formation (Zinsmeister, 2001) (e.g. DJ.952.1, DJ.952.335, DJ.952.423,). This species is found throughout the mid-upper (~650–1003 m in our sections) Maastrichtian on Seymour Island, with the stratigraphically highest recorded occurrence a number of external moulds of small evolute examples found in a 5 m interval below the K–Pg boundary (DJ.953.689).

Genus ZELANDITES Marshall, 1926

Zelandites varuna (Forbes, 1846a)

Figure 3.5B

Material: 2 specimens

These two specimens include one poorly preserved internal mould and cast embedded in well-cemented glauconitic sandstone layer, and one well-preserved internal mould retaining phragmocone and portion of body chamber as well as external ornament. Although both appear to be juveniles, they are very similar to those collected by previous workers (e.g. PRI# 61169) and described by Macellari (1986). *Zelandites varuna* is characterised by a compressed whorl section (Wb/Wh ratio of ~0.7 (DJ.953.684)) with a narrow umbilicus and an initially evolute shell, becomes more involute through ontogeny. This species generally shows weak ornament consisting of very fine growth lines or lirae and occasional prominent constrictions on the flanks — although these are absent in our specimens, perhaps because this feature is only present in larger examples, as noted by Macellari (1986) (e.g. PRI# 61262). All examples of this species found on Seymour Island appear to be from a short stratigraphic interval immediately below the K–Pg boundary (see also Zinsmeister (2001)). Salazar et al. (2010) suggested that specimens from Antarctica described by Macellari (1986) as *Z. varuna* differ from other examples of the species in terms of whorl breadth and whorl height (Wb/Wh) as well as changes during ontogeny. However, it appears that this conclusion is based on an erroneous plot of data from Macellari (1986) who presented shell measurements in cm rather than mm (compare Macellari, 1986 — Table 2, p. 16 with Salazar et al., 2010 — Fig. 12. p. 197). Correcting this and comparing measurements of the best preserved of our samples (DJ.953.684) with those compiled by Salazar et al. (2010), indicates that the Antarctic material sits comfortably within the ontogenetic growth curve expected for *Z. varuna* and should therefore remain assigned to this species.

Family TETRAGONITIDAE Hyatt, 1900

Subfamily TETRAGONITINAE Hyatt, 1900

Genus PSEUDOPHYLLITES Kossmat, 1895

Pseudophyllites cf. *loryi* (Kilian and Reboul, 1909)

Figure 3.5C

Material: 14 specimens

Many of these specimens are rather small and poorly preserved examples
commonly found embedded within well-cemented glauconite-rich sandstone
layers in the mid-upper (700–830 m) portion of the López de Bertodano
Formation hence why they are left in open nomenclature. Nonetheless, a
number of these specimens contain identifiable sutures (e.g. D5.1164.2;
DJ.957.529) and morphological features which compare favourably with
material described from the James Ross Basin by previous workers as
Pseudophyllites loryi and its synonyms such as *Pseudophyllites peregrinus*
(e.g. Spath, 1953; Macellari, 1986) (PRI# 58284, 58728, 60434, 58193).
Several large (>100 mm) but deformed internal moulds with the suture visible
were found in the basal portion (330–350 m) of the López de Bertodano
Formation (D5.855.2, D5.875.2). *P. loryi* is separated from other species of
Pseudophyllites by its evenly rounded whorl section, broader venter, and
vertical rather than inclined umbilical wall. At least one of our specimens
(DJ.957.189) also preserves evidence of extremely fine ribbing/lirae as noted
by Macellari (1986). Differentiation between the various species of
Pseudophyllites present in the Late Cretaceous is challenging and many have
passed into synonymy. Generally speaking three species are recognised:
Pseudophyllites indra (Forbes, 1846a), which ranges from the Santonian to
the latest Maastrichtian and has a virtually pandemic distribution (Kennedy
and Klinger, 1977; Kennedy and Summesberger, 1986; Ward and Kennedy,
1993; Kennedy and Hancock, 1993), *P. loryi* (Kilian and Reboul, 1909) and its
junior synonyms *Pseudophyllites latus*, *Pseudophyllites whangaroaensis*
(Marshall, 1926), *Pseudophyllies peregrinus* (Spath, 1953) and
Pseudophyllites skoui (Birkelund, 1965), which range from the Santonian–
Campanian to the latest Maastrichtian of Antarctica, New Zealand, Australia,
and Greenland, and finally *Pseudophyllites teres* (van Hoepen, 1920), known
only from the Santonian-Campanian of South Africa and Madagascar
(Kennedy and Klinger, 1977). *P. loryi* is clearly quite a rare taxon on Seymour

Island, which coupled with the generally small size of the majority of our specimens perhaps indicates why our records do not match those of Zinsmeister (1998) in terms of the highest stratigraphic occurrence of this genus in Antarctica.

Suborder AMMONITINA Hyatt, 1889

Superfamily DESMOCERATACEAE von Zittel, 1895

Family DESMOCERATOIDEA von Zittel, 1895

Subfamily PUZOSIINAE Spath, 1922

Genus KITCHINITES Spath, 1922

Kitchinites sp.

Figure 3.6E

Material: 53 specimens

This species is a common component of the ammonite fauna throughout the middle portion of the López de Bertodano Formation, occurring between 525 and 673 m in our composite section. Specimens generally show a relatively compressed whorl section (Wb/Wh ratio of 0.6), prominent prorsiradiate to rectiradiate constrictions on an otherwise smooth umbilical wall which become strongly projected forwards as they cross the venter, and coarse forwardly projected ribbing on the ventral margin. This species was previously described as *Kitchinites darwini* by Del Valle and Rinaldi (1976) and Macellari (1986), based on comparison with material from the Quiriquina Formation in Chile by Steinmann (1895) and subsequently Stinnesbeck (1986). Salazar et al. (2010) suggested separation of the Antarctic material from *K. darwini*, based on new collections from Quiriquina which showed differences in shell thickness and whorl outline; although it is clear that Maastrichtian examples of the genus from Chile and Antarctica are closely related. A comprehensive redescription of this species is beyond the scope of the present study so following Salazar et al. (2010) we prefer to leave our material as *Kitchinites* sp.

Kitchinites laurae Macellari, 1986

Figure 3.5F

Material: 13 specimens

Although many of our specimens are fragmentary or rather poorly preserved, this taxon shows a number of morphological features which allow clear differentiation from *Kitchinites* sp. (compare PRI# 58669 (*Kitchinites* sp.) and PRI# 58309 (*Kitchinites laurae*)). It typically exhibits a more inflated whorl section (Wb/Wh ratio of 0.7), much wider venter, more subdued constrictions, and the presence of fine prorsiradiate ribbing on the upper flanks which becomes subdued across the ventral margin. It appears to be rare in the upper Maastrichtian on Seymour Island, occurring sporadically between 679 and 987 m in our sections, and was previously recorded from a stratigraphic interval directly beneath the K–Pg boundary (e.g. Zinsmeister, 1998).

Family KOSSMATICERATIDAE Spath, 1922

Subfamily KOSSMATICERATINAE Spath, 1922

Genus MAORITES Marshall, 1926

Maorites densicostatus (Kilian and Reboul, 1909)

Figure 3.6B

Material: 194 specimens

A full description of this species and its various synonyms is provided by Macellari (1986) and Macellari (1988). Typically for the genus, *Maorites densicostatus* appears to exhibit a large degree of morphological variation, but is easily separated from other species of the genus. Specimens from Seymour Island were separated into three morphotypes by Macellari (1986), α, β, and γ, based mainly on patterns of external shell ornament such as ribbing density and number of constrictions. The stratigraphic ranges of these morphotypes appear to overlap, so for our purposes we refer to them as a single species which occurs between 730 and 1006 m in the composite section. As hypothesised by Macellari (1986), we suggest that these morphotypes may relate to sexual dimorphism; certainly there are places in the upper

Maastrichtian portion of the López de Bertodano Formation on Seymour Island where adult specimens of *M. densicostatus* exhibit a wide range of different sizes and external ornament at the same stratigraphic horizon. All morphotypes of this species are characterised by an involute shell, compressed whorl section (typical Wb/Wh ratio of ~0.45–0.57), and the presence of fine ribbing and constrictions in both adult and juvenile examples, often forming small nodes when several ribs meet at the umbilical margin. Morphotype α (e.g. DJ.952.144) typically shows 10–12 ribs in 1 cm at a whorl height of 3 cm, whereas morphotypes β (e.g. DJ.952.252) is characterised by 12–14 ribs, and γ typically only shows 6–7 ribs per 1 cm at an equivalent whorl height. *M. densicostatus* shows potential as a good stratigraphic marker for the upper Maastrichtian in the Southern Hemisphere, with occurrences in Australia (Henderson and McNamara, 1985), South America (Macellari, 1988; Olivero et al., 2009), South Africa (Kennedy and Klinger, 1985), and New Zealand (Henderson, 1970). Small specimens are also present in the Sandwich Bluff Member of the López de Bertodano Formation on Vega Island, and indicate at least a portion of this deposit to be of late Maastrichtian age (Pirrie et al, 1991).

Maorites seymourianus (Kilian and Reboul, 1909)

Figure 3.6D

Material: 70 specimens

This species can easily be separated from *M. densicostatus* due to its wider umbilicus and thus more evolute shell, coarser ribbing in adult specimens (5–10 ribs in 1 cm at a whorl height of 3 cm), and more rounded whorl section (typical Wb/Wh ratio of 0.6–0.72). Separation from *M. tuberculatus* is mainly possible based on the absence of prominent umbilical tubercules, and straighter and less numerous constrictions. Changes between the three species of *Maorites* present in the López de Bertodano Formation appear to occur over narrow stratigraphic intervals, with little evidence of transitional forms present. As noted by Macellari (1986) however, specimens of *Maorites seymourianus* appear to exhibit a wide range of variation with regard to key morphological features such as shell ornament and size of adult specimens

which like *M. densicostatus*, may be related to sexual dimorphism. This species is very common throughout the middle portion of the López de Bertodano Formation between 440 and 719m in the composite section.

Maorites tuberculatus Howarth, 1958

Figure 3.6C

Material: 17 specimens

All our specimens compare favourably with the descriptions by Howarth (1958) and Macellari (1986) (e.g. PRI# 58278). Examples of *Maorites tuberculatus* are generally small, with rounded flanks and exhibit somewhat tighter coiling of the shell than is seen in *Maorites seymourianus* or *Maorites densicostatus*. The combination of prominent and numerous umbilical tubercles (up to 16 per whorl), numerous and flexuous constrictions (up to 9 per whorl), and fine ribbing also allow differentiation from other kossmaticeratids present on Seymour Island. This species was previously reported from the interval directly above the unconformable contact between the Haslum Crag Member of the Snow Hill Island Formation and the basal López de Bertodano Formation (Olivero et al, 2007, 2008; Olivero, 2012a) where it is the marker species for the base of the MG stratigraphic sequence and ammonite assemblage 11 of Olivero (2012a), but first appears in the composite section of the present study 235 m above this level.

Maorites cf. *weddelliensis* Macellari, 1986

Figure 3.6A

Material: 6 specimens

This species first identified by Macellari (1986) is separated from other examples of *Maorites* on Seymour Island based on the presence of coarse ribbing in both juvenile and adult examples, flat flanks, an evenly rounded venter, prominent tubercules on the umbilical margin, and incised constrictions with a thick adapical border. We tentatively assign several specimens which compare favourably with those presented by Macellari (1986) (e.g. PRI# 58731) to this species, but note that many of the features used to separate

this from other species also assigned to *Maorites* in the López de Bertodano Formation appear to vary among individual specimens.

Genus: GROSSOUVRITES Kilian and Reboul, 1909

Grossouvrites joharae Salazar et al., 2010

Figure 3.5E

Material: 100 specimens

This distinctive taxon is abundant through most of the López de Bertodano Formation on Seymour Island and is easily separated from other species of kossmaticeratid. It exhibits a compressed whorl outline (typical Wb/Wh ratio of 0.8), with vertical almost flat flanks ornamented by thick radial ribs, which arise in either pairs or threes from prominent tubercules at the umbilical margin. Juvenile specimens can also show constrictions. Several large and complete adult specimens containing the aperture are found among our samples (DJ.952.24, DJ.952.336, DJ.952.757, DJ.952.707, D5.1176.2 (×3)). Specimens assigned to *Grossouvrites* are widely distributed in the Late Cretaceous of the Southern Hemisphere with records from the Campanian–Maastrichtian of Antarctica (Macellari, 1986; Olivero, 1992; Olivero, 2012a,b), South America (Macellari, 1988; Salazar et al, 2010), New Zealand (Marshall, 1926; Henderson, 1970) and Australia (Henderson and McNamara, 1985; McNamara et al, 1988), the majority of which have traditionally been assigned to the type species *Grossouvrites gemmatus* (Hupé, 1854). However, differences in shell outline and ornament as well as changes throughout ontogeny have led some authors to suggest several of these may represent distinct species (e.g. Macellari, 1988; Salazar et al, 2010). In their restudy of material from Quiriquina, Chile, Salazar et al. (2010) split *Grossouvrites* into two distinct species; *G. gemmatus* and *Grossouvrites joharae*, in the latter of which they included material described from Antarctica by Macellari (1986) and earlier authors (Kilian and Reboul, 1909; Howarth, 1958). Macellari (1986) claimed that specimens of *Grossouvrites* in the mid portion of the sequence on Seymour Island were characterised by flatter flanks and a more compressed whorl section than those found stratigraphically higher, but did not consider

this grounds for separation into two species. Several of our specimens are crushed which can lead to difficulty in accurately ascertaining the range of variation in whorl outline. We follow Salazar et al. (2010) in identifying the Antarctic material as *G. joharae*. Previous authors have recorded this taxon (as *G. gemmatus*) from the interval directly beneath the K–Pg boundary (Zinsmeister, 1998).

Family PACHYDISCIDAE Spath, 1922

Genus PACHYDISCUS von Zittel, 1895

Pachydiscus (*Pachydiscus*) *ultimus* Macellari, 1986

Figure 3.6F

Material: 29 specimens

This large pachydiscid is easily identified by its very involute shell, compressed whorl outline with flanks sloping gently from maximum width near the umbilicus, sparse ornament consisting of prominent forwardly projecting umbilical ribs and finer ribs across the venter which disappears towards mid-flank. Like other pachydiscids in the López de Bertodano Formation, it exhibits a rather restricted stratigraphic range; with large adult examples appearing suddenly some 62 m below the K–Pg boundary and persisting for only ~30 m before disappearing. There is no evidence that this or any other pachydiscid reaches the K–Pg boundary in any of our section lines.

Pachydiscus (*Pachydiscus*) *riccardi* Macellari, 1986

Figure 3.6G

Material: 19 specimens

As noted by Macellari (1986), this species can be differentiated from *Pachydiscus* (*Pachydiscus*) *ultimus* by its more inflated whorl section, the presence of rectiradiate nodes on the umbilicus, and radial ribbing which is conspicuous across the whole flank in juvenile specimens, but absent in adults. Like *Pachydiscus* (*Pachydiscus*) *ultimus* the suture is complex and typical for the genus. *Pachydiscus* (*Pachydiscus*) *riccardi* is abundant for a

short (25 m) stratigraphic interval in the upper López de Bertodano Formation. Poorly preserved pachydiscids from the Haumurian (Campanian–Maastrichtian) of the Chatham Islands, New Zealand have also been tentatively assigned to this species (Consoli and Stilwell, 2005), which is otherwise only found in the López de Bertodano Formation on Seymour Island.

Pachydiscus (*Pachydiscus*) cf. '*ootacodensis*' (Stoliczka, 1865)

Material: 1 specimen

This specimen is a poorly preserved section of phragmocone with some shell material revealing external ornament, showing coarse radial ribbing on the ventral flank, an inflated whorl section, and overall morphology typical of many pachydiscids (compare Kennedy and Klinger, 2006). The suture is not preserved. Similar specimens from Seymour Island were described by Macellari (1986) as *Pachydiscus* (*Pachydiscus*) *ootacodensis*, a species from the Pacific Northwest of the USA and Canada (Usher, 1952; Jones, 1963) where it is found in deposits of late Campanian–early Maastrichtian age (Mustard, 1994; Shigeta et al., 2010). No systematic revision of pachydiscids from these deposits has been undertaken since the work of Jones (1963), and this single sample from Antarctica is too poorly preserved to allow for a precise identification. *Pachydiscus* (*Pachydiscus*) *ootacodensis* has been used by previous authors to define a distinct biozone within the López de Bertodano Formation (Macellari, 1986; Olivero and Medina, 2000; Olivero, 2012a), but as noted by Crame et al. (2004) and confirmed by the recovery of a single specimen in the present study, it is too rare on Seymour Island for this purpose.

Suborder ANCYLOCERATINA Wiedmann, 1966

Superfamily TURRILITOIDEA Gill, 1871

Family DIPLOMOCERATIDAE Spath, 1926

Subfamily DIPLOMOCERATINAE Spath, 1926

Genus DIPLOMOCERAS Hyatt, 1900

*Diplomoceras cylindrac*eum (Defrance, 1816)

Figure 3.5G

Material: 44 specimens

Specimens of this very large heteromorph are present throughout the López de Bertodano Formation, and include some of the most complete examples of the genus found anywhere in the world (e.g. Zinsmeister and Oleinik, 1995). The genus is characterised by a circular whorl section, uniform ribbing, distinctive suture, and development of 'paper clip-like' morphology. Species-level taxonomy has provoked some debate (Olivero and Zinsmeister, 1989; Kennedy and Henderson, 1992b; Klinger and Kennedy, 2003; Machalski, 2012). Olivero and Zinsmeister (1989) assigned large specimens from the upper Maastrichtian (upper López de Bertodano Formation) of Antarctica to *Diplomoceras maximum* based mainly on changes in ribbing during ontogeny. Machalski (2012) noted that large specimens from the upper Maastrichtian of Europe also appear to conform to *D. maximum*. However, differentiation of *D. maximum* from *Diplomoceras cylindraceum* and its synonyms (e.g. *Diplomoceras lambi*) appears problematic, as pointed out by Kennedy and Henderson (1992b), because specimens are extremely prone to post-mortem crushing. Here we follow Klinger and Kennedy (2003) and others in considering *Diplomoceras* monospecific, with *D. cylindraceum* the single, often rather variable species. This species exhibits a pandemic distribution throughout the latest Campanian–Maastrichtian, and in common with lower latitudes first appears in Antarctica in the late Campanian Sanctuary Cliffs Member of the Snow Hill Island Formation (Pirrie et al., 1997; Olivero, 2012a), remaining a common component of the ammonite fauna until directly beneath the K–Pg boundary (e.g. Landman et al., 2007).

Order NAUTILOIDEA de Blainville, 1825

Family NAUTILIDAE de Blainville, 1825

Genus EUTREPHOCERAS Hyatt, 1894

Eutrephoceras dorbignyanum (Forbes in Darwin, 1846)

Figure 3.5D

Material: 16 specimens

The taxonomy of Southern Hemisphere Late Cretaceous nautiloids has recently been reviewed (Cichowolski et al., 2005; Nielsen and Salazar, 2011). Specimens from the Maastrichtian of Antarctica and southern South America were united under the name *Eutrephoceras dorbignyanum*. All our specimens match the earlier descriptions, and are characterised by a globular shell, inflated whorl section, tiny umbilicus and extremely fine ornament most often seen in juvenile specimens. A number of large incomplete adult specimens are included in the BAS collections, often showing rather flattened flanks and fine growth lines. On Seymour Island *E. dorbignyanum* first appears in the middle of the López de Bertodano Formation, and remains an occasional component of the molluscan fauna until a final occurrence directly beneath the K–Pg boundary.

3.10 References

Alegret, L., Thomas, E., Lohmann, K.C., 2011. End-Cretaceous marine mass extinction not caused by productivity collapse. *Proceedings of the National Academy of Science* **109**, 728–732.

Alvarez, L.W., Alvarez, W., Asaro, F., Michel, H.V., 1980. Extraterrestrial cause for the Cretaceous-Tertiary Extinction. *Science* **208**, 1095–1108.

Archibald, J.D., Clemens, W.A., Padian, K., Rowe, T., MacLeod, N., Barrett, P.M., Gale, A., Holroyd, P., Sues, H.-D., Arens, N.C., Horner, J.R., Wilson, G.P., Goodwin, M.B., Brochu, C.A., Lofgren, D.L., Hurlbert, S.H., Hartman, J.H., Eberth, D.A., Wignall, P.B., Currie, P.J., Weil, A., Prasad, G.V.R., Dingus, L., Courtillot, V., Milner, A., Milner, A., Bajpai, S., Ward, D.J., Sahni, A., 2010. Cretaceous extinctions: multiple causes. *Science* **328**, 973.

Arenillas, I., Arz, J.A.,Molina, E., Dupuis, E., 2000. An independent test of planktonic foraminiferal turnover across the Cretaceous/Paleogene (K/P) boundary at El Kef, Tunisia; catastrophic mass extinction and possible survivorship. *Micropaleontology* **46**, 31–49.

Arkhipkin, A.L., Laptikhovsky, V.V., 2012. Impact of ocean acidification on plankton larvae as a cause of mass extinctions in ammonites and belemnites. *Neues Jahrbuch für Geologie und Paläontologie (Abhandlung)* **266**, 39–50.

Askin, R.A., Jacobsen, S.R., 1996. Palynological change across the Cretaceous-Tertiary boundary on Seymour Island, Antarctica: environmental and depositional factors. In: MacLeod, N., Keller, G. (Eds.), *Cretaceous-Tertiary Mass Extinctions: Biotic and Environmental Changes*. W.W. Norton and Company, New York, pp. 7–25.

Barrera, E., 1994. Global environmental changes preceding the Cretaceous-Tertiary boundary: Early–late Maastrichtian transition. *Geology* **22**, 877–880.

Barrera, E., Savin, S.M., 1999. Evolution of late Campanian–Maastrichtian marine climates and oceans. In: *Barrera, E., Johnson, C.C. (Eds.), Evolution of the Cretaceous Ocean- Climate System*. Geological Society of America Special Paper **332**, pp. 245–282.

Barrera, E., Huber, B.T., Savin, S.M., Webb, P.-N., 1987. Antarctic marine temperatures: Late Campanian through Early Paleocene. *Paleoceanography* **2**, 21–47.

Batenburg, S.J., Gale, A.S., Sprovieri, M., Hilgen, F.J., Thibault, N., Boussaha, M., Orue-Etxebarria, X., 2014. An astronomical time scale for the Maastrichtian based on the Zumaia and Sopelana sections (Basque Country, northern Spain). *Journal of the Geological Society of London* **171**, 165–180.

Birkelund, T., 1965. Ammonites from the Upper Cretaceous of West Greenland. *Bulletin Grønland Geologiske Undersolgese* **56**, 192.

Birkelund, T., 1979. The last Maastrichtian ammonites. In: Birkelund, T., Bromley, R.G. (Eds.), *Cretaceous-Tertiary Boundary Events. I. The Maastrichtian and Danian of Denmark*. University of Copenhagen, Copenhagen, pp. 51–57.

Birkelund, T., 1993. Ammonites from the Maastrichtian White Chalk of Denmark. *Bulletin of the Geological Society of Denmark* **40**, 33–81.

Blainville, H.M.D., 1825. Manuel demalacology et de conchyliologie. *Levrault*, Paris (648 pp.).

Bowman, V.C., Francis, J.E., Riding, J.B., Hunter, S.J., Haywood, A.M., 2012. A latest Cretaceous to earliest Paleogene dinoflagellate cyst zonation from Antarctica, and implications for phytoprovincialism in the high southern latitudes. *Review of Palaeobotany and Palynology* **171**, 40–56.

Bowman, V.C., Francis, J.E., Riding, J.B., 2013a. Late Cretaceous winter sea-ice in Antarctica? *Geology* **41**, 1227–1230.

Bowman, V.C., Riding, J.B., Francis, J.E., Crame, J.A., Hannah, M.J., 2013b. The taxonomy and palaeobiogeography of small chorate dinoflagellate cysts from the Late Cretaceous to Quaternary of Antarctica. *Palynology* **37**, 151–169.

Bowman, V.C., Francis, J.E., Askin, R.A., Riding, J.B., Swindles, G.T., 2014. Latest Cretaceous–earliest Paleogene vegetation and climate change at the

high southern latitudes: palynological evidence from Seymour Island, Antarctic Peninsula. *Palaeogeography Palaeoclimatolology Palaeoecology* **408**, 26–47.

Bown, P., 2005. Selective calcareous nannoplankton survivorship at the Cretaceous-Tertiary boundary. *Geology* **33**, 653–656.

Brecher, H.H., Tope, R.W., 1988. Topographic map of Seymour Island. In: Feldmann, R.M., Woodburne,M.O. (Eds.), *Geology and Paleontology of Seymour Island, Antarctic Peninsula*. Geological Society of America, Memoirs **169**, pp. 17–20.

Casadío, S., Rodriguez, M.F., Reichler, V.A., Camacho, H.H., 1999. Tertiary nautiloids from Patagonia, southern Argentina. *Ameghiniana* **36**, 189–202.

Chenet, A.-L., Courtillot, V., Fluteau, F., Gérard, M., Quidelleur, X., Khadri, S.F.R., Subbarao, K.V., Thordarson, T., 2009. Determination of rapid Deccan eruptions across the Cretaceous-Tertiary boundary using paleomagnetic secular variation: 2. Constraints from analysis of eight new sections and synthesis for a 3500-m-thick composite section. *Journal of Geophysical Research* **114**, B06103. http://dx.doi.org/10.1029/2008JB005644.

Cichowolski, M., Ambrosio, A., Concheyro, A., 2005. Nautilids from the Upper Cretaceous of the James Ross Basin, Antarctic Peninsula. *Antarctic Science* **17**, 267–280.

Consoli, C.P., Stilwell, J.D., 2005. Late Cretaceous Cephalopoda (Mollusca) from the Takatika Grit, Chatham Islands, southwest Pacific. *New Zealand Journal of Geology and Geophysics* **48**, 389–393.

Courtillot, V., Fluteau, F., 2010. Cretaceous extinctions: the volcanic hypothesis. *Science* **328**, 973–974.

Crame, J.A., Luther, A., 1997. The last inoceramid bivalves in Antarctica. *Cretaceous Research* **18**, 179–195.

Crame, J.A., Pirrie, D., Riding, J.B., Thomsen, M.R.A., 1991. Campanian-Maastrichtian (Cretaceous) stratigraphy of the James Ross Island area, Antarctica. *Journal of the Geological Society of London.* **148**, 1125–1140.

Crame, J.A., Lomas, S.A., Pirrie, D., Luther, A., 1996. Late Cretaceous extinction patterns in Antarctica. *Journal of the Geological Society of London.* **153**, 503–506.

Crame, J.A., McArthur, J.M., Pirrie, D., Riding, J.B., 1999. Strontium isotope correlation of the basal Maastrichtian Stage in Antarctica to the European and US biostratigraphic schemes*. Journal of the Geological Society of London.* **156**, 957–964.

Crame, J.A., Francis, J.E., Cantrill, D.E., Pirrie, D., 2004. Maastrichtian stratigraphy of Antarctica. *Cretaceous Research* **25**, 411–423.

Crame, J.A., Pirrie, D., Riding, J.B., 2006. Mid-Cretaceous stratigraphy of the James Ross Basin, Antarctica. In: Francis, J.E., Pirrie, D., Crame, J.A. (Eds.), *Cretaceous–Tertiary High-Latitude Palaeoenvironments, James Ross Basin, Antarctica*, Special Publication vol. **258**. Geological Society, London, pp. 7–19.

Darwin, C., 1846. Geological Observations on South America. Smith, Elder & Co., London 279 pp.

D'Hondt, S., 2005. Consequences of the Cretaceous/Paleogene mass extinction for marine ecosystems. *Annual Reviw of Ecology, Evolution, and Systematics* **36**, 295–317.

Darragh, T.A., 1997. Gastropoda, Scaphopoda, Cephalopoda, and new Bivalvia of the Paleocene Pebble Point Formation, Victoria, Australia. *Proceedings of the Royal Society of Victoria* **109**, 57–108.

Defrance, M.J.L., 1816. . . passim, In: Defrance, M.J.L., De Blainville, H.M.L., Leach,W.E., et al. (Eds.), *Dictionnaire des sciences naturelles, dans lequel on traîte méthodiquement des différents êtres de la nature. Par plusieurs professeurs du Jardin du Roi, et des principales écoles de Paris*. Levrault, Strasbourg and Paris vol. 3 (492 pp. + 174 in suppl.; Plates — Zoologie, Conchyliologie et Malacologie, 1816–1830, 36 pp., 118 pls).

Del Valle, R., Rinaldi, A.C., 1976. Sobre la presencia de Kitchinites darwini (Steinmann) en el Cretacico Superior de la Isla Vicecomodoro Marambio, Antartida. *Contribution Instituto Antartico Argentina* **195**, 1–33.

Ditchfield, P.W., Marshall, J.D., Pirrie, D., 1994. High latitude Palaeotemperature variation: new data from the Tithonian to Eocene of James Ross Island, Antarctica. *Palaeogeography Palaeoclimatolology Palaeoecology* **107**, 79–101.

Doyle, P., 1990. New records of dimitobelid belemnites from the Cretaceous of James Ross Island, Antarctica. *Alcheringa* **14**, 159–175.

Doyle, P., Zinsmeister, W.J., 1988. The new dimitobelid belemnite from the Upper Cretaceous of Seymour Island, Antarctic Peninsula. In: Feldmann, R.M., Woodburne, M.O. (Eds.)*, Geology and Paleontology of Seymour Island, Antarctic Peninsula*. Geological Society of America, Memoirs **169**, pp. 285–290.

Dubicka, Z., Peryt, D., 2012. Latest Campanian and Maastrichtian palaeoenvironmental changes: implications from an epicontinental sea (SE Poland and western Ukraine). *Cretaceous Research* **37**, 272–284.

Dutton, A., Huber, B.T., Lohmann, K.C., Zinsmeister, W.J., 2007. High-resolution stable isotope profiles of a dimitobelid belemnite: implications for paleodepth habitat and late Maastrichtian climate seasonality. *Palaios* **22**, 642–650.

Elliot, D.H., Askin, R.A., Kyte, F.T., Zinsmeister, W.J., 1994. Iridium and dinocysts at the Cretaceous-Tertiary boundary on Seymour Island, Antarctica: implication for the K–T event. *Geology* **22**, 675–678.

Forbes, E., 1846a. Report on the Cretaceous fossil invertebrates from southern India, collected by Mr. Kaye and Mr. Cunliffe. *Transactions of the Geological Society of London* (Part 2) **7**, 97–174 (Plates 7–19).

Forbes, E., 1846b. Descriptions of secondary fossil shells from South America. In: Darwin, C. (Ed.), *Geological Observations on South America*. Smith, Elder & Co., London, pp. 265–268.

Francis, J.E., Poole, I., 2002. Cretaceous and early Tertiary climates of Antarctica: evidence from fossil wood. *Palaeogeography Palaeoclimatolology Palaeoecology* **182**, 47–64.

Friedrich, O., Norris, R.D., Erbacher, J., 2012. Evolution of middle to Late Cretaceous oceans—a 55 m.y. record of Earth's temperature and carbon cycle. *Geology* **40**, 107–110.

Gallagher, W.B., 1991. Selective extinction and survival across the Cretaceous/Tertiary boundary in the northern Atlantic Coastal Plain. *Geology* **19**, 967–970.

Gill, T., 1871. Arrangement of the families of the mollusks. *Smithsonian Miscellaneous Collections* **227** (xvi +49 pp.).

Goolaerts, S., Kennedy, W.J., Dupuis, C., Steurbaut, E., 2004. Terminal Maastrichtian ammonites from the Cretaceous–Paleogene Global Stratotype Section and Point, El Kef, Tunisia. *Cretaceous Research* **25**, 313–328.

Gradstein, F.M., Ogg, J.G., Schmitz, M.D., Ogg, G.M., 2012. The Geologic Time Scale 2012: Oxford. Elsevier, UK (1144 pp.).

Hallam, A., Wignall, P.B., 1999. Mass extinctions and sea-level changes. *Earth Science Reviews* **48**, 217–250.

Hancock, J.M., 1993. Transatlantic correlations in the Campanian-Maastrichtian stages by eustatic changes of sea-level. In: Hailwood, E.A., Kidd, R.B. (Eds.), *High Resolution Stratigraphy*. Geological Society, London, Special Publication **70**, pp. 241–256.

Hansen, T., Surlyk, F., 2014. Marine macrofossil communities in the uppermost Maastrichtian chalk of Stevns Klint, Denmark. *Palaeogeography Palaeoclimatolology Palaeoecology* **399**, 323–344.

Haq, B.U., 2014. Cretaceous eustasy revisited. *Global and Planetary Change* **113**, 44–58.

Hart, M.B., Feist, S.E., Håkansson, E., Heinberg, C., Price, G.D., Leng, M.J., Watkinson, M.P., 2005. The Cretaceous–Palaeogene boundary succession at Stevns Klint, Denmark: foraminifers and stable isotope stratigraphy. *Palaeogeography Palaeoclimatolology Palaeoecology* **224**, 6–26.

Hathway, B., 2000. Continental rift to back-arc basin: Jurassic–Cretaceous stratigraphical and structural evolution of the Larsen Basin, Antarctic Peninsula. *Journal of the Geological Society of London.* **157**, 417–432.

Henderson, R.A., 1970. Ammonoidea from the Mata Series (Santonian-Maastrichtian) of New Zealand. *Special Papers in Palaeontology* **6**, 1–82.

Henderson, R.A., McNamara, K.J., 1985. Maastrichtian non-heteromorph ammonites from the Miria Formation, Western Australia. *Palaeontology* **28**, 35–88.

Hoffman, R., 2010. New insights on the phylogeny of the Lytoceratoidea (Ammonitina) from the septal lobe and its functional interpretation. *Revue de Paléobiolgie* **29**, 1–156.

House, M.R., 1989. Ammonoid extinction events. *Philosophical Transactions of the Royal Society of London, Series B Biological Science* **1228**, 307–325.

Howarth, M.K., 1958. Upper Cretaceous and Jurassic ammonite faunas of Alexander Island and Graham Land*. Falkland Island Dependencies Survey, Scientific Report* **21**, pp. 1–16.

Howarth, M.K., 1965. Cretaceous ammonites and nautiloids from Angola. *Bulletin of the British Museum (Natural History) Geology* **10**, 337–412.

Howarth, M.K., 1966. Ammonites from the Upper Cretaceous of the James Ross Island Group. *British Antarctic Survey Bulletin* **10**, 55–69.

Hsü, K.J., McKenzie, J.A., 1985. A "Strangelove" ocean in the earliest Tertiary. In: Sunquist, E.T., Broecker, W.S. (Eds.), *The Carbon Cycle and Atmospheric CO_2: Natural Variations Archaean to Presen*t. American Geophysical Union, Washington D.C., pp. 487–492.

Huber, B.T., Watkins, D.K., 1992. Biogeography of Campanian–Maastrichtian calcareous plankton in the region of the Southern Ocean: palaeogeographic and palaeoclimatic implications. In: Kennett, J.P., Warnke, D.A. (Eds.), *The Antarctic Palaeoenvironment: A Perspective on Global Change*. AGU Antarctic Research Series **56**, pp. 31–60.

Hull, P.M., Norris, R.D., 2011. Diverse patterns of ocean export productivity change across the Cretaceous-Paleogene boundary: new insights frombiogenic barium. *Paleoceanography* **26**, 1–10.

Hupé, L.H., 1854. Zoologiá. In: Gay, C. (Ed.), *Historia fisica y politica de Chile* **8** (499 pp.).

Husson, D., Galbrun, B., Laskar, J., Hinnov, L.A., Thibault, N., Gardin, S., Locklair, R.E., 2011. Astronomical calibration of the Maastrichtian (Late Cretaceous). *Earth and Planetary Science Letters* **305**, 328–340.

Hyatt, A., 1889. Genesis of the Arietidae. *Smithsonian Contributions to Knowledge* **673**, pp. 1–238 (16 Plates).

Hyatt, A., 1894. Phylogeny of an acquired characteristic. *Proceedings of the American Philosophical Society* **41**, 349–647.

Hyatt, A., 1900. Cephalopoda. In: von Zittel, K.A. (Ed.), *Textbook of Palaeontology*. Macmillan, London and New York, pp. 502–604.

Ifrim, C., Stinnesbeck, W., López-Oliva, J.G., 2004. Maastrichtian cephalopods from Cerralvo, North-Eastern Mexico. *Palaeontology* **47**, 1575–1627.

Ifrim, C., Stinnesbeck, W., Rodríguez Garza, R., Flores Ventura, J., 2010. Hemipelagic cephalopods from the Maastrichtian (Late Cretaceous) Parras Basin at La Parra, Coahuila, Mexico, and their implications for the correlation of the lower Difunta Group. *Journal of South American Earth Science* **29**, 517–618.

Jagt, J.W.M., Goolaerts, S., Jagt-Yazykova, E.A., Cremers, G., Verhesen, W., 2006. First record of *Phylloptychoceras* (Ammonoidea) from the Maastrichtian type area, The Netherlands. *Bulletin de L'Institut Royal des Sciences Naturelles de Belgique, Sciences De La Terre* **76**, 97–103.

Jagt-Yazykova, E.A., 2011. Palaeobiogeographical and palaeobiological aspects of mid and Late Cretaceous ammonite evolution and bio-events in the Russian Pacific. *Scripta Geologica* **143**, 15–121.

Jagt-Yazykova, E.A., 2012. Ammonite faunal dynamics across bio-events during the mid- and Late Cretaceous along the Russian Pacific coast. *Acta Palaeontologica Polonica* **57**, 737–748.

Johnson, C.C., Kauffman, E.G., 1996. Maastrichtian extinction patterns of Carribean province rudistids. In: Macleod, N., Keller, G. (Eds.), *Cretaceous–TertiaryMass Extinctions: Biotic and Environmental Changes*. W.W. Norton, New York, pp. 231–273.

Jones, D.L., 1963. Upper Cretaceous (Campanian and Maestrichtian) ammonites from southern Alaska. *U.S. Geological Survey Professional Papers* **432**, 1–53.

Jung, C., Voigt, S., Friedrich, O., Koch, M.C., Frank, M., 2013. Campanian-Maastrichtian ocean circulation in the tropical Pacific*. Paleoceanography* **28**, 562–573. http://dx.doi.org/10.1002/palo.20051 .

Keller, G., Adatte, T., Tantawy, A.A., Berner, Z., Stinnesbeck, W., Steuben, D., Leanza, H.A., 2007. High stress late Maastrichtian–early Danian palaeoenvironments in the Neuquén Basin, Argentina. *Cretaceous Research* **28**, 939–960.

Keller, G., Adatte, T., Pardo, A., Bajpai, S., Khosla, A., Samant, B., 2010. Cretaceous extinctions: evidence overlooked. *Science* **328**, 974–975.

Kemp, D.B., Robinson, S.A., Crame, J.A., Francis, J.E., Ineson, J., Whittle, R.J., Bowman, V.C., O'Brien, C., 2014. A cool temperate climate on the Antarctic Peninsula through the latest Cretaceous to early Paleogene. *Geology* **42**, 583–586.

Kennedy, W.J., 1989. Thoughts on the evolution and extinction of Cretaceous ammonites. *Proceedings of the Geologists Association* **100**, 251–279.

Kennedy, W.J., Klinger, H.C., 1979. Cretaceous faunas from Zululand and Natal. South Africa. The ammonite family Gaudryceratidae. *Bulletin of the British Museum (Natural History) Geology* **31**, 121–174.

Kennedy, W.J., Henderson, R.A., 1992a. Non-heteromorph ammonites from the Upper Maastrichtian of Pondicherry, Southern India. *Palaeontology* **35**, 381–442.

Kennedy, W.J., Henderson, R.A., 1992b. Heteromorph ammonites from the Upper Maastrichtian of Pondicherry, Southern India. *Palaeontology* **35**, 693–781.

Kennedy, W.J., Klinger, H.C., 1977. Cretaceous faunas from Zululand, Natal, South Africa. The ammonite family Tetragonitidae Hyatt, 1900. *Annals of the South African Museum* **73**, 149–197.

Kennedy, W.J., Klinger, H.C., 1985. Cretaceous faunas from Zululand, Natal, South Africa. The ammonite family Kossmaticeratidae Spath, 1922. *Annals of the South African Museum* **95**, 165–231.

Kennedy, W.J., Klinger, H.C., 2006. Cretaceous faunas from Zululand and Natal, South Africa. The ammonite family Pachydiscidae Spath, 1922. *African Natural History* **2**, 17–166.

Kennedy, W.J., Summesberger, H., 1986. Lower Maastrichtian ammonites from Neuberg, Steirmark, Austria. Separatdruck von Beiträge zur Paläontologie von Österreich **12**, 181–242.

Kennedy, W.J., Landman, N.H., Christensen, W.K., Cobban, W.A., Hancock, J.M., 1998. Marine connections in North America during the late Maastrichtian: palaeogeographic and palaeobiogeographic significance of *Jeletzkytes nebrascensis* Zone cephalopod fauna from the Elk Butte member of the Pierre Shale, SE Dakota and NE Nebraska. *Cretaceous Research* **19**, 745–755.

Kennedy, W.J., Crame, J.A., Bengston, P., Thompson, M.R.A., 2007. Coniacian ammonites from the James Ross Island, Antarctica. *Cretaceous Research* **28**, 509–531.

Kilian, W., Reboul, P., 1909. Les Céphalopodes néocrétacés des Îles Seymour et Snow Hill. *Wissenschafliche Ergebnisse der Schweidschen Südpolar-Expedition 1901–1903, Stockholm* **3**, pp. 1–75.

Klinger, H.C., Kennedy, W.J., 2003. Observations on the systematics, geographic and stratigraphic distribution and origin of *Diplomoceras cylindraceum* (DeFrance, 1816) (Cephalopoda: Ammonoidea). *Annals of the South African Museum* **110**, 171–198.

Kominz, M.A., Browning, J.V., Miller, K.G., Sugarman, P.J., Misintseva, S., Scotese, C.R., 2008. Late Cretaceous to Miocene sea-level estimates from the New Jersey and Delaware coastal plain coreholes: an error analysis. *Basin Research* **20**, 211–226.

Korn, D., Klug, C., 2012. Paleozoic ammonoids— diversity and development of conch morphology. In: Talent, J.D. (Ed.), *Earth and Life*. Springer, Dordrecht, pp. 491–534.

Kossmat, F., 1895. Untersuchungen über die Südindische Kreideformation. Erster Theil. *Beiträge zur Paläontologie Österreich-Ungarns und des Orient* **9**, pp. 97–203 ((1–107) (Plates 15–25 (1–11))).

Kruta, I., Landman, N.H., Rouget, I., Cecca, F., Tafforeau, P., 2011. The role of ammonites in the Mesozoic marine food web revealed by jaw preservation. *Science* **331**, 70–72.

Landman, N.H., Tanabe, K., Shigeta, Y., 1996. Ammonoid embryonic development. In: Landman, N.H., Tanabe, K., Davis, R.A. (Eds.), *Ammonoid Paleobiology*. Topics in Geobiology **13**, pp. 607–707.

Landman, N.H., Johnson, R.O., Edwards, L.E., 2004a. Cephalopods from the Cretaceous/Tertiary boundary interval on the Atlantic coastal plain, with a description of the highest ammonite zones in North America. Part 1. Maryland and North Carolina. *American Museum Novitates* **3454**, 1–64.

Landman, N.H., Johnson, R.O., Edwards, L.E., 2004b. Cephalopods from the Cretaceous/Tertiary boundary interval on the Atlantic coastal plain, with a description of the highest ammonite zones in North America. Part 2. Northeastern Monmouth County, New Jersey. *Bulletins of the American Museum of Natural History* **287**, 1–107.

Landman, N.H., Johnson, R.O., Garb, M.P., Edwards, L.E., Kyte, F.T., 2007. Cephalopods from the Cretaceous/Tertiary boundary interval on the Atlantic coastal plain, with a description of the highest ammonite zones in North America. Part III. Manasquan River Basin, Monmouth County, New Jersey. *Bulletins of the American Museum of Natural History* **303**, 1–122.

Landman, N.H., Goolaerts, S., Jagt, J.W.M., Jagt-Yazykova, E.A., Machalski, M., Yacobucci, M.M., 2014. Ammonite extinction and nautilid survival at the end of the Cretaceous. *Geology* **42**, 707–710.

Lawver, L.A., Gahagan, L.M., Coffin, M.F., 1992. The development of paleoseaways around Antarctica. In: Kennett, J.P., Warnke, D.A. (Eds.), Antarctic Research Series **56**, pp. 7–30.

Li, L., Keller, G., 1998a. Maastrichtian climate, productivity and faunal turnovers in planktic foraminifera in South Atlantic DSDP Sites 525A and 21. *Marine Micropaleontology* **33**, 55–86.

Li, L., Keller, G., 1998b. Abrupt deep-sea warming at the end of the Cretaceous. *Geology* **26**, 995–998.

Linnert, C., Robinson, S.A., Lees, J.A., Bown, P.R., Pérez-Rodríguez, I., Falzoni, F., Littler, K., Arz, J.A., Russell, E.R., 2014. Evidence for global cooling in the Late Cretaceous. *Nature Communications* **5**. http://dx.doi.org/10.1038/ncomms5194 (Article number 4194).

Macellari, C.E., 1986. Late Campanian–Maastrichtian ammonite fauna from Seymour Island (Antarctic Peninsula). *Memoirs of the Paleontological Society* **18**, 1–55.

Macellari, C.E., 1988. Stratigraphy, sedimentology and paleoecology of Upper Cretaceous/Paleocene shelf-deltaic sediments of Seymour Island (Antarctic Peninsula). In: Feldmann, R.M., Woodburne, M.O. (Eds.), *Geology and Paleontology of Seymour Island, Antarctic Peninsula*. Geological Society of America, Memoirs **169**, pp. 25–53.

Machalski, M., 2005. The youngest Maastrichtian ammonite faunas from Poland and their dating by scaphitids. *Cretaceous Research* **26**, 813–836.

Machalski, M., 2012. Stratigraphically important ammonites from the Campanian-Maastrichtian boundary interval of the Middle Vistula River section, central Poland. *Acta Geologica Polonica* **62**, 91–116.

Machalski, M., Heinberg, C., 2005. Evidence for ammonite survival into the Danian (Paleogene) from the Cerithium Limestone at Stevns Klint, Denmark. *Bulletin of the Geological Society of Denmark* **52**, 97–111.

MacLeod, K.G., 1994. Bioturbation, inoceramid extinction, and mid-Maastrichtian ecological change. *Geology* **22**, 139–142.

MacLeod, K.G., Huber, B.T., 2001. The Maastrichtian record at Blake Nose (western North Atlantic) and implications for global palaeoceanographic and biotic changes. In: Kroon, D., Norris, R.D., Klaus, A. (Eds.), *Western North Atlantic Palaeogene and Cretaceous Palaeoceanography*. Geological Society, London, Special Publications **183**, pp. 111–130.

MacLeod, K.G., Huber, B.T., Ward, P.D., 1996. The biostratigraphy and paleobiogeography of Maastrichtian inoceramids. In: Ryder, G., Fastovsky, D., Gartner, S. (Eds.), *The Cretaceous-Tertiary Event and Other Catastrophes in Earth History*. Geological Society of America Special Paper **307**, pp. 361–373.

Maeda, H., Shigeta, Y., Fernando, A.G.S., Okada, H., 2005. Stratigraphy and fossil assemblages of the Upper Cretaceous system in the Makarov Area, Southern Sakhalin, Russian Far East. In: Shigeta, Y., Maeda, H. (Eds.), *The Cretaceous System in the Makarov Area, Southern Sakhalin, Russian Far East*. National Science Museum Monographs **31**, pp. 25–120.

Marshall, S., 1926. The upper Cretaceous ammonites of New Zealand. *Transactions and Proceedings of the Royal Society of New Zealand* **56**, 129–210 (Plates 19–47).

Marshall, C.R., 1995. Distinguishing between sudden and gradual extinctions in the fossil record: predicting the position of the Cretaceous-Tertiary iridium anomaly using the ammonite fossil record on Seymour Island, Antarctica. *Geology* **23**, 731–734.

Marshall, C.R., Ward, P.D., 1996. Sudden and gradual molluscan extinctions in the Latest Cretaceous of Western European Tethys. *Science* **274**, 1360–1363.

Martin, J.E., 2006. Biostratigraphy of the Mosasauridae (Reptilia) from the Cretaceous of Antarctica. In: Francis, J.E., Pirrie, D., Crame, J.A. (Eds.), *Cretaceous–Tertiary High-Latitude Palaeoenvironments, James Ross Basin, Antarctica.* Special Publication vol. **258**. Geological Society, London, pp. 101–108.

Martin, J.E., Crame, J.A., 2006. Palaeobiological significance of high-latitude Late Cretaceous vertebrate fossils from the James Ross Basin, Antarctica. In: Francis, J.E., Pirrie, D., Crame, J.A. (Eds.), *Cretaceous–Tertiary high-Latitude Palaeoenvironments, James Ross Basin, Antarctica*. Special Publication vol. **258**. Geological Society, London, pp. 109–124.

McArthur, J.M., Thirlwall, M.F., Engkilde, M., Zinsmeister, W.J., Howarth, R.J., 1998. Strontium isotope profiles across K/T boundary sequences in Denmark and Antarctica. *Earth and Planetetary Science Letters* **160**, 179–192.

McArthur, J.M., Crame, J.A., Thirlwall, M.F., 2000. Definition of Late Cretaceous stage boundaries in Antarctica using strontium isotope stratigraphy. *Journal of Geology* **108**, 623–640.

McNamara, K.J., Rexilius, J.P., Marshall, N.G., Henderson, R.A., 1988. The first record of a Maastrichtian ammonite from the Perth Basin, Western Australia, and its biostratigraphical significance. *Alcheringa* **12**, 163–168.

Meldahl, K.H., 1990. Sampling, species abundance, and the stratigraphic signature, of mass extinction: a test using Holocene tidal flat molluscs. *Geology* **18**, 890–893.

Miller, K.G., Sugarman, P.J., Browning, J.V., Kominz, M.A., Hernandez, J.C., Olsson, R.K., Wright, J.D., Feigenson, M.D., Van Sickel, W., 2003. Late Cretaceous chronology of large, rapid sea-level changes: glacioeustasy during the greenhouse world. *Geology* **31**, 585–588.

Montes, M., Nozal, F., Santillana, S., Marenssi, S.A., Olivero, E., 2010. Mapa Geológico de la isla Marambio (Seymour). Escala 1:20,000. Institute Instituto Antártico Argentino & Instituto Geológico y Minero de España.

Mustard, P.S., 1994. The Upper Cretaceous Nanaimo Group, Georgia Basin. In: Monger, J.W.H. (Ed.), Geology and Geological Hazards of the Vancouver Region, Southwestern British Columbia. *Geological Survey of Canada Bulletin* **481**, pp. 27–95.

Nielsen, S.N., Salazar, C., 2011. *Eutrephoceras subplicatum* (Steinmann, 1895) is a junior synonym of *Eutrephoceras dorbignyanum* (Forbes in Darwin, 1846) (Cephalopoda, Nautiloidea) from the Maastrichtian Quiriquina Formation of Chile. *Cretaceous Research* **32**, 833–840.

O'Dogherty, L., Sandoval, J., Vera, J.A., 2000. Ammonite faunal turnover tracing sea-level changes during the Jurassic (Betic Cordillera, southern Spain). *Journal of the Geological Society of London.* **157**, 723–736.

Olivero, E.B., Zinsmeister, W.J., 1989. Large heteromorph ammonites from the Upper Cretaceous of Seymour Island, Antarctica. *Journal of Paleontology* **63**, 626–636.

Olivero, E.B., 1992. Asociaciones de ammonites de la Formación Santa Marta (Cretácico tardio), isla James Ross, Antártida. In: Rinaldi, C.A. (Ed.), *Geologia de la Isla James Ross, Antártida*. Instituto Antártico Argentino, Buenos Aires, pp. 47–76.

Olivero, E.B., 1998. Large mud-filled channels in the Maastrichtian of the López de Bertodano Formation (Seymour Island, Antarctica): stratigraphical implications. *Revista de la Asociación Geológica Argentina* **53**, 553–556.

Olivero, E.B., 2012a. Sedimentary cycles, ammonite diversity and palaeoenvironmental changes in the Upper Cretaceous Marambio Group, Antarctica. *Cretaceous Research* **34**, 348–366.

Olivero, E.B., 2012b. New Campanian kossmaticeratid ammonites from the James Ross Basin, Antarctica, and their possible relationships with

Jimboiceras? *antarcticum* Riccardi. *Revue de Paléobiologie*, Genève Volume spécial **11**, pp. 133–149.

Olivero, E.B., Medina, F.A., 2000. Patterns of Late Cretaceous ammonite biogeography in the southern high latitudes: the family Kossmaticeratidae in Antarctica. *Cretaceous Research* **21**, 269–279.

Olivero, E.B., Ponce, J.J., Marsicano, C.A., Martinioni, D.R., 2007. Depositional settings of the basal López de Bertodano Formation, Maastrichtian, Antarctica. *Revista de la Asociación Geológica Argentina*. **62**, 521–529.

Olivero, E.B., Ponce, J.J., Martinioni, D.R., 2008. Sedimentology and architecture of sharp based tidal sandstones in the Upper Marambio Group, Maastrichtian of Antarctica. *Sedimentary Geology* **210**, 11–26.

Olivero, E.B., Medina, F.A., López, C.M.I., 2009. The stratigraphy of Cretaceous mudstones in the Eastern Fuegian Andes: new data from body and trace fossils. *Revista de la Asociación Geológica Argentina* **64**, 60–69.

Olsson, R.K., Wright, J.D., Miller, K.G., 2001. Paleobiogeography of *Pseudotextularia elegans* during the latest Maastrichtian global warming event. *Journal of Foraminiferal Research* **31**, 275–282.

Pirrie, D., Crame, J.A., Riding, J.B., 1991. Late Cretaceous stratigraphy and sedimentology of Cape Lamb, Vega Island, Antarctica. *Cretaceous Research* **12**, 227–258.

Pirrie, D., Crame, J.A., Lomas, S.A., Riding, J.B., 1997. Late Cretaceous stratigraphy of the Admiralty Sound region, James Ross Basin, Antarctica. *Cretaceous Research* **18**, 109–137.

Pujalte, V., Baceta, J.I., Orue-Etexebarria, X., Payros, A., 1998. Paleocene strata of the Basque Country, W. Pyrenees, Northern Spain: facies and sequence development in a deep-water starved basin. In: De Gaciansky, P.-C., Hardenbol, J., Jacquin, T., Vail, P.R., Farley, M.B. (Eds.), *Sequence Stratigraphy of European Basins*. SEPM (Society for Sedimentary Geology), Special Publication vol. **60**, pp. 311–325.

Rampino, M.R., Adler, A.C., 1998. Evidence for abrupt latest Permian extinction of foraminifera: results of tests for the Signor–Lipps effect. *Geology* **26**, 415–418.

Renne, P.R., Deino, A.L., Hilgen, F.J., Kuiper, K.F., Mark, D.F., Mitchell III, W.S., Morgan, L.E., Mundil, R., Smit, J., 2013. Time scales of critical events around the Cretaceous-Paleogene Boundary. *Science* **339**, 684–687.

Robertson, D.S., Lewis, W.M., Sheehan, P.M., Toon, O.B., 2013. K–Pg extinction patterns in marine and freshwater environments: the impact winter model. *Journal of Geophysical Research: Biogeosciences* **118**, 1–9.

Sadler, P., 1988. Geometry and stratification of uppermost Cretaceous and Paleogene units on Seymour Island, northern Antarctic Peninsula. In: Feldmann, R.M., Woodburne, M.O. (Eds.), *Geology and Paleontology of Seymour Island, Antarctic Peninsula*. Geological Society of America, Memoirs **169**, pp. 303–320.

Salazar, C., Stinnesbeck, W., Quinzio-Sinn, L.A., 2010. Ammonites from the Maastrichtian (Upper Cretaceous) Quiriquina Formation in Central Chile. *Neues Jahrbuch für Geologie und Paläontologie (Abhandlung)* **257**, 181–236.

Scasso, R.A., Olivero, E.B., Buatois, L.A., 1991. Lithofacies, biofacies, and ichnoassemblage evolution of a shallow submarine volcaniclastic fan-shelf depositional system (Upper Cretaceous, James Ross Island, Antarctica). *Journal of South American Earth Science* **4**, 239–260.

Schulte, P.D., Alegret, L., Arenillas, I., Arz, J.A., Barton, P.J., Bown, P.R., Bralower, T.J., Chisteson, G.L., Claeys, P., Cockell, C.S., Collins, G.S., Deutsch, A., Goldin, T.J., Goto, K., Grajales-Nishimura, J.M., Grieve, R.A.F., Gulick, S.P.S., Johnson, K.R., Kiessling, W., Koeberl, C., Kring, D.A., MacLeod, K.G., Matsui, T., Melosh, J., Montanari, A., Morgan, J.V., Neal, C.R., Nichols, D.J., Norris, R.D., Pierazzo, E., Ravizza, G., Rebolledo-Vieyra, M., Reimold, W.U., Robin, E., Salge, T., Speijer, R.P., Sweet, A.R., Urrutia-Fucugauchi, J., Vajda, V., Whalen, M.T., Willumsen, P.S., 2010. The Chicxulub asteroid impact and mass extinction at the Cretaceous-Paleogene boundary. *Science* **327**, 1214–1218.

Sepulveda, J., Wendler, J.E., Summons, R.E., Hinrichs, K.U., 2009. Rapid resurgence of marine productivity after the Cretaceous-Paleogene mass extinction. *Science* **326**, 129–132.

Shigeta, Y., 1993. Post-hatching early life history of Cretaceous Ammonoidea. *Lethaia* **26**, 133–145.

Shigeta, Y., Tanabe, K., Izukura, M., 2010. *Gaudryceras izumiense* Matsumoto and Morozumi, a Maastrichtian ammonoid from Hokkaido and Alaska and its biostratigraphic implications. *Paleontological Research* **14**, 202–211.

Shimizu, S., 1934. Ammonites. In: Shimizu, S., Obata, T. (Eds.), *Cephalopoda*. Iwanami's Lecture Series of Geology and Palaeontology. Tokyo, pp. 1–137 (in Japanese).

Signor, P.W., Lipps, J.H., 1982. Sampling bias, gradual extinction patterns, and catastrophes in the fossil record. In: Silver, L.T., Schulz, P.H. (Eds.), *Geological Implications of Large Asteroids and Comets on the Earth*. Geol. Soc. Am. Spec. Publ. **190**, pp. 291–296.

Sogot, C.E., Harper, E.M., Taylor, P.D., 2013. Biogeographical and ecological patterns in bryozoans across the Cretaceous-Paleogene boundary: Implications for the phytoplankton collapse hypothesis. *Geology* **41**, 631–634.

Song, H., Wignall, P.B., Tong, J., Yin, H., 2013. Two pulses of extinction during the Permian-Triassic crisis. *Nature Geoscience* **6**, 52–56.

Spath, L.F., 1922. On the Senonian ammonite fauna of Pondoland. *Transactions of the Royal Society of South Africa* **10**, 113–148 (Plates 5–9).

Spath, L.F., 1926. On new ammonites from the English Chalk. *Geological Magazine* **3**, 77–83 (1 Plate).

Spath, L.F., 1927. Revision of the Jurassic Cephalopod Fauna of Kachh (Cutch), part 1. Memoirs of the Geological Survey of India. *Palaeontologia Indica (new series)* **9**, 1–71.

Spath, L.F., 1953. The Upper Cretaceous cephalopod fauna of Graham Land. *Falkland Island Dependencies Survey, Scientific Report* **3**, pp. 1–60.

Steinmann, G., 1895. Die Cephalopoden der Quiriquina-Schisten. *Neues Jahrbuch für Minerologie Geologie und Paläontologie* **10**, 64–94.

Stilwell, J.D., Grebneff, A., 1996. Records of Nautiloidea (Mollusca: Cephalopoda) across the Cretaceous-Tertiary boundary in Otago and Chatham Islands, New Zealand. *New Zealand Journal of Geology and Geophysics* **39**, 83–91.

Stilwell, J.D., Zinsmeister, J.D., Oleinik, A.E., 2004. Early Paleocene mollusks of Antarctica: systematics, palaeoecology and palaeobiogeographic significance. *Bulletins of American Paleontology* **367**, 1–89.

Stinnesbeck,W., 1986. Faunistic and paleoecological conditions of the Quiriquina Formation (Maastrichtian) of central Chile. *Palaeontographica A* **194**, 99–237.

Stinnesbeck, W., Ifrim, C., Salazar, C., 2012. The last Cretaceous ammonites in Latin America. *Acta Palaeontologica Polonica* **57**, 717–728.

Stoliczka, F., 1865. The fossil Cephalopoda of the Cretaceous rocks of southern India. Vol. 3. Ammonitidae. *Memoirs of the Geological Survey of India. Palaeontolia Indica* **6–9**, 107–154.

Stott, L.D., Kennett, J.P., 1990. The paleoceanographic and paleoclimatic signature of the Cretaceous/Paleogene boundary in the Antarctic: stable isotopic results from ODP Leg 113. In: Barker, P.F., Kennett, J.P. (Eds.), *Proceedings of the Ocean Drilling Program, Scientific Results* **13**, pp. 829–848.

Surlyk, F., 1997. A cool-water carbonate ramp with bryozoan mounds: Late Cretaceous-Danian of the Danish Basin. In: James, N.P., Clarke, J.D.A. (Eds.), *Cool-Water Carbonates*. SEPM Special, Publication **56**, pp. 293–307.

Surlyk, F., Nielsen, J.M., 1999. The last ammonite? *Bulletins of the Geological Society of Denmark* **46**, 115–119.

Tajika, A., Wani, R., 2011. Intraspecific variation of hatchling size in Late Cretaceous ammonoids from Hokkaido, Japan: implication for planktic duration at early ontogentic stage. *Lethaia* **44**, 287–293.

138

Tanabe, K., 2011. The feeding habits of ammonites. *Science* **331**, 37–38.

Teichert, C., Glenister, B.F., 1952. Fossil nautiloid faunas from Australia. *Journal Paleontology* **26**, 730–752.

Thibault, N., Gardin, S., 2006. Maastrichtian calcareous nannofossil biostratigraphy and paleoecology in the Equatorial Atlantic (Demerara Rise, ODP Leg 207 Hole 1258A). *Revue de Micropaléontologie* **49**, 199–214.

Thibault, N., Gardin, S., 2010. The calcareous nannofossil response to the end-Cretaceous warm event in the tropical Pacific. *Palaeogeography Palaeoclimatololology Palaeoecology* **291**, 239–252.

Thibault, N., Gardin, S., Galbrum, B., 2010. Latitudinal migration of calcareous nannofossil *Micula murus* in the Maastrichtian: implications for global climate change. *Geology* 38, 203–206.

Thorn, V.C., Thorn, V.C., Francis, J.E., Riding, J.B., Raiswell, R.W., Pirrie, D., Haywood, A.M., Crame, J.A., Marshall, J.M., 2007. Terminal Cretaceous climate change and biotic response in Antarctica. In: Cooper, A., Raymond, C., 10th ISAES Editorial Team (Eds.), *Antarctica; A Keystone in a Changing World—Online Proceedings for the 10th International Symposium on Antarctic Earth Sciences*. U.S. Geological Survey Open-File Report 2007-1047 (http://pubs.usgs.gov/of/2007/1047/ . Extended abstract 096).

Thorn, V.C., Riding, J.B., Francis, J.E., 2009. The Late Cretaceous dinoflagellate cyst Manumiella - Biostratigraphy, systematics, and palaeoecological signals in Antarctica. *Review of Palaeobotany and Palynology* **156**, 436–448.

Tobin, T.S.,Ward, P.D., Steig, E.J., Olivero, E.B., Hilburn, I.A.,Mitchell, R.N., Diamond,M.R.,Raub, T.D., Kirschvink, J.L., 2012. Extinction patterns, $\delta_{18}O$ trends, and magnetostratigraphy from a southern high-latitude Cretaceous-Paleogene section: links with Deccan volcanism. *Palaeogeography Palaeoclimatololology Palaeoecology* **350–352**, 180–188.

Usher, J.L., 1952. Ammonite faunas of the Upper Cretaceous rocks of Vancouver Island, British Columbia. *Bulletin of the Geological Survey of Canada* **21**, 1–182.

van Hoepen, E.C.N., 1920. Description of some Cretaceous ammonites from Pondoland. *Annals of the Transvaal Museum* **7**, 142–147.

Voigt, S., Gale, A.S., Jung, C., Jenkyns, H.C., 2012. Global correlation of upper Campanian–Maastrichtian successions using carbon-isotope stratigraphy: development of a new Maastrichtian timescale. *Newsletters on Stratigraphy* **45**, 25–53.

Vonhof, H.B., Jagt, J.W.M., Immenhauser, A., Smit, J., van den Berg, Y.W., Saher, M., Keutgen, N., Reijme, J.J.G., 2011. Belemnite-based strontium, carbon, and oxygen isotope stratigraphy of the type area of the Maastrichtian Stage. *Netherlands Journal of Geoscience: Geologie en Mijnbouw* **90**, 259–270.

Wang, S.C.,Marshall, C.R., 2004. Improved confidence intervals for estimating the position of a mass extinction boundary. *Paleobiology* **30**, 5–18.

Ward, P.D., 1990. A review of Maastrichtian ammonite ranges. In: Sharpton, V.L., Ward, P.D. (Eds.), *Global Catastrophes in Earth History; An Interdisciplinary Conference on Impacts, Volcanism, and Mass Mortality*. GSA Special Paper **247**, pp. 519–530.

Ward, P.D., Kennedy, W.J., 1993. Maastrichtian ammonites from the Biscay region (France, Spain). *Paleontological Society Memoirs* **34**, 1–58.

Ward, P.D., Kennedy, W.J., Macleod, K.G., Mount, J.F., 1991. Ammonite and inoceramid bivalve extinction patterns in Cretaceous/Tertiary boundary sections of the Biscay region (southwestern France, northern Spain). *Geology* **19**, 1181–1184.

Whiteside, J.H., Ward, P.D., 2009. Ammonoid diversity and disparity track episodes of chaotic carbon cycling during the early Mesozoic. *Geology* **39**, 99–102.

Wiedmann, J., 1966. Stammesgeschichte und System der posttriadischen Ammonoideen: ein Überblick. *Neues Jahrbuch für Geologie und Paläontologie (Abhandlung).* **125**, 49–78 (127, 113–181).

Wiedmann, J., Kullman, J., 1996. Crises in ammonoid evolution. In: Landman, N.H., Tanabe, K., Davis, R.A. (Eds.), *Ammonoid Paleobiology.* Topics in Geobiology **13**, pp. 795–811.

Wilf, P., Johnson, K., Huber, B.T., 2003. Correlated terrestrial andmarine evidence for global climate change before mass extinction at the Cretaceous-Paleogene boundary. *Proceedings of the National Acadamey of Science* **100**, 599–604.

Wrenn, J.H., Hart, G.F., 1988. Paleogene dinoflagellate cyst biostratigraphy of Seymour Island, Antarctica. In: Feldmann, R.M., Woodburne, M.O. (Eds.), *Geology and Paleontology of Seymour Island, Antarctic Peninsula*. Geological Society of America, Memoirs **169**, pp. 321–448.

Wright, C.W., Calloman, J.H., Howarth, M.K., 1996. Cretaceous Ammonoidea. In: Kaesler, R.L. (Ed.), *Treatise on Invertebrate Paleontology, Part L, Mollusca 4, Revised*. The Geological Society of America, Boulder & The University of Kansas, Lawrence (362 pp.).

Yacobucci, M.M., 2005. Multifractal and white noise evolutionary dynamics in Jurassic-Cretaceous Ammonoidea. *Geology* **33**, 97–100.

Zinsmeister, W.J., 1988. Early geological exploration of Seymour Island, Antarctica. In: Feldmann, R.M., Woodburne, M.O. (Eds.), *Geology and Paleontology of Seymour Island, Antarctic Peninsula*. Geological Society of America, Memoirs **169**, pp. 1–16.

Zinsmeister, W.J., 1998. Discovery of fish mortality horizon at the K–T boundary on Seymour Island: re-evaluation of events at the end of the Cretaceous. *Journal of Paleontology* **72**, 556–571.

Zinsmeister, W.J., 2001. Late Maastrichtian short-term biotic events on Seymour Island, Antarctic Peninsula. *Journal of Geology* **109**, 213–229.

Zinsmeister, W.J., Feldmann, R.M., 1996. Late Cretaceous faunal changes in the high southern latitudes: a harbinger of global biotic catastrophe? In: Macleod, N., Keller, G. (Eds.), *Cretaceous–Tertiary Mass Extinctions: Biotic and Environmental Changes*. W.W. Norton, New York, pp. 303–325.

Zinsmeister, W.J., Oleinik, A.E., 1995. Discovery of a remarkably complete specimen of the giant cephalopod *Diplomoceras maximum* from the Late Cretaceous of Seymour Island, *Antarctic Journal of the United States* **30**, 9.

Zinsmeister, W.J., Feldmann, R.M., Woodburne, M.O., Elliot, D.H., 1989. Latest Cretaceous/Tertiary transition on Seymour Island, Antarctica. *Journal of Paleontology* **63**, 731–738.

Zittel, K.A., 1884. Cephalopoda, Handbuch der Paläontologie 1, Abteilung 2, Lieferung 3. R. Oldenburg, München, Leipzig, pp. 329–522.

Zittel, K.A., 1895. Grundzüge der Paläontologie, Oldenburg (viii + 971 pp.).

Chapter 4 : Benthic macrofossil evidence for a rapid and severe Cretaceous–Paleogene mass extinction in Antarctica

This chapter has been published as;

4.1 Abstract

Debate continues about the nature of the Cretaceous–Paleogene (K–Pg) mass extinction event. An abrupt crisis triggered by a bolide impact contrasts with ideas of a more gradual extinction involving flood volcanism or climatic changes. Evidence from high latitudes has also been used to suggest that the severity of the extinction decreased from low latitudes towards the poles. Here we present a record of the K–Pg extinction based on extensive assemblages of marine macrofossils (primarily new data from benthic molluscs) from a highly expanded Cretaceous–Paleogene succession: the López de Bertodano Formation of Seymour Island, Antarctica. We show that the extinction was rapid and severe in Antarctica, with no significant biotic decline during the latest Cretaceous, contrary to previous studies. These data are consistent with a catastrophic driver for the extinction, such as bolide impact, rather than a significant contribution from Deccan Traps volcanism during the late Maastrichtian.

4.2 Introduction

The Cretaceous–Paleogene (K–Pg) mass extinction at 66 Ma is the most intensively studied of the 'Big Five' crises to have affected life during the Phanerozoic (Alvarez et al., 1980; Archibald et al., 2010; Bambach, 2006; Brusatte et al., 2015; Keller et al., 2010; McGhee et al., 2013; Raup and Sepkoski, 1982; Schulte et al., 2010).The extinction led to a fundamental restructuring of global ecosystems and the rise of modern taxonomic groups (Aberhan and Kiessling, 2014; Aberhan and Kiessling, 2015; Krug et al., 2009; McGhee et al., 2013). Despite this interest, debate continues as to the duration of the crisis as well as the relative contributions of the bolide impact at Chicxulub (Alvarez et al., 1980; Schulte et al., 2010), voluminous eruptions from the Deccan Traps large igneous province (Schoene et al., 2014; Renne et al., 2015), and dynamic climate instability during the preceding Maastrichtian stage (72.1–66 Ma) (Archibald et al., 2010; Renne et al., 2013).

Parts of this discourse have particularly focused on the Antarctic fossil record. Previous studies on high southern latitude biotas have claimed the extinction to be either a gradual diversity decline (Zinsmeister et al., 1989; Zinsmeister, 1998), a series of extinction pulses linked to episodes of Deccan volcanism (Tobin et al., 2012) or, for ammonites at least, a single rapid event (Witts et al., 2015). In addition, it has been suggested that the intensity of the extinction and environmental stress varied with latitude and was related to the proximity of the impact site or the volcanism (both at mid to low latitudes) (Powell and MacGregor, 2011; Punekar et al., 2014). As a result, the high southern latitudes are thought to have weathered the crisis better than lower latitude regions (Zinsmeister et al., 1989; Jablonski, 1998; Jiang et al., 2010).

The López de Bertodano Formation of southern Seymour Island, Antarctica (Figure 4.1) represents one of the most highly expanded onshore Maastrichtian–Danian sedimentary successions in the world with ~1,000m of sedimentation in ~4 Myr (Tobin et al., 2012; Bowman et al., 2013; Bowman et al., In Press). At a palaeolatitude of 65°S during the latest Cretaceous (Hathway, 2000), this succession represents a true high latitude record of

events during this critical time period. The succession exposed on Seymour Island is dominated by silty clays with occasional, thin glauconite-rich sandstone horizons becoming more prevalent in the uppermost 300 m, along with indurated layers formed of early diagenetic concretions and thin bioturbated sands (Macellari, 1988; Crame et al., 2004; Olivero, 2012). Despite the lithological homogeneity of the succession, several environmental changes have been proposed that have a bearing on marine biodiversity. The depositional environment of the López de Bertodano Formation is broadly transgressive; the lower portion has been interpreted as relatively shallow water, outer estuarine facies (Olivero et al., 2007; Olivero, 2012), with a low-energy, marine shelf facies forming the remainder of the succession (Crame et al., 2004; Elliot et al., 1994).

Here we address these debates on the timing and intensity of Antarctic marine extinctions with a detailed analysis of marine diversity trends during the Maastrichtian to earliest Paleocene ~70–65.6 Ma (Bowman et al., 2013) from the López de Bertodano Formation. We evaluate the nature of the K–Pg extinction, its abruptness and intensity in this region. In addition, we test the relationship between palaeoenvironmental changes and diversity, using pyrite petrography as an indicator of palaeoenvironmental conditions. Besides comparisons of existing low-resolution faunal range charts with oxygen isotope data as a proxy for marine palaeotemperature trends (e.g. Tobin et al., 2012), there have been few previous attempts to relate faunal diversity trends in this succession to other local environmental conditions, for example benthic redox changes. We suggest that the K–Pg extinction in Antarctica was as rapid and severe as that seen at lower latitudes, with no evidence for significant precursor extinction events during the latest Maastrichtian, which can be related to the onset of Deccan volcanism or climatic instability.
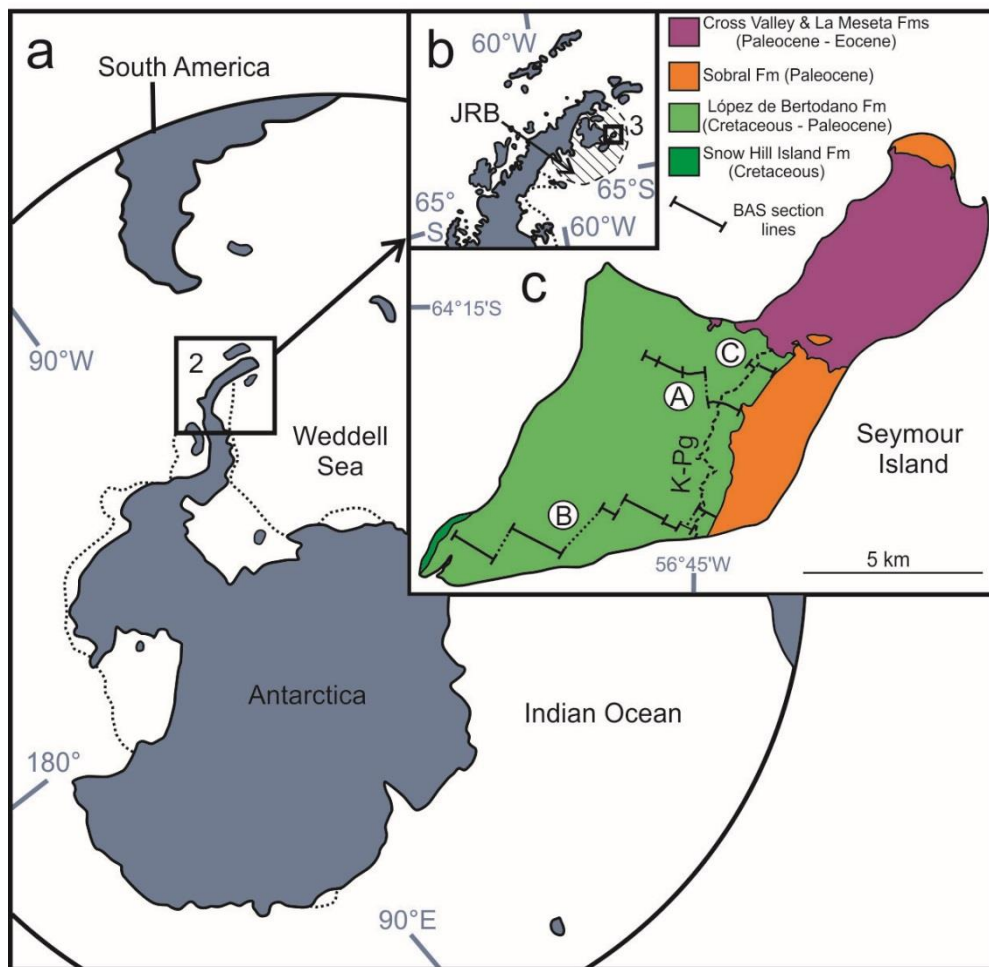
Figure 4.1: Location map of Seymour Island. (a) Modern Southern Hemisphere geography showing location of Antarctica, Antarctic Peninsula highlighted. (b) Map of northern Antarctic Peninsula, location of James Ross Basin (JRB) circled and highlighted. (c) Geological map of Seymour Island showing locations of principal lithological units, their ages, as well as the locations of British Antarctic Survey section lines mentioned in the text. Location of K–Pg boundary indicated by dotted line on c. Circled letters in c correspond to individual British Antarctic Survey sections lines, A, 1999 field season, B, 2006 field season, C, 2010 field season. Scale bar, 5 km. See Figs. B1–B4 for more details.

4.3 Results

4.3.1 Fossil evidence for diversity and extinction

The primary data for this study more than 6,000 benthic molluscan fossils (bivalves and gastropods) from 377 individual sampling stations accurately located within a series of detailed measured sedimentary sections through the

146

López de Bertodano Formation (Figure 4.1; Figs B.1–B.4). Species range charts based on these collections were combined and compared directly with data from nektonic and nekto-benthic cephalopod molluscs from the same sections (Chapter 3) (Figure 4.2) and from previous studies of the K–Pg boundary interval on Seymour Island undertaken by Zinsmeister et al. (1998) (Fig.B. 6). The K–Pg boundary on Seymour Island occurs in a 2.5–3-m-thick glauconite-rich horizon 1,007.5m above the base of our composite section, based on biostratigraphic data from marine palynology (Elliot et al., 1994; Bowman et al., 2012; Bowman et al., In Press) (Figure 4.2; Figs B.1–B.5) and the presence in a parallel section of the globally recognized iridium (Ir) anomaly used as a marker for the K–Pg boundary (Elliot et al., 1994; Molina et al., 2006) (Figure 4.1).

Besides an abundant and diverse molluscan fauna, other common faunal elements found throughout the Maastrichtian portion of the López de Bertodano Formation include serpulid worm tubes (*Rotularia*), cidaroid echinoid spines, scaphopods, rare solitary corals, decapod crustaceans, marine reptiles, shark vertebrae and fossil wood bored by *Teredolites* (Macellari, 1988; Francis and Poole, 2002; Crame et al., 2004). Recent work has also revealed the presence of fossil methane seeps, which are periodically developed on the Maastrichtian sea-floor and are characterized by a distinctive benthic molluscan fauna (Little et al., 2015).

On the basis of the combined data sets, a total of 44 species and 39 genera of benthic molluscs occur within the Maastrichtian portion of the López de Bertodano Formation (Figure 4.2) along with 15 species and 9 genera of nektonic and nekto-benthic cephalopods (Chapter 3; Witts et al., 2015). Focusing on the benthos, a total of 25 out of 37 benthic molluscan species (67%) have their last occurrence at or below the K–Pg boundary and 15 out of 35 benthic molluscan genera disappear during the Maastrichtian (43%) (Excluding those represented by a single occurrence: 7 species and 4 genera, respectively).

148
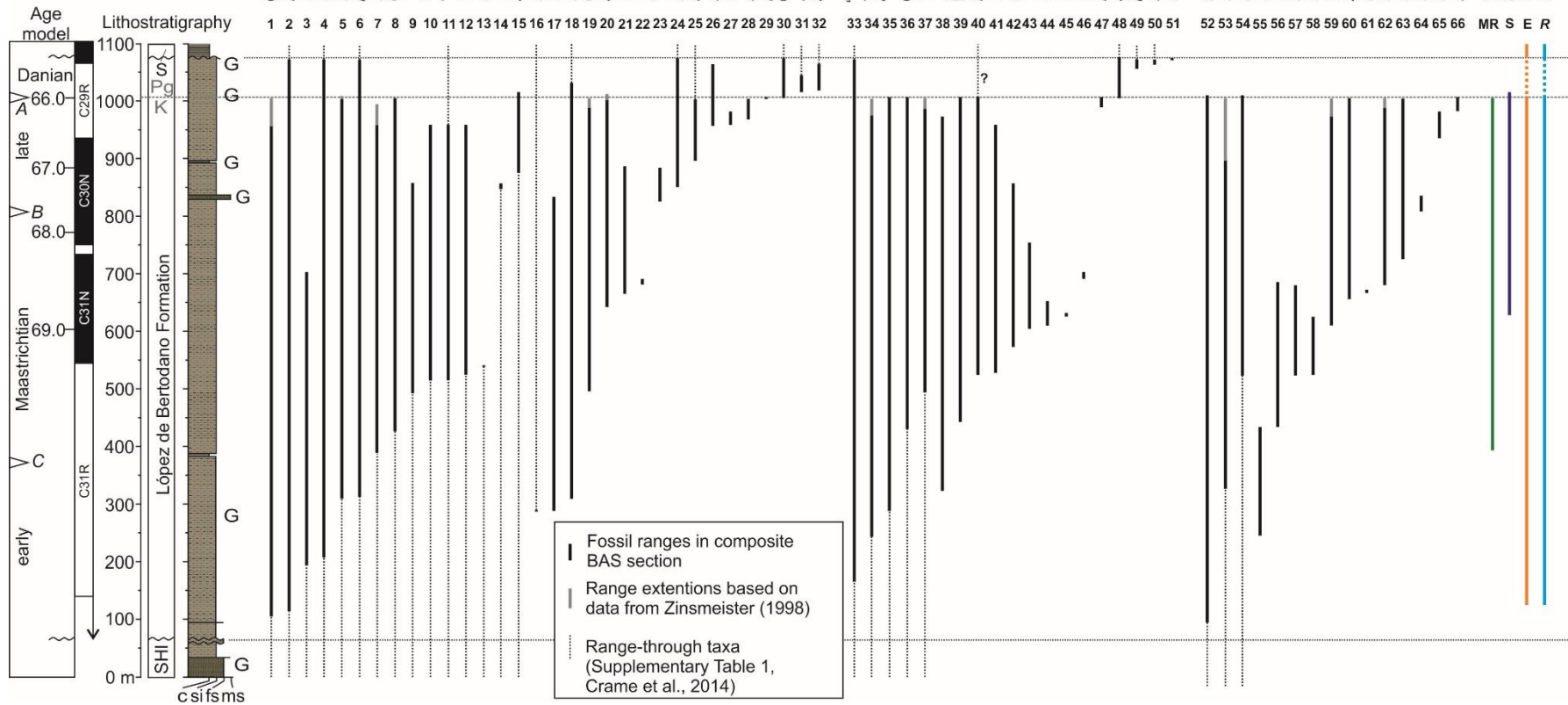
Figure 4.2 (previous page): Composite stratigraphic range data for molluscan taxa from the López de Bertodano Formation. Range data is plotted against composite lithostratigraphy and age model. Includes new data from this study (see Section 4.5 and Figs. B.1 to B.4, and from Zinsmeister (1998) and Chapter 3 (Witts et al., 2015)). Separated into bivalves (B) (1–32), gastropods (G) (33–51), and cephalopods (A and N) (52–66), with taxa ordered by first appearance in the composite section. Range extensions calculated based on a literature review of molluscan occurrences from underlying formations (Table B.1), in addition to collections from overlying Paleocene strata (Crame et al., 2014; Bowman et al., In Press). Also illustrated are the stratigraphic ranges of marine reptile fossils (MR), lamniform shark vertebrae (S), echinoid spines (E) and serpulid worm tubes (*Rotularia* .spp (*R*) in the composite section. Age model is derived from Bowman et al. (2013). Time scale is based on Sr isotope chemostratigraphy (italicized A–C) (McArthur et al., 1998) and magnetostratigraphy (Tobin et al., 2012), updated with ages from the Geological Time Scale 2012 (Gradstein et al., 2012) and using the K–Pg boundary datum. G, glauconite-rich intervals. S, Sobral Formation. See Appendix B.1 for details of species identifications.

Standing species richness based on range-through data gives a good approximation of taxonomic diversity, and indicates an overall increase in benthic molluscan diversity up-section from the base of the López de Bertodano Formation, culminating in a maximum of 33 species at 690m (310m below the K–Pg boundary in our composite section) (Figure 4.3a).

Standing species richness of bivalve and gastropod faunas remains stable until a level ~40m below the K–Pg interval (Figure 4.2; Figure 4.3). Above this horizon, there is a slight decline due to the apparent loss of six species, before a significant extinction event between 1,000 and 1,007.5m in our composite section (that is, the interval directly beneath the K–Pg boundary) where 11 benthic species disappear along with all eight remaining species and genera of cephalopods (Witts et al., 2015) (Figure 4.2; Fig. B.7). Turnover metrics clearly indicate a significant peak in extinction rate at this level, which is apparent in both a combined analysis (Figure 4.3 a and b) and when data are separated into benthos and nekton (Fig. B.7).
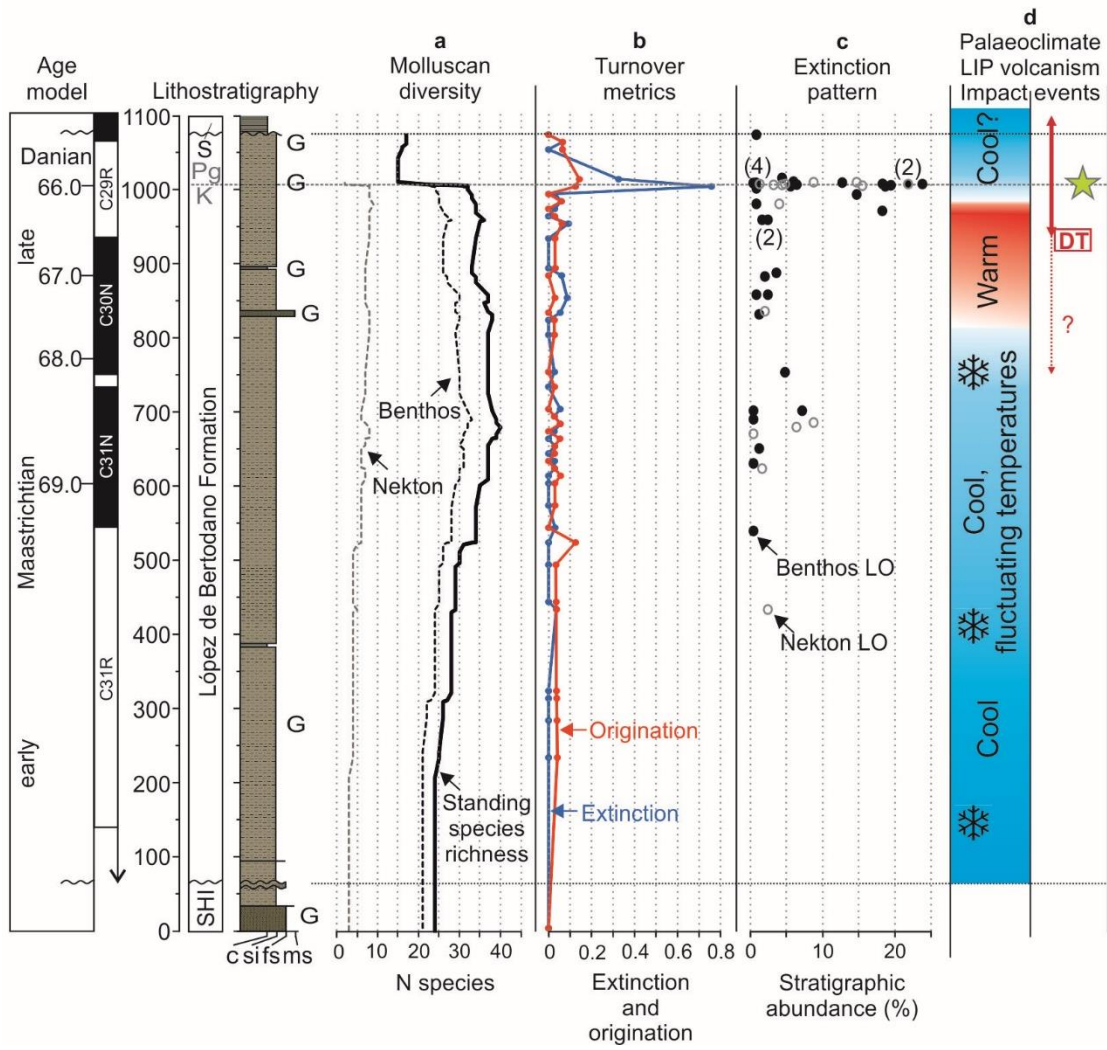
Figure 4.3: (previous page) Molluscan diversity and extinction data compared with evidence for Cretaceous–Paleogene palaeoenvironmental change. (a) Molluscan diversity for benthos (bivalves and gastropods) and nekton (ammonites and nautiloid) measured as standing species richness in the composite section (Tables B.3-B.11), plotted against age model and lithostratigraphy. Composite standing species richness for all molluscan groups plotted as solid black line. Note all nektonic molluscan taxa disappear at the K–Pg boundary (grey dashed line, defined by dinoflagellate cyst biostratigraphy and iridium (Ir) anomaly in parallel section (Elliot et al., 1994; Zinsmeister, 1998; Bowman et al., 2012). All nekton species richness and extinction data reanalysed from Chapter 3 (Witts et al., 2015). (b) Extinction and origination rates through time based on boundary-crosser methodology (Foote, 2000), calculated for the entire molluscan fauna in 10m bins (see Section 4.5 and Tables B.3-B.11). See Fig. B.6 for metrics calculated for benthos and nekton individually. (c) Analysis of extinction pattern based on 'Meldahl's method (Meldahl, 1990; Song et al., 2012) with last occurrences (LO) in the composite section plotted against stratigraphic abundance _S_ (measured as a %), separated into benthos and nekton. Numbers in parentheses indicate number of overlapping datapoints (where taxa have the same value of S). Data are consistent with a single mass extinction event affecting common molluscan taxa (those with higher value of _S_) coincident with the K–Pg boundary. (d) Palaeoclimate interpretation based on published data from multiple sections on Seymour Island (Tobin et al., 2012; Bowman et al., 2013; Kemp et al., 2014; Bowman et al., 2014). Snowflake symbols are 'cold snaps' of Bowman et al. (2013), red arrow labelled DT, approximate duration of the main phase of Deccan Trap volcanism (correlated to section and age model using magnetostratigraphy, based on Schoene et al. (2014) and Renne et al. (2015). Dashed red line and '?' illustrates uncertainty surrounding timing of initial onset of Deccan volcanism (Chenet et al., 2009; Schoene et al., 2014). Yellow star, position of Ir anomaly at the K–Pg boundary in a parallel section (Elliot et al., 1994), taken as a global marker of the Chicxulub impact event (Molina et al., 2006). (See Figs. B.6 and B.7 for further information).

Two bivalve species (_Panopea clausa_ and _Seymourtula antarctica_) range into the glauconite-rich beds in the earliest Paleocene before disappearing, and based on existing data from Zinsmeister et al. (1998), another species (_Surobula nucleus_) also shows this pattern (Fig. B.6). These taxa are classed as additional victims of the extinction (Figure 4.2). Thus combined raw stratigraphic range data suggest the benthic molluscan community at Seymour Island saw a species-level extinction of 56% (14 out of 25 species) at the K–Pg event. Local generic level extinction was lower at only 30% (9 out of 30

genera), although several genera (*Cryptorhytis, Haustator*) were extirpated in Antarctica but may have survived the K–Pg event at lower latitudes (Aberhan and Kiessling, 2014).

These are also likely to be conservative estimates because many of the taxa that disappear within the Maastrichtian are rare and could therefore be under-sampled with respect to their true stratigraphic range (that is, the 'Signor-Lipps' effect) (Signor and Lipps, 1982). To examine this phenomenon, we first employed a modified version of Meldahl's Method (Meldahl, 1990; Song et al., 2012) to our combined records (see Section 4.5). Significantly, the majority of the most common molluscs (those most likely to give a true picture of their stratigraphic range (Meldahl, 1990)) disappear immediately below the K–Pg boundary (Figure 4.3c). This suggests that the preceding decline is likely due to the apparent loss of rare taxa, known as 'backward smearing' (Signor and Lipps, 1982; Meldahl, 1990; Song et al., 2012).

Application of confidence intervals to raw range and occurrence data in the two longest stratigraphic sections (A and B in Figure 4.1c and Fig. B.1) in the form of range extensions (Marshall, 2010) support this assertion, showing a cluster of both 50 and 95% confidence intervals around the K–Pg boundary interval outlined above (Figs. B.2 and B.3). Only two benthic taxa with a stratigraphic abundance >10% (*Austroaporrhais* sp. and *Eselaevitrigonia regina*) disappear >10m below the K–Pg boundary, and only one of these disappearances is close to the interval identified by Tobin et al. (2012) as containing a supposed precursor extinction event (see Appendix B for more details). Furthermore, extension of their 95% confidence intervals into the K–Pg interval in the two BAS section lines suggests that both these taxa, plus a further rare species of bivalve (*Dozyia drygalskiana*), could be additional victims of extinction in the boundary interval. Assuming this is the case would raise the benthic species-level extinction to 61% (17 out of 28) and generic-level extinction to 36% (12 out of 33).

Directly above the K–Pg boundary a low-diversity molluscan assemblage occurs, dominated by large numbers of the bivalves *Lahillia larseni* and *Cucullaea ellioti*, along with the gastropod *Struthiochenopus hurleyi* (Crame et

al., 2004; Stilwell et al., 2004). Beds immediately above the Ir anomaly level also contain a large number of diagenetic concretions containing articulated and disarticulated fish remains (Zinsmeister, 1998), the only such horizon in the Seymour Island succession. A total of eight benthic molluscan species range through the K–Pg boundary and occur in the 60-m-thick Paleocene portion of the López de Bertodano Formation. This number increases to 11 when taxa that disappear in the Maastrichtian but reappear in the overlying Paleocene Sobral Formation are included (Stilwell et al., 2004; Crame et al., 2014) (Figure 4.2 and Figure 4.3; Appendix B). Origination rates peak in the interval containing the extinction horizon and directly above in the earliest Paleocene, and seven benthic molluscan species make their first appearances in the 60-m between the K–Pg boundary and the base of the Sobral Formation, an interval that represents ~350 kyr (Tobin et al., 2012; Bowman et al., 2013; Bowman et al., In Press) with only one of these taxa disappearing during the same interval (Figure 4.2 and Figure 4.3). However, diversity of the molluscan fauna fails to recover to levels attained during the Maastrichtian.

4.3.2 Benthic environmental conditions from pyrite petrography

Pyrite petrography was undertaken according to the established procedures (Wignall and Newton, 1998). This revealed highly variable pyrite abundance with framboids either being absent (in 10 samples) or present in abundance (in 13 samples). When present, the framboid populations have small mean diameters varying between 4 and 7 µm, and often a considerable 'tail' of large examples (Fig. B.8; Table B.2); this size range is typical of dysoxic (low oxygen) environments in modern settings (Wilkin et al., 1996). Samples with abundant framboid populations are more common in the lower part of the López de Bertodano Formation. Several samples, from closer to the base of the formation, have a narrow size distribution of framboids (minimum diameter 1.5 mm, maximum diameter 14 mm) and a smaller s.d. (1.5–2), more typical of modern anoxic–euxinic environments (Wilkin et al., 1996) (Figure 4.4)
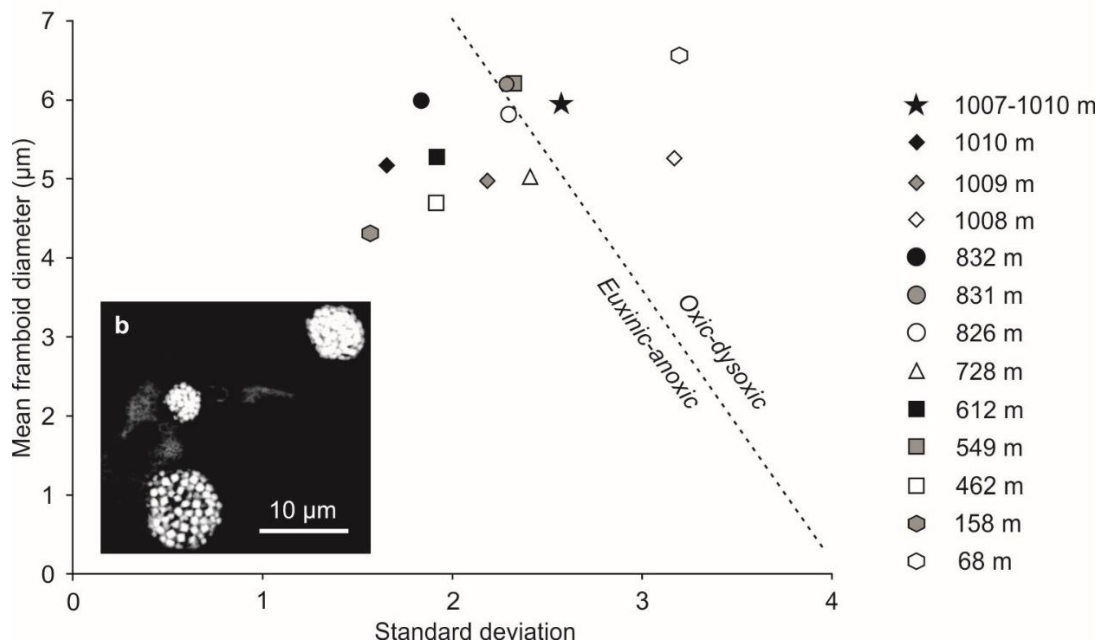
Figure 4.4: Mean versus s.d. plot of framboid populations from the López de Bertodano Formation. Samples ordered stratigraphically in composite section. Dashed line separates redox conditions and is based on modern calibration (Wilkin et al., 1996). Samples plot in both oxic–dysoxic and anoxic–euxinic fields, indicating rapid redox fluctuations. Inset (b) represents pyrite framboids from sample D5.481.2 (158m). Scale bar, 10μm. See Table B.2 for more information.

It is notable that samples from both of the glauconite-rich sandstone units examined in the petrographic analysis, including the interval that yields articulated fish remains immediately above the K–Pg boundary, also have a framboid population typical of rapid fluctuations between dysoxic and anoxic conditions. However, samples from the latest Maastrichtian strata and those above the glauconite-rich interval in the earliest Danian do not contain framboids, possibly indicating that fully oxygenated conditions prevailed on the sea-floor both before and after the K–Pg boundary.

4.4 Discussion

In contrast to all previous studies on the molluscan fauna from Seymour Island (Zinsmeister et al., 1989; Tobin et al., 2012; Elliot et al., 1994), our results identify a single, severe K–Pg extinction event in Antarctica affecting both benthic and nektonic taxa, without precursor extinction events. In contrast,

154

Tobin et al. (2012) argued for two extinction events, one at the K–Pg boundary itself, and an earlier extinction 40m below (~300 kyr prior to the K–Pg boundary), which primarily affected benthic taxa. Tobin and colleagues argued that the earlier crisis was related to a phase of climate warming that has been linked to the onset of Deccan Traps eruptions prior to the K–Pg boundary (Thibault and Gardin, 2010; Thibault and Husson, 2016). However, there remains significant uncertainty in the precise timing of the main phase of Deccan eruptions relative to the K–Pg extinction (Schoene et al., 2014; Renne et al., 2015), as well as the magnitude and potential for global environmental change driven by this volcanism (Schmidt et al., 2016), and even the possibility of a cause-and-effect relationship between Deccan eruptions and the Chicxulub impact event (Richards et al., 2015). In addition, marine and terrestrial proxy data indicate evidence for regional climate warming in the Antarctic Peninsula region commencing up to 2 million years prior to the K–Pg boundary (Bowman et al., 2013; Bowman et al., 2014) (Figure 4.3d).

It seems unlikely that any late Maastrichtian warming event significantly stressed the marine fauna. Throughout this interval of warming temperatures, macrofaunal diversity in our composite section remained stable, and extinction rates were low in both the benthic and nekton/nekto-benthic molluscan faunas (Figure 4.2 and Figure 4.3; Fig. B.7). The difference in findings compared with previous studies (e.g. Zinsmeister et al., 1989; Tobin et al., 2012) can be explained by our much expanded fossil data set from Seymour Island, which has extended stratigraphic ranges through both the Maastrichtian and the Early Paleocene, and the addition of updated taxonomic information, in particular for benthic molluscs (Crame et al., 2014; Beu, 2009) (see Section B.1).

The majority of macrofaunal last occurrences are confined to a short interval directly beneath the K–Pg boundary where previously common benthic, and all nektonic molluscs disappear alongside evidence for severe losses in the wider marine community (Figure 4.2 and Figure 4.3). For example, remains of large marine vertebrates (marine reptiles, lamniform sharks) are present until the extinction interval, with marine reptiles disappearing only 1m beneath the

K–Pg boundary on Seymour Island (Zinsmeister, 1998; Martin, 2006). Providing further evidence for a major benthic disruption, serpulid worm tubes (*Rotularia* spp.) and cidaroid echinoid spines, the most common of all Maastrichtian benthic fossils on Seymour Island, temporarily disappear from the succession at the K–Pg boundary (Zinsmeister, 1998) (Fig. B.6), only reappearing in the basal levels of the Sobral Formation some ~350 kyr later (Figure 4.2).

The record from microfossils is more equivocal. In common with low latitude sections, dinoflagellate cysts exhibit a turnover of taxa at the K–Pg boundary on Seymour Island, but show no significant extinction events (Elliot et al., 1994; Bowman et al., 2012; Bowman et al., In Press), as do diatoms (Harwood, 1988). This may be due to the ability to encyst (dinoflagellates) or create resting spores (diatoms) during periods of environmental stress (Lewis et al., 1999; Ribeiro et al., 2011). Cretaceous planktonic and benthic foraminifera also disappear beneath the K–Pg boundary following a long period of apparent faunal stability in the López de Bertodano Formation (Huber, 1988). Silicoflagellate assemblages show a similar pattern of stasis followed by an abrupt turnover coincident with the K–Pg boundary on Seymour Island (Harwood, 1988).

The 30–43% extinction of bivalves and gastropods at generic level on Seymour Island is similar to that seen in other Southern Hemisphere molluscan faunas (for example, 21.7–32.1% in Patagonia (Aberhan and Kiessling, 2014)) These values are also comparable to extinction estimates from Northern Hemisphere K–Pg boundary sections (for example, 30.5% for bivalves and gastropods in the clastic facies of the Gulf Coast, USA (Aberhan and Kiessling, 2014; Hansen et al., 1993), and 22.5% for bivalves in the chalk facies of Stevns Klint, Denmark (Aberhan and Kiessling, 2014; Heinberg, 1999). Estimates for the magnitude of the extinction are similar despite significant differences in the diversity (in terms of generic richness) of these different benthic molluscan faunas from different palaeolatitudes (Hansen et al., 1993; Raup and Jablonski, 1993; Heinberg, 1999; Aberhan and Kiessling, 2014; Crame et al., 2014). Our data are thus also in broad agreement with the

suggestion made using global databases, albeit analysed at stage level, that there was no latitudinal variation to the K–Pg losses in these groups (Raup and Jablonski, 1993). A latitudinal diversity gradient provided no protection against mass extinction for molluscs at the K–Pg boundary, with the Polar Regions seemingly no safer than the tropics.

Previous studies have postulated that longer-term biotic changes recorded in the James Ross Basin, such as changes in molluscan faunas during the Campanian–Maastrichtian interval, were 'harbingers' of the K–Pg extinction itself (Zinsmeister et al., 1989; Elliot et al., 1994; Crame et al., 1996). We infer that these changes are more likely recording high-latitude biotic response to environmental perturbations on a longer time-scale, such as the long-term global cooling trend evident at this time (Friedrich et al., 2012; Linnert et al., 2014; Witts et al., 2015), and are thus independent of events at the K–Pg boundary.

Nevertheless, existing geochemical, palaeontological and sedimentological data sets from Seymour Island support ideas of a relationship between local palaeoenvironmental changes and marine diversity during the Maastrichtian–Paleocene interval in Antarctica. The lower part of the succession on Seymour Island contains evidence for predominantly cool ocean temperatures during the early Maastrichtian (Dutton et al., 2007; Tobin et al., 2012; Bowman et al., 2013) (Figure 4.2; Fig. B.7) supporting records from lower latitudes (Friedrich et al., 2012; Linnert et al., 2014). Although lithological homogeneity and lack of key horizons makes a detailed analysis of water depth changes difficult, the shallow water setting proposed for this interval (Macellari, 1988; Olivero et al., 2007; Olivero, 2012), correlates to a period of low molluscan diversity in our sections (Figure 4.2 and Figure 4.3; Fig. B.7). A transition to a more offshore environment occurred during the mid-Maastrichtian (Macellari, 1988; Olivero et al., 2007; Olivero, 2012), under a variable temperate climate with fluctuating temperatures and occasional 'cold-snaps' when sea ice may have developed on the Antarctic margin (Tobin et al., 2012; Bowman et al., 2013; Bowman et al., 2014). This interval is linked to an increase in diversity and establishment

of a more diverse and stable benthic and nektonic molluscan fauna (Figure 4.2; Figure 4.3).

Warming in the late Maastrichtian occurred alongside a slight facies change, with more frequent deposition of glauconite-rich horizons perhaps indicative of subtle changes in water depth and the nature of the substrate (Macellari, 1988). This may account for the minor increase in benthic extinction rates recorded in this interval (Fig. B.7). Warming is followed by further cooling in the latest Maastrichtian (Tobin et al., 2012; Bowman et al., 2014; Kemp et al., 2014; Bowman et al., In Press), and evidence for an overall shallowing of the basin into the Paleocene (Macellari, 1988; Elliot et al., 1994; Olivero et al., 2007; Olivero, 2012). The cluster of last occurrences at the K–Pg boundary appear unrelated to significant facies change.

Integration of our new pyrite petrographic analysis with these data reveals a broadly inverse relationship between diversity in the López de Bertodano Formation and the occurrence of framboid-rich samples. This suggests that, contrary to previous studies of the López de Bertodano Formation that assumed fully oxic conditions throughout deposition (Macellari, 1988; Zinsmeister, 1998; Olivero et al., 2007), fluctuating redox conditions on the Maastrichtian sea-floor may have been a further factor influencing benthic diversity. Initial low molluscan diversity during the early Maastrichtian also corresponded with evidence for the periodic development of shallow water dysoxia, anoxia and even euxinia (Figure 4.4; Fig. B.8). Significantly, the apparent reappearance of a large number of range-through taxa from underlying formations (Table B.1) in the mid-López de Bertodano Formation indicates that early Maastrichtian environmental fluctuations were not accompanied by any significant extinction events, at least in the benthos, and any reduction in diversity was temporary (Figure 4.2 and Figure 4.3). Oxygenation levels and benthic diversity subsequently improved, although framboid evidence for redox conditions fluctuating between dysoxia and anoxia–euxinia is present in samples in at least three distinct levels in the upper López de Bertodano Formation (Figure 4.4; Fig. B.8).

Interestingly, these include the glauconite-rich sandstone horizons immediately above the K–Pg boundary, suggesting the development of local bottom-water anoxia in the aftermath of the extinction. Although the occurrence of similar conditions associated with another, older, glauconite-rich horizon in the Maastrichtian suggest this is not unusual (Fig. B.8), certain characteristics of the extinction interval suggest the development of harsh conditions in the water column as well as on the sea-floor at this time.

These characteristics include the loss of pelagic and nektonic/nektobenthic macrofauna (Witts et al., 2015; Martin, 2006) (Figure 4.2), disruption to planktonic microfauna and flora (Harwood, 1988; Huber, 1988; Bowman et al., 2012), and occurrence of large numbers of articulated fish remains immediately above the K–Pg boundary on Seymour Island (Zinsmeister, 1998). The origin of recurrent 'fish-kill' events in this short stratigraphic interval is unclear; Zinsmeister (1998) suggested they may have resulted from large-scale algal or bacterial blooms, or unspecified changes in water chemistry following the end-Cretaceous impact event. Such blooms of opportunistic primary producers and geographically heterogeneous high-stress marine conditions have been hypothesized worldwide in the aftermath of the Chicxulub impact (Alegret and Thomas, 2009), following perturbation or collapse of the global marine food web due to mass extinction of many groups of phytoplankton (Schulte et al., 2010).

In Antarctica, local benthic anoxia likely led to enhanced preservation potential for victims of the subsequent 'fish-kills' by limiting the activity of benthic scavengers. The loss of common scavenging taxa such as many epifaunal gastropods and echinoids in the aftermath of the extinction event on Seymour Island (Figure 4.2), may also have favoured enhanced preservation of fish carcasses. The benthos of this immediate post-extinction interval is also characterized by unusual high abundance 'blooms' of presumably opportunistic molluscan taxa, primarily represented by the infaunal bivalve *Lahillia larseni* and the aporrhaid gastropod *Struthiochenopus hurleyi* (Crame et al., 2004; Stilwell et al., 2004).

Pyrite framboid data probably indicate a return to oxygenated sea-floor conditions above the boundary interval (Fig. B.8). However, successive acmes of several species of dinoflagellate cyst (Bowman et al., 2012), and an increase in diatom resting spores (Harwood, 1988) in the 60 m stratigraphic interval above the K–Pg boundary may indicate the persistence of unstable marine conditions and a perturbed marine ecosystem following the extinction on Seymour Island. Despite a peak in origination rates at and above the K–Pg interval (Figure 4.3), significant recovery of benthic species richness only commenced, ~350 kyr after the extinction, just prior to initial deposition of the Sobral Formation (Crame et al., 2014; Bowman et al., In Press). This provides some support for the hypothesized continuation of unusual environmental conditions into the early Danian.

In summary, intensive collecting of marine fossils from the Maastrichtian-earliest Paleocene López de Bertodano Formation on Seymour Island, Antarctica, reveals that, contrary to all previous studies, there was a single, abrupt extinction at the end of the Cretaceous at this location. We find no counterevidence for any precursor biotic crises at this high southern palaeolatitude. Our results support the idea that a sudden event such as the Chicxulub bolide impact and associated rapid environmental deterioration (Molina et al., 2006; Schulte et al., 2010; Jiang et al., 2010) was the most probable cause of the K–Pg mass extinction. Although recent dating estimates for onset of the main phase of the Deccan Traps large igneous province do suggest a complex temporal coincidence between volcanism and impact at this time (Schoene et al., 2014; Renne et al., 2015), the precise environmental effects of this volcanism on global ecosystems remain unclear (Schmidt et al., 2016).

Prior to the K–Pg extinction interval, minor diversity fluctuations in Antarctica were linked to local water depth changes with associated changes in seawater temperature. Pyrite framboid data indicates fluctuations in local benthic oxygenation levels may also have played a role in controlling diversity of the marine fauna. In conjunction with the temporary absence of scavenging benthic taxa in the immediate aftermath of the mass extinction event, this

provided favourable conditions for fossilization of well-preserved fish directly above the K–Pg boundary in Antarctica, perhaps related to transient unstable marine conditions following the Chicxulub impact.

Although evidence for rapid climate oscillations and a late Maastrichtian warming event are present on Seymour Island (Tobin et al., 2012; Bowman et al., 2013; Bowman et al., 2014), they are not associated with any significant diversity decline in the marine macrofauna prior to the K–Pg boundary. This argues against models that invoke rapid Maastrichtian climate changes as a significant stressor on pre-extinction communities (Archibald et al., 2010; Renne et al., 2013). The losses among the benthic invertebrates in Antarctica due to the K–Pg extinction are closely comparable with those recorded from lower latitudes, despite the overall lower diversity of the Antarctic molluscan fauna, and do not support the theory of latitudinal extinction selectivity during this major mass extinction event (Jiang et al., 2010; Raup and Jablonski, 1993).

4.5 Methods

4.5.1 Sampling strategy

Our primary data are derived from extensive macrofossil collecting in three sedimentary section lines spanning the López de Bertodano Formation and K–Pg interval. All sub-sections that comprise the composite section were measured perpendicular to strike using a Jacob's staff and tape measure. Fieldwork was undertaken during three field seasons to Seymour Island and encompassed the main outcrop of the López de Bertodano Formation in the southern part of the island (Crame et al., 2004; Crame et al., 2014; Bowman et al., 2014; Bowman et al., In Press). The island is ice-free and exposure excellent.

Sections DJ.959, DJ.957, DJ.952 and DJ.953 were made during the 1999 field season, and are located close to the central portion of the outcrop, commencing in the mid-levels of the López de Bertodano Formation representing the informal mapping units Klb7–9 and Ktplb10 of Macellari

(1988) (Figure 4.1). Section D5.251 (comprising sub-sections D5.212, D5.215, D5.218, D5.219, D5.220, D5.222 and D5.229) was measured and sampled during the 2006 field season and runs perpendicular to strike and approximately parallel to the southern coast of the island, beginning within the uppermost levels of the Snow Hill Island Formation. Sections D9.205, D9.206 and D9.207 were located at the northern end of the outcrop during the 2010 field season, and begin immediately below the K–Pg boundary. All three composite sections extend through the K–Pg boundary and the informal mapping unit Ktplb10 to the unconformable contact with the overlying Sobral Formation (Figs B.1–B.4).

Macrofossil collections were made systematically at varying scales during the different field seasons, with sample bins ranging on average from 1m to intervals 10–15m thick (see Figs B.2–B.4 and Section B.1 for illustration of sampling intervals and bin length in each individual section line). Changes in the size of sample bins within and between individual section lines were necessary during field collecting due to the nature of the 'scarp and dip-slope' topography that predominates on southern Seymour Island, whereby fossils are invariably more common on dip-slopes than scarps.

Collections were made at each station until a representative collection of all the obvious macrofossil types had been obtained; just as it was not possible to standardize sample bin size, so it was not possible to use a standard collecting time either. For these reasons we chose to focus only on range-through data and standing species richness to estimate changes in taxonomic diversity across the K–Pg boundary. In Fig. B.7, we have plotted variations in sample species richness through all three of our sections, including data from Zinsmeister (1998) (Fig. B.6). These all show fairly regular variation around a sample mean, but no major trends that could be linked to any obvious form of either local or global environmental variation. Such small-scale fluctuations in species richness are an inevitable consequence of specimen collection in a scarp and dip-slope terrain, and are unlikely to represent any true response to environmental change.

162

Correlation between section lines and the construction of a composite section was achieved using several stratigraphic tie-points, notably the glauconite-rich beds that mark the K–Pg boundary and a further prominent glauconite-rich horizon present in all section lines ~174m below the K–Pg. To enable a full analysis of extinction patterns at the K–Pg boundary, field data derived from British Antarctic Survey sampling was also supplemented with additional data from Zinsmeister (1998) (Fig. B.6). These macrofossil collections were taken from a series of short (20 m) sections measured and sampled during a detailed along-strike mapping study of the K–Pg boundary across ~5.5 km of southern Seymour Island. When plotting these additional fossil occurrences the base of the 'Lower Glauconite' horizon of Zinsmeister (1998) is taken as a reference plane, and assumed to be equivalent to the base of the glauconite-rich beds and K–Pg boundary in our composite measured section at a stratigraphic height of 1,007.5m (Bowman et al., 2012; Bowman et al., 2014). For all these stratigraphic correlations, we assume planar bedding along strike. The unconformable contact at the base of the Sobral Formation is also useful as a tie-point, although it can be demonstrated that on a regional scale the degree of erosion of the upper levels of the López de Bertodano Formation changes subtly along strike across the island (Macellari, 1988; Montes et al., 2010).

The occurrence of glauconite-rich horizons, such as those that mark the K–Pg interval, suggest periods of slower, condensed sedimentation. The base of these units appears gradational in the field (Elliot et al., 1994; Zinsmeister, 1998; Crame et al., 2004; Bowman et al., In Press) and high-resolution palynological studies (Bowman et al., 2013; Bowman et al., In Press) show they are not associated with significant sedimentary hiatuses in the studied sections, but probably represent conformable facies boundaries (Bowman et al., In Press).

4.5.2 Fossil data analysis

Over 6,000 fossils of benthic molluscs (bivalves and gastropods) were examined during this study, with 5,710 identified to at least generic level, these have been combined with 4,700 cephalopod macrofossils (Witts et al.,

2015) for an examination of overall diversity of the molluscan fauna. Following taxonomic identification and reassessment (Section B.1), first and last occurrence data from individual section lines were used to construct a composite range chart using the stratigraphic tie points outlined above. Changes in stratigraphic bin size were accounted for by taking the base of the stratigraphic bin in which a species first occurred as the first appearance, and the top of the stratigraphic bin in which a species last occurred as the last appearance. While this introduces a degree of error into the results (for example, where a sampling bin straddles the K–Pg boundary in a single stratigraphic section), it is negligible given the expanded nature of the succession.

A presence–absence data set based on this range data (see Appendix B tables) was used to calculate standing species richness variations throughout the section, supplemented with additional collections from the overlying Paleocene Sobral Formation (Crame et al., 2014; Bowman et al., In Press) and a literature review to identify range-through taxa from older, underlying formations (Table B.1). To assess changing rates of biotic turnover through the succession, the presence–absence data set was split into 10m bins and both extinction (E_r) and origination (O_r) rates calculated for each 10m bin using the boundary-crosser methodology outlined by Foote (2000):

$$O_r = - ln \frac{N_{bt}}{N_{ft} + N_{bt}}$$

Equation 1

$$E_r = - ln \frac{N_{bt}}{N_{bl} + N_{bt}}$$

Equation 2

where N_{bt} = number of range-through taxa, N_{ft} =number of taxa that originate within any given 10m bin and cross the top boundary of that bin and N_{bl} -= number of taxa that cross the bottom boundary of the bin but have their last occurrence within the bin. These should be considered as 'extinction' and 'origination' rates only in the local context, and are not expressed relative to

164

bin duration. Available evidence suggests overall sedimentation rates remained high throughout deposition of the López de Bertodano Formation at 0.1–0.2mm per year (Tobin et al., 2012) (Fig. B.5) indicating that any variation in bin duration is likely to have a negligible effect on the magnitude of biotic turnover rates.

To test the hypothesis of multiple extinction events and visually assess the pattern of taxonomic turnover more generally through the Maastrichtian, we also employed the stratigraphic abundance method of Meldahl (1990). Stratigraphic abundance (S, the percentage of sample intervals in which a given taxon occurs) was calculated using a recently modified method (Song et al., 2012) to enable us to include data from all three studied sedimentary sections in addition to data from Zinsmeister (1998):

$$S = (\frac{N_{occurrence\ 1} + N_{occurrence\ 2} + N_{occurrence\ 3}}{(N_{sample\ 1} + N_{sample\ 2} + N_{sample\ 3})} \times 100$$

Equation 3

where $N_{occurrence\ 1}$ is the number of occurrences of a given species in section 1, and $N_{sample\ 1}$ is the number of samples in section 1. A plot of S versus last occurrence provides a visual estimate of the likely position of an extinction horizon based on the disappearance of the most common taxa in an assemblage (Figure 4.3c), and along with a plot of the frequency distribution of last occurrences in a stratigraphic section (Fig. B.7), can be compared with simulated models of sudden and gradual extinction (Meldahl, 1990). We included all molluscan taxa in this analysis, including a reanalysis of the nekton to include additional data from field collections made in 2010 (data reanalysed from Witts et al., 2015). To investigate the extent to which the data is influenced by the 'Signor-Lipps Effect' (Signor and Lipps, 1982) due to the sampling strategy, 50 and 95% confidence intervals were calculated for all benthic taxa with >5 occurrences during the Maastrichtian within two BAS section lines (sections A and B, Figure 4.1c). We applied the 'classical' method as summarised by Marshall (2010), and illustrate these confidence intervals as range extensions (Figs B.3 and B.4) using the following equation:

$$r_{C,i} = [(1 - C)^{-1/(H-1)} - 1]R$$

Equation 4

Average gap size between fossil occurrences also provides an unbiased point estimate of the true time of appearance or disappearance in any given stratigraphic section assuming random fossil recovery (Marshall, 2010), and was calculated for the same taxa using:

$$r_{unbiased} = R/(H - 1)$$

Equation 5

where $r_{C,i}$ is the length of the range extension, $r_{unbiased}$ is the average gap between fossil occurrences as a percentage of that taxon's stratigraphic range, C is the desired confidence level (expressed as a decimal; 0.5 and 0.95), H is the number of observed fossil occurrences for a species in an individual section line and R is the observed stratigraphic range of the taxon in the same section line. Confidence intervals were only calculated for data from two sections directly sampled by the authors (sections A and B in Figure 4.1c), both of which have extended records from the Maastrichtian into the Paleocene. Because of the constraints of the sampling strategy outlined above, confidence intervals were not applied to any composite data set that is derived only from range-through data (Figure 4.2).

4.5.3 Pyrite petrography

Polished blocks were made from 21 bulk sediment samples collected throughout composite section D5.251 (Table B.2). These were examined using an FEI Quanta 650 scanning electron microscope (SEM) in back-scatter mode to identify microfacies and quantify the diameter of pyrite framboid populations. The size and distribution of pyrite framboids in both ancient and modern sediments are interpreted to result from local redox conditions (Wilkin et al., 1996; Wignall and Newton, 1998). In modern environments, syngenetic framboids form in a narrow iron reduction region developed at the redox boundary, but cease growing in the underlying fully anoxic sulphate reduction

zone. Under fully euxinic conditions (where free H_2S occurs in the water column), syngenetic framboids grow to a maximum diameter of 6–7 µm in the water column before gravity causes them to sink to the seabed (Wignall and Newton, 1998). Framboid populations formed under these conditions will exhibit both a small size range and a small s.d. In dysoxic settings, conditions on the seabed are often weakly oxygenated, leading to framboid development in the pore water of the underlying sediments. Here the size range is controlled primarily by the availability of reactants and therefore framboid populations typically grow to larger sizes (up to 20 µm) with a correspondingly higher s.d. (Wilkin et al., 1996). Figure B.8 presents a 'Box and Whisker' plot showing the stratigraphic distribution of the sampled horizons and illustration of framboid populations.

4.6 References

Aberhan, M., Kiessling, W., 2014. Rebuilding biodiversity of Patagonian marine molluscs after the end-Cretaceous mass extinction. *PLoS ONE* **9**, e106269.

Aberhan, M., Kiessling, W., 2015. Persistent ecological shifts in marine molluscan assemblages across the end-Cretaceous mass extinction. *Proceedings of the National Academy of Science, USA* **112**, 7207–7212.

Alegret, L., Thomas, E., 2009. Food supply to the seafloor in the Pacific Ocean after the Cretaceous/Paleogene boundary event. *Marine Micropalaeontology* **73**, 105–116.

Alvarez, L.W., Alvarez, W., Asaro, F., Michel, H.V., 1980. Extraterrestrial cause for the Cretaceous-Tertiary Extinction. *Science* **208**, 1095–1108.

Archibald, J.D., Clemens, W.A., Padian, K., Rowe, T., MacLeod, N., Barrett, P.M., Gale, A., Holroyd, P., Sues, H.-D., Arens, N.C., Horner, J.R., Wilson, G.P., Goodwin, M.B., Brochu, C.A., Lofgren, D.L., Hurlbert, S.H., Hartman, J.H., Eberth, D.A., Wignall, P.B., Currie, P.J., Weil, A., Prasad, G.V.R., Dingus, L., Courtillot, V., Milner, A., Milner, A., Bajpai, S., Ward, D.J., Sahni, A., 2010. Cretaceous extinctions: multiple causes. *Science* **328**, 973.

Bambach, R.K., 2006. Phanerozoic biodiversity mass extinctions. *Annual Reviews of Earth and Planetary Science* **34**, 127–155.

Beu, A. G., 2009. Before the ice: biogeography of Antarctic Paleogene molluscan faunas. *Palaeogeography Palaeoclimatology Palaeoecology* **284**, 191–226.

Bowman, V. C., Francis, J. E., Riding, J. B., Hunter, S. J., Haywood, A. M., 2012. A latest Cretaceous to earliest Paleogene dinoflagellate cyst zonation from Antarctica, and implications for phytoprovincialism in the high southern latitudes. *Review of Palaeobotany and Palynology* **171,** 40–56.

Bowman, V. C., Francis, J. E., Riding, J. B., 2013. Late Cretaceous winter sea ice in Antarctica? *Geology* **41**, 1227–1230.

Bowman, V. C., Francis, J. E., Askin, R. A., Riding, J. B. Swindles, G. T., 2014. Latest Cretaceous–earliest Paleogene vegetation and climate change at the high southern latitudes: palynological evidence from Seymour Island, Antarctic Peninsula. *Palaeogeography Palaeoclimatology Palaeoecology* **408**, 26–47.

Bowman, V.C. *et al.*, In Press. The Paleocene of Antarctica: Dinoflagellate cyst biostratigraphy, chronostratigraphy and implications for the palaeo-Pacific margin of Gondwana. *Gondwana Research* doi:10.1016/j.gr.2015.10.018 .

Brusatte, S.L., Butler, R.J., Barrett, P.M., Carrano, M.T., Evans, D.C., Lloyd, G.T., Mannion, P.D., Norell, M.A., Peppe, D.J., Upchurch, P., Williamson, T.E. 2015. The Extinction of the Dinosaurs. *Biological Reviews* **90**, 628–642.

Chenet, A. L., Courtillot, V., Fluteau, F., Gerard, M., Quidelleur, X., Khadri, S.F.R., Subbarao, K.V., Thordarson, T., 2009. Determination of rapid Deccan eruptions across the Cretaceous–Tertiary boundary using paleomagnetic secular variation: 2. constraints from analysis of eight new sections and synthesis for a 3500-m-thick composite section. *Journal of Geophysical Research* **114**, BO6103.

Crame, J. A., Lomas, S. A., Pirrie, D., Luther, A., 1996. Late Cretaceous extinction patterns in Antarctica. *Journal of the Geological Society of London* **153**, 503–506.

Crame, J. A., Francis, J. E., Cantrill, D. J., Pirrie, D., 2004. Maastrichtian stratigraphy of Antarctica. *Cretaceous Research* **25**, 411–423.

Crame, J. A., Beu, A. G., Ineson, J. R., Francis, J. E., Whittle, R. J. & Bowman, V. C., 2014. The early origins of the Antarctic marine fauna and its evolutionary implications. *PLoS ONE* **9**, e114732.

Dutton, A., Huber, B. T., Lohmann, K. C., Zinsmeister, W. J. 2007. High-resolution stable isotope profiles of a dimitobelid belemnite: implications for paleodepth habitat and late Maastrichtian climate seasonality *Palaios* **22**, 642–650.

Elliot, D. H., Askin, R. A., Kyte, F. T., Zinsmeister, W. J, 1994. Iridium and dinocysts at the Cretaceous–Tertiary boundary on Seymour Island, Antarctica: implications for the K–T event. *Geology* **22**, 675–678.

Foote, M., 2000. Origination and extinction components of taxonomic diversity: general problems. *Paleobiology* **26**, 74–102.

Francis, J. E., Poole, I., 2002. Cretaceous and early Tertiary climates of Antarctica: Evidence from fossil wood. *Palaeogeography Palaeoclimatology Palaeoecology* **182**, 47–64 (2002).

Friedrich, O., Norris, R. D., Erbacher, J., 2012. Evolution of middle to Late Cretaceous oceans – a 55 m.y. record of Earth's temperature and carbon cycle. *Geology* **40**, 107–110.

Gradstein, F. M., Ogg, J. G., Schmitz, M. & Ogg, G., 2012. *The Geological Time Scale 2012* Elsevier Science Ltd: Boston.

Hansen, T. A., Farrell, B. R. & Upshaw, B III., 1993. The first 2 million years after the Cretaceous–Tertiary boundary in east Texas: rate and paleoecology of the molluscan recovery. *Paleobiology* **19**, 251–265.

Harwood, D. M., 1988. Upper Cretaceous and lower Paleocene diatom and silicoflagellate biostratigraphy of Seymour Island, eastern Antarctic Peninsula. In: Feldmann, R.M., Woodburne, M.O. (Eds.), *Geology and Paleontology of Seymour Island, Antarctic Peninsula*. Geological Society of America, Memoirs **169,** 55–130.

Hathway, B., 2000. Continental rift to back-arc basin: Jurassic–Cretaceous stratigraphical and structural evolution of the Larsen Basin, Antarctic Peninsula. *Journal of the Geological Society London* **157**, 417–432.

Heinberg, C., 1999. Lower Danian bivalves, Stevns Klint, Denmark. Continuity across the K/T boundary. *Palaeogeography Palaeoclimatology Palaeoecology* **154**, 87–106.

Huber, B. T., 1988. Upper Campanian–Paleocene foraminfera from the James Ross Island region, Antarctic Peninsula. In: Feldmann, R.M., Woodburne,

M.O. (Eds.), *Geology and Paleontology of Seymour Island, Antarctic Peninsula*. Geological Society of America, Memoirs **169,** 163–252.

Jablonski, D., 1998. Geographic variation in the molluscan recovery from the end-Cretaceous extinction. *Science* **279**, 1327–1330.

Jiang, S., Bralower, T. J., Patzkowsky, M. E., Kump, L. R., Schueth, J. D., 2010. Geographic controls on nannoplankton extinction across the Cretaceous/Paleogene boundary. *Nature Geoscience* **3**, 280–285.

Keller, G., Adatte, T., Pardo, A., Bajpai, S., Khosla, A., Samant, B., 2010. Cretaceous extinctions: evidence overlooked. *Science* **328**, 974–975.

Kemp, D. B., Robinson, S.A., Crame, J.A., Francis, J.E., Ineson, J., Whittle, R.J., Bowman, V.C., O'Brien, C., 2014. A cool temperate climate on the Antarctic Peninsula through the latest Cretaceous to early Paleogene. *Geology* **42**, 583–586.

Krug, A.Z., Jablonski, D., Valentine, J.W., 2009. Signature of the end-Cretaceous mass extinction in the modern biota. *Science* **323**, 767–771.

Lewis, J., Harris, A. S. D., Jones, K. J., Edmonds, R. L., 1999. Long term survival of marine planktonic diatoms and dinoflagellates in stored sediment samples. *Journal of Plankton Research* **21**, 343–354.

Linnert, C., Robinson, S.A., Lees, J.A., Bown, P.R., Pérez-Rodriguez, I., Petrizzo, M.R., Falzoni, F., Littler, K., Arz, J.A., Russell, E.E. 2014. Evidence for global cooling in the Late Cretaceous. *Nature Communications.* **5**, 4194, doi:10.1038/ncomms5194.

Little, C.T.S., Birgel, D., Boyce, A.J., Crame, J.A., Francis, J.E., Kiel, S., Peckmann, J., Pirrie, D., Rollinson, G.K., Witts, J.D., 2015. Late Cretaceous (Maastrichtian) shallow water hydrocarbon seeps from Snow Hill and Seymour Islands, James Ross Basin, Antarctica. *Palaeogeography Palaeoclimatology Palaeoecology* **418**, 213–228.

Macellari, C.E., 1988. Stratigraphy, sedimentology and paleoecology of Upper Cretaceous/Paleocene shelf-deltaic sediments of Seymour Island (Antarctic Peninsula). In: Feldmann, R.M., Woodburne, M.O. (Eds.), *Geology and*

Paleontology of Seymour Island, Antarctic Peninsula. Geological Society of America, Memoirs **169**, pp. 25–53.

Marshall, C. R., 2010. in: *Quantitative methods in paleobiology.* (eds Alroy, J. and Hunt, G.) The Palentological Society Papers **16**, 291–316.

Martin, J. E. Biostratigraphy of the Mosasauridae (Reptilia) from the Cretaceous of Antarctica. In: Francis, J.E., Pirrie, D., Crame, J.A. (Eds.), *Cretaceous–Tertiary high-Latitude Palaeoenvironments, James Ross Basin, Antarctica*. Special Publication vol. **258**. Geological Society, London, pp. 101–108.

McArthur, J. M., Thirlwall, M. F., Engkilde, M., Zinsmeister, W. J. & Howarth, R. J. 1998. Strontium isotope profiles across K/T boundary sequences in Denmark and Antarctica. *Earth and Planetary Science Letters* **160**, 179–192.

McGhee, G.R., Clapham, M.E., Sheehan, P.M., Bottjer, D.J., Droser, M.L., 2013. A new ecological severity ranking of major Phanerozoic biodiversity crises. *Palaeogeography Palaeoclimatolology Palaeoecology* **283**, 260–270.

Meldahl, K.H., 1990. Sampling, species abundance, and the stratigraphic signature, of mass extinction: a test using Holocene tidal flat molluscs. *Geology* **18**, 890–893.

Molina, E., Alegret, L., Arenillas, I., Arz, J.A., Gallala, N., Hardenbol, J., von Salis, K., Steurbaut, E., Vandenberghe, N., Zaghbib-Turki, D., 2006. The global boundary stratotype section and point for the base of the Danian stage (Paleocene, Paleogene, "Tertiary", Cenozoic) at El Kef, Tunisia – original definition and revision. *Episodes* **29**, 263–273.

Montes, N., Nozal, F., Santillana, S., Marenssi, S. A., Olivero, E. B., 2010. Mapa geológioco de la Isla Marambio (Seymour). Escala 1:20,000. *Inst. Ant. Arg. & Inst. Geol. Min. España.*

Olivero, E.B., Ponce, J.J., Marsicano, C.A., Martinioni, D.R., 2007. Depositional settings of the basal López de Bertodano Formation, Maastrichtian, Antarctica. *Revista de la Asociación Geológica Argentina*. **62**, 521–529.

Olivero, E. B., 2012. Sedimentary cycles, ammonite diversity and palaeoenvironmental changes in the Upper Cretaceous Marambio group, Antarctica. *Cretaceous Research* 34, 348–**366**.

Pirrie, D., Crame, J. A., Lomas, S. A., Riding, J. B., 1997. Late Cretaceous stratigraphy of the Admiralty Sound region, James Ross Basin, Antarctica. *Cretaceous Research* **18,** 109–137.

Powell, M. G., MacGregor, J., 2011. A geographic test of species selection using planktonic foraminifera during the Cretaceous/Paleogene mass extinction. *Paleobiology* **37**, 426–437.

Punekar, J., Mateo, P., Keller, G., 2014. Effects of Deccan volcanism on paleoenvironment and planktonic foraminifera: a global survey. In: *Volcanism, Impacts, and Mass Extinctions: Causes and Effects*. (eds Keller, K. & Kerr, A. C.) Geological Society of America Special Publications **505**, SPE504–505.

Raup, D.M., Sepkoski, J.J. 1982. Mass extinctions in the marine fossil record. *Science* **215**, 1501–1503.

Raup, D. M., Jablonski, D., 1993. Geography of end-Cretaceous marine bivalve extinctions. *Science* **260**, 971–973.

Renne, P. R., Deino, A.L., Hilgen, F.J., Kuiper, K.F., Mark, D.F., Mitchell, W.S.III., Morgan, L.E., Mundil, R., Smit, J., 2013. Time scales of critical events around the Cretaceous–Paleogene boundary. *Science* **339**, 684–687 (2013).

Renne, P.R., Sprain, C.J., Richards, M.A., Self, S., Vanderkluysen, L., Pande, K., 2015. State shift in Deccan volcanism at the Cretaceous–Paleogene boundary, possibly induced by impact. *Science* **350**, 76–78.

Ribeiro, S., Berge, T., Lundholm, N., Andersen, T.J., Abrantes, F., Ellegaard, M., 2011. Phytoplankton growth after a century of dormancy illuminates past resilience to catastrophic darkness. *Nature Commsunications* **2**, doi:10.1038/ncomms1314.

Richards, M. A., Alvarez, W., Self, S., Karlstrom, L., Renne, P.R., Manga, M., Sprain, C.J., Smit, J., Vanderkluysen, L., Gibson, S.A., 2015. Triggering of the

largest Deccan eruptions by the Chicxulub impact. *Geological Society of America Bulletin* **127**, 1507–1520.

Scasso, R. A., Olivero, E. B., Buatois, L., 1991. Lithofacies, biofacies, and ichnoassemblage evolution of a shallow submarine volcaniclastic fan-shelf depositional system (Upper Cretaceous, James Ross Island, Antarctica). *Journal of South American Earth Science* **4,** 239–260.

Schmidt, A., Skeffington, R.A., Thordarson, T., Self, S., Forster, P.M., Rap, A., Ridgwell, A., Fowler, D., Wilson, M., Mann, G.W., Wignall, P.B., Carslaw, K.S., 2016. Selective environmental stress from sulphur emitted by continental flood basalt eruptions. *Nature Geoscience* **9**. 77–82 (2016).

Schoene, B., Samperton, K.M., Eddy, M.P., Keller, G., Adatte, T., Bowring, S.A., Khadri, S.F.R., Gertsch, B., 2014. U-Pb geochronology of the Deccan Traps and relation to the end-Cretaceous mass extinction. *Science* **347**, 182–184.

Schulte, P.D., Alegret, L., Arenillas, I., Arz, J.A., Barton, P.J., Bown, P.R., Bralower, T.J., Chisteson, G.L., Claeys, P., Cockell, C.S., Collins, G.S., Deutsch, A., Goldin, T.J., Goto, K., Grajales-Nishimura, J.M., Grieve, R.A.F., Gulick, S.P.S., Johnson, K.R., Kiessling, W., Koeberl, C., Kring, D.A., MacLeod, K.G., Matsui, T., Melosh, J., Montanari, A., Morgan, J.V., Neal, C.R., Nichols, D.J., Norris, R.D., Pierazzo, E., Ravizza, G., Rebolledo-Vieyra, M., Reimold, W.U., Robin, E., Salge, T., Speijer, R.P., Sweet, A.R., Urrutia-Fucugauchi, J., Vajda, V., Whalen, M.T., Willumsen, P.S., 2010. The Chicxulub asteroid impact and mass extinction at the Cretaceous-Paleogene boundary. *Science* **327**, 1214–1218.

Signor, P.W., Lipps, J.H., 1982. Sampling bias, gradual extinction patterns, and catastrophes in the fossil record. In: Silver, L.T., Schulz, P.H. (Eds.), *Geological Implications of Large Asteroids and Comets on the Earth*. Geol. Soc. Am. Spec. Publ. **190**, pp. 291–296.

Song, H., Wignall, P. B., Tong, J. Yin, H., 2012. Two pulses of extinction during the Permian–Triassic crisis. *Nature Geoscience* **6**, 52–56.

Stilwell, J. D., 2002. Geological exploration of Cockburn Island, Antarctic Peninsula. *Polish Polar Research* **23,** 47–73.

Stilwell, J. D., Zinsmeister, W. J., Oleinik, A. E., 2004. Early Paleocene mollusks of Antarctica: systematics, paleoecology and paleogeographic significance. *Bulletins of American Paleontology* **367**, 1–89.

Thibault, N., Gardin, S. 2010. The nannofossil response to the end-Cretaceous warm event in the tropical Pacific. *Palaeogeography Palaeoclimatology Palaeoecology* **291**. 239–252.

Thibault, N. & Husson, D., 2016. Climatic fluctuations and sea-surface water circulation patterns at the end of the Cretaceous era: Calcareous nannofossil response. *Palaeogeography Palaeoclimatology Palaeoecology* **441**, 152–164.

Tobin, T. S., Ward, P.D., Steig, E.J., Olivero, E.B., Hilburn, I.A., Mitchell, R.N., Diamond, M.R., Raub, T.D., Kirschvink, J.L., 2012. Extinction patterns, $\delta^{18}O$ trends, and magnetostratigraphy from a southern high-latitude Cretaceous–Paleogene section: links with Deccan volcanism. *Palaeogeography Palaeoclimatology Palaeoecology* **350–352**, 180–188.

Wignall, P. B. & Newton, R., 1998. Pyrite framboid diameter as a measure of oxygen deficiency in ancient mudrocks. *American Journal of Science* **298**, 537–552.

Wilkin, R. T., Barnes, H. L. & Brantley, S. L., 1996. The size distribution of framboidal pyrite in modern sediments: an indicator of redox conditions. *Geochimica et Cosmochimica Acta* **60**, 3897–3912.

Witts, J. D., Bowman, V. C., Wignall, P. B., Crame, J. A., Francis, J. E., Newton, R. J., 2015. Evolution and extinction of Maastrichtian (Late Cretaceous) cephalopods from the López de Bertodano Formation, Seymour Island, Antarctica. *Palaeogeography Palaeoclimatology Palaeoecology* **418**, 193–212.

Zinsmeister, W. J., Feldmann, R. M., Woodburne, M. O., Elliot, D. H., 1989. Latest Cretaceous/earliest Tertiary transition on Seymour Island, Antarctica. *Journal of Palaeontology* **63**, 731–738.

Zinsmeister, W. J., 1998. Discovery of fish mortality horizon at the K–T boundary on Seymour Island: re-evaluation of events at the end of the Cretaceous. *Journal of Palaeontology* **72**, 556–571.

Chapter 5 : A biogenic and sedimentary sulphur isotope record across the Cretaceous–Paleogene (K–Pg) boundary in Antarctica: relationship to environmental change, mass extinction and recovery

Witts, J.D., Newton, R.J., Wignall, P.B., Bottrell, S.H., Hall, J.L.O., Francis, J.E., Crame, J.A. A biogenic and sedimentary sulphur isotope record across the Cretaceous–Paleogene (K–Pg) boundary in Antarctica: relationship to environmental change, mass extinction and recovery

5.1 Abstract

The Cretaceous–Paleogene (K–Pg) mass extinction event (66 Ma) had a profound effect on both life and the broader Earth system. Despite the well-studied nature of this extinction event and its effects on global biota and the carbon cycle, the effects on the global sulphur cycle are less well known. This study aims to provide the first record of seawater sulphate sulphur isotope variations across the extended K–Pg mass extinction interval covering both the interval of Deccan trap eruptions and the initial stages of recovery from an expanded and fossiliferous high latitude sedimentary succession on Seymour Island, Antarctica. Using carbonate-associated-sulphate (CAS) from well-preserved marine bivalves, alongside sedimentary sulphide (pyrite) sulphur isotopes this study also constrains local changes in sedimentary sulphur cycling. A rigorous assessment of sample preservation and fidelity of the sulphur isotope record reveal a complex picture, where the preservation of primary CAS records is controlled by the presence and isotopic composition of pyrite contamination, and the degree and diagenetic environment of recrystalisation. The relationship of pyrite and primary-CAS isotopes is partially controlled by the non-steady state behaviour of pore water chemistry driven by changes in sedimentation rate. These processes act to alter primary

seawater signals in both fossil samples and sedimentary sulphides in the sedimentary sub-surface. A primary seawater sulphate record is generated that shows significant variation and rapid rates of change, linked to Maastrichtian palaeoenvironmental and climate change prior to the K–Pg extinction. Some of these changes imply decoupling of the sulphur and carbon cycle during portions of the Maastrichtian. These data also suggest no direct influence of sulphur release from Deccan volcanism and the Chicxulub impact event on the seawater sulphate reservoir during the late Maastrichtian or at the K–Pg boundary itself, probably due to the buffering capacity of the large oceanic reservoir relative to the size of the inputs, and the nature of the target rocks during the impact event. Changes associated with the mass extinction event such as a temporary increase in anoxia and pyrite burial, and an apparent global productivity decrease produce rapid changes in the sulphur cycle in the aftermath of the extinction. Recovery of the sulphur cycle occurs on the same timescale as initial recovery of the carbon cycle, and the first stages of biotic recovery, emphasising close links between the biosphere and geosphere in the aftermath of mass extinction events. Estimates of the likely size of the Cretaceous–Paleogene seawater sulphate reservoir based on paired sulphate and sulphide isotope data and estimated rates of change, suggest it may have been ~50% smaller than today, consistent with existing data from other proxies for this time period. The K–Pg ocean sulphate reservoir was small enough for its isotopic composition to respond rapidly to environmental change. Correlation of the sulphur isotope records with previous work on seasonally resolved shell carbonate-carbon isotopes suggests that a lower sulphate concentration is likely to have underpinned a style of sedimentary biogeochemical cycling quite different from modern, with an increased role for methane. Increased sedimentary production and oxidation of methane at shallower depths in the sediment may therefore have characterised marine sedimentary carbon-cycling during the large portions of the Phanerozoic likely to have had low ocean sulphate.

5.2 Introduction

The Cretaceous–Paleogene (K–Pg) mass extinction event of 66 Ma is not only the most recent of the Phanerozoic 'Big Five' mass extinctions (Bambach, 2006), but also the most well-known and best-studied. The leading hypothesis for the cause of this extinction remains a bolide impact (Alvarez et al., 1980), creating the 180–200 km-wide Chicxulub crater in the Gulf of Mexico (Hildebrand et al., 1991), and leading to rapid and severe global environmental changes and mass extinction (Schulte et al., 2010). However, the K–Pg extinction event occurred during a time of longer-term environmental changes. These include geologically rapid climate (Wilf et al., 2003; Bowman et al., 2013; Thibault, 2016) and sea level (Kominz et al., 2008; Haq, 2014) fluctuations, and large igneous province (LIP) volcanism from the Deccan Traps in India (Schoene et al., 2014; Renne et al., 2015). There remains significant debate as to the importance and relative contributions of each of these to the extinction event itself (e.g. Archibald et al., 2010; Courtillot and Fluteau, 2010; Keller et al., 2010; Schmidt et al., 2016), and even the possibility of cause-and-effect relationships (Richards et al., 2015; Renne et al., 2015).

Surprisingly little is known about how the global sulphur cycle may have responded to the events that surround the K–Pg mass extinction. This is despite the fact that many of the Earth system changes that occurred at this time (e.g. climate change, bolide impact and productivity collapse, LIP volcanism, anoxia) have the potential to affect the global sulphur cycle sufficiently to leave a stratigraphic record of isotopic change.

The global sulphur cycle is also intimately linked to the carbon cycle: Up to 80% of organic matter remineralisation in shallow settings in the modern ocean occurs as a result of microbial sulphate reduction (MSR) in marine sediments (Jorgensen and Kasten, 2006). Coincident changes in the carbon and sulphur cycles are linked by organic matter and pyrite burial, ultimately linked to nutrient flux, productivity, and life (Berner, 1982). Several of these factors vary through time – especially during episodes of rapid environmental

change such as mass extinction events. Despite its importance, there remain fewer records and reconstructions of changes to the sulphur cycle through geological time (see Fike et al., 2015 for a recent review).

The oceans represent the largest reservoir of sulphur at the Earth's surface. Oxidative weathering of sulphide minerals and dissolution of evaporite deposits on land lead to the delivery of sulphate to the oceans via rivers. Volcanism and hydrothermal inputs also constitute a minor flux. Sulphur is removed from the ocean reservoir to the sediment either in an oxidised state (as carbonate associated sulphate (CAS), or evaporites) or reduced state (mainly FeS or FeS_2 (pyrite)) following MSR in marine sediments. It is the balance of these factors which drive the sulphur cycle and control the sulphur isotopic composition of seawater over geological timescales.

Sulphur as seawater sulphate has a long residence time (~10-20 Ma) and a relatively high concentration (29 mM) in the modern ocean (Bottrell and Newton, 2006), and therefore rapid perturbations to its sulphur isotope composition are unlikely. However, a variety of studies have demonstrated that during various periods of environmental change in the Phanerozoic, such as mass extinction events, rapid changes are recorded by sulphur isotope proxies such as sedimentary pyrite and carbonate associated sulphate (CAS) (e.g. Newton et al., 2004; Gill et al., 2011; Schobben et al., 2016). In some cases these can be linked directly to changes in ocean redox structure that relate to mass extinction kill mechanisms and other drivers of such environmental change (e.g. Newton et al., 2004; Schobben et al., 2016). These rapid changes are usually explained by lower concentrations of sulphate in ancient oceans in the geological past, leading to concomitant lower residence times in ancient oceans compared to present day and allowing the cycle to respond rapidly to environmental perturbations. Reconstructions of sulphate concentrations through time lend support to this model (e.g. Algeo et al., 2015), and suggest that examination of sulphur cycle changes through Earth history have the potential to provide new interpretations for the cause and effect of environmental change during mass extinction events.

As a proxy for reconstructing seawater sulphate, CAS relies on trace amounts of sulphate incorporated into biogenic carbonates. Studies on modern biota and limestones indicate CAS faithfully records the isotopic composition of ambient seawater (e.g. Kampschulte et al., 2001; Kampschulte and Strauss, 2004). CAS is resistant to diagenesis (Lyons et al., 2004; Marenco et al., 2008a; 2008b; Gill et al., 2008), and also reproduces the record from other proxies for long-term Phanerozoic sulphur cycle changes such as evaporite minerals and marine barite (Claypool et al., 1980; Paytan et al., 1998; Paytan et al., 2004; Kampschulte and Strauss, 2004).

CAS has also proven to be a robust proxy for sulphur cycle changes during intervals of rapid environmental change throughout the Phanerozoic; including the end-Ordovician (Jones and Fike, 2013), late Devonian (John et al., 2010), and Permo–Triassic (Newton et al., 2004; Song et al., 2014; Schobben et al., 2016) extinction events. CAS also records sulphur cycle changes across various Oceanic Anoxic Events (OAE's) during the Jurassic (Newton et al., 2011; Gill et al., 2011) and Cretaceous (Adams et al., 2010; Owens et al., 2013; Poulton et al., 2015; Gomes et al., 2016). The isotopic composition of sulphide minerals (primarily pyrite) is also useful for examining sulphur cycling in ancient marine sediments, especially when used in conjunction with $\delta^{34}S_{CAS}$ data ($\Delta^{34}S$) (e.g. Algeo et al., 2015). However, its isotope composition is sensitive to local geochemical conditions, and thus untangling signals of global sulphur cycle change is more problematic.

Only two detailed studies from condensed deep water marine sections in Japan (Kajiwara et al., 1992) and Spain (Kaiho et al., 1999) contain stratigraphically constrained sulphur isotope records across the K–Pg boundary from both the latest Cretaceous (Maastrichtian stage, 72.1–66 Ma) and earliest Paleogene (Danian stage, 66–61.6 Ma). Both of these studies suggest changes to the sulphur cycle at the K–Pg boundary. Their interpretations primarily focus on the development of a period of transient ocean anoxia following the mass extinction event. However, only one of these studies (Kaiho et al., 1999) produces a record from bulk rock CAS as a proxy for seawater sulphate. Both studies also cover an extremely restricted

stratigraphic interval centred on the K–Pg boundary itself, which does not overlap with all the events that have a potential impact on the K–Pg mass extinction such as the possible effects of Deccan volcanism. They are also unable to examine longer-term changes during the Late Cretaceous or early Paleogene which could have an effect on the sulphur cycle, such as apparently rapid and dynamic climate, sea level and associated carbon cycle fluctuations (Miller et et al., 2005; Voigt et al., 2012; Thibault, 2016).

Under some circumstances, the isotopic signal from CAS can be altered towards either positive or negative values. The use of biogenic calcite and aragonite for CAS studies as opposed to bulk sedimentary carbonate reduces the risk of contamination of the primary isotope signal from sedimentary sulphide and its weathering products (Staudt and Schoonen, 1995; Kampschulte and Strauss, 2004). Biogenic carbonates also contain a higher concentration of CAS when compared to bulk sedimentary limestones, buffering them from diagenetic alteration (Staudt and Schoonen, 1995) and making them potentially the best source for the generation of CAS records. Nevertheless, careful consideration must still be made of possible diagenetic alteration and contamination of samples, as well as ensuring the data are placed in a sedimentary and palaeoenvironmental context before interpretation (e.g. Fike et al., 2015).

This study aims to generate records from biogenic CAS and bulk sedimentary (pyrite) sulphur from an expanded and fossiliferous high latitude Cretaceous–Paleogene section located in the James Ross Basin, Antarctica. The overall aim is to examine sulphur cycle changes before, during, and after the K–Pg mass extinction event over a ~4 million year time span.

Recently Hall et al. (In Prep) presented intriguing data from these same high latitude sections which have direct relevance to the sulphur cycle. They demonstrated periodic development of exceptionally negative carbon-isotope compositions in bivalve shell aragonite, resolved on a sub-annual resolution. They suggested these recorded periods where carbon derived from the anaerobic oxidation of methane (AOM) dominated the bottom water dissolved inorganic carbon (DIC) pool, and that the cyclic nature of the signal indicated

that the system of methane production or oxidation must have been sensitive to environmental variables on a seasonal timescale. Additional evidence for methane generation and flux in the Cretaceous of the James Ross Basin is provided by Little et al. (2015), who describe similar negative carbon isotope signatures in rare authigenic burrow-filling carbonate derived from methane-oxidation, and putative chemosynthetic bivalve assemblages at distinct stratigraphic levels through the same succession.

In modern marine settings, the high concentration of seawater sulphate controls the depth of AOM in the sediment and ultimately severely limits methane release from sediments (e.g. Jørgensen and Kasten, 2006). Methane produced in sulphate-depleted sub-surface sediment diffuses upwards until it reaches the zone of AOM and becomes oxidised by a consortia of archaea and bacteria (Regnier et al., 2011).

In most modern marine settings, these reactions occur deep enough that there is no influence on the isotopic composition of DIC as recorded in carbonate shell material of marine organisms. However, under hypothesised lower seawater sulphate conditions of the past (e.g. Holt et al., 2014), AOM would likely occur closer to the sediment surface. Thus generation of a seawater sulphur isotope curve, and estimates for concentration of sulphate in the Cretaceous–Paleogene Ocean, would provide additional data on the validity of the signals, and biogeochemical model of Hall et al. (In Prep).

5.2.1 Geological setting

Samples were collected from the shallow marine López de Bertodano Formation, which crops out over 70 km^2 of southern Seymour Island and neighbouring Snow Hill Island (Crame et al., 2004; Olivero et al., 2008), in the James Ross Basin, Antarctic Peninsula (Figure 5.1 A–D). The López de Bertodano Formation forms the upper part of the 3000 m-thick Marambio Group (McArthur et al., 2000; Crame et al., 2004; Olivero, 2012), and records deposition in inner-mid shelf conditions (Macellari, 1988; Olivero, 2012; Bowman et al., 2012) in a large back-arc basin (the Larsen Basin) which opened into the Weddell Sea to the east (Hathway, 2000). During the Late

Cretaceous–Paleocene the Antarctic Peninsula, located to the west of present-day Seymour Island, was an active and emergent volcanic arc (Elliot, 1988; Hathway, 2000). Large quantities of fine-grained sediment were eroded and transported by extensive river systems before accumulating in the back-arc basin (Olivero, 2012; Bowman et al., 2014). Palaeogeographic reconstructions indicate that during the Late Cretaceous the James Ross Basin was located close to its present day high latitude of 65°S (Lawver et al., 1992).

The López de Bertodano Formation itself is unconformably intercalated between the underlying Snow Hill Island Formation and overlying Sobral Formation (Olivero et al., 2008; Crame et al., 2014), and comprises ~1000 m of unconsolidated silty clays and clayey silts, with occasional glauconite–rich horizons becoming more prevalent in the uppermost 300 m. The studied section contains no field evidence for significant hiatuses.
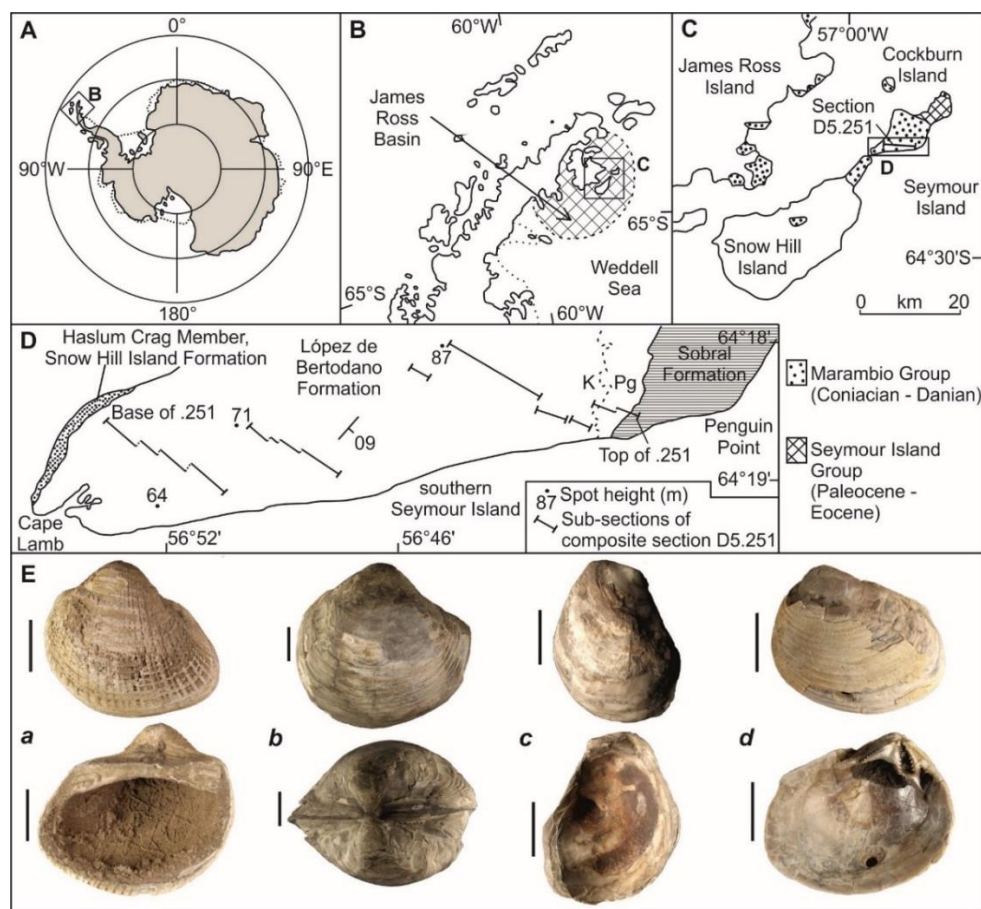
Figure 5.1 (previous page): Location map, geological setting, and images of fossil taxa used in this study. A-C, maps showing present-day geography of Antarctica (A) with the northern Antarctic Peninsula highlighted, location of the James Ross Basin (B), and outcrops of the Marambio and Seymour Island groups on islands in the James Ross Basin. D, measured section D5.251 across the southern portion of Seymour Island is a composite of various sub-sections (see Figure 5.2 for more details). K, Cretaceous; Pg, Paleogene. Position of the K–Pg boundary in the upper portion of the López de Bertodano Formation is indicated by the dashed line. E, examples of fossil bivalve taxa from the López de Bertodano Formation sampled for CAS in this study. *a Cucullaea antarctica; b Lahillia larseni; c Pycnodonte* (*Pycnodonte*) *vesicularis; d Eselaevitrigonia regina.* All scale bars are 2 cm.

An age model based on macrofossil and dinoflagellate biostratigraphy, strontium isotope chemostratigraphy, and magnetostratigraphy (McArthur et al., 1998; Crame et al., 2004; Tobin et al., 2012; Bowman et al., 2013; Witts et al., 2016), as well as the presence of an iridium (Ir) anomaly at the K–Pg boundary (Elliot et al., 1994), dates this unit as Maastrichtian–Danian. This age model indicates high sediment accumulation rates of 0.1–0.2 mm/yr (Elliot et al., 1994; Bowman et al., 2013), indicating that this is one of the most expanded sequences of this age anywhere in the world. The López de Bertodano Formation has thus been the subject of extensive palaeontological and stratigraphic studies over the last 30 years (Feldmann and Woodburne, 1988 and authors therein; Crame et al., 2004; Olivero, 2012; Bowman et al., 2012), and contains the best onshore record in the Southern Hemisphere of the K–Pg mass extinction event (Zinsmeister, 1998; Witts et al., 2015; Witts et al., 2016).

Fossil molluscs from the James Ross Basin are generally thought to show excellent preservation, and have proved suitable for isotope analyses aiming to reconstruct palaeoceanographic conditions (e.g. Pirrie and Marshall, 1990; Ditchfield et al., 1994; McArthur et al., 2000; Tobin et al., 2012). This level of preservation is consistent with the idea that the sediments of the Marambio Group have undergone burial to minimal depths of 1–2km at low temperatures and pressures (Askin and Jacobsen, 1988; Svojtka et al., 2009).

5.3 Material and methods

Macrofossil and bulk sediment samples were collected from southern Seymour Island during the 2006 BAS field season, where a composite measured section (D5.251) comprising individual measured sections (in stratigraphic order; D5.212, .215, .218, .219, .220, .222, .229) was made through the entire 1074m thickness of the López de Bertodano Formation (Figure 5.1D). Sedimentary section lines were measured perpendicular to strike in the field using a Jacobs staff and tape measure. Macrofossil collections were made at varying scales within each sub-section, with sample bins ranging on average from 1 m to intervals 5–6 m thick. All fossil occurrences are illustrated at the mid-point of the stratigraphic bin from which they were collected. Bulk sediment was collected at either 1m or 0.5m intervals through the same section.

Examples of 6 different genera of bivalve mollusc were utilised in this study (Figure 5.1E) covering a stratigraphic range of 166 to 1074m in the composite section (Figure 5.2). Each genus has a well-established mode of life and palaeoecology based on comparison with modern relatives and shell morphology (e.g. Macellari, 1988; Zinsmeister and Macellari, 1988; Crame et al., 2014). Samples included representatives of the genera *Lahillia* (14 samples)*, Cucullaea* (6 samples), *Eselaevitrigonia* (1 sample), *Oistotrigonia* (1 sample) (shallow infaunal suspension feeders), *Pycnodonte* (16 samples) (epifaunal suspension feeder) and *Leionucula* (1 sample) (deep infaunal deposit feeder).

5.3.1 CAS and Pyrite ^{34}S extraction

CAS extraction was carried out using a modified version of a procedure developed at the University of Leeds (e.g. Newton et al., 2004; John et al., 2010; Newton et al., 2011). Fossil bivalve samples taken from composite BAS section D5.251 were screened visually to assess preservation, and shell material was picked from the specimens by hand or using a small chisel and tweezers. These were then washed in an ultrasonic bath for 20–30 minutes to remove any adhering sediment or matrix material. Between 2 and 4 g of shell

material was used for CAS analyses. A total of 58 shell samples were powdered by hand, and powdered samples were left in an excess of sodium hypochlorite (NaOCl) 5% for at least 24 hours, in order to remove sulfur contained in organic matter and sulphate or sulphide minerals. Filtered leachate was retained and its sulphate precipitated as $BaSO_4$ by adjusting the pH of the solution to 2.5 – 3.0 using hydrochloric acid (HCl), warming gently on a hotplate and adding excess 10% $BaCl_2$ solution at ~70°C. Cellulose nitrate filter membranes were then weighed and used to filter the $BaSO_4$ precipitate. The weight of the $BaSO_4$ precipitate was measured to determine the NaOCl-S ($\delta^{34}S_{hypochlorite-S}$) yield.

The bleached and rinsed shell powders were reacted with 50% HCl in an anaerobic chamber in order to release the CAS from the calcite lattice and avoid oxidation of any surviving sulphide minerals. 50% HCl was added until there was no more reaction. The solution was then filtered through a Whatman 40 filter paper to remove any residue. When the leachates were removed from the anaerobic chamber, they were immediately vacuum filtered through a 0.45 μm cellulose nitrate membrane. Great care was taken to minimise the amount of time during which the released CAS was present as dissolved sulphate in the acidic solution as isotopic exchange between sulphate-O and water-O is known to occur increasingly rapidly as pH decreases (Lloyd, 1967). The pH of the filtered solution was adjusted to >9.5 with concentrated ammonia solution and the samples left stirring overnight or longer in order to precipitate out any dissolved metals. Any precipitated metals and the leachate were separated using a Whatman 40 filter paper. Finally, $BaSO_4$ was precipitated from the HCl leachate by adjusting the pH to between 2.5 and 3 with HCl and ammonia solution, and adding 10% $BaCl_2$ solution in excess at ~70°C. The weight of the $BaSO_4$ precipitate was measured to determine the CAS yield. The weight of the NaOCl- and CAS-BaSO4 precipitates was corrected using the weight percent sulfur derived during isotopic analysis. Subsamples of the CAS-$BaSO_4$ precipitate powders were analysed for sulphur and oxygen isotope composition.

Pyrite⁻S was extracted using a modified version of the chromous chloride technique (Canfield et al., 1986; Poulton and Canfield, 2005) on a sub-set of 50 bulk sediment samples from composite BAS section D5.251. Sulphides (in the form of H_2S) were liberated from 0.5–1 g of sediment and trapped as Ag_2S by reaction with $AgNO_3$. Pyrite S (wt%) was determined stoichiometrically from the weight of the Ag_2S precipitate and original sample weights.

5.3.2 CAS and Pyrite ³⁴S and CAS ¹⁸O isotope analysis

Sulphate and Sulphide-S isotopic analyses were performed on a Micromass Isoprime continuous flow mass spectrometer coupled to a Eurovector Elemental Analyser. $BaSO_4$ and Ag_2S were weighed out in tin cups and converted to SO_2 by flash combustion at 1020°C in the presence of oxygen. Excess oxygen was removed by reaction with copper wire at 650°C and the SO_2 separated from other impurities using a chromatographic column and a helium carrier gas. The $\delta^{34}S$ of the sample is derived from the integrated mass 66 and 64 signals from the pulse of sample SO_2, compared to those in an independently introduced pulse of reference gas. These ratios were then calibrated using an internal seawater derived barium sulphate standard (SWS-3B) (+20.3‰) and CP-1 a chalcopyrite inter-laboratory standard (-4.56‰). The value for SWS-3B was calibrated using international standards (NBS-127 (+20.3‰), IAEA-S1 (-0.30‰), NBS-123 (+17.01‰), IAEA-s3 (-32.06‰) to the Vienna-Canyon Diablo Troilite (V-CDT) scale in per mille notation (‰). The precision obtained for repeat analysis of standard materials is better than ±0.3‰ (1 standard deviation).

The isotopic composition of the oxygen in the sulphate ion was measured by mixing $BaSO_4$ precipitates with spectroscopically pure graphite and placing the resulting mixture on platinum foils. These were then degassed and conductively heated under vacuum to about 1100°C. A quantitative yield of CO_2 was achieved by converting any CO to CO_2 using a high voltage applied across platinum electrodes, whilst water was removed cryogenically. The $^{18}O/^{16}O$ ratios were measured on the CO_2 gas using VG SIRA 10 dual inlet, 90° magnetic sector gas source mass spectrometer and calibrated to the Vienna-Standard Mean Ocean Water (V-SMOW) scale using an internal

188

standard (SWS-3B) calibrated to the V-SMOW scale using the international standard NBS-127 (+9.3‰). The precision obtained for the sulphate-O isotope measurements is 0.5‰ (1 standard deviation).

5.3.3 Carbonate carbon and oxygen isotopes ($\delta^{13}C_{carb}$, $\delta^{18}O_{carb}$), Trace Element (ICP-MS), and XRD analyses

Powdered shell material from all 58 samples used in CAS extraction were analysed for their bulk stable carbonate oxygen and carbon isotope compositions using a Micromass Multicarb Sample Preparation System attached to a VG SIRA Mass Spectrometer at the Godwin Laboratory, University of Cambridge. Each run of samples was accompanied by 10 reference carbonates and 2 control samples. The results are reported with reference to the international standard Vienna Pee Dee Belemnite (VPDB). The precision on repeat measurements is better than ±0.06‰ for $\delta^{13}C$ and ±0.08‰ for $\delta^{18}O$.

Shell powders were also analysed for their trace element content (Mg, Ca, Sr, Mn, Fe, Ba) in the labs of the National Oceanographic Center, Southampton. 2 mg of carbonate was dissolved in 20ml of 3% HNO_3 containing 20 ppb Be and 5 ppb In and Re, with the addition of 10ul of concentrated sub-boiled HNO_3. This solution was analysed on a ThermoFisher XSeries2 ICP-MS calibrated using synthetic standards also made up in 3% HNO_3 containing In, Re and Be at the same concentration to act as internal standards.

For XRD analyses, the powdered samples were front loaded into apertured low background silicon holders. The samples were analysed with a Bruker D8 using Cu Kα1 radiation, a Germanium primary monochromator and a Lynx Eye detector. All the samples were scanned at 40kV, 40mA from 2-86°, with an increment of 0.0105° and a count time of 2s/step. The data was analysed using the Bruker's EVA for phase identification and TOPAS Rietveld refinement for phase quantification.

5.3.4 Cathodoluminescence and Scanning Electron Microscopy

Shell material from total of seven specimens was cut and polished into thin sections using standard techniques, these were then examined visually on a

cold cathode cathodoluminescence system (CITL 8200 Mk 3A mounted on a Nikon Optiphot petrological microscope) to identify areas of recrystallized carbonate. The same samples were also analysed using a nFEI Quanta 650 scanning electron microscope (SEM) in both back-scatter and secondary electron mode to identify original shell structure and contaminant sulphide minerals.

5.3.5 Total Organic Carbon (TOC) and Total Sulphur (TS) analyses

A total of 133 samples of bulk sediment from composite section D5.251 were analysed for their Total Organic Carbon content. Approximately 1g of bulk sediment was weighed and then reacted for 24 hours with ~5ml of 10% HCl to remove all carbonate and non-organic material. Excess liquid was drawn off and the samples washed 3 times with milli-Q de-ionised water to remove residual acid and dissolved species. Samples were then dried at 85°C in a heating cabinet for 36 hours and reweighed to establish the mass of carbonate removed. 4-5mg of this acid-washed sediment was then weighed out into tin cups and run in sequence with standards on a Micromass Isoprime continuous flow mass spectrometer coupled to a Eurovector or Elementar Pyrocube Elemental Analyser. Organic carbon was completely combusted at 1020°C or 1150°C (Eurovector and Pyrocube respectively) to CO_2 in a medium of pure oxygen injected into a stream of helium. Excess oxygen was removed by reaction with metallic copper heated to 650°C, H_2O was removed in a magnesium perchlorate trap and the CO_2 separated from other impurities using a chromatographic column or temperature controlled adsorbtion desorption columns (Eurovector and Pyrocube respectively). Calculation of Total Organic Carbon (TOC) was derived from the mass spectrometer traces relative to a sucrose standard, and corrected for weight loss during the acidification process. A sub-set of 50 untreated bulk sediment samples were also analysed for their total sulphur content using a LECO SC-144 DR analyser at the University of Leeds. Relative Standard Deviation (%RSD) on the analysis is estimated at ±10%.

5.4 Results

5.4.1 Sulphur isotopes: $\delta^{34}S_{CAS}$, $\delta^{18}O$ CAS, $\delta^{34}S_{hypochlorite-S.}$ CAS-S and $\delta^{34}S_{hypochlorite-S}$ concentrations

Overall $\delta^{34}S_{CAS}$ values show significant variation, ranging from -10.7‰ to +57.7‰ with a mean of +16.1‰. As expected for biogenic samples, CAS-S concentration data are high (Staudt and Schoonen, 1995). These range from 45 pm to 24318ppm with an average of 1241 ppm. Taxa which secreted a shell originally made of calcite (*Pycnodonte*) generally have significantly higher concentrations than those taxa with a primary aragonite shell (*Lahillia*, *Cucullaea*, *Eselaevitrigonia*) (Appendix C, Table C1). The $\delta^{18}O$ CAS ranges from -1.4‰ to +16.9‰, with a mean of +9.01‰, while $\delta^{34}S_{hypochlorite-S}$ values range from -28.2‰ to +17.1‰ with an average of -3.55‰ (Figure 5.2). Despite these broad ranges, much of the dataset overlaps with published records of sulphur cycling for the latest Cretaceous (Paytan et al., 1998; Paytan et al., 2004; Kampschulte and Strauss, 2004; Turchyn and Schrag, 2006) and show several congruent stratigraphic trends between the various records that are relevant for interpreting the primary nature and fidelity of the isotope record.
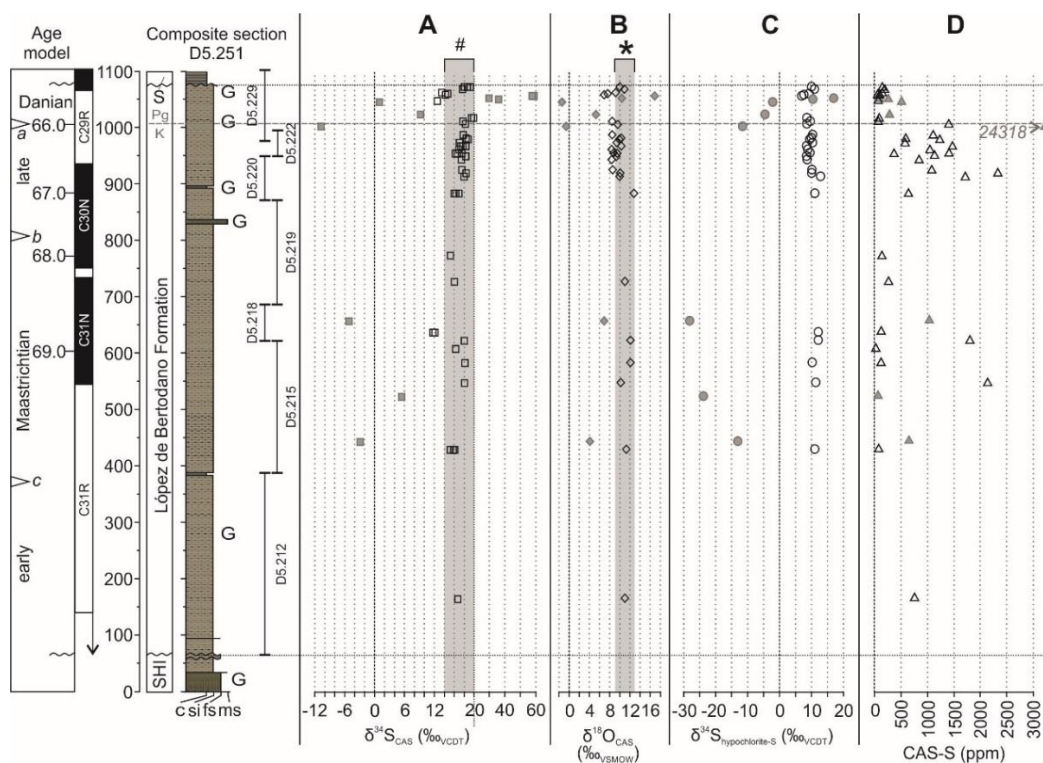
Figure 5.2: A: δ³⁴S$_{CAS}$ (open and filled squares), B: δ¹⁸O$_{CAS}$ (open and filled diamonds), C: δ³⁴S$_{hypochlorite-S}$ (open and filled circles), D: CAS concentration data (open and filled triangles) from the López de Bertodano Formation. Filled symbols are datapoints considered unreliable through either contamination or alteration (see section 5.5 below). Vertical grey bars labelled # and * indicate the range of published δ³⁴S (from CAS and marine barite) and δ¹⁸O-S data respectively for the Maastrichtian–Paleocene intervals. Data from Claypool et al. (1980), Paytan et al. (1998; 2004), Kampschulte and Strauss (2004), and Turchyn and Schrag (2006). Number and arrow on D is single altered sample that plots outside the scale presented here. The sub-section overlap between D5.222 and D5.229 has been taken into account when plotting and interpreting the isotope data. Age model is derived from Bowman et al. (2013). Time scale is based on Sr isotope chemostratigraphy (italicized *a–c*) (McArthur et al., 1998) and magnetostratigraphy (Tobin et al., 2012), updated with ages from the Geological Time Scale 2012 (Gradstein et al., 2012) and using the K–Pg boundary datum. G, glauconite-rich intervals. S, Sobral Formation.

5.4.2 δ³⁴S$_{Pyrite}$

Like δ³⁴S$_{CAS}$ isotopes, δ³⁴S$_{Pyrite}$ values are also highly variable throughout the section (Figure 5.3); ranging from -47.3‰ to +39.8‰ with an average of -12.6‰. Stratigraphically coherent trends are apparent, with mostly depleted

values between -41‰ and +2‰ between the base of the Lopez de Bertodano Formation and a stratigraphic height of ~730 m. Above this rapid fluctuations between depleted and enriched values are apparent (-47‰ to +39‰); especially coinciding with the glauconite-rich horizon at ~830 m stratigraphic height. This is followed by a return to mostly depleted values (range -41‰ to -5‰) between 883 and 905 m, before a cluster of highly enriched values (+11‰ to +25‰) between 915 and 944 m. Above this, values return to a depleted average of -10‰, with a single enriched datapoint at 969 m (+26.8‰). Minor fluctuations occur over the K–Pg boundary and through the early Danian, but with the exception of a further single ~enriched datapoint (+2‰) at 1032 m, values remain around -10‰ until the base of the Sobral Formation.

The isotopic difference between $\delta^{34}S_{CAS}$ and $\delta^{34}S_{Pyrite}$ ($\Delta^{34}S$) also provides important information about the sulphur cycling, but is only informative after the primary nature of the CAS isotope record has been assessed. Hence this is discussed after section 5.5 where this is addressed.

5.4.3 Carbonate $\delta^{13}C$ and $\delta^{18}O$, trace element concentrations

The preservation of a primary CAS signal is likely to be related to the preservation of primary biogenic carbonate. Both carbonate isotopes and trace element compositions of carbonate have been shown to be sensitive to diagenesis and have therefore been analysed to assess preservation of the CAS isotope signal. Bulk fossil shell powders yielded variable $\delta^{13}C_{carb}$ (range -7.19‰ to +4.13‰, average +0.82‰) and $\delta^{18}O_{carb}$ (range -0.58‰ to 2.15‰, average +0.78‰) values and highly variable trace element concentrations (Appendix C, Table C1) (Figure 5.4). These data are nevertheless within the range of previously published datasets using molluscan carbonate from the López de Bertodano Formation on Seymour Island (McArthur et al., 1998; Tobin et al., 2012; Tobin and Ward, 2015), and underlying formations (Pirrie and Marshall, 1990; Ditchfield et al., 1994; Crame et al., 1999).
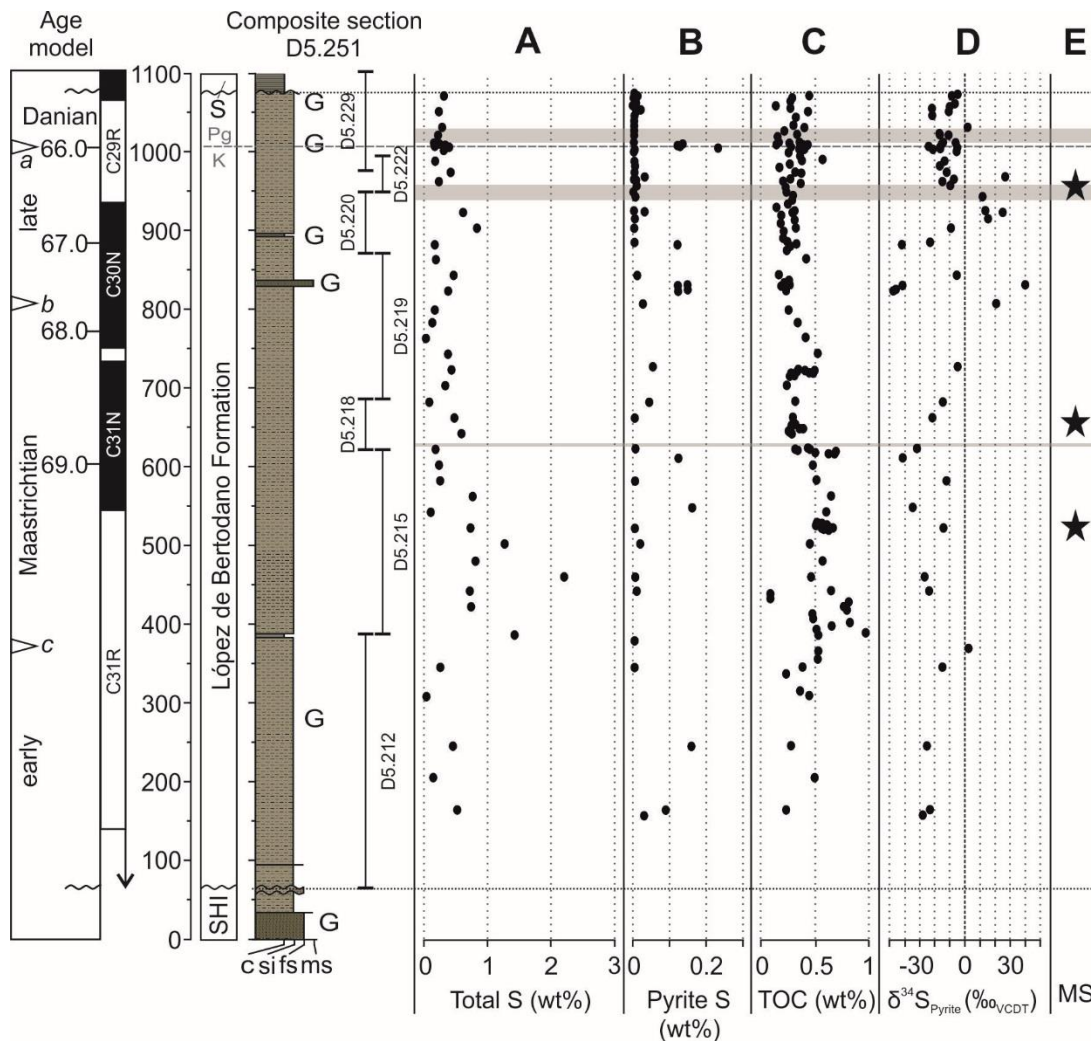
Figure 5.3: Sedimentary geochemistry. A: Total S, B: Pyrite S, C: TOC (all wt%) D: δ³⁴S_Pyrite derived from bulk sediment samples from composite section D5.251. Data are plotted against lithostratigraphy and age model (see caption to Figure 5.2 for details). E: stratigraphic locations of methane seeps based on the occurrence of chemosynthetic bivalve taxa from Little et al. (2015), and intervals of hypothesised methane flux from the sediment (horizontal grey bars) (from Hall et al. (In prep) Appendix E.

5.4.4 SEM, Cathodoluminescence, XRD

Examination using SEM and cathodoluminescence of thin sections of bivalve shell material revealed most shell carbonate shows excellent preservation. Most samples were generally non-luminescent and with original shell microstructure preserved (Figure 5.5). Exceptions to this included examples of

contaminant minerals inside micro-borings or natural tubles in the shell, and luminescent cements within the shell material of many *Pycnodonte* oysters.

In general, comparison of carbonate stable isotope and quantitative XRD data, trace element concentrations, and visual examination of fossil shells using cathodoluminescence and scanning electron microscopy (SEM) broadly confirmed that these samples likely represent a mixture of primary and diagenetically altered data (see full discussion in section 5.5).

5.4.5 Sedimentary geochemistry: Total Sulphur, Wt% $S_{Pyrite,}$ Total Organic Carbon

Total sulphur content of the sediments is low (average of 0.42 wt%, maximum of 2.29 wt%, and minimum of 0.03 wt%). These data show a pattern with the highest values (>0.5 wt%) in the stratigraphically lower portion of the formation (up to 500 m above the base of the succession). Fluctuations between 0.1 and 1 wt% characterise the remainder of the record.

Calculation of weight percent (Wt%) S_{Pyrite} from the chromous chloride extraction revealed significantly lower values; (average of 0.04 wt%, maximum of 0.23 wt%) with some samples recording values indistinguishable from 0. The presence of iron oxides in microfacies analysis of these same samples (Chapter 4; Witts et al., 2016) as well as contaminant gypsum in fossil mollusc shell material (see section 5.5) suggests that oxidation of pyrite has occurred in the section leading to values lower than those during deposition. It is therefore likely that the total sulphur data is elevated due to the presence of pyrite oxidation products, or sulphur bound to organic matter. The latter is less likely given the relatively low average organic carbon content.

Total organic carbon content of the sediments is also low (average value of 0.38 wt%, maximum of 0.96 wt%, minimum of 0.09 wt%), in line with previous studies which focused on the K–Pg boundary interval (Askin and Jacobson, 1988). Like total sulphur, higher values are apparent in the lower ~600 m of the López de Bertodano Formation, with the remainder of the data averaging between 0.2 and 0.5 wt% (Figure 5.3).

5.5 Preservation and assessment of a primary seawater isotopic signal from CAS

A variety of studies on the durability and reliability of CAS indicate that alteration of the primary isotopic signal can occur as both an enrichment or depletion of $\delta^{34}S$ relative to known contemporaneous seawater values, and that such alteration can be the result of multiple processes (e.g. Lyons et al., 2004; Marenco et al., 2008a; 2008b; Gill et al., 2008; Newton et al., 2011; Rennie and Turchyn, 2014).

Most existing studies however, focus either on bulk CAS records from ancient and modern limestones or deep-sea carbonate oozes, or are derived from biogenic carbonates secreted by extinct organisms (e.g. belemnites). Here we examine biogenic carbonates from thick-shelled marine bivalves of differing mineralogies.

The initial dataset contains a range of $\delta^{34}S_{CAS}$ values, the majority of which are comparable to published Late Cretaceous and early Paleogene records (e.g. Paytan et al., 2004; Turchyn and Schrag, 2006). In order to test the validity of this CAS dataset, a range of screening techniques were applied to the sample suite to distinguish primary isotope values (Figure 5.4, Figure 5.5).

Although the carbonate powders were bleached and the CAS extraction is completed under anaerobic conditions, oxidation of sulphides during extraction is still possible. Fine-grained sulphide-mineral grains can be wholly encapsulated by larger carbonate grains, shielding them from the bleaching pre-treatment. Anaerobic oxidation is possible via dissolved oxidised metal species released during extraction. The sulphur added from sulphide minerals is derived from sulphide produced during MSR or sulphate-driven AOM (Jørgensen and Kasten, 2006) in anoxic sedimentary pore waters. Since this is generally depleted in ^{34}S relative to seawater sulphate, the isotopic effect of this process is to decrease the apparent $\delta^{34}S$ of CAS as well as increasing the apparent CAS concentration (e.g. Marenco et al., 2008a; Mazumdar et al., 2008 Fike et al., 2015) (Figure 5.6).

The oxidation of sulphide minerals during extraction will also effect the oxygen isotope composition of the sulphate. Leeds laboratory de-ionised water has a $\delta^{18}O_{V-SMOW}$ value of around -7‰. Incorporation of this water oxygen during oxidation of sulphide minerals to sulphate will therefore also lead to a depletion in $\delta^{18}O_{CAS}$. Since pyrite emplacement in shell material can occur in pre-existing natural voids in the shell structure (such as tubules or borings), measures of carbonate preservation (e.g. cross-plots of $\delta^{18}O_{carb}$ and $\delta^{13}C_{carb}$, and trace element composition) are not relevant when assessing this process and should show no distinct correlation as contamination can occur with no effect on the structure and composition of shell carbonate.

A total of six fossil samples (four Maastrichtian (7-2, 9-2, 16-2, 20-1), two Danian (24-1, 29-1) record $\delta^{34}S_{CAS}$ values significantly depleted relative to the overall trend of the remaining dataset and of contemporaneous published seawater values (e.g. Paytan et al., 1998; Paytan et al., 2004; Kampschulte and Strauss, 2004; Turchyn and Schrag, 2006) (Figure 5.4 A,C,D,E,F). In addition, these samples also record negative $\delta^{18}O_{CAS}$ and $\delta^{34}S_{hypochlorite-S}$ values (Figure 5.2), and elevated concentrations of non-CAS-S (represented by hypochlorite-S ppm values) although by other measures of carbonate preservation they are well preserved (Figure 5.4 B). Correlation of these variables alone indicates these samples are likely not recording a seawater signature. Measurement of the isotopic composition of sulphur removed by the sodium hypochlorite bleach in these samples (range +17.1 to -17‰, mean of -1.47‰) indicates that the sum of sulphide plus organic sulphur in these samples broadly conform to the hypothesised addition of isotopically depleted sulphide to the samples.

An additional sample (15-2) exhibits a low $\delta^{34}S_{CAS}$ value (+11.86‰) compared to stratigraphically adjacent samples (Figure 5.2). This sample also has quite a negative $\delta^{34}S_{hypochlorite-S}$ value, indicating some addition of light sulphur. Against this hypothesis it exhibits low CAS concentration, and ultimately lacks confirmation from a $\delta^{18}O_{CAS}$ value. It is included in the final dataset with these caveats.
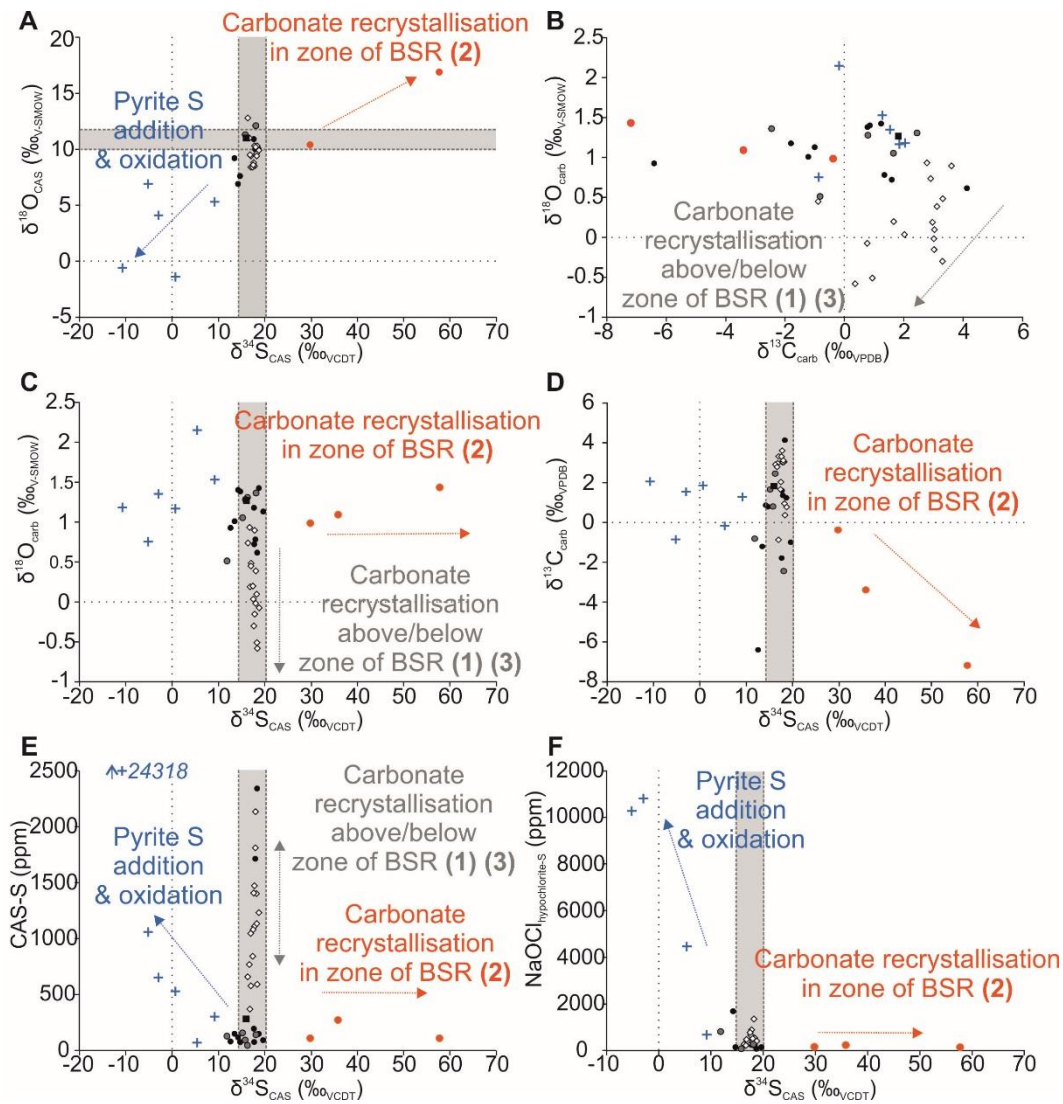
Figure 5.4: Cross-plots of isotope data for the full CAS dataset for all species. A: δ³⁴S_CAS versus δ¹⁸O_CAS, B: δ¹³C_carb versus δ¹⁸O_carb, C: δ³⁴S_CAS vs δ¹⁸O_carb, D: δ³⁴S_CAS versus δ¹³C_carb, E: δ³⁴S_CAS versus CAS concentration (ppm), F: δ³⁴S_CAS versus δ³⁴S_hypochlorite-S concentration. Grey boxes in A, C, D, E, and F illustrate range of published Cretaceous–Paleogene seawater δ³⁴S and δ¹⁸O-S values (Claypool et al., 1980; Paytan et al., 1998; Paytan et al., 2004; Turchyn and Schrag, 2006). Filled black and red circles, *Lahillia*, filled grey circles, *Cucullaea*, filled white diamonds, *Pycnodonte*, filled black square *Eselaevitrigonia*. Numbers in parentheses represent possible zones of recrystallization in Figure 5.6, with arrows indicating direction of change expected in isotope data. Blue crosses represent samples from a range of genera, likely contaminated with light sulphur from oxidation of sulphide minerals.

SEM examination of several shells (6-2, 12-1, 18-1, 35-1) in the total dataset

revealed that pyrite framboids are present within the infill of micro-borings or

natural tubules in shell structure of the genera *Lahillia* and *Cucullaea* which otherwise preserve pristine original shell microstructure and are non-luminescent during examination under CL (Figure 5.5). This suggests that pyrite addition is variable, and $\delta^{34}S_{Pyrite}$ in fossil samples themselves (as represented by the $\delta^{34}S_{hypochlorite-S}$) clearly has a variable isotope composition. Therefore the potential for alteration of the primary CAS isotope signal is also variable at the level of each individual shell. In only a few examples oxidation of sulphides has occurred – perhaps as a result of the aforementioned failure to remove sulphides during sample bleaching. Due to the high probability of contamination, the six datapoints described above are removed from subsequent analysis and discussion of the primary record.
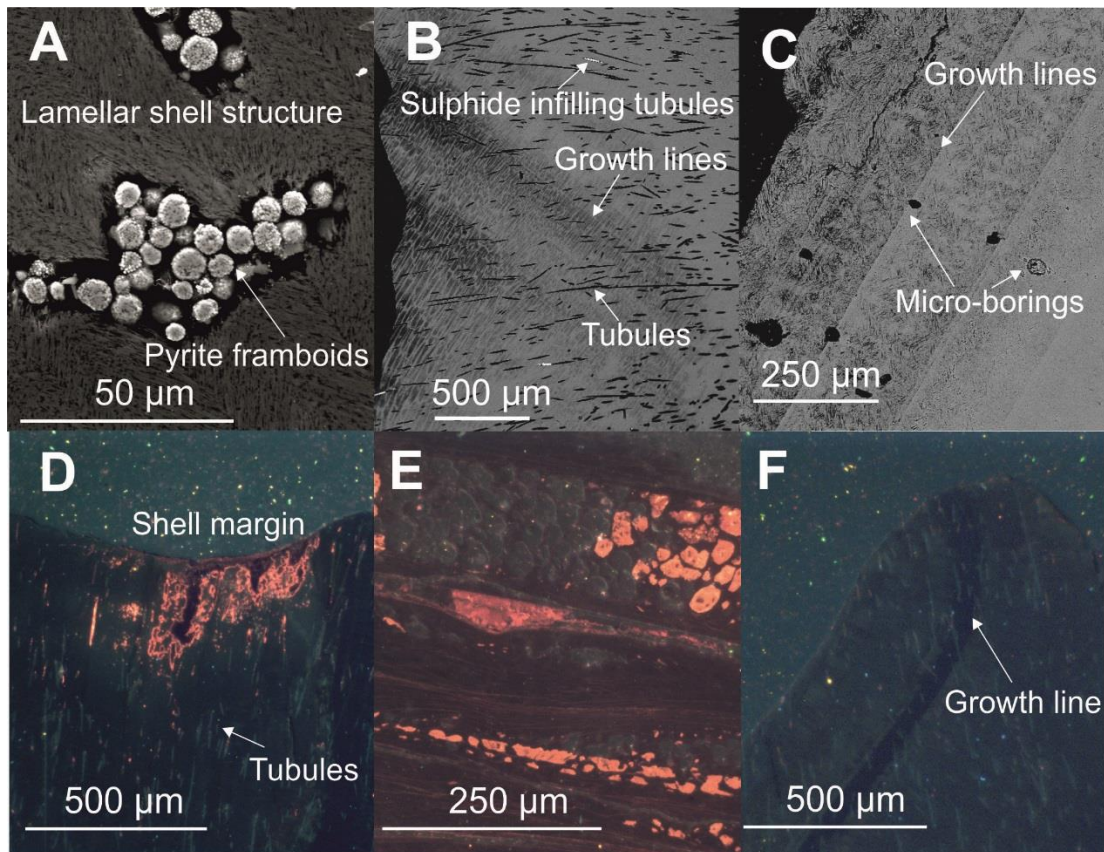
Figure 5.5: Examples of shell preservation from fossil bivalve samples of the López de Bertodano Formation. Taken from SEM (A–C) and CL (D–F) imaging of fossil shells. A, (sample D5.1355.2, *Lahillia*) original pristine lamellar shell structure, with pyrite framboids inside micro-boring. B, (sample D5.955.2, *Cucullaea*) well-preserved shell structure including growth lines and tubules, some infilled with small amounts of sulphide (pyrite framboids). C, (sample D5.1355.2, *Lahillia*) further examples of lamellar shell structure, with growth lines and algal micro-borings into shell. D, (D5.955.2, *Cucullaea*) shell margin with non-luminescent primary shell structure, thin external layer showing a degree of luminescence and alteration. E, (D5.1277.2, *Pycnodonte*) showing generally non-luminescent shell with typical lenticular texture and areas in-filled with high magnesium luminescent calcite cements. F, (D5.955.2, *Cucullaea*) shell margin with well-preserved (non-luminescent) shell material and original growth lines.

A second suite of processes linked directly to the preservation of original carbonate material also have the potential to alter the CAS from a primary seawater isotope composition. To explore the effects of these processes on the studied samples, a conceptual model based around a pore-water profile with typical biogeochemical zonation seen in marine sediments during the

breakdown of organic matter (Jorgensen and Kasten, 2006) is used to consider the likely effect of recrystallisation on CAS isotope values in three hypothetical 'zones of alteration' following burial (Figure 5.6):

1) Shallow zone with concentrations of sulphate near seawater. Here porewater sulphate isotope compositions will also be near those of seawater, but concentrations of iron and manganese are likely to be elevated. Incorporation of sulphate into recrystalised carbonate here will not result in any significant deviation from a primary signal.

2) Intermediate depth zone with depleted porewater sulfate concentrations relative to seawater. The porewater sulphate has a more positive sulphur isotope composition than seawater due to MSR and/or AOM. Here, sulphate concentrations are still sufficient to produce a significant concentration of CAS in recrystalised carbonate, but addition of recrystalised carbonate will now shift the CAS-S isotope composition towards heavier values. The isotope composition of dissolved inorganic carbon (DIC) is becoming increasingly more negative for both carbon and oxygen in this zone.

3) Deep zone where sulphate concentrations are negligible. Recrystalisation here has a minimal effect on CAS sulphur isotope compositions because the new carbonate will contain little or no sulphate. The carbon and oxygen isotope compositions of DIC are shifted to more negative values here.
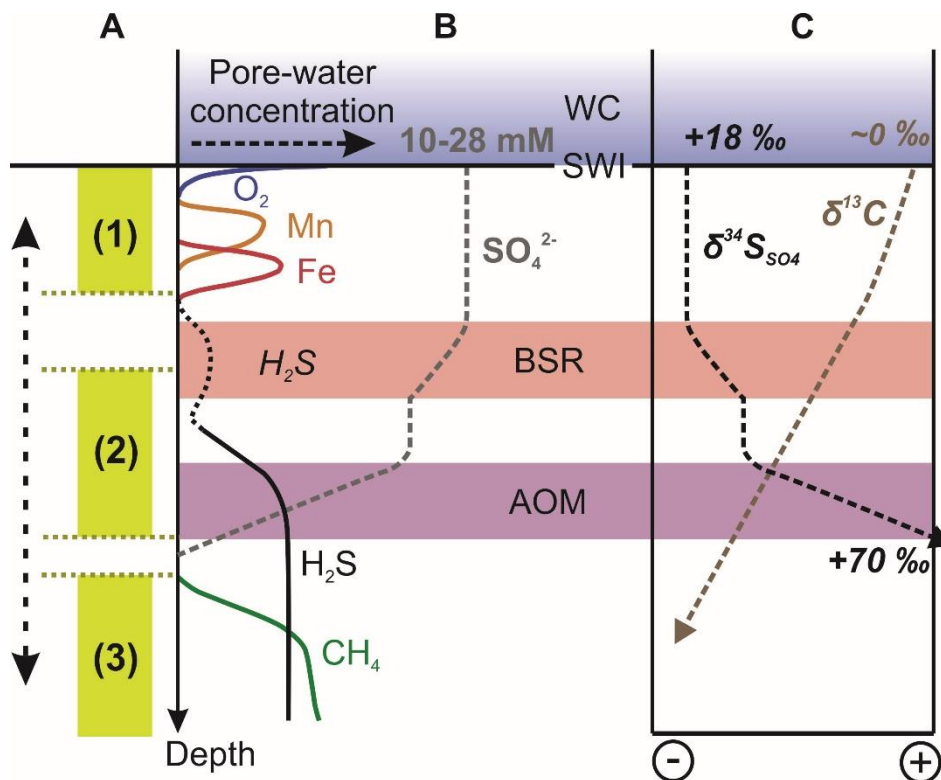
Figure 5.6: Schematic pore water profile (not to scale). A: potential zones of alteration for fossil samples following burial and diagenesis. B: pore water concentration for various ions used as electron acceptors, and the concentration of sulphate. C: effect on the isotopic composition of sulphate ($\delta^{34}S_{SO4}$) and dissolved inorganic carbon ($\delta^{13}C$). BSR, bacterial sulphate reduction, AOM, anaerobic oxidation of methane, WC, water column, SWI, sediment-water interface. Vertical dashed arrow next to A indicates the potential for these zones to migrate vertically through time due to a variety of factors.

The zone of recrystallization of carbonate is likely to vary depending on carbonate mineralogy and sedimentation rate. Rennie and Turchyn (2014) suggested a relationship between CAS alteration and sedimentation rate; such that preservation of primary $\delta^{34}S_{CAS}$ values was more likely in sites with low sedimentation rates, where recrystallization would occur above a deeper zone containing isotopically evolved pore fluids (Zone 1 of Figure 5.6), or in settings with very high sedimentation rates where samples would be rapidly placed below this critical region before recrystallization could occur (e.g. into Zone 3 of Figure 5.6). CAS was thus most prone to alteration at intermediate sedimentation rates – estimated at 50–150 m Myr^{-1}, which would be comparable to estimates for the López de Bertodano Formation on Seymour

Island (100–150 m Myr^{-1} based on average calculated sedimentation rate) (Tobin et al., 2012; Bowman et al., 2013; Witts et al., 2016). Although this is an average rate for the whole formation, the presence of a number of glauconite-rich horizons in the uppermost ~300m indicate intervals of significantly lower sedimentation rate and reworking of sediment (Macellari, 1988; Witts et al., 2016). Application of this general model to the present study should be approached with caution given the differing palaeoenvironmental setting. In deep sea carbonate dominated sediments, such as those studied by Rennie and Turchyn (2014), high rates of carbonate recrystallization occur at shallow depths in the sediment column in association with pore waters containing relatively unevolved $\delta^{34}S_{SO4}$, whereas the zones of MSR and AOM may be >1 m (and in some cases, tens of meters) below the sediment-water interface (Rennie and Turchyn, 2014; Turchyn et al., 2016).

In shallower water settings, such as those considered in this study, the zones of MSR and AOM may occur a lot closer (mm's to cm-scale for BSR, cm to m-scale for AOM) to the surface (e.g. Jorgensen, 1982; Jorgensen and Kasten, 2006; Rooze et al., 2016) potentially in association with higher rates of recrystallization. Biogeochemical zones are also more likely to migrate over time with changes in sedimentation rate, organic matter delivery, or concentration of ions diffusing from the overlying water column (Figure 5.6A), making relationships with sedimentation rate in particular more complicated. Samples of biogenic carbonate from thick-shelled marine bivalves are also substantially different to deep sea foraminiferal oozes since they have a much lower surface area to volume ratio. Our data also indicate that calcitic taxa such as *Pycnodonte* oysters start with an initially higher CAS concentration than foraminfera and aragonitic taxa and are therefore less vulnerable to alteration. Aragonitic taxa have the advantage that their progressive recrystalisation can be monitored by the percentage of calcite in their shell (see below).

Many specimens of the oyster *Pycnodonte*, which originally secrete a calcite shell, contain significant enrichment in Mn and Fe and exhibit a relationship between decreasing values of $\delta^{18}O_{carb}$ $\delta^{13}C_{carb}$, and decreasing Sr content, as

would be expected during diagenetic recrystallization in Zone 1 (Figure 5.6). Examination using Cathodoluminescence and SEM revealed good preservation of original porous shell structure (Figure 5.5 E), but the presence of significant portions of luminescent, presumably early diagenetic cement. This has been noted by previous studies (Pirrie and Marshall, 1990; Ditchfield et al., 1994), and led to the exclusion of *Pycnodonte* samples from palaeotemperature reconstructions from the James Ross Basin using $\delta^{18}O_{carb}$.

Importantly for this study, $\delta^{34}S_{CAS}$ and $\delta^{18}O_{CAS}$ values for all *Pycnodonte* samples are within the range of contemporaneous seawater (range 16.3–18.8‰), and they exhibit high CAS-S concentrations (minimum 370 ppm, maximum 2134 ppm, average 1102 ppm), with no relationship between $\delta^{18}O_{carb}$ (Figure 5.7C) and CAS concentration, and only a very weak relationship between $\delta^{18}O_{carb}$ (Figure 5.7B) and $\delta^{34}S_{CAS}$. This strongly suggests that despite recrystallization, $\delta^{34}S_{CAS}$ values in these bivalves are buffered from alteration (e.g. Gill et al., 2008) and likely record primary seawater values.
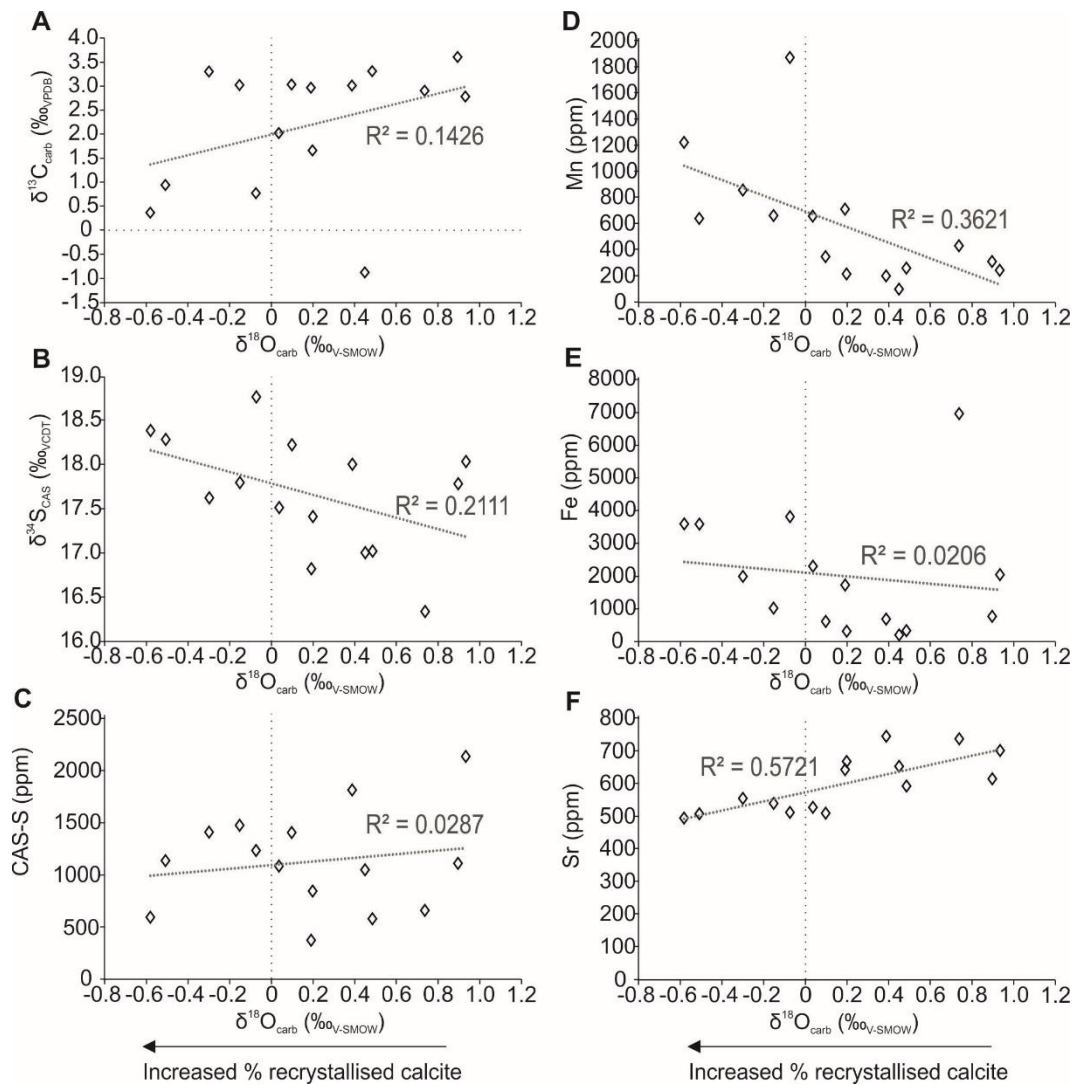
Figure 5.7: Cross-plots between δ¹⁸O$_{carb}$ and A: δ¹³C$_{carb}$, B: δ³⁴S$_{CAS}$, C: CAS-S ppm, D: Mn, E: Fe, F: Sr for calcitic *Pycnodonte* oysters. Significant correlations between decreasing δ¹⁸O$_{carb}$ and any of these variables is often interpreted as a sign of increasing recrystallization and loss of primary CAS isotope signal (e.g. Brand and Veizer, 1980; Gill et al., 2008).

Those samples with originally primary aragonite shells (*Lahillia*, *Cucullaea*, *Eselaevitrigonia*) show mostly good preservation of original shell microstructure with little or no development of diagenetic cements (Figure 5.5), indicating significant amounts of recrystallization has likely not occurred in the majority of samples. Assessment of preservation for originally aragonite samples is important because it has been demonstrated that sulphate incorporation occurs more favourably in calcite than aragonite (Busenberg and

Plummer, 1985). Compatible with this notion, these bivalves show lower CAS concentrations than the calcitic *Pycnodonte* oysters (mean 332ppm, s.d. 473 ppm), suggesting that they are less buffered from the effects of diagenesis on their CAS record. Detailed examination of specimens of *Lahillia* and *Cucullaea* reveal that these taxa can develop an organic-rich outer layer, possibly the remains of a periostracum (Appendix E; Hall et al., In prep), which appears prone to early diagenetic alteration and shows luminescence under CL imaging (Figure 5.5D). This outer layer can be removed or avoided during detailed microsampling. The surface of the shell material used in this study was not cleaned in this way and this layer is therefore potentially included in the homogenised samples.

To assess the amount of recrystallization and potential alteration of CAS in these bivalves, quantitative XRD was used to estimate the proportion of aragonite to calcite in each shell (Figure 5.8), and compared to isotope values and trace element concentrations. Incorporation or contamination of shells with other minerals (i.e. sediment not removed during sample cleaning), could lead to anomalous trace element values, so estimates of the percentage of 'other' minerals included in the shells were also examined.

Cross-plots of these variables (Figure 5.8) indicate that several samples of *Lahillia* show significant alteration of original 'pure' aragonite shell to calcite during recrystallisation. *Cucullaea* samples are generally better preserved, showing minimal alteration of calcite, and negligible incorporation of contaminating minerals from the surrounding sediment.

Sample 30-1 shows a moderate degree of recrystallization (36.8% calcite) and records a CAS value that is lower than expected Cretaceous seawater sulphate (Figure 5.8A), but is not different to stratigraphically adjacent samples (Figure 5.2A – 1049m). This sample also shows evidence for enrichment in Fe and Mn, as would be expected from recrystallization in zone 1 (Figure 5.6). Two samples (3-1 and 4-1) are highly recrystallized (65.5 and 98.3% calcite respectively), but record CAS values in the range of seawater values from other studies. They also have elevated CAS-S concentrations consistent with the addition of calcite with high sulfate concentrations relative

to aragonite. These samples are also considered recrystallized in Zone 1, despite the lack of significant Fe and Mn enrichment. This inconsistency would initially suggest Zone 3, but a prediction of conditions in this interval would be for addition of calcite with little or no CAS within it – clearly not the case with these samples.

Three samples (32-1, 33-1, 34-1) with very enriched CAS values flagged previously (Figure 5.4) exhibit varying levels of recrystallization (26, 16, and 37% calcite respectively). This evidence of conversion from aragonite to calcite in conjunction with their elevated $\delta^{34}S_{CAS}$ values are likely to be indicative of recrystallization in Zone 2; in an interval where pore-waters concentrations and isotope compositions are modified by MSR or AOM. One of these samples (34-1), as well as a further *Lahillia* which records expected seawater CAS values (38-1) show also elevated Mn and Fe values, as would be expected by recrystallization in Zone 1. However, both of these samples appear to be contaminated by incorporation of other minerals, probably as a result of failure to remove adhering sediment during cleaning or shell bleaching with NaOCl (Figure 5.8H, J) which is likely to have elevated measurements of carbonate Fe and Mn.

To conclude an assessment of preservation, aragonite samples that recrystallized in Zone 2 are removed from the final dataset due to their modified $\delta^{34}S_{CAS}$ values (Table 5-1), along with samples considered non-primary from pyrite-S addition. Remaining samples where there is no evidence of pyrite oxidation during extraction, no evidence of alteration to the primary shell carbonate, or where alteration to the shell carbonate has occurred in such a way as to preserve the primary seawater signal are considered to represent a primary record of seawater sulphate, and are discussed in the next section.

Table 5-1: List of CAS samples removed from final analysis following assessment of preservation.

Sample #	Strat height (m)	Reason for removal	$\delta^{34}S_{CAS}$
34-1 (D5.1351.2)	1058	Recrystalisation in Zone 2	+57.70‰
33-1 (D5.1343.2	1054	Recrystalisation in Zone 2	+29.81
32-1 (D5.1339.2)	1052	Recrystalisation in Zone 2	+35.8
29-1 (D5.1334.2)	1047	Pyrite-S addition	+0.72
24-1 (D5.1313.2)	1022-1028	Pyrite-S addition	+9.2
20-1 (D5.1298.2)	1004	Pyrite-S addition	-10.72
16-2 (D5.1040.2)	656-661	Pyrite-S addition	-5.16
9b-2 (D5.347.2)	522-527	Pyrite-S addition	+5.4
7-2 (D5.970.2)	442-447	Pyrite-S addition	-2.94
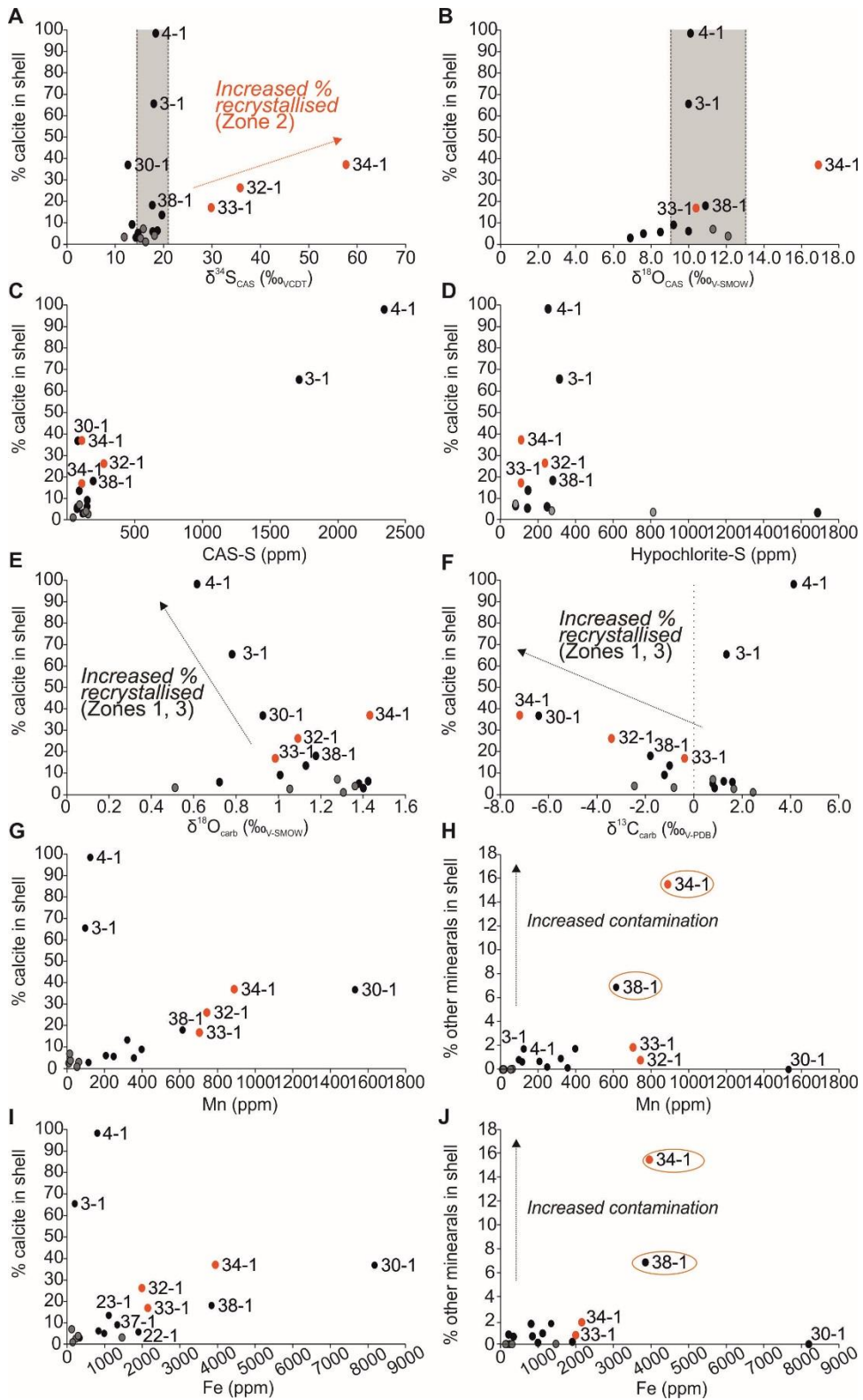
Figure 5.8 (previous page): Cross-plots for originally aragonite taxa (*Lahillia, Cucullaea*). Cross plots based on quantified XRD analysis between % calcite in shell (A, B, C, D, E, G, I) and A: $\delta^{34}S_{CAS}$, B: $\delta^{18}O_{CAS}$, C: CAS-S, D: Hypochlorite-S, E: $\delta^{18}O_{carb}$, F: $\delta13^{C}_{carb}$, G: Mn (ppm), I: Fe (ppm). H and J: % other (contaminating) minerals in shell and H: Mn (ppm) and J: Fe (ppm). Black and red circles represent *Lahillia*, grey circles *Cucullaea*. Samples numbers correspond to Table C1. Arrows represent direction of change expected during recrystallization or contamination in zones of alteration from Figure 5.6. Grey bars on A and B are range of Cretaceous–Paleogene values of $\delta^{34}S_{CAS}$ and $\delta^{18}O_{CAS}$.

5.6 Discussion

5.6.1 Sulphur-cycle changes across the Maastrichtian and the K–Pg interval.

The $\delta^{34}S_{CAS}$ dataset remaining after screening for preservation is presented in Figure 5.9. Once data suspected to be contaminated or altered are removed, several stratigraphic and temporal trends in $\delta^{34}S_{CAS}$ become apparent which are interpreted to represent a true picture of the evolution of seawater sulphate during the Maastrichtian and early Danian.

No directly compatible data are available in terms of the temporal resolution of this study, as existing datasets either focus on a narrow window around the K–Pg boundary interval itself (Kajiwara et al., 1992; Kaiho et al., 1999) or are long-term records derived from marine barite at low resolution and with significant gaps (Paytan et al., 1998; Paytan et al., 2004).

These low-resolution marine barite records, all taken from the Pacific Ocean, show a distinct lack of fluctuation in the Maastrichtian, all data ranging between +18 and +19‰ (Paytan et al., 2004). Kampsculte and Strauss (2004) reported values from CAS for the 65–70 Ma time bin of between +18.1 and +18.6‰, and +16.9 to +17.4‰ from evaporites of the same age. Kaiho et al. (1999) CAS data fluctuates from values of +15 to +22‰ across the K–Pg boundary (Figure 5.10). These data are from a short (80 cm) interval across the K–Pg boundary; representing a very short time interval in the latest Maastrichtian and early Danian.

Attempted comparison between Seymour Island and contemporaneous lower latitude sulphur isotope K–Pg datasets is shown in Figure 5.10. Absolute correlation is not possible beyond the known position of the K–Pg boundary due to the lack of datum levels for direct correlation. Magnetochron reversals are also used as tie-points from Seymour Island, but both of the published datasets come from a short interval in chron C29R. Published age models (Kaiho and Saito, 1986; Arenillas et al., 2004) would suggest the perturbations to the sulphur cycle recorded at the K–Pg boundary are confined to the P0 (*Guembelitria cretacea*) foraminiferal biozone in both Spain and Japan, with a suggested duration of 18-21 kyrs of the early Paleocene (Arenillas et al., 2004).

Using published age models from the López de Bertodano Formation (Tobin et al., 2012; Bowman et al., 2013; Chapter 4 (Witts et al., 2016), an equivalent interval on Seymour Island would bracket a 4m-thick glauconite-rich interval immediately above the K–Pg boundary (Figure 5.10), although this must also be regarded as a tentative correlation given the fact that glauconite-rich horizons may represent intervals of slow sedimentation associated with lateral facies boundaries (Bowman et al. In Press).

Broadly speaking, therefore our primary CAS data are comparable with existing estimates of the isotopic composition of seawater sulphur for the Maastrichtian and Danian from published datasets (Figure 5.10) (e.g. Kaiho et al., 1999; Paytan et al., 1998; Paytan et al., 2004), but add new detail, particularly in an interval spanning around 2 million year across the K–Pg boundary itself (the consecutive magnetochrons C30N and C29R) (Figure 5.9). Whilst CAS data are in broad agreement with published data, $\delta^{34}S_{Pyrite}$ data show significant differences (Figure 5.10), suggesting this record is responding to local sulphur cycle changes.

The precision of CAS in recording seawater $\delta^{34}S_{CAS}$ means that variability is generally only considered significant when changes exceed >1‰ (Rennie and Turchyn, 2014). With this in mind we interpret the remaining record in terms of three main features:

1) Early-mid Maastrichtian stability 100–800m: In the basal portion of the López de Bertodano Formation (100–600m) corresponding to the early Maastrichtian (magnetochron C31R), data density is low but $\delta^{34}S_{CAS}$ values average 17‰ ±1‰, with values at the higher end of this range around 600m, during the mid–Maastrichtian (~69 Ma, close to the base of chron C31N). This interval finishes with slightly lower values (15–16.5‰) between 700 and 800m, (corresponding to magnetochrons C30R and C30N and an age of ~68 Ma).

2) Late Maastrichtian increase 750–1020m: The low point of ~15.5 per mille between 750 and 800m is followed by a near continuous increase to 19.6‰ at 1019m, ~10m above the K–Pg boundary (corresponding to the upper portion of magnetochron C30N and lower two thirds of C29R, 67–66 Ma). This feature occurs where data density is highest, although the most positive value is only recorded by one sample.

3) An early Paleocene negative excursion 1000–1080m: From the most positive value in the record in the earliest Palaeocene there is a rapid excursion to a prominent cluster of depleted values defined by four datapoints (range 12.6‰ – 14.7‰, mean 13.8‰) occurring in stratigraphically adjacent samples between 1049 and 1064m, 40m above the K–Pg boundary (corresponding to the upper portion of chron C29R, ~65.7 Ma). $\delta^{34}S_{CAS}$ values then return to values of 17–19‰, similar to those of the late Maastrichtian in the highest portion of the section (1070–1074m), directly below the unconformable contact with the overlying Sobral Formation.

Each of these intervals is described in more detail in the following sections, which also examine evidence from palaeoenvironmental proxies for possible mechanisms which could drive changes to the sulphur cycle during the Maastrichtian–Danian interval.

213

Figure 5.9: A: Primary δ³⁴S$_{CAS}$ **dataset. B: δ³⁴S**$_{Pyrite}$ **dataset. C: Δ³⁴S dataset. Dashed circle highlights interval where values approach 0. D: δ¹³C**$_{Carb}$ **dataset, values from bulk powders of this study (open symbols) and Hall et al. (In Prep) (closed symbols). For explanation of differing symbology relating to different taxa see Figure 5.4. Horizontal grey bars are range of δ¹³C values recorded from microsampling growth bands of individual shells. E: Stratigraphic locations of putative chemosymbiotic bivalve taxa, in this and adjacent stratigraphic sections (Appendix D; Little et al., 2015). Horizontal grey bars are intervals where methane derived carbon becomes apparent in annually resolved aragonite shell records (Appendix E; Hall et al., In Prep). F: summary palaeoclimate information, timing and evidence for LIP volcanism, and impact events. Data derived from oxygen isotope temperatures (Tobin et al., 2012), marine (Bowman et al., 2013) and terrestrial (Bowman et al., 2014) palynology. Snowflake symbols are 'cold snaps' of Bowman et al. (2013). Grey bar extending from K–Pg boundary represents uncertainty in palynological climate proxy data due to disruption of marine and terrestrial communities following the K–Pg mass extinction. Red arrow labelled DT is the inferred duration of the Deccan Traps LIP – solid red line marks timing of Main Phase eruptions (Schoene et al., 2015; Renne et al., 2015) dashed red line and ? mark timing of phase 1 (Chenet et al., 2009). The K–Pg boundary is represented by the dashed horizontal grey line at 1008m. Yellow star marks position of the iridium anomaly, taken as a marker for the Chicxulub impact event (Molina et al., 2006). Dashed horizontal green line indicates the local initiation of significant glauconite deposition and inferred change in mean sedimentation rate at ~830m.**

A Seymour Island, Antarctica (This study)

B Kawaruppu, Japan (Kajiwara & Kaiho, 1992)

C Caravaca, Spain (Kaiho et al. 1999)

215
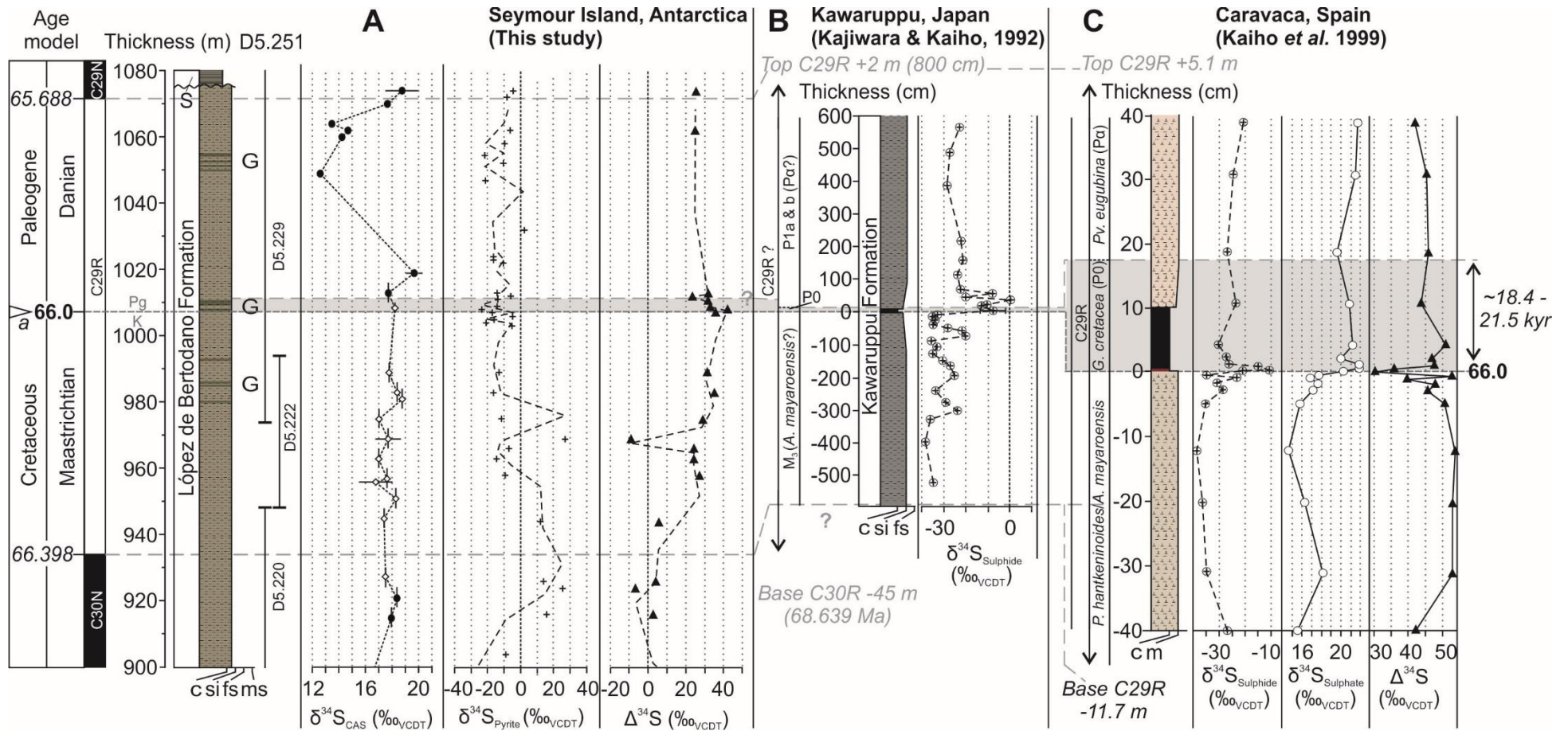
Figure 5.10 (Previous page): Correlation of K–Pg sulfur isotope data from this study (Seymour Island, Antarctica - $\delta^{34}S_{CAS}$, $\delta^{34}S_{Pyrite}$, $\Delta^{34}S$) compared and correlated with existing datasets from Kawaruppu, Japan (Kajiwara and Kaiho, 1992) ($\delta^{34}S_{Sulphide}$) and Caravaca, Spain (Kaiho et al., 1999) ($\delta^{34}S_{Sulphide}$, $\delta^{34}S_{Sulphate}$, $\Delta^{34}S$). Attempted correlation (horizontal dashed grey lines and shaded grey box) using age models. Primarily magnetostratigraphy (Arenillas et al., 2004 (Caravaca); Tobin et al., 2012 (Seymour Island); Kurihara et al., 2016 (Kawaruppu)) and biostratigraphy –estimates for the duration of the P0 foraminiferal biozone found in both the Kawaruppu (Kaiho and Saito, 1986) and Caravaca sections (Arenillas et al., 2004; Molina et al., 2009). The base of this biozone is the K–Pg boundary itself (Molina et al., 2006; 2009). Estimated correlation with Seymour Island is based on sedimentation rates of 0.1–0.2 mm/yr (Tobin et al., 2012; Witts et al., 2016). Vertical error bars on $\delta^{34}S_{CAS}$ dataset in A represent thickness of stratigraphic sampling bins from which fossils were collected. Horizontal error bars represent range of multiple $\delta^{34}S_{CAS}$ values, with marker located at the mean value. Dashed lines in Seymour Island $\delta^{34}S_{Pyrite}$ $\Delta^{34}S$ datasets are 2 point running averages. G, glauconite-rich horizons, also marked as green bands in lithostratigraphy. S, Sobral Formation. Expanded foraminiferal species names from biostratigraphy in B and C: *M. mayaroensis = Abathomphalus mayaroensis, P. hantkeninoides = Plummerita hantkeninoides, G. cretacea = Guembelitria cretacea, Pv. eugubina = Paravularugoglobigerina eugubina.

5.6.2 Early-mid Maastrichtian sulphur cycle stability

The early Maastrichtian record probably represents subtle fluctuations within a system close to steady state; the apparent small increase and decrease in $\delta^{34}S_{CAS}$ values ~400–700m is defined by a limited number of datapoints (Figure 5.9), and given the expected variability of 1–2‰ around a true seawater value in CAS data, may have a primary significance but is rather difficult to interpret. This interval does contain several global palaeoenvironmental changes that could have affected the sulphur cycle.

Climate can influence the sulphur cycle and the isotopic composition of seawater sulphate via carbon cycle feedbacks produced by changes in nutrient inputs to the ocean, in turn affecting productivity and therefore driving change in the pyrite burial flux.

Sea level change can also cause changes to the sulphur cycle. Sea-level rise would be expected to lead to a general increase in seawater sulphate-$\delta^{34}S$ due to an increase in pyrite burial in expanded shallow shelf environments

where the relative contribution of MSR to the anaerobic remineralisation of organic matter is higher than in deeper waters (Jorgensen, 1982). Increased weathering and flux of sulphides to the ocean during sea level fall would be expected to lead to an overall decrease in seawater sulphate.

The Maastrichtian is well known to contain climate fluctuations preceding the K–Pg mass extinction (e.g. Barrera and Savin,1999; Jung et al., 2013; Bowman et al., 2014), with a long-term cooling trend from mid-Cretaceous 'super greenhouse' conditions reaching its peak across the Campanian–Maastrichtian boundary and during the early Maastricthian (Friedrich et al., 2012; Thibault, 2016). Large and rapid sea level changes (25-75 m amplitude over < 1myr) also occurred during the Maastrichtian superimposed on an overall long-term fall from a mid-Cretaceous high (e.g. Miller et al., 2005; Haq, 2014).

The early Maastrichtian cooling trend was followed by a warming event and positive carbon isotope fluctuations recorded globally in the mid-Maastrichtian (the 'Mid-Maastrichtian Event' or MME) ~69 Ma, during magnetochron C31N (Voigt et al., 2012; Jung et al., 2013). This warming event is also associated with a eustatic sea level rise, changes to ocean circulation patterns, and was followed by some minor extinction events – most prominently the disappearance of the majority of the inoceramid bivalves (MacLeod et al., 1996; Dubicka and Peryt, 2012; Jung et al., 2013).

Due to the low density of data in the portion of the CAS record that correlates with this interval, it is difficult to test whether these global events had a significant effect on the sulphur cycle. A slight increase in $\delta^{34}S_{CAS}$ values between 400 and 600 m in the composite section could plausibly reflect increased global pyrite burial during the MME sea level rise and climate warming (Figure 5.9), and occurs in parallel with a positive shift in global carbon isotope records reflecting a period of increased carbon burial (Voigt et al., 2012). However, it is difficult to draw a definitive conclusion based on the available data.

5.6.3 Late Maastrichtian increase in seawater-δ^{34}S

The later Maastrichtian increase of ~4–5‰, from magnetochron C30N, to a maximum just above the K–Pg boundary is well constrained by multiple data points, representing a true shift in the isotopic value of seawater sulphate during this time interval.

The effect of climate or sea level on the record from $\delta^{34}S_{CAS}$ during the late Maastrichtian is not easily linked to a known change in global climate or tectontics. The major positive shift (+4‰) in the CAS record from Seymour Island begins in magnetochron C30N (Figure 5.9;Figure 5.10), an interval where most climate proxies globally show evidence for significant cooling (e.g. Li and Keller, 1998; Thibault, 2016). Although the global sea level record for this interval lacks precise temporal constraints, it is broadly characterised by a rise in C30N followed by a fall into C29R (Miller et al., 2005; Haq, 2014), at odds with a role in controlling a persistent increase in pyrite burial.

Because of the tight coupling apparent in marine sediments between the burial of isotopically depleted organic-carbon and pyrite-sulphur, any increase in pyrite burial, indicated by a significant positive shift in the sulphur isotope record, should be mirrored by an increase in carbon burial (Berner, 1982). If this is large enough it will impact on the isotopic composition of ocean DIC and be recorded in the record of marine carbonates. Numerous carbon isotope curves derived from bulk carbonate (e.g. Voigt et al., 2012; Thibault, 2016) or foraminifera (Li and Keller, 1998) are available for the Maastrichtian from a variety of ocean basins (Wendler, 2013). They generally show a long-term decreasing trend in the late Maastrichtian, followed by a short and rapid positive peak immediately preceding the K–Pg boundary, this is seen in deep sea records from the Pacific, Southern, and Tethys oceans (Cramer et al., 2009; Voigt et al., 2012) (Figure 5.11A). Several of these records come from epeiric seas (e.g. 1 and 2 in Figure 5.11a) which have the potential to record an isotopic composition different to the global ocean (e.g. Panchuk et al., 2005; Voigt et al., 2012). Despite this, few carbon isotope records show any significant (>1‰) increase prior to this during the late Maastrichtian, as might be expected during a period of increased linked carbon and pyrite burial

inferred from the increase in $\delta^{34}S_{CAS}$ values during magnetochrons C30N–29R.

There are several possibilities to explain this apparent contradiction; A decoupling of the carbon and sulphur cycles via terrestrial carbon cycle changes (e.g. Kurtz et al., 2003), or a reduced significance of marine sulphate-sulphur isotopic change for the carbon cycle due to lower marine sulphate concentrations. Decoupling of the carbon and sulphur cycles has previously been hypothesised for the early Paleogene (Kurtz et al., 2003), in this case a decrease in pyrite burial alongside a concomitant increase in organic carbon burial in terrestrial environments. Hence increases in marine organic carbon burial may be balanced by decreases in terrestrial organic-carbon burial such that the net effect on the DIC-carbon isotope composition of the ocean is only small. There is also evidence that the late Cretaceous was a time of reduced concentrations of sulphate in the oceans (Holt et al., 2014) (see section 5.6.5 below for more detail). A lower marine sulphate concentration would make the marine sulphate sulphur more sensitive to change for any given amount of carbon/pyrite burial. Therefore there could be sufficient pyrite burial to impact the CAS record significantly whilst having only a minimal effect on the isotopic composition of ocean DIC.

Large-scale volcanism has also been suggested as a driver of change in the Cretaceous sulphur cycle (Paytan et al., 2004; Adams et al., 2010; Gomes and Hurtgen, 2016). As well as causing or exacerbating climate-driven changes, LIP volcanism could contribute significant amounts of volcanic or mantle sulphur (isotopic composition of 0‰) to the ocean (e.g. Adams et al., 2010; Gomes and Hurtgen, 2016), causing a decrease in $\delta^{34}S$. Extensive continental flood basalt volcanism from the Deccan Traps LIP in India commenced ~1.2 myrs prior to the K–Pg boundary (Chenet et al., 2009), with the main phase of eruptions (accounting for ~80% of the total eruptive volume) confined to a 750 kyr interval in magnetochron C29R (Schoene et al., 2015; Renne et al., 2015). Evidence for the onset of this phase of eruptive activity is seen as a prominent negative excursion in Os istope records from numerous deep sea cores, commencing close to the C30N/29R chron boundary (Robinson et al., 2009), representing weathering of freshly exposed Deccan

basalt on the Indian continent – at that time located at a palaeolatitude of ~20°S.

An estimated >1.3 x 10^6 km^3 of lava was erupted from the Deccan Traps, with total volatile emissions generally thought to be high compared to other LIP's (totals of 3.5-6.5 x 10^6 Mt (SO_2), 1.4 x 10^7 Mt (CO_2), and 1 x 10^6 Mt (Cl) respectively) (Self et al., 2014). Individual eruptions probably occurred as short-lived pulses, and Callegaro et al. (2014) suggested that each 1km^3 of Deccan lava erupted would outgas 8 Mt of SO_2. The potential for environmental change resulting from release of these volatiles is still debated (Schmidt et al., 2016; Tobin et al., In Press).

The lack of significant excursions in the CAS record during the stratigraphic interval correlated to C29R below the K–Pg boundary on Seymour Island (930–1007m) (Figure 5.10), suggests Deccan eruptions did not perturb the seawater sulphate reservoir significantly during this interval. Assuming the volumes and flux estimates outlined above are correct, sulphur release from Deccan eruptions would equate to 5.02 x 10^6 MT of S. This is large, but is likely to be buffered by the larger size of the oceanic reservoir, even at lower concentrations (see 5.6.5 below). An indirect forcing via CO_2 induced climate warming in the late Maastrichtian might be plausible, but as previously mentioned, the increase in $\delta^{34}S_{CAS}$ values occurs prior to chron C29R and the onset of Deccan main phase eruptions (Figure 5.9) (Schoene et al., 2015; Henehan et al., 2016). A volumetrically small, earlier phase of volcanism did occur during chron C30N (Chenet et al., 2009; Keller et al., 2015), but there is little or no evidence that this caused any perturbation to global climate (e.g. Thibault, 2016).

$\delta^{34}S_{CAS}$ and $\delta^{34}S_{Pyrite}$ values appear to show little change at the K–Pg boundary itself, but a positive peak in CAS values (+19.6) is reached ~10m (50-100kyrs) above the boundary interval (Figure 5.10). Sulphur release from the Chicxulub impact event at the K–Pg boundary itself (Arenillas et al., 2006; Renne et al., 2013) also appears to have a negligible effect on seawater $\delta^{34}S$. The Chicxulub impact occurred in a shallow water carbonate platform underlain by significant evaporite deposits (Claypool et al., 1980; Brett, 1992),

so sulphur release was probably substantial and rapid (Ohno et al., 2014; Tyrrel et al., 2015). However, these target rocks likely have an isotopic composition very close to contemporaneous seawater (+18‰ in the compilation of Claypool et al. (1980), meaning any addition is unlikely to alter records of $\delta^{34}S$ directly.

Kajiwara and Kaiho (1992) and Kaiho et al. (1999) suggested on the basis of rapid positive excursions in $\delta^{34}S_{Sulphide}$ and $\delta^{34}S_{CAS}$ at the K–Pg boundary in sections from Japan (Kawaruppu) and Spain (Caravaca), the development of a low oxygen interval in the immediate aftermath of the mass extinction event (Figure 5.10B and C). $\delta^{34}S_{Sulphate}$ values at Caravaca also rise above the boundary and continue at +22‰ during the earliest Danian.

Trace metal proxies have confirmed this low oxygen event in the Caravaca section, but suggest it was confined to the 'impact layer' of fallout located directly at the K–Pg boundary (stratigraphc extent of 1mm) and therefore extremely short-lived (<500 years) (De Oca et al., 2013). There remains rather limited evidence for the extent of any significant anoxic event globally (e.g. Alegret and Thomas, 2005) which may simply represent a short-lived increase in the oxygen minimum zone at intermediate water depths following the extinction.

Nevertheless, evidence from the size range of pyrite framboids does provide evidence for fluctuating benthic redox conditions in the post-boundary interval on Seymour Island (Chapter 3; Witts et al., 2016), which also contains a large number of articulated and disarticulated fish remains; the only such horizon on Seymour Island (Zinsmeister, 1998). This could indicating temporary development of harsh conditions in the water column in the immediate aftermath of the mass extinction. It is therefore possible that this final increase in $\delta^{34}S_{CAS}$ values above the K–Pg boundary on Seymour Island was driven by a short-lived increase in anoxic deposition and pyrite burial just after the boundary interval.

A

$\delta^{13}C_{Carb}$ (‰$_{VPDB}$)

Danian

late Maastrichtian

C29R

C30N

66.02

66.298

67.0

68.0

1
2
3
4
5

B

C29N

65.688

C29R

66.298

C30N (part)

López de Bertodano Formation

$\delta^{34}S_{CAS}$ (‰$_{VCDT}$)

C

i   ii   iii   iv   v

C29N

C29R

65.6
65.7
65.8
65.9
66
66.1

2

Danian

Paleogene

1

66.02

Pre-extinction

Maastrichtian

Cretaceous

$\delta^{13}C_{Carb}$ (‰$_{VPDB}$)

Species richness

N. trumpyi (Benthic)
H. holmdelensis (Surface)
G. falsostuarti (Mixed layer)
S. trivalis (Thermocline)
Pr. taurica (Mixed layer)
Bulk carbonate

222

Figure 5.11 (previous page): Comparison between sulphur and carbon cycling, and biotic change before, during, and in the aftermath of the K–Pg mass extinction event. A: compilation of bulk rock (carbonate) carbon isotope curves from a variety of different ocean basins for the late Maastrichtian taken from Wendler (2013). 1= Lägerdorf-Kronsmoor-Hemmoor (German Chalk), 2=Stevns-1 core (Danish Chalk), 3=Bottaccione/Gubbio (Italian Apennines), 4=Site 762C (Exmouth Plateau, NW Australian Shelf), 5=Site 1210B (Shatsky Rise, Pacific Ocean). Horizontal black dashed line is the K–Pg boundary. Gubbio record has been extended into the Danian based on Husson et al. (2014). B: $\delta^{34}S_{CAS}$ dataset from Seymour Island, Antarctica. Plotted stratigraphically and correlated to magnetostratigraphy of Tobin et al. (2012), ages of chron reversals from GTS2012 (Ogg et al., 2012). Dashed line in the early Paleocene record represents absence of well-preserved CAS data. S, Sobral Formation. C: Record of carbon isotope and biotic change at ODP Site 1262 (Walvis Ridge, central Atlantic). Age model from Dinares-Turrell et al. (2014). i= carbon isotope data from planktonic and benthic foraminifera across the K–Pg boundary, showing collapse of surface-deep water carbon isotope gradient. Coloured lines are different species of foraminifera. Full generic names: _N. truempyi = Nuttalides_, _H.holmdelensis = Hedbergella, G. falsostuarti = Globotruncana, , S. trivalis = Subbotina, Pr. taurica = Praemurica_,. ii= bulk carbon isotope data from Kroon et al. (2007) showing characteristic decrease coinicident with the K–Pg boundary and mass extinction. Dashed circle indicates location of the Dan-C2 carbon isotope excursion in the early Danian. iii and iv = species richness data from benthic foraminifera (Alegret and Thomas, 2007) (iii) and calcareous nannofossils (Jiang et al., 2010) (iv) v= ecological recovery stages of Birch et al. (2016). Stage 1/2 boundary occurs close to base of magnetochron C29N, and the initital recovery of the carbon isotope gradient between surface and deep waters, (increase in export productivity) and coincides with recovery of the Seymour Island $\delta^{34}S_{CAS}$ dataset to pre-extinction values (B). Dashed grey lines mark tentative correlation between magnetostratigraphic tie-points

5.6.4 The early Paleocene negative seawater-sulphate sulphur isotope excursion and the effects of the K–Pg extinction

In Antarctica, $\delta^{34}S_{CAS}$ values show a drop to +12.6‰ some 41.5m above the K–Pg boundary following a ~30m gap due to elimination of samples due to alteration (Figure 5.11) before recovering to a pre-extinction baseline of ~+17–18‰ at the base of the Sobral Formation. This drop and recovery occurs entirely within an interval that is correlated to magnetochron C29R, representing ~320kyrs following the K–Pg (Chapter 3; Appendix B) (Tobin et al., 2012; Bowman et al., 2013).

A significant body of evidence suggests that the K–Pg extinction was followed by a decrease in the primary and export productivity of the oceans (Zachos et al., 1989; D'Hondt, 2005; Esmeray-Senlet et al., 2016; Birch et al., 2016). This is primarily seen in the collapse of the vertical gradient in $\delta^{13}C$ between surface and deep water foraminifera (Zachos et al., 1989; D'Hondt, 2005; Birch et al., 2016), a proxy for the biological carbon pump; sinking of organic matter to deep water with associated remineralisation releasing ^{12}C to the surrounding water (Figure 5.11C-i). Various models exist for this post-extinction ocean, varying from the 'Strangelove' Ocean (Hsü and Mackenzie, 1985) with essentially no primary productivity, to the 'Living Ocean' where primary productivity itself recovers relatively quickly, perhaps driven initially by organic-walled phytoplankton and bacteria (Sepulveda et al., 2009) but where export of organic material to the deep ocean is retarded. Recent studies show strong support for such a 'Living Ocean' model (D'Hondt, 2005; Esmeray-Senlet et al., 2016). Pronounced geographic heterogeneity is also apparent in the response of different ocean basins to the K–Pg event (Hull and Norris, 2011; Esmeray-Senlet et al., 2016).

Reduced carbonate accumulation rates, a decrease in the value bulk carbonate $\delta^{13}C$, and no or little offset in $\delta^{13}C$ between benthic and planktonic taxa characterise the initial aftermath of the K–Pg extinction in the majority of deep ocean sites (Figure 5.11C using ODP Site 1262 on Walvis Ridge, South Atlantic as an example) and in shelf sections (Esmeray-Senlet et al., 2016). Geochemical models suggest that a reduction of 30-40% in organic export or 10% reduction in organic carbon burial (Kump, 1991) is required to achieve the collapse in surface-deep $\delta^{13}C$ gradient seen at this time (Birch et al., 2016). Recovery of the carbon cycle took place in several stages over a >1 myr period, and is closely tied to initial recovery of ecological and taxonomic diversity (D'Hondt, 2005; Coxall et al. 2006; Birch et al., 2016).

The negative excursion in $\delta^{34}S_{CAS}$ followed by recovery could therefore be the result of a significant decrease in pyrite burial associated with large drop in organic export and carbon burial globally. The timing of the subsequent rise to pre-extinction 'background' values occurs close to the base of magnetochron

C29N; ~320 kyrs after the K–Pg boundary. This is very close to the timing of initial recovery of the surface-deep water isotopic gradient in the deep ocean (Stage 1-2 boundary of Birch et al., 2016 (Figure 5.11C-v), and occurs in an interval characterised by stabilising diversity in benthic foraminifera (Alegret and Thomas, 2007 Figure 5.11-iii) and calcareous nannoplankton recovery (Jiang et al., 2010) (Figure 5.11-iv). Intriguingly, this also corresponds with the short-lived 'Dan-C2' hyperthermal event recorded as a series of prominent carbon isotope excursions in deep sea and land-based sections (Coccioni et al., 2010) (Figure 5.11C-ii) although any link between the two has not been established.

On Seymour Island, this also coincides with the stratigraphic interval where species richness in benthic molluscan faunas (bivalves and gastropods) begins to increase following the extinction, with the immigration of new species from South America (Crame et al., 2014) (Chapter 3). These various data would suggest close links between stabilisation of carbon and sulphur cycling, and ecosystem recovery following the K–Pg extinction event in both the Deep Ocean and relatively shallow shelf ecosystems, supporting models of post-extinction ecosystems which closely link processes in both the biosphere and geosphere (e.g. Hull, 2015).

To summarise, a productivity collapse at the K–Pg boundary would lead to a concomitant decline in global pyrite burial and decrease in ocean sulphate $\delta^{34}S$ as light weathered sulphate continues to be added to the system. About 300 kyrs after the extinction, the biological system starts to recover, and carbon is once more exported to the deep ocean. Global pyrite burial flux therefore increases, and re-exerts its influence on the isotopic composition of seawater sulphate, driving it back towards pre-extinction values.

5.6.5 Seawater sulphate concentrations; $\Delta^{34}S_{CAS-Pyrite}$ – stratigraphic fluctuations and their implications

The excursions and rates of change in $\delta^{34}S$ described in the previous section are large; approaching the levels of variability seen during the OAE events during the Jurassic and early-mid Cretaceous (Newton et al., 2011; Owens et

al., 2013; Gomes and Hurtgen, 2016). They are significantly larger than variability recorded in the low-resolution marine barite record for the equivalent time period to this study (Paytan et al., 1998; Paytan et al., 2004). For such large shifts to be primary requires a much lower concentration of seawater sulphate relative to modern oceans. Data from the study of halite fluid inclusion chemistry suggest that Cretaceous sulphate concentrations are generally thought to be >50% lower than today (Holt et al., 2014; Algeo et al., 2015; Gomes and Hurtgen, 2016).

Several methods have been proposed for estimating seawater sulphate concentrations using geological datasets (Kah et al., 2004; Algeo et al., 2015); one utilising the rate of change recorded by CAS datasets through time, and a second relying on the value of $\Delta^{34}S_{CAS-Pyrite}$. This isotopic difference ($\Delta^{34}S$) between seawater ($\delta^{34}S_{CAS}$) and sedimentary ($\delta^{34}S_{Pyrite}$) sulphides in general reflects the kinetic fractionation between microbially-produced hydrogen sulphide (a by-product of MSR), and coeval sulphate derived from seawater (e.g. Canfield, 2001; Brunner and Bernasconi, 2005; Fike et al., 2015). There are many factors that have been shown to influence the size of the isotopic enrichment between sulphate and sulphide but the interactions between these factors and microbial sulphate reduction are complex and not well understood. Algeo et al. (2015) show that whilst there is a lot of scatter in the data, the magnitude of fractionation can be primarily related to sulphate concentration of both seawater and subsequently pore waters (Canfield, 2001; Habicht et al., 2002; Algeo et al., 2015), such that lower fractionations are achieved under lower sulphate concentrations. Other factors such as organic substrate (Canfield, 2001), rates of BSR (Brunner and Bernasconi, 2005) and temperature (Canfield et al., 2006) are considered of secondary importance in the majority of sedimentary environments (Algeo et al., 2015).

We have used Algeo et al's (2015) methodology to derive an estimate for end Cretaceous seawater sulphate concentration. $\Delta^{34}S$ was calculated by subtracting values of $\delta^{34}S_{CAS}$ from stratigraphically equivalent $\delta^{34}S_{Pyrite}$ values. Because the fossils used for CAS isotope study were sometimes collected in binned intervals several meters thick and sediment samples were collected

226

every meter on average, these should be regarded as average values for any given interval (Appendix C- Table C4). The stratigraphic distribution of $\Delta^{34}S$ values in the López de Bertodano Formation can be split into two distinct sections (Figure 5.9), from 166–886m the mean $\Delta^{34}S$ is 43‰, (minimum 21‰, maximum 58‰). Above this, from a stratigraphic height of 916–944m, a cluster of values record significantly lower fractionations; with a mean of 1.27‰ (minimum -6.84‰, maximum 5.6‰). Across the K–Pg boundary, values are tightly clustered around a mean of 31‰ (minimum 24.8‰, maximum 36.8‰).

$\Delta^{34}S$ values approaching 0 fractionation are difficult to explain by simple concentration changes. To achieve this would likely require sulphate concentrations significantly <1 mM (Habicht et al., 2002; Algeo et al., 2015) and would likely be accompanied by substantial variability in the seawater sulphate isotope record. Not such major shift is visible in the CAS data across the interval where $\Delta^{34}S$ values decrease (Figure 5.9; Figure 5.10). A more likely explanation relates to local carbon and sulphur cycling in the subsurface driven by closed system sulphur cycling, anaerobic oxidation of methane (AOM) and the position of the sulphate methane transition in the sediment column driven by sedimentation rate change (Figure 5.6). In many studies of modern marine pore waters, a second locus of sulphate reduction is identified, linked to the disappearance of sulphate and the appearance of methane in pore waters (Lin et al., 2016. This is termed the sulphate methane transition zone (SMTZ) (Sivan et al., 2007). The SMTZ is linked to the production of isotopically heavy pyrite (Peketi et al., 2012; Borowski et al., 2013), which increases the bulk isotopic composition of sedimentary pyrite reservoir, with the potential to affect the relationship between $\Delta^{34}S$ and seawater sulphate concentrations.

The position of the SMTZ in the sediment column is controlled by a number of factors (e.g. Jørgensen and Kasten, 2006; Regnier et al., 2011). These either act from above, relating to diffusion through the overlying sediment column, or from below. Processes acting from above would include the sulphate concentration of the overlying seawater, porosity of the sediment, and amount

of organic carbon burial. In order for organic matter to be available for AOM, it must pass through the overlying biogeochemical zones. Methane flux from below the SMTZ is controlled by diffusion and advection, which is partly a function of sedimentation rate. In an ocean with lower sulphate concentrations, the SMTZ will always be closer to the sediment water interface at any given time (thus setting a higher sensitivity for the system to react to palaeoenvironmental changes) (Appendix E; Hall et al., In Prep).

Alterations to the sedimentation rate in particular could trigger a non-steady state change in the location of the SMTZ; driving it to a higher or lower position in order to achieve equilibrium of advection and diffusion of methane with diffusion of sulphate and organic carbon from overlying seawater (Borowski et al., 2013). In this scenario, production of isotopically heavy pyrite would accompany this change, and potentially be increasingly preserved in the rock record. SMTZ changes could also be driven by increased production and flux of methane from below (e.g. Lin et al., 2016). Non-steady state movement of the SMTZ generates pyrite with a distinctly different isotopic signature to that of pyrite formed from the by-products of BSR (Borowski et al., 2013).

Evidence for an overall change in sedimentation rates in the López de Bertodano Formation is provided by the increased occurrence of glauconite-rich horizons above a stratigraphic height of 830m in the composite section (Figure 5.9). Biostratigraphic data indicates these do not represent significant time gaps (Bowman et al., 2012; Bowman et al., In Press), but are likely periods of periodic lowered sedimentation and reworking. The overall effect of an increased number of these intervals would lead to lower overall sedimentation rates compared to stratigraphically lower in the succession.

This interval broadly overlaps with the occurrence of extremely negative carbon isotope signatures recorded in bivalve carbonate (Appendix E; Hall et al., In Prep), suggesting changes to the location of the SMTZ and AOM drive increased imprint of methane carbon on the isotopic composition of DIC. Such changes might also be expected to manifest themselves in an increase in pyrite abundance (e.g. Lin et al., 2016), but due to the evidence for pyrite

oxidation in this succession (Figure 5.3), it is impossible to test this. An overall increase in $\delta^{34}S_{Pyrite}$ and drop in $\Delta^{34}S$ in the same stratigraphic interval (Figure 5.9B, C; Figure 5.10) also support increased contribution of isotopically heavy pyrite from non-steady state SMTZ behaviour. Lack of change in other parameters that might affect fractionation during MSR such as significant changes in the style of sedimentation or increased TOC (Figure 5.3), indicate the SMTZ hypothesis is the primary control on the isotopic signal from pyrite and therefore $\Delta^{34}S$ values in this succession.

Identification of this local control indicates that values of $\Delta^{34}S$ from the upper portion of the section (>830m) may be influenced by secondary processes and local sulphur cycling. Thus the equations of Algeo et al. (2015) were only applied to data from below the interval where the SMTZ signature becomes apparent, where this effect is probably minimised.

Using the rate method, and assuming a rate of change of 2.75‰ Myr^{-1} (based on the 3‰ shift from around +15‰ to +18‰ between 728m and 920m – a time interval representing slightly more than ~2 myr (Tobin et al., 2012; Bowman et al., 2013) (Figure 5.9), a pyrite flux of 4 x 10^{13} g yr^{-1} – equivalent to modern sink flux – and $\Delta^{34}S$ range of 21 to 58‰ (mean 43‰) gives a mean seawater concentration of 13 mM (range 7 to 18 mM using minimum and maximum values of $\Delta^{34}S$) . The value of pyrite flux used by Algeo et al. (2015) may not be appropriate for the K–Pg time interval, as a warmer Cretaceous ocean likely contained lower dissolved bottom water oxygen levels (Hay, 2008). Kah et al. (2004) suggested a flux of 10 x 10^{13} g yr^{-1} for a fully euxinic Proterozoic ocean which provides an extreme end-member.

Therefore, adjusting for a moderately increased pyrite flux in the less well-oxygenated (but not euxinic) Mesozoic ocean (6 x 10^{13} g yr^{-1}) yields a mean seawater concentration value of 21 mM (range 10 to 28 mM). The rate method also allows a calculation of the mass of seawater sulphate reservoir (Msw); assuming a mean concentration of 21 mM, would equate to a mass of 9.3 x 10^{20} g, an order of magnitude lower than today (1.3 x 10^{21} g).

The MSR method using empirical equations derived by Algeo et al. (2015) yields a mean concentration of 18 mM, a minimum of 2 mM and maximum of

47 mM. Mean values derived from both methods are lower than today, but overlap with estimated values from other proxies and modelling of seawater concentrations for the late Mesozoic and early Cenozoic (e.g. lower values during the early Cretaceous; 6 to 14 mM from 94–112 Ma, rising into the Cenozoic to 13 to 23 mM at ~37 Ma Holt et al., 2014; Lowenstein et al., 2003; Wortmann and Paytan, 2012). They also compare extremely well with estimated values from Algeo et al. (2015), using the Phanerozoic compilation of $\Delta^{34}S$ from Wu et al. (2010).

These data confirm that the concentration of sulphate in Latest Cretaceous and early Paleogene seawater was significantly lower than today, indicating that the sulphur cycle may have been able to respond rapidly to contemporaneous environmental changes. This data also lends support to the model of Hall et al. (In prep) for fundamentally different forms of biogeochemical cycling in these ancient oceans, with increased importance of processes such as methanogenesis in influencing the isotopic composition of the DIC of bottom waters, as recorded by fossil carbonates. Such processes are only possible at lower seawater sulphate concentrations than modern.

5.7 Conclusions

- This is the highest resolution seawater sulphate record ever generated for this time period, revealing changes to the global sulphur cycle before, and after the K–Pg mass extinction event.
- Detailed assessment of sample preservation and fidelity of the record suggest factors affecting preservation of primary seawater CAS isotopes are complex and not necessarily linked to the preservation of original carbonate mineralogy or chemistry. The influence of local pore water chemistry and biogeochemical processes in driving changes to sulphur cycle proxies such as CAS should be considered before the primary record is interpreted.
- This study provides clear evidence of the influence of pyrite oxidation on CAS isotope compositions, and emphasises the importance of $\delta^{18}O_{CAS}$ as a tool for assessing the influence of this process.

- Interpretation of the primary record and comparison with contemporaneous environmental change reveals evidence for a relatively stable sulphur cycle in the early to mid-Maastrichtian (69 Ma).

- A +4‰ shift in $\delta^{34}S_{CAS}$ suggests a late Maastrichtian increase in pyrite burial, possibly decoupled from global carbon cycle changes in the late Maastrictian-earliest Danian. This record may be partly influenced by short term anoxia immediately following the K–Pg boundary.

- There is no evidence of the direct influence of Deccan volcanism on seawater sulphate record during the late Maastrichtian, probably due to the buffering effect of the much larger seawater reservoir.

- There is also no evidence of a direct influence of the Chicxulub impactor on the seawater sulphate record, probably because of the nature and composition of the target rocks.

- Changes to the carbon cycle as a result of the K–Pg mass extinction event also affected the global sulphur cycle. This is recorded in a prominent negative excursion in sulphate-S isotopes during the earliest Paleogene (66 – 65.7 Ma) driven by productivity collapse and drop in pyrite burial.

- Recovery of seawater sulphate isotopes to pre-extinction values occurs at the same time as the initial recovery of the global carbon cycle following in the extinction, as well as evidence for biotic and ecological recovery ~350 kyrs aftr the mass extinction

- Coupled pyrite and CAS sulphur isotope records record local non-steady state processes acting on the sulphur cycle in the James Ross Basin; specifically the effects of the repositioning of the SMTZ which coincides with evidence for sedimentation rate changes, as well as coinciding with methane dominated DIC in bottom waters in the late Maastrichtian and across the K–Pg boundary.

- Estimates of seawater sulphate concentrations from coupled isotopic records agree with previous independent estimates from halite fluid inclusions for the Cretaceous and Paleogene time periods. The K–Pg seawater sulphate reservoir was around 50% smaller than the modern,

consistent with the potential for it to record dynamic changes of the type outlined above.

5.8 References

Adams D.D., Hurtgen, M.T., Sageman, B.B., 2010. Volcanic triggering of a biogeochemical cascade during Oceanic Anoxic Event 2. *Nature Geoscience* **3**, 201–204.

Alegret, L., Thomas, E., 2005. Cretaceous/Paleogene boundary bathyal palaeoenvironments in the central North Pacific (DSDP Site 465), the Northwestern Atlantic (ODP Site 1049), the Gulf of Mexico and the Tethys: the benthic foraminiferal record. *Palaeogeography, Palaeoclimatology, Palaeoecology* **224**, 53–82.

Alegret, L., Thomas, E., 2007. Deep-sea environments across the Cretaceous/Paleogene boundary in the eastern South Atlantic Ocean (ODP Leg 208, Walvis Ridge). *Marine Micropaleontology* **64**, 1–17.

Algeo, T.J., Luo, G.M., Song, H.Y., Lyons, T.W., Canfield, D.E., 2015. Reconstruction of secular variation in seawater sulfate concentrations. *Biogeosciences* **12**, 2131–2151.

Alvarez, L.W., Alvarez, W., Asaro, F., Michel, H.V., 1980. Extraterrestrial cause for the Cretaceous-Tertiary Extinction. *Science* **208**, 1095–1108.

Archibald, J.D., Clemens, W.A., Padian, K., Rowe, T., MacLeod, N., Barrett, P.M., Gale, A., Holroyd, P., Sues, H.-D., Arens, N.C., Horner, J.R., Wilson, G.P., Goodwin, M.B., Brochu, C.A., Lofgren, D.L., Hurlbert, S.H., Hartman, J.H., Eberth, D.A., Wignall, P.B., Currie, P.J., Weil, A., Prasad, G.V.R., Dingus, L., Courtillot, V., Milner, A., Milner, A., Bajpai, S., Ward, D.J., Sahni, A., 2010. Cretaceous extinctions: multiple causes. *Science* **328**, 973.

Arenillas, I., Arz, J., Molina, E., 2004. A new high resolution planktic foraminiferal zonation and subzonation for the lower Danian. *Lethaia* **37**, 79–95.

Askin, R.A., Jacobson, S.R., 1988. Total Organic Carbon content and Rock Eval pyrolysis on outcrop samples across the Cretaceous/Tertiary boundary, Seymour Island, Antarctica. *Antarctic Journal of the United States* **1988,** 37–39

Bambach, R.K., 2006. Phanerozoic biodiversity mass extinctions. *Annual Reviews of Earth and Planetary Science* **34**, 127–155.

Barrera, E., Savin, S.M., 1999. Evolution of late Campanian–Maastrichtian marine climates and oceans. In: *Barrera, E., Johnson, C.C. (Eds.), Evolution of the Cretaceous Ocean- Climate System*. Geological Society of America Special Paper **332**, pp. 245–282.

Berner, R.A., 1982. Burial of organic carbon and pyrite sulfur in the modern ocean: its geochemical and environmental significance. *American Journal of Science* **282**, 451–473.

Birch, H.S., Coxall, H.K., Pearson, P.N., Kroon, D. and Schmidt, D.N. 2016. Partial collapse of the marine carbon pump after the Cretaceous-Paleogene boundary. *Geology* **44**, 287–290.

Borowski, W.S., Rodriguez, N.M., Paull, C.K., Ussler, III, W., 2013. Are ^{34}S-enriched authigenic sulfide minerals a proxy for elevated methane flux and gas hydrates in the geologic record? *Marine and Petroleum Geology* **43**, 381–395.

Bottrell, S.H., Newton, R.J., 2006. Reconstruction of changes in global sulfur cycling from marine sulfate isotopes. Earth-Science Reviews **75**, 59–83.

Bowman, V. C., Francis, J. E. & Riding, J. B. 2013. Late Cretaceous winter sea ice in Antarctica? *Geology* **41**, 1227–1230.

Bowman, V.C. *et al.*, In Press. The Paleocene of Antarctica: Dinoflagellate cyst biostratigraphy, chronostratigraphy and implications for the palaeo-Pacific margin of Gondwana. *Gondwana Research* doi:10.1016/j.gr.2015.10.018 .

Bowman, V.C., Francis, J.E., Askin, R.A., Riding, J.B., Swindles, G.T., 2014. Latest Cretaceous–earliest Paleogene vegetation and climate change at the

high southern latitudes: palynological evidence from Seymour Island, Antarctic Peninsula. *Palaeogeography Palaeoclimatolology Palaeoecology* **408**, 26–47.

Bowman, V.C., Francis, J.E., Riding, J.B., Hunter, S.J., Haywood, A.M., 2012. A latest Cretaceous to earliest Paleogene dinoflagellate cyst zonation from Antarctica, and implications for phytoprovincialism in the high southern latitudes. *Review of Palaeobotany and Palynology* **171**, 40–56.

Brett, R., 1992. The Cretaceous-Tertiary extinction: A lethal mechanism involving anhydrite target rocks. *Geochimica et Cosmochimica Acta* **56**, 3603-3606.

Brunner, B., Bernasconi, S.M., 2005. A revised isotope fractionation model for dissimilatory sulfate reduction in sulfate reducing bacteria. *Geochemica Cosmochemica Acta* **69**, 4759–4771.

Busenberg, E., Plummer, L.N., 1985. Kinetic and thermodynamic factors controlling the distribution of SO_4 an $Na+$ in calcites and selected aragonites. *Geochemica Cosmochemica Acta* **49**, 713–725.

Callegaro, S., Baker, D.R., de Min, A., Marzoli, A., Geraki, K., Bertrand, H., Viti, C., Nestola, F., 2014. Microanalyses link sulfur from large igneous provinces and Mesozoic mass extinctions. *Geology* **42**, 895-898.

Canfield, D.E., Raiswell, R., Westrich, J.T., Reaves, C.M., Berner, R.A., 1986. The use of chromium reduction in the analysis of reduced inorganic sulfur in sediments and shales. *Chemical Geology* **54**, 149–155.

Canfield, D.E., Rosing, M., Bjerrum, C., 2006. Early anaerobic metabolisms. *Philosophical Transactions of the Royal Society B: Biological Sciences* **361**,

Canfield, D.E., 2001. Biogeochemistry of Sulfur Isotopes. *Reviews in Mineralogy and Geochemistry* **43**, 607–636.

Chenet, A.-L., Courtillot, V., Fluteau, F., Gérard, M., Quidelleur, X., Khadri, S.F.R., Subbarao, K.V., Thordarson, T., 2009. Determination of rapid Deccan eruptions across the Cretaceous-Tertiary boundary using paleomagnetic secular variation: 2. Constraints from analysis of eight new sections and

synthesis for a 3500-m-thick composite section. *Journal of Geophysical Research* **114**, B06103. http://dx.doi.org/10.1029/2008JB005644.

Claypool, G. E., W. T. Holser, I. R. Kaplan, H. Sakai, and I. Zak (1980), The age curves of sulfur and oxygen isotopes in marine sulfate and their mutual interpretation, *Chemical Geology* **28**, 199–260.

Coccioni, R., Frontalini, F., Bancalá, G., Fornaciari, E., Jovane, L., Sprovieri, M., 2010. The Dan-C2 hyperthermal event at Gubbio (Italy): Global implications, environmental effects, and cause(s). *Earth and Planetary Science Letters* **297**, 298–305.

Courtillot, V., Fluteau, F., 2010. Cretaceous extinctions: the volcanic hypothesis. *Science* **328**, 973–974.

Coxall, H.K., D'Hondt, S., Zachos, J.C., 2006. Pelagic evolution and environmental recovery after the Cretaceous-Paleogene mass extinction. *Geology* **34,** 297-300.

Crame, J.A., McArthur, J.M., Pirrie, D., Riding, J.B., 1999. Strontium isotope correlation of the basal Maastrichtian Stage in Antarctica to the European and US biostratigraphic schemes*. Journal of the Geological Society of London.* **156**, 957–964.

Crame, J. A., Beu, A. G., Ineson, J. R., Francis, J. E., Whittle, R. J. & Bowman, V. C., 2014. The early origins of the Antarctic marine fauna and its evolutionary implications. *PLoS ONE* **9**, e114732.

Crame, J.A., Francis, J.E., Cantrill, D.E., Pirrie, D., 2004. Maastrichtian stratigraphy of Antarctica. *Cretaceous Research* **25**, 411–423.

Cramer, B.S., Toggweiler, J.R., Wright, J.D., Katz, M.E., Miller, K.G., 2009. Ocean overturning since the late cretaceous: Inferences from a new benthic foraminiferal isotope compilation. *Paleoceanography* **24.**

D'Hondt, S., 2005. Consequences of the Cretaceous/Paleogene mass extinction for marine ecosystems. *Annual Reviw of Ecology, Evolution, and Systematics* **36**, 295–317

De Oca, C.S.M., Martínez-Ruiz, F., Rodríguez-Tovar, F.J., 2013. Bottom-water conditions in a marine basin after the Cretaceous-Paleogene impact event: timing the recovery of oxygen levels and productivity. PLOS One http://dx.doi.org/10.1371/journal.pone.0082242

Dinarès-Turrell, J., Westerhold, T., Pujalte, V., Röhl, U., Kroon, D., 2014. Astronomical calibration of the Danian stage (Early Paleocene) revisited: Settling chronologies of sedimentary records across the Atlantic and Pacific Oceans. *Earth and Planetary Science Letters* **405**, 119–131.

Ditchfield, P.W.,Marshall, J.D., Pirrie, D., 1994. High latitude Palaeotemperature variation: new data from the Tithonian to Eocene of James Ross Island, Antarctica. *Palaeogeography Palaeoclimatolology Palaeoecology* **107**, 79–101.

Dubicka, Z., Peryt, D., 2012. Latest Campanian and Maastrichtian palaeoenvironmental changes: implications from an epicontinental sea (SE Poland and western Ukraine). *Cretaceous Research* **37**, 272–284.

Elliot, D.H., 1988. Tectonic setting and evolution of the James Ross Basin, northern Antarctic Peninsula. In: Feldmann, R.M., Woodburne, M.O. (Eds.), *Geology and Paleontology of Seymour Island, Antarctic Peninsula*. Geological Society of America, Memoirs **169**. 541-555.

Elliot, D.H., Askin, R.A., Kyte, F.T., Zinsmeister, W.J., 1994. Iridium and dinocysts at the Cretaceous-Tertiary boundary on Seymour Island, Antarctica: implication for the K–T event. *Geology* **22**, 675–678.

Esmeray-Senlet, S., Wright, J.D., Olsson, R.K., Miller, K.G., Browning, J.V., Quan, T.M., 2015. Evidence for reduced export productivity following the Cretaceous/Paleogene mass extinction. *Paleoceanography* **30**, 718-738.

Feldmann R. M., Woodburne M. O.*, eds (1988) Geology and Paleontology of Seymour Island, Antarctic Peninsula* **169***:*Memoir, Geological Society of America*.

Fike, D.A., Bradley, A.S., Rose, C.V., 2015. Rethinking the Ancient Sulfur Cycle. *Annual Reviews of Earth and Planetary Science* **43**, 593–622.

Friedrich, O., Norris, R.D., Erbacher, J., 2012. Evolution of middle to Late Cretaceous oceans—a 55 m.y. record of Earth's temperature and carbon cycle. *Geology* **40**, 107–110.

Gill B.C., Lyons, T.W., Frank, T.D., 2008. Behavior of carbonate-associated sulfate during meteoric diagenesis and implications for the sulfur isotope paleoproxy. *Geochemica Cosmochemica Acta* **72**, 4699–4711.

Gill B.C., Lyons, T.W., Young, S.W., Kump, L.R., Knoll, A.H., Saltzmann, M.R., 2011. Geochemical evidence for widespread euxinia in the Later Cambrian Ocean. *Nature* **469**, 80–83.

Gomes M.L., Hurtgen, M.T., Sageman, B.B., 2016. Biogeochemical sulphur cycling during Cretaceous oceanic anoxic events: a comparison of OAE1a and OAE2. *Paleoceanography* **31**, 233–251.

Gradstein, F. M., Ogg, J. G., Schmitz, M. & Ogg, G., 2012. *The Geological Time Scale 2012* Elsevier Science Ltd: Boston.

Gradstein, F. M., Ogg, J. G., Smith, A.G., 2004. *A Geologic Time Scale 2004* Cambridge University Press, Cambridge, 589p.

Habicht, K.S., Gade, M., Thamdrup, B., Berg, P., Canfield, D.E., 2002. Calibration of sulphate levels in the Archaean Ocean. *Science* **298**, 2372–2374.

Hall, J.L.O., Newton, R.J., Witts, J.D., Francis, J.E., Harper, E.M., Crame, J.A., Haywood, A.M., Hunter, S.J., In preperation. Sedimentary carbon cycling in a low sulfate ocean: evidence of episodic seasonal methane oxidation in the Cretaceous Antarctic.

Haq, B.U., 2014. Cretaceous eustasy revisited. *Global and Planetary Change* **113**, 44–58.

Hathway, B., 2000. Continental rift to back-arc basin: Jurassic–Cretaceous stratigraphical and structural evolution of the Larsen Basin, Antarctic Peninsula. *Journal of the Geological Society of London.* **157**, 417–432.

Hay, W.W., 2008. Evolving ideas about the Cretaceous climate and ocean circulation. *Cretaceous Research* **29**, 725–753.

Henehan, M.J., Hull, P.M., Penman, D.E., Rae, J.W.B. and Schmidt, D.N. 2016. Biogeochemical significance of pelagic ecosystem function: An end-cretaceous case study. *Philosophical Transactions of the Royal Society B: Biological Sciences* **371**.

Hildebrand, A.R., Penfield, G.T., Kring, D.A., Pilkington, M., Camargo Z, A., Jacobsen, S.B., Boynton, W.V., 1991. Chicxulub crater: A possible Cretaceous/Tertiary boundary impact crater on the Yucatán Peninsula, Mexico. *Geology* **19**, 867–871.

Holt, N.M., Garcia-Veiga, J., Lowenstein, T.K., Giles, P.S., Williams-Stroud, S., 2014. The major ion composition of Carboniferous seawater. *Geochemica Cosmochemica Acta* **134**, 317–334.

Hsü, K.J., McKenzie, J.A., 1985. A "Strangelove" ocean in the earliest Tertiary. In: Sunquist, E.T., Broecker,W.S. (Eds.), *The Carbon Cycle and Atmospheric CO_2: Natural Variations Archaean to Present*. American Geophysical Union, Washington D.C., pp. 487–492.

Hull, P.M., Norris, R.D., 2011. Diverse patterns of ocean export productivity change across the Cretaceous-Paleogene boundary: new insights frombiogenic barium. *Paleoceanography* **26**, 1–10.

Jiang, S., Bralower, T. J., Patzkowsky, M. E., Kump, L. R., Schueth, J. D., 2010. Geographic controls on nannoplankton extinction across the Cretaceous/Paleogene boundary. *Nature Geoscience* **3**, 280–285.

John, E.H., Wignall, P.B., Newton, R.J., Bottrell, S.H., 2010. $\delta^{34}S_{CAS}$ and $\delta^{18}O_{CAS}$ records during the Frasnian-Fammenian (Late Devonian) transition and their bearing on mass extinction models. *Chemical Geology* **275**, 221–234.

Jones, D.S., Fike, D.A., 2013. Dynamic sulfur and carbon cycling through the end-Ordovician extinction revealed by paired sulfate-pyrite $\delta^{34}S$. *Earth and Planetary Science Letters* **363**, 144–155.

Jørgensen, B.B., 1982. Mineralization of organic matter in the sea bed – the role of sulphate reduction. *Nature* **296**, pp. 643–645

Jørgensen, B.B., Kasten, S., 2006. Sulfur cycling and methane oxidation. In *Marine Geochemistry*, pp. 271–309.

Jung, C., Voigt, S., Friedrich, O., Koch, M.C., Frank, M., 2013. Campanian-Maastrichtian ocean circulation in the tropical Pacific. *Paleoceanography* **28**, 562–573. http://dx.doi.org/10.1002/palo.20051 .

Kah, L.C., Lyons, T.W., Frank, T.D., 2004. Low marine sulphate and protracted oxygenation of the Proterozoic biosphere. *Nature* **431**, 834–838.

Kaiho, K., Saito, T., 1986. Terminal Cretaceous sedimentary sequence recognized in the northernmost Japan based on planktic foraminiferal evidence. *Proceedings of the Japanese Academy of Science Series B*, **62**, 145–148.

Kaiho K., Kajiwara, Y., Tazaki, K., Ueshima, M., Takeda, N., Kawahata, H., Arinobu, T., Ishiwatari, R., Hirai, A., Lamolda, M., 1999. Oceanic primary productivity and dissolved oxygen levels at the Cretaceous/Tertiary boundary: their decrease, subsequent warming, and recovery. *Paleoceanography* **14**, 511–524.

Kajiwara, Y., Kaiho, K., 1992. Oceanic anoxia at the Cretaceous/Tertiary boundary supported by the sulfur isotopic record. *Palaeogeography, Palaeoclimatology, Palaeoecology* **99**, 151–162.

Kampschulte A., Strauss, H., 2004. The sulfur isotopic evolution of Phanerozoic seawater based on the analysis of structurally substituted sulfate in carbonates. *Chemical Geology* **204**, 255–286.

Kampschulte A., Bruckschen, P., Strauss, H., 2001. The sulphur isotopic composition of trace sulphates in Carboniferous brachiopods: implications for coeval seawater, correlation, with other geochemical cycles and isotope stratigraphy. *Chemical Geology* **175**, 149–173.

Keller, G., Adatte, T., Pardo, A., Bajpai, S., Khosla, A., Samant, B., 2010. Cretaceous extinctions: evidence overlooked. *Science* **328**, 974–975.

Keller, G., Punekar, J., Mateo, P., 2016. Upheavals during the Late Maastrichtian: Volcanism, climate and faunal events preceding the end-

Cretaceous mass extinction. *Palaeogeography, Palaeoclimatology, Palaeoecology* **441**, 137–151.

Komintz, M.A., Browning, J.V., Miller, K.G., Sugarman, P.J., Misintseva, S., Scotese, C.R., 2008. Late Cretaceous to Miocene sea-level estimates from the New Jersey and Delaware coastal plain coreholes: an error analysis. *Basin Research* **20**, 211–226.

Kroon, D., J. C. Zachos, and the Leg 208 Scientific Party (2007), Leg 208 synthesis: Cenozoic climate cycles and excursions, Proc. Ocean Drill. Program Sci. Results, 208, 55 pp

Kump, L.R. 1991. Interpreting carbon-isotope excursions: Strangelove oceans. *Geology* **19**, 299-302.

Kurtz, A.C., Kump, L.R., Arthur, M.A., Zachos, J.C., Paytan, A., 2003. Early Cenozoic decoupling of the global carbon and sulfur cycles. *Paleoceanography* **18**, 1090, doi:10.1029/2003PA000908, 4.

Lawver, L.A., Gahagan, L.M., Coffin, M.F., 1992. The development of paleoseaways around Antarctica. In: Kennett, J.P., Warnke, D.A. (Eds.), *Antarctic Research Series* **56**, pp. 7–30.

Li, L., Keller, G., 1998. Abrupt deep-sea warming at the end of the Cretaceous. *Geology* **26**, 995–998.

Lin Q., Wang, J., Algeo, T.J., Sun, F., Lin, R., 2016. Enhanced framboidal pyrite formation related to anaerobic oxidation of methane in the sulfate-methane transition zone of the northern South China Sea. *Marine Geology* **379**, 100–108.

Little C.T.S., Birgel, D., Boyce, A.J., Crame, J.A., Francis, J.E., Kiel, S., Peckmann, J., Pirrie, D., Rollinson, G.K., Witts, J.D., 2015. Late Cretaceous (Maastrichtian) shallow water hydrocarbon seeps from Snow Hill and Seymour Islands, James Ross Basin, Antarctica. *Palaeogeography, Palaeoclimatology, Palaeoecology* **418**, 213–228.

Lowenstein, T.K., Hardie, L.A., Timofeeff, M.N., Demicco, R.V., 2003. Secular variation in seawater chemistry and the origin of calcium chloride basinal brines. *Geology* **31**, 857–860.

Lyons T.W., Walter, L.M., Gellatly, A.M., Martin, A.M., Blake, R.E., 2004. Sites of anomalous organic remineralization in the carbonate sediments of South Florida, USA: the sulfur cycle and carbonate associated sulfate. In: J.P. Amend, K.J. Edwards, T.W. Lyons (Eds.), *Sulfur Biogeochemistry—Past and Present*, Geological Society of America Special Papers vol. **379**, pp. 161–176.

Macellari, C.E., 1988. Stratigraphy, sedimentology and paleoecology of Upper Cretaceous/Paleocene shelf-deltaic sediments of Seymour Island (Antarctic Peninsula). In: Feldmann, R.M., Woodburne, M.O. (Eds.), *Geology and Paleontology of Seymour Island, Antarctic Peninsula*. Geological Society of America, Memoirs **169**, pp. 25–53.

MacLeod, K.G., Huber, B.T., Ward, P.D., 1996. The biostratigraphy and paleobiogeography of Maastrichtian inoceramids. In: Ryder, G., Fastovsky, D., Gartner, S. (Eds.), *The Cretaceous-Tertiary Event and Other Catastrophes in Earth History*. Geological Society of America Special Paper **307**, pp. 361–373.

Marenco, P.J., Corsetti, F.A., Hammond, D.E., Kaufman, A.J., Bottjer, D.J., 2008a. Oxidation of pyrite during extraction of carbonate associated sulfate. *Chemical Geology* **247**, 124–132.

Marenco, P.J., Corsetti, F.A., Kaufman, A.J., Bottjer, D.J., 2008b. Environmental and diagenetic variations in carbonate associated sulfate: An investigation of CAS in the Lower Triassic of the western USA. *Geochemica Cosmochemica Acta* **72**, 1570–1582.

Mazumdar A., Goldberg, T., Strauss, H., 2008. Abiotic oxidation of pyrite by Fe(III) in acidic media and its implications for sulfur isotope measurements of lattice-bound sulfate in sediments. *Chemical Geology* **253**, 30–37.

McArthur, J.M., Thirlwall, M.F., Engkilde, M., Zinsmeister, W.J., Howarth, R.J., 1998. Strontium isotope profiles across K/T boundary sequences in Denmark and Antarctica. *Earth and Planetetary Science Letters* **160**, 179–192.

McArthur, J.M., Crame, J.A., Thirlwall, M.F., 2000. Definition of Late Cretaceous stage boundaries in Antarctica using strontium isotope stratigraphy. *Journal of Geology* **108**, 623–640.

Miller, K.G., Kominz, M.A., Browning, J.V., Wright, J.D., Mountain, G.S., Katz, M.E., Sugarman, P.J., Cramer, B.S., Christie-Blick, N., Pekar, S.F., 2005. The Phanerozoic record of global sea-level change. *Science* **310**, 1293-1298.

Molina, E., Alegret, L., Arenillas, I., Arz, J.A., Gallala, N., Grajales-Nishimura, Murillo-Muneton, G., Zaghbib-Turki, D., 2009. The Global Boundary Stratotype Section and Point for the base of the Danian Stage (Paleocene, Paleogene, "Tertiary", Cenozoic), auxiliary sections and correlation. *Episodes* **32**, 84–95.

Molina, E., Alegret, L., Arenillas, I., Arz, J.A., Gallala, N., Hardenbol, J., von Salis, K., Steurbaut, E., Vandenberghe, N., Zaghbib-Turki, D., 2006. The global boundary stratotype section and point for the base of the Danian stage (Paleocene, Paleogene, "Tertiary", Cenozoic) at El Kef, Tunisia – original definition and revision. *Episodes* **29**, 263–273.

Newton, R.J., Pevitt, E.L., Wignall, P.B., Bottrell, S.H., 2004. Large shifts in the isotopic composition of seawater sulphate across the Permo-Triassic boundary in northern Italy. Earth and Planetary Science Letters 218, 331-345.

Newton R.J., Reeves, E.P., Kafousia, N., Wignall, P.B., Bottrell, S.H., Sha, J.G., 2011. Low marine sulfate concentrations and the isolation of the European epicontinental sea during the Early Jurassic. Geology 39, 7–10.

Ohno, S., Kadono, T., Kurosawa, K., Hamura, T., Sakaiya, T., Shigemori, K., Hironaka, Y., Sano, T., Watari, T., Otani, K. and Matsui, T., 2014. Production of sulphate-rich vapour during the Chicxulub impact and implications for ocean acidification. *Nature Geoscience*, **7**, 279-282.

Olivero, E.B., 2012. Sedimentary cycles, ammonite diversity and palaeoenvironmental changes in the Upper Cretaceous Marambio Group, Antarctica. *Cretaceous Research* **34**, 348–366.

Olivero, E.B., Ponce, J.J., Martinioni, D.R., 2008. Sedimentology and architecture of sharp based tidal sandstones in the Upper Marambio Group, Maastrichtian of Antarctica. *Sedimentary Geology* **210**, 11–26.

Owens, J.D., Gill, B.C., Jenkyns, H.C., Bates, S.M., Severmann, S., Kuypers, M.M.M., Woodfine, R.G., Lyons, T.W., 2013. Sulfur isotopes track the global extent and dynamics of euxinia during Cretaceous Oceanic Anoxic Event 2. *Proceedings of the National Academy of Science* **110**, 18407–18412.

Panchuk K. L., Holmden, C.E., Leslie, S.A., 2006. Local controls on carbon cycling in the Ordovician midcontinent regions of North America, with implications for carbon isotope secular curves. *Journal of Sedimentary Research* **76**, 200–211.

Paytan A., Kastner, M., Campbell, D., Thiemens, M.H., 1998. Sulfur isotopic composition of Cenozoic seawater sulfate. *Science* **282**, 1459–1462.

Paytan A., Kastner, M., Campbell, D., Thiemens, M.H., 2004. Seawater sulfur isotope fluctuations in the Cretaceous. *Science* **304**, 1663–1665.

Peketi, A., Mazumdar, A., Joshi, R.K., Patil, D.J., Srinivas, P.L., Dayal, A.M., 2012. Tracing the Paleo sulfate-methane transition zones and H_2S seepage events in marine sediments: an application of C-S-Mo systematics. *Geochemistry, Geophysics, Geosystems* **13**, DOI 10.1029/2012GC004288

Pirrie, D., Marshall, J.D., 1990. High-paleolatitude Late Cretaceous palaeotemperatures: New data from James Ross Island, Antarctica. *Geology* **18**, 31–34.

Poulton, S.W., Canfield, D.E., 2005. Development of a sequential extraction procedure for iron: Implications for iron partitioning in continentally derived particulates, *Chemical Geology* **214**, 209–221

Poulton, S.W., Henkel S., März C., Urquhart H., Flögel S., Kasten S., Sinninghe Damsté JS., Wagner T., 2015. A continental-weathering control on orbitally driven redox-nutrient cycling during Cretaceous Oceanic Anoxic Event 2, *Geology* **43**, 963–966

Regnier P., Dale, A., Arndt, S., LaRowe, D.E., Mogollen, J., Van Cappellen, P., 2011. Quantitative analysis of Anaerobic Oxidation of Methane (AOM) in marine sediments: a modelling perspective. *Earth-Science Reviews* **106**, 105–130.

Renne, P. R., Deino, A.L., Hilgen, F.J., Kuiper, K.F., Mark, D.F., Mitchell, W.S.III., Morgan, L.E., Mundil, R., Smit, J., 2013. Time scales of critical events around the Cretaceous–Paleogene boundary. *Science* **339**, 684–687 (2013).

Renne, P.R., Sprain, C.J., Richards, M.A., Self, S., Vanderkluysen, L., Pande, K., 2015. State shift in Deccan volcanism at the Cretaceous–Paleogene boundary, possibly induced by impact. *Science* **350**, 76–78.

Rennie, V.C.F., Turchyn, A.V., 2014. The preservation of $\delta^{34}S_{SO4}$ and $\delta^{18}O_{SO4}$ in carbonate-associated sulfate during marine diagenesis: a 25 Myr test case using marine sediments. *Earth and Planetary Science Letters* **395**, 13–23.

Richards, M. A., Alvarez, W., Self, S., Karlstrom, L., Renne, P.R., Manga, M., Sprain, C.J., Smit, J., Vanderkluysen, L., Gibson, S.A., 2015. Triggering of the largest Deccan eruptions by the Chicxulub impact. *Geological Society of America Bulletin* **127**, 1507–1520.

Robinson, N., Ravizza, G., Coccioni, R., Peucker-Ehrenbrink, B., Norris, R.D., 2009. A high resolution marine $^{187}Os/^{188}Os$ record for the late Maastrichian: distinguishing the chemical fingerprints of Deccan volcanism and the KP impact event. *Earth and Planetary Science Letters* **281**, 159–168.

Rooze, J., Egger, M., Tsandve, I., Slomp, C.P., 2016. Iron-dependent anaerobic oxidation of methane in coastal surface sediments: potential controls and impact. *Limnology and Oceanography* **00**, 1–26.

Schmidt, A., Skeffington, R.A., Thordarson, T., Self, S., Forster, P.M., Rap, A., Ridgwell, A., Fowler, D., Wilson, M., Mann, G.W., Wignall, P.B., Carslaw, K.S., 2016. Selective environmental stress from sulphur emitted by continental flood basalt eruptions. *Nature Geoscience* **9**. 77–82 (2016).

Schoene, B., Samperton, K.M., Eddy, M.P., Keller, G., Adatte, T., Bowring, S.A., Khadri, S.F. and Gertsch, B., 2015. U-Pb geochronology of the Deccan

Traps and relation to the end-Cretaceous mass extinction. *Science* **347,** 182-184.

Schulte, P.D., Alegret, L., Arenillas, I., Arz, J.A., Barton, P.J., Bown, P.R., Bralower, T.J., Chisteson, G.L., Claeys, P., Cockell, C.S., Collins, G.S., Deutsch, A., Goldin, T.J., Goto, K., Grajales-Nishimura, J.M., Grieve, R.A.F., Gulick, S.P.S., Johnson, K.R., Kiessling, W., Koeberl, C., Kring, D.A., MacLeod, K.G., Matsui, T., Melosh, J., Montanari, A., Morgan, J.V., Neal, C.R., Nichols, D.J., Norris, R.D., Pierazzo, E., Ravizza, G., Rebolledo-Vieyra, M., Reimold, W.U., Robin, E., Salge, T., Speijer, R.P., Sweet, A.R., Urrutia-Fucugauchi, J., Vajda, V., Whalen, M.T., Willumsen, P.S., 2010. The Chicxulub asteroid impact and mass extinction at the Cretaceous-Paleogene boundary. *Science* **327**, 1214–1218.

Self, S., Schmidt, A. and Mather, T.A., 2014. Emplacement characteristics, time scales, and volcanic gas release rates of continental flood basalt eruptions on Earth. In: *Keller, G., Kerr, A.C. (Eds.), Volcanism, Impacts, and Mass Extinctions: Causes and Effects.* Geological Society of America Special Paper **505**

Sepúlveda, J., Wendler, J., Summons, R.E., Hindrichs, K.U., 2009. Rapid resurgence of marine productivity after the Cretaceous-Paleogene mass extinction. *Science* **326**, 129–132.

Sivan, O., Schrag, D.P., Murray, R.W., 2007. Rates of methanogenesis and methanotrophy in deep-sea sediments. *Geobiology* **5**, 141–151.

Song, H., Wignall, P. B., Tong, J. Yin, H., 2012. Two pulses of extinction during the Permian–Triassic crisis. *Nature Geoscience* **6**, 52–56.

Staudt W.J., Schoonen, M.A.A., 1995; Sulfate incorporation into sedimentary carbonates. In: M.A. Vairavamurthy, M.A.A. Schoonen (*Eds.*), Geochemical Transformations of Sedimentary Sulfur, American Chemical Society, Washington (1995), pp. 332–345

Svojtka, M., Nyvlt, D., Murakami, M., Vavrova, J., Filip, J., Mixa, P., 2009. Provenance and post-depositional low-temperature evolution of the James

Ross Basin sedimentary rocks (Antarctic Peninsula) based on fission track analysis. *Antarctic Science* **21**, 593–607.

Thibault, N., 2016. Calcareous nannofossil biostratigraphy and turnover dynamics in the late Campanian–Maastrichtian of the tropical South Atlantic.

Tobin, T.S., Ward, P.D., 2015. Carbon isotope (δ^{13}C) differences between Late Cretaceous ammonites and benthic mollusks from Antarctica. *Palaeogeography, Palaeoclimatology, Palaeoecology* **428**, 50-57

Tobin, T.S., Bitz, C.M., Archer, D., In Press. Modeling climatic effects of carbon dioxide emissions from the Deccan Traps Volcanic Eruptions around the Cretaceous–Paleogene boundary. *Palaeogeograpgy, Palaeoclimatology, Palaeoecology*. doi:10.1016/j.palaeo.2016.05.028

Tobin, T.S.,Ward, P.D., Steig, E.J., Olivero, E.B., Hilburn, I.A.,Mitchell, R.N., Diamond,M.R.,Raub, T.D., Kirschvink, J.L., 2012. Extinction patterns, δ_{18}O trends, and magnetostratigraphy from a southern high-latitude Cretaceous-Paleogene section: links with Deccan volcanism. *Palaeogeography Palaeoclimatololology Palaeoecology* **350–352**, 180–188.

Turchyn, A.V., Schrag, D.P., 2006. Cenozoic evolution of the sulfur cycle: Insight from oxygen isotopes in marine sulfate. *Earth and Planetary Science Letters*, **241**, 763–779.

Turchyn A.V., Antler, G., Byrne, D., Miller, M., Hodell, D.A., 2016. Microbial sulfur metabolism evidenced from pore fluid isotope geochemistry at Site U1385. *Global and Planetary Change* **141**, 82–90.

Tyrrell, T., Merico, A. and McKay, D.I.A., 2015. Severity of ocean acidification following the end-Cretaceous asteroid impact. *Proceedings of the National Academy of Sciences* **112**, 6556-6561.

Voigt, S., Gale, A.S., Jung, C., Jenkyns, H.C., 2012. Global correlation of upper Campanian–Maastrichtian successions using carbon-isotope stratigraphy: development of a new Maastrichtian timescale. *Newsletters on Stratigraphy* **45**, 25–53.

Wendler, I., 2013. A critical evaluation of carbon isotope stratigraphy and biostratigraphic implications for Late Cretaceous global correlation. *Earth-Science Reviews* **126**, 116–146.

Wilf, P., Johnson, K., Huber, B.T., 2003. Correlated terrestrial andmarine evidence for global climate change before mass extinction at the Cretaceous-Paleogene boundary. *Proceedings of the National Acadamey of Science* **100**, 599–604.

Witts, J.D., Bowman, V.C., Wignall, P.B., Crame, J.A., Francis, J.E., Newton, R.J., 2015. Evolution and extinction of Maastrichtian (Late Cretaceous) cephalopods from the López de Bertodano Formation, Seymour Island, Antarctica. *Palaeogeography Palaeoclimatololology Palaeoecology* **418**, 193–212.

Witts, J.D., Whittle, R.J., Wignall, P.B., Crame, J.A., Francis, J.E., Newton, R.J., Bowman, V.C., 2016. A rapid and severe Cretaceous–Paleogene mass extinction in Antarctica. *Nature Communications* **7**.

Wortmann, U.G., Paytan, A., 2012. Rapid variability of Seawater Chemistry over the past 130 million years. *Science* **337**, 334–336.

Wu, N., Farquhar, J., Strauss, H., Kim, S.T., Canfield, D.E., 2010. Evaluating the S-isotope fractionation associated with Phanerozoic pyrite burial. *Geochemica Cosmochemica Acta* **74**, 2053–2071.

Zachos, J.C., Arthur, M.A., Dean, W.E., 1989. Geochemical evidence for suppression of pelagic marine productivity at the Cretaceous–Tertiary boundary. *Nature* **337**, 61–64.

Zinsmeister, W. J. & Macellari, C. E., 1988. Bivalvia (Mollusca) from Seymour Island, Antarctic Peninsula. *Geological Society of America Memoirs* **169,** 25–53.

Chapter 6 : Discussion, conclusions, and further work

In the following discussion, I attempt to bring together and discuss the main findings of each of the preceding data chapters, and contrast the data and conclusions against the research rationale and research questions (as outlined in Chapter 1). A compilation of the main datasets presented in this thesis, focused on the K–Pg boundary interval is presented in Figure 6.1.

The overall aims of the thesis were to attempt to provide answers to the following questions and hypotheses;

1. What is the nature, rate, and timing of the Cretaceous–Paleogene extinction event in Antarctica? Is there evidence for a single, catastrophic event, a gradual diversity drawdown through the Late Cretaceous, or is the extinction in Antarctica the sum of multiple, different events?
2. How did hypothesised Earth system changes (e.g. sea level, climate) occurring at high latitudes during the Cretaceous–Paleogene interval affect marine biodiversity?
3. How does the record of environmental and biotic change recorded in the López de Bertodano Formation compare with existing records from contemporaneous lower latitude sections?
4. How do these new data from Antarctica add to the various hypotheses surrounding the K–Pg mass extinction event and its probable causes, effects, and the subsequent recovery of life?

6.1 Research question 1: Nature, rate, and timing of the Cretaceous–Paleogene extinction event in Antarctica

In contrast to previous work (e.g. Zinsmeister et al., 1989; Zinsmeister, 1998; Tobin et al., 2012), the data presented in this thesis indicate that the record of the Cretaceous–Paleogene mass extinction event in the López de Bertodano Formation on Seymour Island is similar to contemporaneous data from lower latitudes. ~65–70% of the molluscan fauna at species level (cephalopods, bivalves, and gastropods) suffer extinction at, or close to the K–Pg boundary,

248

with little or no evidence for precursor biodiversity decline. Other groups with less well-resolved fossil records (sharks, marine reptiles, echinoids) disappear at the same stratigraphic level, confirming the severity of the extinction.

Data presented in Chapter 3 confirm that a sudden extinction of ammonoid cephalopods, and the disappearance of the single species of nautiloid, at the K–Pg boundary in Antarctica was coincident with extinctions seen in other macrofossil and microfossil groups (e.g. Martin, 2006; Bowman et al., 2012). In total, seven ammonite species belonging to seven genera, range to the final few metres below the K–Pg boundary in Antarctica, with only a single genus (*Pachydiscus*) disappearing prior to this in the late Maastrichtian. This conclusion was reached by integrating fossil data from BAS section lines and collections examined during this thesis, with published information from other sections (Zinsmeister, 1998). For this correlation the K–Pg boundary was employed as a datum, along with a prominent glauconite-rich horizon stratigraphically ~173m below. Examining the overall record from Seymour Island there is no evidence for a significant reduction in the diversity of the ammonite fauna prior to a sudden mass extinction at the K–Pg boundary, despite evidence for dynamic environmental fluctuations during the Maastrichtian (see below).

It is important to place this record into a longer-term context, which does reveal a waxing and waning in the diversity of ammonites and other molluscan groups in Antarctica during the Coniacian–Maastrichtian time interval. Others (Zinsmeister et al., 1989; Zinsmeister and Feldmann, 1996; Zinsmeister, 1998) have suggested that these diversity patterns should be considered a 'harbinger' of the final extinction at the end of the Cretaceous; and that ammonites were in long-term decline prior to any extinction event at the boundary.

However, a much better explanation for these earlier diversity changes probably relates to research question 2; culminations of longer term environmental changes such as climate, sea level and tectonically-driven ocean circulation changes (c.f. Barrera and Savin, 1999; Miller et al., 2005; Friedrich et al., 2012).

Species ranges (molluscs and non-molluscan taxa)
Numbers refer to Fig. 2 of Witts et al. (2016)

B — Species richness (molluscs)

C — Last occurrence vs stratigraphic abundance (%)

D — Marine palaeotemp. (clumped isotopes)

E — Terrestrial palaeotemp. (GDGT)

F — $\delta^{34}S_{CAS}$ (‰$_{VCDT}$)

G — $\delta^{34}S_{Pyrite}$ (‰$_{VCDT}$)

H — $\Delta^{34}S$ (‰$_{VCDT}$)

Legend:

— Molluscs (benthos)
— Molluscs (nekton/nekto-benthic)
— Vertebrates (marine reptiles (MR), sharks (S))
— Other benthos (echinoid debris (E), *Rotularia* (R))
- - - Range extensions based on data from Zinsmeister (1998)
······ Temporary absence from section (range through)

** True last occurrence lower due to sampling bin size?
K-Pg glauconite interval
Deccan-induced (?) warming (Petersen et al., 2016) and location of precursor extinction (Tobin et al., 2012)
Last appearance (ammonite/nautiloid)
Last appearance (bivalve/gastropod)

S isotope panels
◇ *Pycnodonte* oyster
● *Lahillia larseni*
+ Bulk sediment

250

Figure 6.1 (previous page): Compilation of primary datsets presented in this thesis with published age model, palaeotemperature and extinction information (Tobin et al., 2012; Bowman et al., 2013; Kemp et al., 2014; Petersen et al., 2016), focusing on the upper portion of the composite BAS section and K–Pg boundary interval (900 – 1080 m). A–C, species range and extinction data (Chapters 3 and 4). A, molluscan species range-through data (numbers refer to those in Figure 4.2, page 149). B, species richness variations for molluscs (ammonites and nautiloids, bivalves and gastropods, and total). C, stratigraphic abundance (%) versus last appearance datums for molluscan taxa. D, marine palaeotemperature variation based on clumped isotope palaeothermometry (Petersen et al., 2016). E, terrestrial palaeotemperature, based on organic geochemical proxies (GDGT's) (Kemp et al., 2014). F–H, sulphur isotope geochemical data (Chapter 5). F, $\delta^{34}S_{CAS}$ variations from molluscan carbonate. G, $\delta^{34}S_{Pyrite}$ data from bulk sediment. H, $\Delta^{34}S$ variations ($\delta^{34}S_{CAS}$ - $\delta^{34}S_{Pyrite}$). K–Pg boundary glauconite beds indicated by grey box. Late Maastrichtian warming event (Petersen et al., 2016) and location of supposed precursor extinction (Tobin et al., 2012) marked by orange box. S, Sobral Formation. Ages in age model from Gradstein et al. (2012).

Ammonites appear to have been particularly sensitive to environmental changes on both a local and global scale throughout their long evolutionary history (e.g. Whiteside and Ward, 2009), which may have been particularly amplified in the climatically sensitive high latitudes. As pointed out in Chapter 3 and by others (e.g. Landman et al., 2007), many groups of ammonites that disappeared from Antarctica prior to the Maastrichtian flourished until close to the K–Pg boundary at lower latitudes (e.g. the heteromorph *Scaphitidae* and *Baculitidae* and the long-ranging *Phylloceratidae*). These early disappearance events in the James Ross Basin are thus unrelated to the end-Cretaceous extinction itself.

The relative stability of diversity through the Maastrichtian succession on Seymour Island, which includes evidence for a diversity increase during the mid-Maastrichtian (~69 Ma) appears compatible with a sudden extinction event. An attempt was made to estimate the likelihood of sampling playing a role in driving diversity patterns in Chapter 3, through implementation of stratigraphic abundance method (Meldahl, 1990), and stratigraphic confidence intervals (Marshall, 2010) as per previous work on existing datasets from this site (Marshall, 1995). At the time this chapter was written, access to a full

dataset from all three BAS section lines was not possible, hence the discrepancy between the absolute values of stratigraphic abundance methods presented here and in Chapter 4.

In Chapter 4, the extinction record is significantly expanded to include other molluscan groups (bivalves and gastropods) (Figure 6.1A–C). Tobin et al. (2012) hypothesised for the existence of a separate, 'precursor' extinction event during the late Maastrichtian on Seymour Island, located some 40 m below, and 300 kyr prior, to the K–Pg boundary itself. They linked this precursor extinction to a significant warming event seen in oxygen isotope data from molluscan carbonate, and suggested based on existing fossil data taken from Zinsmeister et al. (1989), that it preferentially affected benthic taxa. This warming event has recently been confirmed by a new clumped isotope temperature record published following completion of this thesis (Petersen et al., 2016) (Figure 6.1D).

Benthic molluscan faunas are well known from the Maastrichtian–Paleocene interval on Seymour Island (e.g. Zinsmeister and Macellari, 1988; Stilwell, et al., 2004). However, this thesis contains the first attempt to use updated taxonomic information (Beu, 2009; Crame et al., 2014), in particular from the previously undescribed gastropod fauna, to assess stratigraphic ranges and faunal diversity through the López de Bertodano Formation. Again, direct comparison was made where possible with published range data from close to the stratigraphically well-constrained K–Pg boundary, and estimates were made of the effect of sampling and rarity of taxa using similar methods to Chapter 3. This analysis revealed convincing evidence for only a single benthic extinction event at the K–Pg boundary; where 30–43% of benthic molluscan genera disappear. This may seem a low number, but it is close to the global average for these groups (Raup and Jablonski, 1993; Aberhan and Kiessling, 2014), suggesting that lower diversity polar faunas in the southern high latitudes were no more buffered from extinction than those in the tropics. Gastropods, in particular epifaunal neogastropods, seem to have been badly affected at the K–Pg boundary. This paves the way for a subsequent radiation of this group in the Paleogene (Crame et al., 2014).

Faunal range data in this chapter were presented in a slightly differing way to Chapter 3; this was due to a greater understanding of sampling variations in and between the various sedimentary section lines used in this thesis. Ultimately, range-through data was considered the most reliable (and conservative) methodology to combat this, and was used to estimate 'origination' and 'extinction' rates through the section (Foote, 2000). These confirmed the pattern from raw diversity (measured as species richness) data; with a single significant peak in extinction at the K–Pg boundary. Only a single species of gastropod disappears in the interval identified by Tobin et al. (2012) as containing a 'precursor' extinction event, suggesting this event may have been an artefact of low sampling resolution below the K–Pg boundary (Figure 6.1A–D). As pointed out in Chapter 4, this interval in at least one of the BAS sections corresponds to a subtle change in outcrop, whereby scarp slopes become more prevalent than fossiliferous dip-slops.

Data in Chapter 5 were perhaps less relevant to answering this research question, although the lack of perturbation to the sulphur cycle in the stratigraphic interval correlate with chron C29R - with no apparent impact from the Deccan Traps or sulphur release from the Chicxulub impactor on the global sulphur cycle (Figure 6.1F–H), despite a likely significantly lower concentration in seawater during the Cretaceous – is perhaps relevant to this discussion.

6.2 Research question 2: Earth system changes and marine biodiversity

This research question was stimulated by the wealth of data now available for Maastrichtian environmental change (e.g. Barrera and Savin, 1999; Miller et al., 2005; Voigt et al., 2012; Jung et al., 2013; Thibault, 2016). In a high latitude setting sensitive to such changes, it would be reasonable to suggest these would have an effect on marine biodiversity.

Chapter 3 clearly demonstrates that cephalopod diversity in the James Ross Basin during the Late Cretaceous was controlled by a combination of sea level

and temperature (climate) change (c.f. Olivero, 2012) on both a long and short-term time scale. During the Santonian–early Campanian sea level appears to have been the dominant control, but during the late Campanian–Maastrichtian, data from the Snow Hill Island and López de Bertodano formations indicate the long-term global cooling trend which began during the Campanian and reached its peak across the Campanian–Maastrichtian boundary (Friedrich et al., 2012), may have led to the exclusion of a large number of common cosmopolitan ammonite genera from the James Ross Basin. This faunal change was coincident with the rise to dominance of endemic Austral ammonite taxa in the López de Bertodano Formation, and regional extinction events and temporary disappearances recorded by other molluscan groups such as inoceramid bivalves and belemnites (Doyle and Zinsmeister, 1988; Crame and Luther, 1997).

In Chapter 4, similar controls are shown to influence the diversity of benthic taxa, which show an apparent increase in diversity up-section from the base of the López de Bertodano Formation. A larger number of range-through taxa from underlying formations are apparent in the benthic dataset (Appendix B), suggesting the environmental effects of the Campanian–Maastrichtian boundary cooling event and associated sea level fall were insufficient to cause significant extinctions in the Antarctic benthos.

Integrating data from Chapter 4, both nektonic cephalopods and benthic molluscs seem to have responded to an interval of unfavourable conditions during the early Maastrichtian, with a low diversity assemblage in the basal López de Bertodano Formation on Seymour Island comprising just two species of ammonite, and 10–15 species of bivalve and gastropod. This interval coincides with evidence for shallow waters and low temperatures following the Campanian–Maastrichtian boundary event (Olivero et al., 2008; Bowman et al., 2013). Despite the assumption that the López de Bertodano Formation was deposited in a fully oxygenated setting, microfacies analysis and analysis of the size range of pyrite framboids provides some evidence for short-term redox fluctuations through the section. Shallow water dysoxia may also have controlled early Maastrichtian diversity, with evidence for recurrence

254

throughout the section – especially coinciding with the deposition of glauconite horizons. The mechanism and nature of these redox fluctuations would be an obvious area of future work. The presence of complex local geochemical conditions in the sediments of the James Ross Basin is borne out by sedimentary geochemistry and pyrite sulphur isotope work, as well as fossil data recording the influence of methane carbon on a seasonally resolved timescale.

Climate warming in the late Maastrichtian is apparent in Antarctica (Bowman et al., 2013; Bowman et al., 2014), commencing nearly 2 million years prior to the K–Pg boundary. It is probable that several distinct warming and cooling events occurred in this interval prior to the K–Pg boundary itself (Petersen et al., 2016) (Figure 6.1D, E). It is difficult to ascribe much effect on biodiversity to these events. The brief stratigraphic appearance of certain ammonite taxa (pachydiscids, *Zelandites*) could be related to climate and oceanographic fluctuations prior to the K–Pg boundary (c.f. Thibault et al., 2010). If so, ammonites may show a similar pattern to microfossil groups such as calcareous nannofossil and planktonic foraminifera, with repeated pole-ward and equator-ward migrations as a result of these climate changes and biotic exchange between low and high latitude assemblages (Huber and Watkins, 1992). The Maastrichtian ammonite record is perhaps of insufficient temporal and spatial resolution globally to examine this hypothesis in detail.

A greater control on benthic diversity during the late Maastrichtian in Antarctica may well be sea level; deposition of thick beds rich in glauconite coincident with the appearance of 'flat clams' ("*Entolium*") and increases in *Pycnodonte* oysters perhaps indicating a related substrate control.

 In Chapter 5, seawater sulphur isotope data would suggest that that several of the Earth system changes in the Maastrichtian had the potential to alter global sulphur cycling. Especially given concentration estimates for a reservoir ~50% smaller than modern, leading to a concomitant lower residence time in the ocean. Despite this, low data density suggests a ~stable early Maastrichtian sulphur cycle, with big changes occurring only later in the Maastrichtian and after the K–Pg boundary.

6.3 Research question 3: How do the new data from Antarctica compare with lower latitude sites?

Ammonite data presented in Chapter 3 from the high southern latitudes are in accordance with those from well-studied lower latitude sections in the Tethyan, Atlantic seaboard, and Boreal regions (e.g. Marshall and Ward, 1996; Landman et al., 2007; Hansen and Surlyk, 2014), and indicate no evidence of elevated extinction rates for ammonites globally prior to the sudden K–Pg mass extinction event. An argument has been made for the short-lived survival of several genera of heteromorph ammonite into the Paleogene (e.g. Landman et al., 2014). These appear to be taxa with large geographic ranges, presumably ecological generalists, very different to the highly endemic taxa present on Seymour Island. Benthic molluscan data are also comparable with published datasets in terms of patterns at the K–Pg boundary (e.g. Hansen et al., 1993; Aberhan et al., 2007; Hansen and Surlyk, 2014), although there is little evidence for substantial increase in deposit-feeding taxa following the K–Pg extinction on Seymour Island. This would suggest a model whereby the magnitude of the extinction is the same everywhere, but pronounced regional heterogeneities in the response of ecosystems depend largely on local factors (e.g. Hull and Norris, 2011; Aberhan and Kiessling, 2015).

The sulphur isotope curve generated in Chapter 5 also provides new data for comparison with lower latitudes. Most strikingly they record an apparent decoupling between the sulphur and carbon cycles in the late Maastrichtian, with evidence for a positive shift in $\delta^{34}S$ values in a time interval where most global carbon isotope records are either static or show a slight negative shift (Cramer et al., 2009; Voigt et al., 2012). The precise mechanisms behind this are also not well understood, although they could relate to terrestrial carbon cycle changes, or reduced significance of sulphur isotopic change for the carbon cycle because of a smaller concentration of sulphur in seawater. The role of eperic seas causing local changes to both the carbon and sulphur cycle in the latest Cretaceous should also not be ruled out; evidence from Nd isotopes suggests development of local water masses and lack of deep water

connectivity were a feature of the Maastrichtian ocean (Voigt et al., 2013; Jung et al., 2013).

The seawater sulphur isotope data shows broad agreement with lower latitude records from a restricted time interval over the K–Pg boundary (e.g. Kaiho et al., 1999) (Figure 6.1F). Pyrite sulphur isotopes however do not show a good relationship (Figure 6.1G); perhaps an effect of local conditions (organic matter delivery, sedimentation rate etc). Sulphur data also compares favourably to lower latitude records of the aftermath of the K–Pg extinction; specifically evidence for a global decrease in productivity to the ocean. For the first time, data presented here suggest this event, which lasted up several 100 kyrs, affected the global sulphur as well as carbon cycle.

6.4 Research question 4: How do these new data add to hypotheses about the probable causes and effects of the K–Pg mass extinction event?

Data generated in this thesis add important new information and evidence to the ongoing debate over the cause and nature of the K–Pg extinction. Firstly they do not support hypotheses that it was somehow 'safer in the south' during this mass extinction event (Zinsmeister et al., 1989; Jiang et al., 2010; Barreda et al., 2012), at least in the oceans. Extinction data from marine mollusc species richness variations suggest the magnitude, and timing of the extinction were the same at 65°S as elsewhere (e.g. Aberhan and Kiessling, 2014). These data do not support models for a significant destabilisation of polar ecosystems (in terms of any significant decline in species richness) caused by the main phase eruptions of the Deccan LIP prior to the K–Pg boundary (Tobin et al., 2012), and rule out precursor late Maastrichtian extinction events in this expanded and fossiliferous section. Importantly, they also indicate that regional disappearances in Antarctica during the Campanian and early Maastrichtian were not 'harbingers' of the K–Pg event, but likely the response of taxa not adapted to the cooler temperatures migrating away from the James Ross Basin.

Geochemical data from sulphur isotopes also suggest minimal perturbation prior to the K–Pg boundary from sulphur emissions from Deccan volcanism (e.g. Schmidt et al., 2016), although this may be due to the buffering effect of the ocean reservoir. Importantly they also suggest minimal input of sulphur from the Chicxulub impact. The after-effects of the impact event however, may drive changes in the sulphur cycle; specifically a drop in pyrite burial related to less organic carbon burial and export productivity crash during the first 300 kyrs of the Danian. This is further evidence for the global reach of the after-effects of the Chicxulub impact on marine ecosystems and biogeochemical cycles.

The timing of geochemical (S and C cycle) and biotic (species richness, ecology) recovery following the extinction event appears to be the same; the recovery of sulphur isotope data to a pre-extinction values occurs at the same time as deep sea carbon cycle beings to recover, 300 kyrs after the K–Pg boundary. In the shallow shelf seas of Antarctica, this also coincides with the initial recovery of marine diversity, and return of certain ecologies (e.g. epifaunal molluscs) in the molluscan record.

Recent high-precision dating of the Deccan Traps does suggest that the most voluminous portions of the lava pile overlap temporally with the K–Pg boundary (Renne et al., 2015). However, there remains uncertainty in using lava thickness as proxy for volume and volatile release which could drive climate/environmetnal changes. Species range and richness data from high latitude molluscan faunas produced in this thesis, also question whether any Deccan-induced climate changes were enough to drive significant ecosystem destabilisation and/or extinction events in marine or terrestrial communities, and thus whether this LIP played a significant role in the K–Pg mass extinction event itself. Further high precision refinement to the age of the Deccan, and the volatile content of each distinct 'phase' of volcanism may help resolve this. Until then, it must be concluded that the Chicxulub impact remains the most plausible driving mechanism for a sudden mass extinction at the close of the Cretaceous.

6.5 Conclusions

To summarise the main conclusions of this thesis;

- A single, rapid extinction event (measured in loss of species richness) occurred at the K–Pg in Antarctica, affecting both benthic and nektonic molluscs, and coincident with evidence for losses in the wider marine community.

- We find no evidence on Seymour Island for a precursor biotic crisis in the high southern latitudes. Data are congruent with a similar response (in terms of magnitude of the extinction event) globally; although regional heterogeneities in the aftermath of the extinction may develop due to local factors.

- Prior to the K–Pg extinction, dynamic environmental changes may have played a role in driving both diversity dynamics, and global biogeochemical cycles. Sea level, and temperature changes seem to be the main control on molluscan diversity during the Campanian–Maastrichtian of the James Ross Basin.

- For the first time, benthic redox fluctuations have been identified in the López de Bertodano Formation. These may have some bearing on the fossil record of the immediate aftermath of the extinction event in Antarctica, alongside a loss of grazing benthos (the 'fish-kill' layer (Zinsmeister, 1998).

- New high resolution seawater sulphur isotope record reveals evidence for both stability (early Maastrichtian) and variability (late Maastrichtian; early Paleogene) in the sulphur cycle, probably an effect of global environmental changes.

- Data demonstrate a direct effect of the K–Pg extinction on the sulphur cycle; specifically productivity crash. This has previously only been demonstrated for the carbon cycle.

- Congruent recovery times seen in the carbon and sulphur cycle, and biotic and ecological recovery highlight the close links between biosphere and geosphere during times of rapid environmental change.

6.6 Outlook and suggestions for future work

Data generated during the course of this thesis has raised several interesting questions which could be explored with further work.

1.) *Deccan-induced palaeoenvironmental change prior to the K–Pg boundary in Antarctica – does it exist*? Data outlined in Chapters 3 and 4 would suggest Deccan volcanism had a minimal effect on marine biodiversity in terms of species richness variations at high latitudes, and therefore was likely not a major contributing factor to the K–Pg extinction event. However, species richness is only one measure of diversity and ecosystem stability. An alternative approach could be to examine another variable for ecological change, such as body-size variations.

   The onset of the main phase of Deccan volcanism is well constrained to the base of chron C29R (Robinson et al., 2009), and it is now the prevailing hypothesis to link Deccan eruptions with a prominent (and probably global) late Maastrichtian climate warming event (e.g. Thibault and Husson, 2016; Henehan et al., 2016; Petersen et al., 2016). Evidence for environmental changes linked to this warming appear rather subtle; but dwarfing has been reported in planktonic foraminifera (Abramovich and Keller, 2003) and calcareous nannofossil show a temporary drop in diversity (Thibault and Husson, 2016). Recent data also suggest a link to potential ocean acidification and shoaling of the lysocline shown by variations in deep sea carbonate proxies at the same time as warming (Henehan et al., 2016). Importantly, nannofossil species richness and these carbonate proxies subsequently recover towards the K–Pg boundary. A detailed examination of body size variations in molluscan taxa from Seymour Island in the stratigraphic interval correlated to chron 29R could reveal the effects of these events at high latitudes.

2.) *Recovery from the K–Pg extinction in Antarctica – ecological versus taxonomic decoupling?* – Following the K–Pg extinction, global environments, particularly in the ocean, remained significantly

perturbed for 100's of kyrs (Coxall et al., 2006; Esmeray-Senlet et al., 2015). Data in this thesis has demonstrated the potential links between carbon and sulphur cycle recovery and biotic recovery. This could be further explored by examining in more detail the early Danian record from Seymour Island; perhaps in terms of the ecological change at the boundary, and subsequent recovery from the extinction. Did this occur on the same time scale? Does it compare well to the general models from lower latitudes in the face of evidence for regional heterogeneity in the pattern of recovery from the K–Pg? (E.g. Hull and Norris, 2011; Aberhan and Kiessling, 2015).

3.) *Rapid redox fluctuations physical and geochemical evidence, driving mechanisms* – Benthic redox fluctuations seem to have occurred throughout the López de Bertodano Formation, despite the presence of a diverse marine fauna, and hypothesised bioturbated nature of the sediment. Further examination of these using geochemical proxies (iron speciation, trace metal analysis) could lead to an understanding of their drivers and the scale at which they occur relative to the evidence for a fully-developed marine fauna (e.g. pyrite framboid record may be time-averaged to a greater degree than the fossil record). A proper examination of sedimentary fabric is difficult in the field due to freeze-thaw weathering of surface exposure, but would certainly help constrain this further.

4.) *Further exploration of sulphur cycle changes during this interval, regional versus global signal?* – Further CAS records for the Maastrichtian would validate the record generated here. Although the null hypothesis would be that these data represent a global signal, evidence for the development of regional water masses in the Late Cretaceous–Paleogene ocean (Voigt et al., 2012; Jung et al., 2013) mean that this requires validation to rule out development of regional variability in the signal from sulphur cycling.

Additional sulphur data from Seymour Island could greatly increase the resolution of the CAS curve – in particular in the early Maastrichtian, and during the early Danian. One intriguing archive could be *Rotularia* –

hugely abundant calcitic serpulid worm tubes in the López de Bertodano Formation that secrete in equilibrium with seawater (c.f. Tobin et al., 2012).

5.) *Geochemical modelling: global and local-scale?* To further constrain the results from the CAS data, and its implications for both the carbon cycle pre-and post-extinction, global biogeochemical box modelling could be used to explore variations in carbon and sulphur reservoirs during the K–Pg time interval. On a smaller scale, biogeochemical reaction transport modelling could further tease out local non-steady state behaviour arising as a result of low sulphate conditions in the oceans during this time (e.g. the SMTZ signal).

6.) *Better constrained sampling of K–Pg interval* – It is perhaps obvious that any study of mass extinction event where timing of extinctions and environmental change is so important, is only as good as the field sampling that underlies the fossil dataset. This study utilised large fossil collections made over a long time period (10's years). Inevitably, collecting was not entirely standardised, which impacts the kind of analysis that can be done. The methods employed to study the mass extinction in this thesis are therefore relatively conservative, and perhaps provide a blueprint for other studies working with similar constraints. Nevertheless, proper quantified logging and sampling of the extended K–Pg boundary interval on Seymour Island would greatly increase the resolution of the fossil dataset, as well as the potential analytical methodologies available for analysis of data from this important site. The hypothesis that no significant destabilisation of the high latitude marine community occurred prior to the K–Pg boundary could be better tested by employing quantified diversity metrics (e.g. Shannon Diversity, Evenness etc), and by directly comparing geochemical and fossil datasets.

6.7 References

Aberhan, M., Kiessling, W., 2014. Rebuilding biodiversity of Patagonian marine molluscs after the end-Cretaceous mass extinction. *PLoS ONE* **9**, e106269.

Aberhan, M., Kiessling, W., 2015. Persistent ecological shifts in marine molluscan assemblages across the end-Cretaceous mass extinction. *Proceedings of the National Academy of Science, USA* **112**, 7207–7212.

Aberhan, M., Weidemeyer, S., Kiessling, W., Scasso, R.A., Medina, F.A., 2007. Faunal evidence for reduced productivity and uncoordinated recovery in Southern Hemisphere Cretaceous-Paleogene boundary sections. *Geology* **35**, 227-230.

Abramovich, S., Keller, G., 2003. Planktonic foraminiferal response to the latest Maastrichtian abrupt warm event: A case study from South Atlantic DSDP Site 525A. *Marine Micropaleontology* **48**, 225-249.

Barreda, V.D., Cúneo, N.R., Wilf, P., Currano, E.D., Scasso, R.A., Brinkhuis, H., 2012. Cretaceous/Paleogene Floral Turnover in Patagonia: Drop in Diversity, Low Extinction, and a Classopollis Spike. *PLoS ONE* **7**.

Barrera, E., Savin, S.M., 1999. Evolution of late Campanian–Maastrichtian marine climates and oceans. In: *Barrera, E., Johnson, C.C. (Eds.), Evolution of the Cretaceous Ocean- Climate System.* Geological Society of America Special Paper **332**, pp. 245–282.

Beu, A. G., 2009. Before the ice: biogeography of Antarctic Paleogene molluscan faunas. *Palaeogeography Palaeoclimatology Palaeoecology* **284**, 191–226.

Bowman, V. C., Francis, J. E., Riding, J. B., Hunter, S. J., Haywood, A. M., 2012. A latest Cretaceous to earliest Paleogene dinoflagellate cyst zonation from Antarctica, and implications for phytoprovincialism in the high southern latitudes. *Review of Palaeobotany and Palynology* **171,** 40–56.

Bowman, V. C., Francis, J. E., Riding, J. B., 2013. Late Cretaceous winter sea ice in Antarctica? *Geology* **41**, 1227–1230.

Bowman, V. C., Francis, J. E., Askin, R. A., Riding, J. B. Swindles, G. T., 2014. Latest Cretaceous–earliest Paleogene vegetation and climate change at the high southern latitudes: palynological evidence from Seymour Island, Antarctic Peninsula. *Palaeogeography Palaeoclimatology Palaeoecology* **408**, 26–47.

Coxall, H.K., D'Hondt, S., Zachos, J.C., 2006. Pelagic evolution and environmental recovery after the Cretaceous-Paleogene mass extinction. *Geology* **34,** 297-300.

Crame, J.A., Luther, A., 1997. The last inoceramid bivalves in Antarctica. *Cretaceous Research* **18**, 179–195.

Crame, J. A., Beu, A. G., Ineson, J. R., Francis, J. E., Whittle, R. J. & Bowman, V. C., 2014. The early origins of the Antarctic marine fauna and its evolutionary implications. *PLoS ONE* **9**, e114732.

Cramer, B.S., Toggweiler, J.R., Wright, J.D., Katz, M.E., Miller, K.G., 2009. Ocean overturning since the late cretaceous: Inferences from a new benthic foraminiferal isotope compilation. *Paleoceanography* **24.**

Doyle, P., Zinsmeister, W.J., 1988. The new dimitobelid belemnite from the Upper Cretaceous of Seymour Island, Antarctic Peninsula. In: Feldmann, R.M., Woodburne, M.O. (Eds.)*, Geology and Paleontology of Seymour Island, Antarctic Peninsula*. Geological Society of America, Memoirs **169**, pp. 285–290.

Esmeray-Senlet, S., Wright, J.D., Olsson, R.K., Miller, K.G., Browning, J.V., Quan, T.M., 2015. Evidence for reduced export productivity following the Cretaceous/Paleogene mass extinction. *Paleoceanography* **30**, 718-738.

Foote, M., 2000. Origination and extinction components of taxonomic diversity: general problems. *Paleobiology* **26**, 74–102.

Friedrich, O., Norris, R. D., Erbacher, J., 2012. Evolution of middle to Late Cretaceous oceans – a 55 m.y. record of Earth's temperature and carbon cycle. *Geology* **40**, 107–110.

Gradstein, F. M., Ogg, J. G., Schmitz, M. & Ogg, G., 2012. *The Geological Time Scale 2012* Elsevier Science Ltd: Boston.

Hansen, T., Surlyk, F., 2014. Marine macrofossil communities in the uppermost Maastrichtian chalk of Stevns Klint, Denmark. *Palaeogeography Palaeoclimatolology Palaeoecology* **399**, 323–344.

Hansen, T. A., Farrell, B. R. & Upshaw, B III., 1993. The first 2 million years after the Cretaceous–Tertiary boundary in east Texas: rate and paleoecology of the molluscan recovery. *Paleobiology* **19**, 251–265.

Henehan, M.J., Hull, P.M., Penman, D.E., Rae, J.W.B. and Schmidt, D.N. 2016. Biogeochemical significance of pelagic ecosystem function: An end-cretaceous case study. *Philosophical Transactions of the Royal Society B: Biological Sciences* **371**.

Huber, B.T., Watkins, D.K., 1992. Biogeography of Campanian–Maastrichtian calcareous plankton in the region of the Southern Ocean: palaeogeographic and palaeoclimatic implications. In: Kennett, J.P.,Warnke, D.A. (Eds.), *The Antarctic Palaeoenvironment: A Perspective on Global Change*. AGU Antarctic Research Series **56**, pp. 31–60.

Hull, P.M., Norris, R.D., 2011. Diverse patterns of ocean export productivity change across the Cretaceous-Paleogene boundary: new insights frombiogenic barium. *Paleoceanography* **26**, 1–10.

Jiang, S., Bralower, T. J., Patzkowsky, M. E., Kump, L. R., Schueth, J. D., 2010. Geographic controls on nannoplankton extinction across the Cretaceous/Paleogene boundary. *Nature Geoscience* **3**, 280–285.

Jung, C., Voigt, S., Friedrich, O., Koch, M.C., Frank, M., 2013. Campanian-Maastrichtian ocean circulation in the tropical Pacific*. Paleoceanography* **28**, 562–573. http://dx.doi.org/10.1002/palo.20051 .

Kaiho K., Kajiwara, Y., Tazaki, K., Ueshima, M., Takeda, N., Kawahata, H., Arinobu, T., Ishiwatari, R., Hirai, A., Lamolda, M., 1999. Oceanic primary productivity and dissolved oxygen levels at the Cretaceous/Tertiary boundary:

their decrease, subsequent warming, and recovery. *Paleoceanography* **14**, 511–524.

Landman, N.H., Johnson, R.O., Garb,M.P., Edwards, L.E., Kyte, F.T., 2007. Cephalopods from the Cretaceous/Tertiary boundary interval on the Atlantic coastal plain, with a description of the highest ammonite zones in North America. Part III. Manasquan River Basin, Monmouth County, New Jersey. *Bulletins of the American Museum of Natural History* **303**, 1–122.

Landman, N.H., Goolaerts, S., Jagt, J.W.M., Jagt-Yazykova, E.A., Machalski, M., Yacobucci, M.M., 2014. Ammonite extinction and nautilid survival at the end of the Cretaceous. *Geology* **42**, 707–710.

Marshall, C.R., Ward, P.D., 1996. Sudden and gradual molluscan extinctions in the Latest Cretaceous of Western European Tethys. *Science* **274**, 1360–1363.

Marshall, C.R., 1995. Distinguishing between sudden and gradual extinctions in the fossil record: predicting the position of the Cretaceous-Tertiary iridium anomaly using the ammonite fossil record on Seymour Island, Antarctica. *Geology* **23**, 731–734.

Marshall, C. R., 2010. in: *Quantitative methods in paleobiology.* (eds Alroy, J. and Hunt, G.) The Palentological Society Papers **16**, 291–316.

Martin, J.E., 2006. Biostratigraphy of the Mosasauridae (Reptilia) from the Cretaceous of Antarctica. In: Francis, J.E., Pirrie, D., Crame, J.A. (Eds.), *Cretaceous–Tertiary High-Latitude Palaeoenvironments, James Ross Basin, Antarctica.* Special Publication vol. **258**. Geological Society, London, pp. 101–108.

Meldahl, K.H., 1990. Sampling, species abundance, and the stratigraphic signature, of mass extinction: a test using Holocene tidal flat molluscs. *Geology* **18**, 890–893.

Miller, K.G., Kominz, M.A., Browning, J.V., Wright, J.D., Mountain, G.S., Katz, M.E., Sugarman, P.J., Cramer, B.S., Christie-Blick, N., Pekar, S.F., 2005. The Phanerozoic record of global sea-level change. *Science* **310**, 1293-1298.

Olivero, E.B., Ponce, J.J., Martinioni, D.R., 2008. Sedimentology and architecture of sharp based tidal sandstones in the Upper Marambio Group, Maastrichtian of Antarctica. *Sedimentary Geology* **210**, 11–26.

Olivero, E.B., 2012. Sedimentary cycles, ammonite diversity and palaeoenvironmental changes in the Upper Cretaceous Marambio Group, Antarctica. *Cretaceous Research* **34**, 348–366.

Petersen, S.V., Dutton, A., Lohmann, K.C., 2016. End-Cretaceous extinction in Antarctica linked to both Deccan volcanism and meteorite impact via climate change. *Nature Communications* **7.** 12079, doi: 10.1038/ncomms12079.

Raup, D. M., Jablonski, D., 1993. Geography of end-Cretaceous marine bivalve extinctions. *Science* **260**, 971–973.

Renne, P.R., Sprain, C.J., Richards, M.A., Self, S., Vanderkluysen, L., Pande, K., 2015. State shift in Deccan volcanism at the Cretaceous–Paleogene boundary, possibly induced by impact. *Science* **350**, 76–78.

Schmidt, A., Skeffington, R.A., Thordarson, T., Self, S., Forster, P.M., Rap, A., Ridgwell, A., Fowler, D., Wilson, M., Mann, G.W., Wignall, P.B., Carslaw, K.S., 2016. Selective environmental stress from sulphur emitted by continental flood basalt eruptions. *Nature Geoscience* **9**. 77–82 (2016).

Stilwell, J.D., Zinsmeister, J.D., Oleinik, A.E., 2004. Early Paleocene mollusks of Antarctica: systematics, palaeoecology and palaeobiogeographic significance. *Bulletins of American Paleontology* **367**, 1–89.

Thibault, N. & Husson, D., 2016. Climatic fluctuations and sea-surface water circulation patterns at the end of the Cretaceous era: Calcareous nannofossil response. *Palaeogeography Palaeoclimatology Palaeoecology* **441**, 152–164.

Thibault, N., Gardin, S., Galbrum, B., 2010. Latitudinal migration of calcareous nannofossil *Micula murus* in the Maastrichtian: implications for global climate change. *Geology* 38, 203–206.

Thibault, N., 2016. Calcareous nannofossil biostratigraphy and turnover dynamics in the late Campanian–Maastrichtian of the tropical South Atlantic. *Revue de Micropaléontologie* **59**, 57-69.

Tobin, T.S.,Ward, P.D., Steig, E.J., Olivero, E.B., Hilburn, I.A.,Mitchell, R.N., Diamond,M.R.,Raub, T.D., Kirschvink, J.L., 2012. Extinction patterns, δ_{18}O trends, and magnetostratigraphy from a southern high-latitude Cretaceous-Paleogene section: links with Deccan volcanism. *Palaeogeography Palaeoclimatolology Palaeoecology* **350–352**, 180–188.

Voigt, S., Gale, A.S., Jung, C., Jenkyns, H.C., 2012. Global correlation of upper Campanian–Maastrichtian successions using carbon-isotope stratigraphy: development of a new Maastrichtian timescale. *Newsletters on Stratigraphy* **45**, 25–53.

Whiteside, J.H.,Ward, P.D., 2009. Ammonoid diversity and disparity track episodes of chaotic carbon cycling during the early Mesozoic. *Geology* **39**, 99–102.

Zinsmeister, W.J., 1998. Discovery of fish mortality horizon at the K–T boundary on Seymour Island: re-evaluation of events at the end of the Cretaceous. *Journal of Paleontology* **72**, 556–571.

Zinsmeister, W. J. & Macellari, C. E., 1988. Bivalvia (Mollusca) from Seymour Island, Antarctic Peninsula. *Geological Society of America Memoirs* **169,** 25–53.

Zinsmeister, W.J., Feldmann, R.M., Woodburne, M.O., Elliot, D.H., 1989. Latest Cretaceous/Tertiary transition on Seymour Island, Antarctica. *Journal of Paleontology* **63**, 731–738.

Zinsmeister,W.J., Feldmann, R.M., 1996. Late Cretaceous faunal changes in the high southern latitudes: a harbinger of global biotic catastrophe? In: Macleod, N., Keller, G. (Eds.), *Cretaceous–Tertiary Mass Extinctions: Biotic and Environmental Changes*. W.W. Norton, New York, pp. 303–325

Appendix A : Supplementary data from Chapter 3

Supplementary data to accompany Chapter 3 (Evolution and extinction of Maastrichtian (Late Cretaceous) cephalopods from the López de Bertodano Formation, Seymour Island, Antarctica).
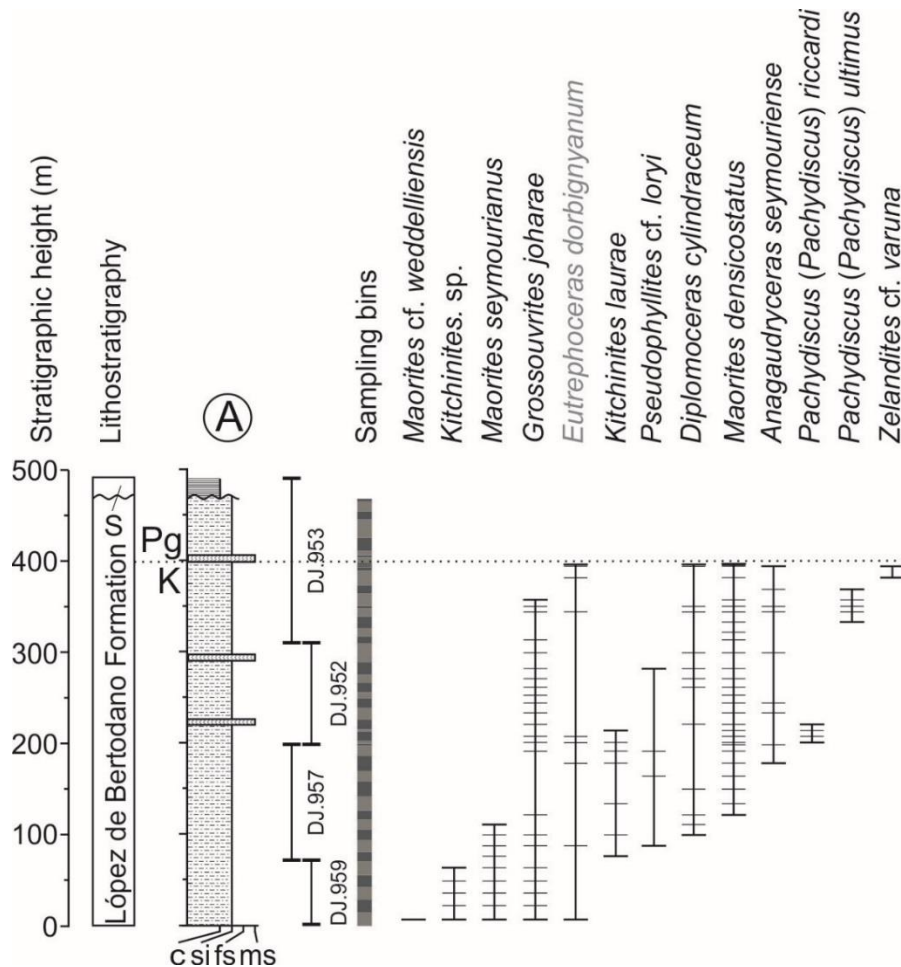
Figure A.1 Lithostratigraphy, sedimentology and stratigraphic range chart of cephalopod taxa from the López de Bertodano Formation found in the 1999 BAS field season (sections DJ.959, 957, 952, 953) (see also Crame et al., 2004) See Figure 3.1 for location of individual section lines and Figure 3.2 for correlation with other sections. K = Cretaceous, Pg = Paleogene, S = Sobral Formation. Position of the K–Pg boundary marked by dotted line at 398.5 m. Tick marks in stratigraphic range chart denote individual fossil occurrences plotted at the stratigraphic mid-point of sampling bins as indicated on the left of the figure by alternating grey squares. Sampling bins range in size from 1.5 m to 19.5 m stratigraphic height. Taxa are ordered by the first occurrence.
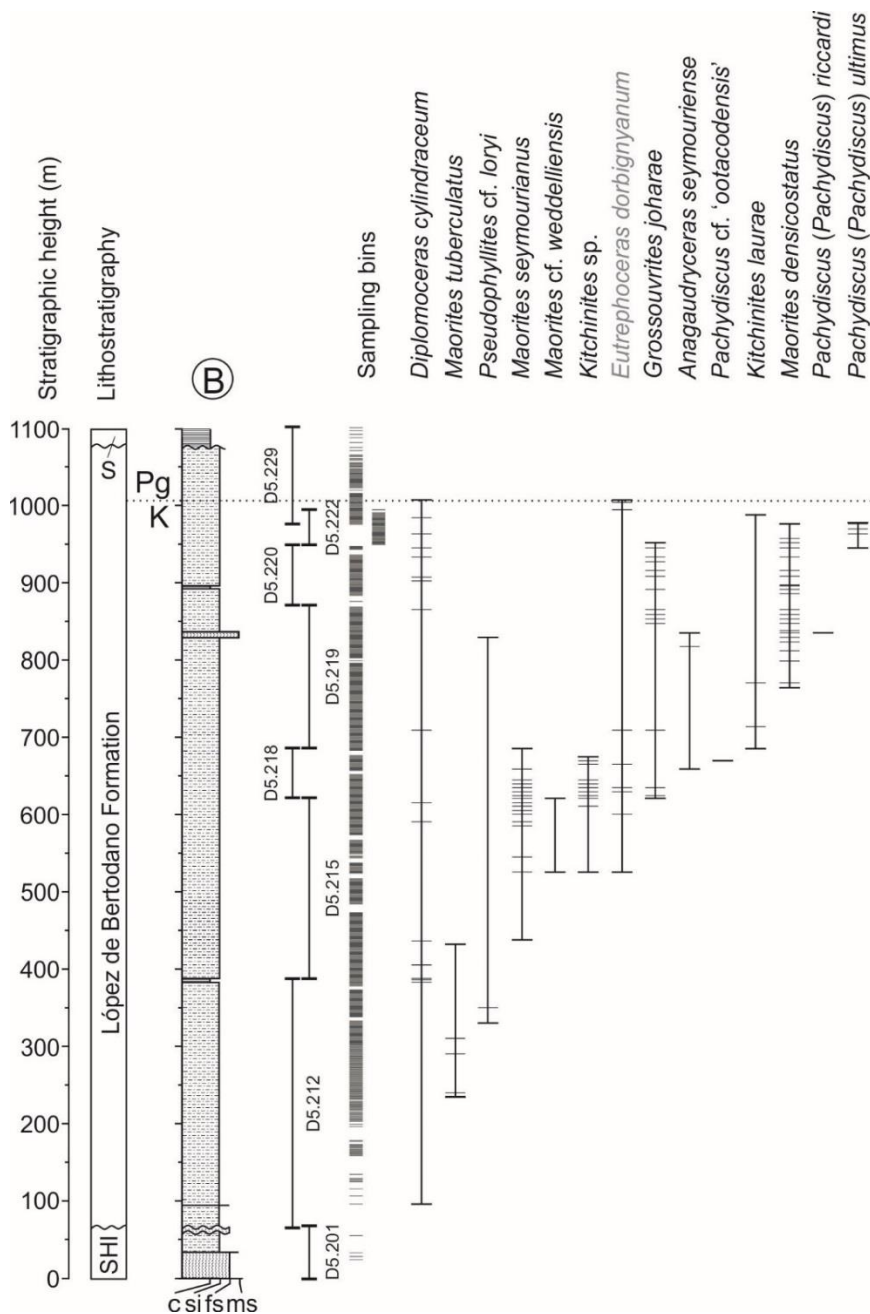
Figure A.2 Lithostratigraphy, sedimentology and stratigraphic range chart of cephalopod taxa from the López de Bertodano Formation found in the 2006 BAS field season (composite section D5.251) (see also Bowman et al., 2012; Bowman et al., 2013a; 2013b and Bowman et al., 2014). See Figure 3.1 for location of individual section lines and Figure 3.2 for correlation with other sections. K = Cretaceous, Pg = Paleogene, S = Sobral Formation. Position of the K–Pg boundary marked by dotted line at 1007.5 m. Tick marks in stratigraphic range chart denote individual fossil occurrences plotted at the stratigraphic mid-point of sampling bins as indicated on the left of the figure by alternating grey squares and lines. Sampling bins range in size from 1 m to 7 m in stratigraphic height. Taxa are ordered by the first occurrence.

Appendix B   Supplementary data for Chapter 4
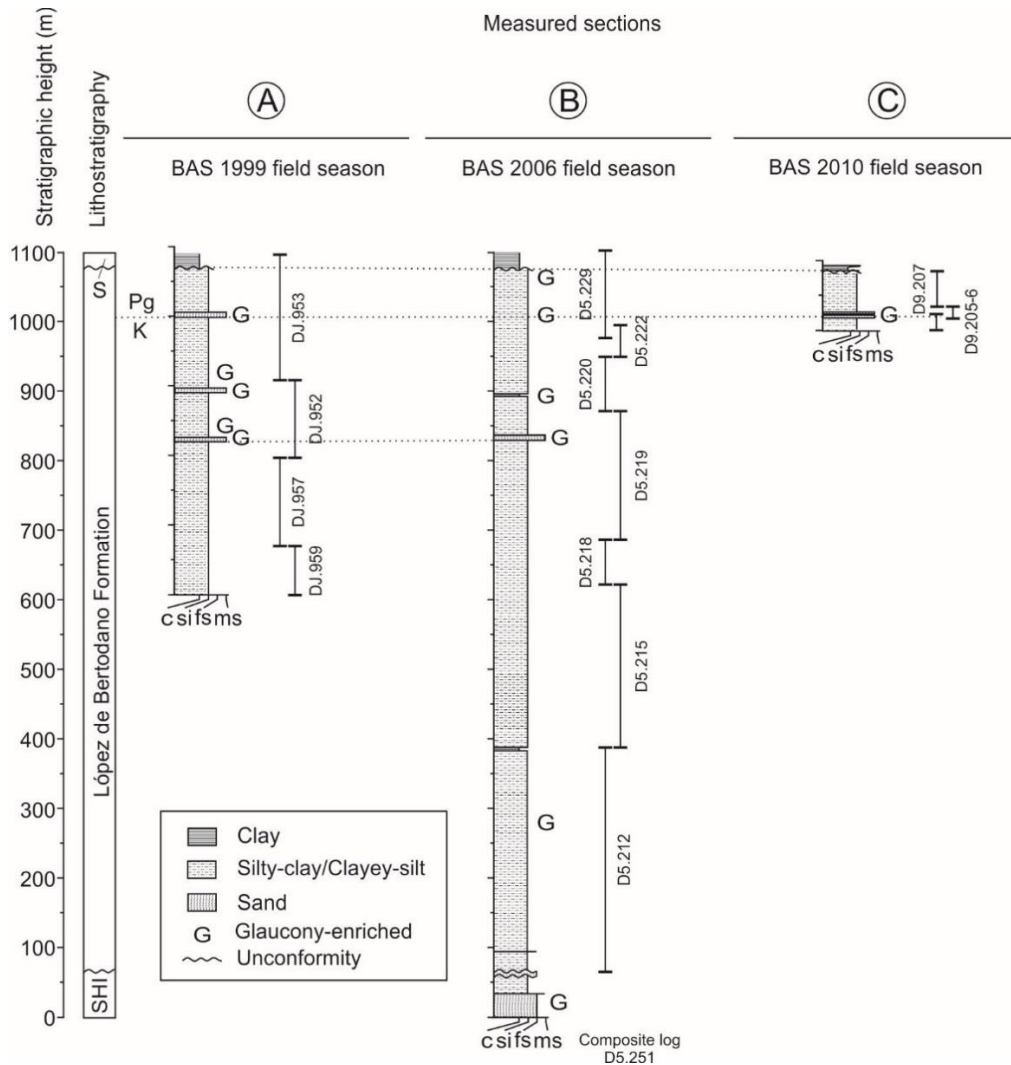
Figure B.1 Lithostratigraphy and correlation within the López de Bertodano Formation on Seymour Island. BAS (British Antarctic Survey) sedimentary sections A–C used to construct composite section. Tie points for correlation: K–Pg boundary, unconformable contact with overlying Sobral Formation, and prominent glauconitic horizon 174 m below the K–Pg interval. A–C refer to section identifications used in Main Text Fig. 1. SHI, Snow Hill Island Formation, S, Sobral Formation, K, Cretaceous, Pg, Paleogene. For further details on individual field seasons and section lines see Crame et al., 2004; Bowman et al., 2015; Bowman et al., 2012; Bowman et al., 2013; Witts et al., 2015; Bowman et al., 2014; Crame et al., 2014.
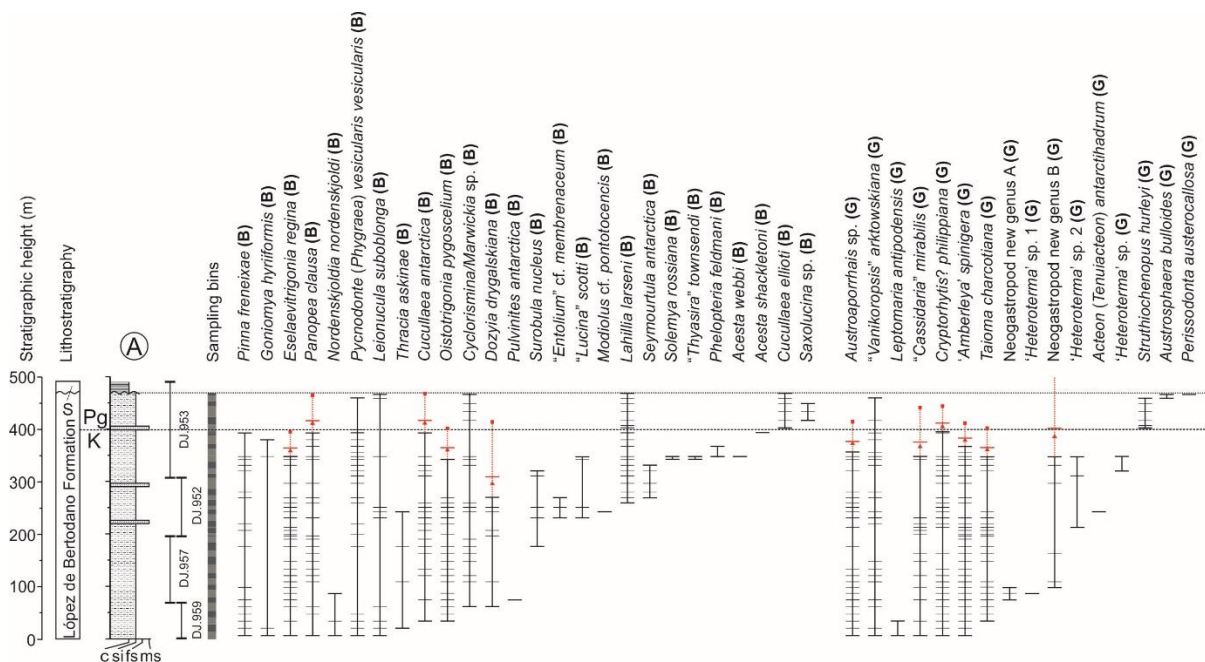
Figure B.2 Stratigraphic range and occurrence data for molluscan taxa from the BAS 1999 field season. Lithostratigraphy, sampling bins, and raw stratigraphic range (vertical solid black lines) and occurrence (horizontal black ticks) data for benthic molluscan taxa (bivalves (B) and gastropods (G)) from sub-sections DJ.959, DJ.957, .952, and .953 (Crame et al., 2004; Crame et al., 2014). 50% confidence intervals (red triangles), 95% confidence intervals (red squares), and average gap size between occurrences (horizontal red ticks) calculated for Maastrichtian taxa with more than five occurrences. Illustrated as range extensions (vertical red dashed line) calculated using 'classic' confidence interval methodology as summarised by Marshall, 2010. See B.1 for raw field data and Fig. B.1 for lithostratigraphic key.
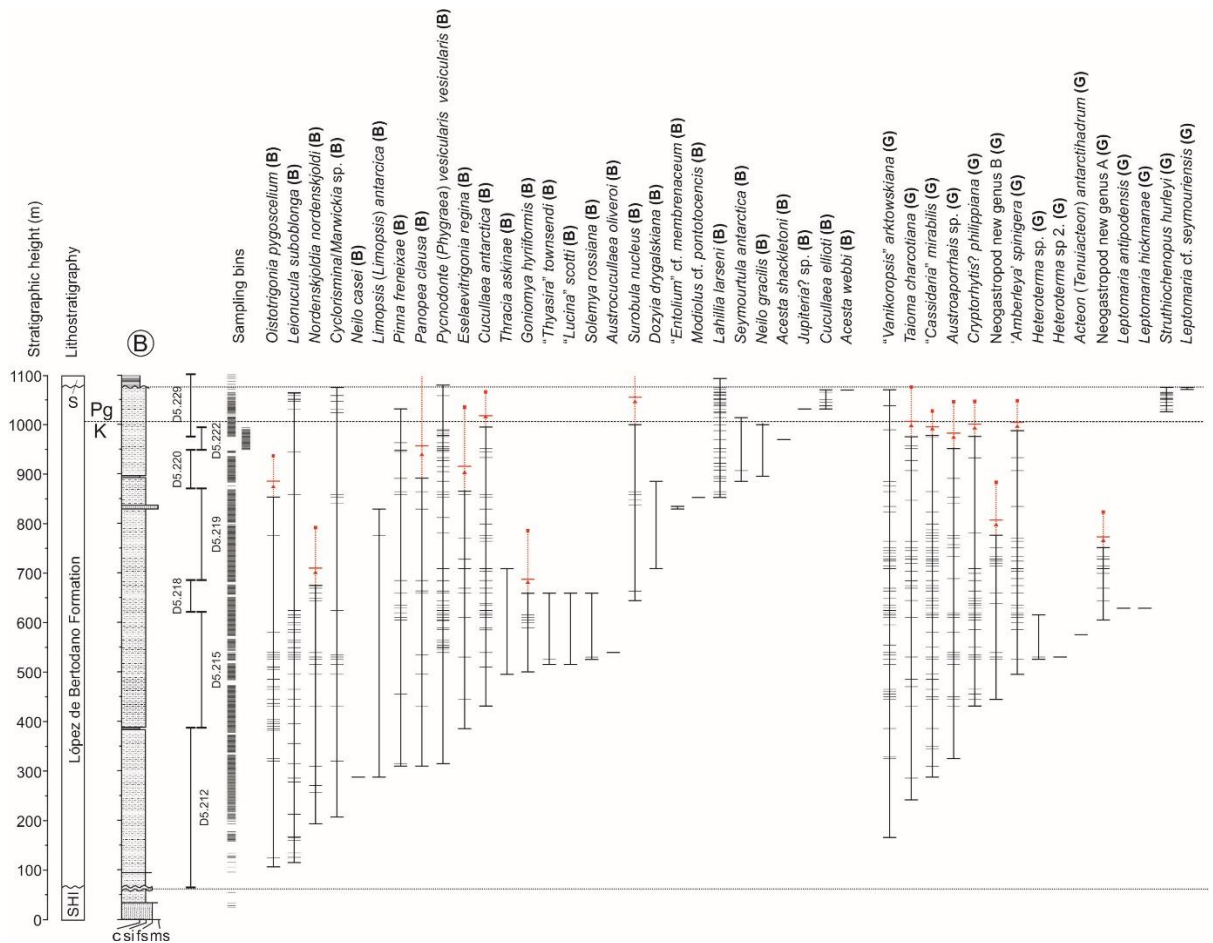
Figure B.3 Stratigraphic range and occurrence data for molluscan taxa from the BAS 2006 field season. Lithostratigraphy, sampling bins, and raw stratigraphic range data for benthic molluscan taxa (bivalves (B) and gastropods (G) from sub-sections D5.212, .D5.215, D5.218, D5.219, D5.220, D5.222, D5.229 (Bowman et al., 2012; Bowman et al., 2013; Witts et al., 2015; Bowman et al., 2014). 50% confidence intervals (red triangles), 95% confidence intervals (red squares), and average gap size between occurrences (horizontal red ticks) calculated for Maastrichtian taxa with more than five occurrences. Illustrated as range extensions (vertical red dashed line) calculated using 'classic' confidence interval methodology as summarised by Marshall, 2010. See Section B.1 for raw field data and Fig. B.1 for lithostratigraphic key.
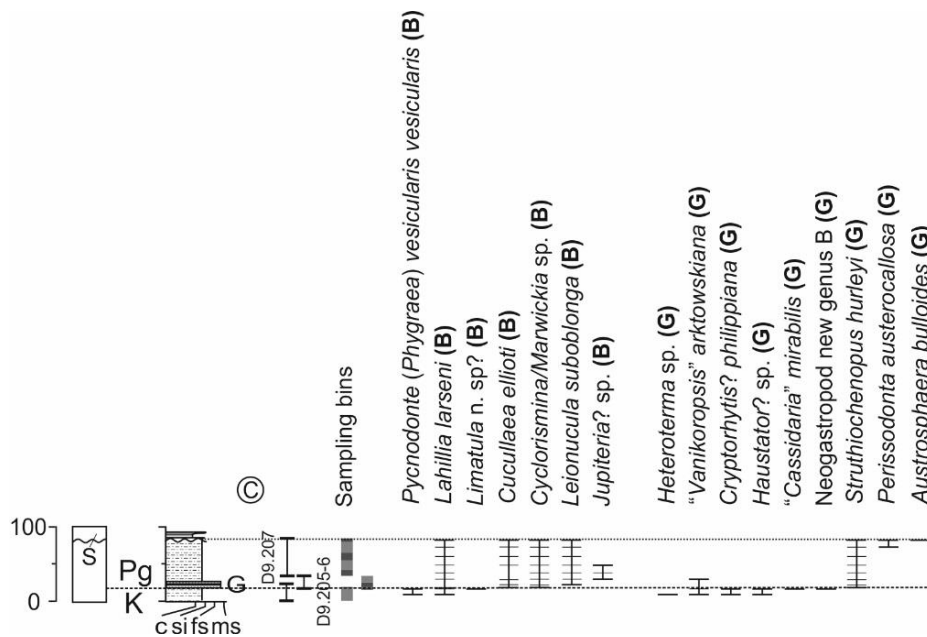
Figure B.4 Stratigraphic range and occurrence data for molluscan taxa from the BAS 2010 field season. Lithostratigraphy, sampling bins, and raw stratigraphic range data for benthic molluscan taxa (bivalves (B) and gastropods (G)) from sub-sections D9.205, D9.206, D9.207 (Bowman et al., 2015; Bowman et al., 2013; Crame et al., 2014). Due to the limited number of Maastrichtian samples, confidence intervals could not be calculated for these sections. See Section B.1 for raw field data, and Fig. B.1 for lithostratigraphic key.
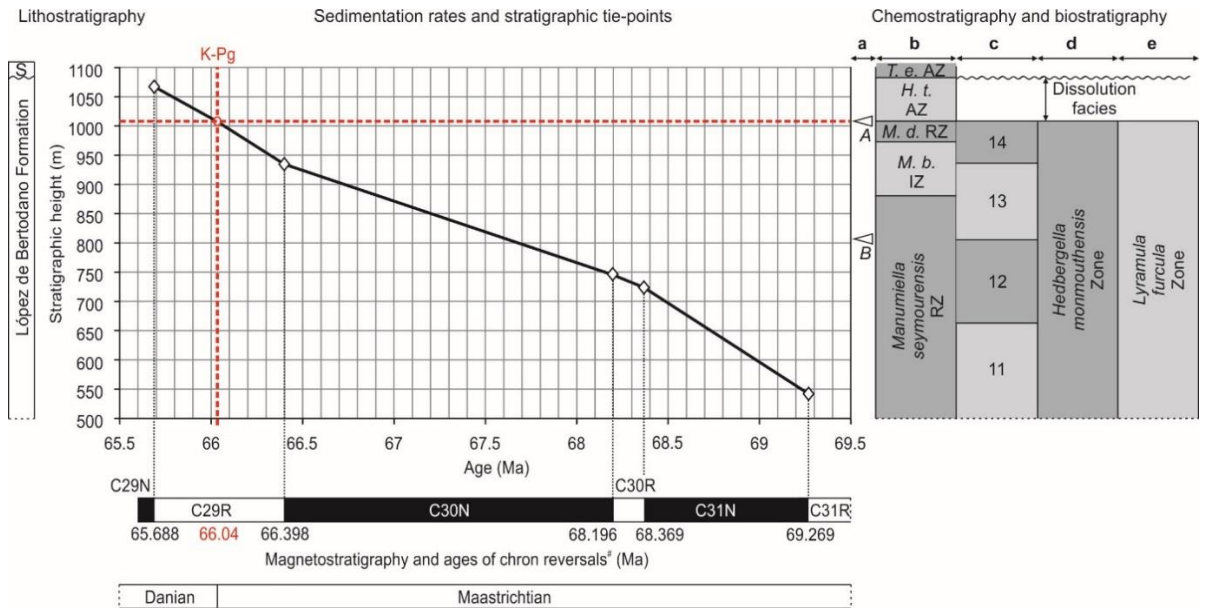
Figure B.5 Summary of age model for the López de Bertodano Formation. Magnetostratigraphy taken from Tobin et al., 2012 correlated to British Antarctic Survey (BAS) composite section using the K–Pg boundary as a stratigraphic tie-point and assuming planar bedding along strike. # updated chron reversal ages from Gradstein et al., 2012. a–e chemostratigraphy and biostratigraphy. a, strontium (Sr) isotope chemostratigraphy (McArthur et al., 1998). Arrow A = bivalve *Pycnodonte* cf. *P. vesiculosa*, 0m (relative to K–Pg boundary, ^{87}Sr/^{86}Sr = 0.707833. Arrow B = bivalve '*Linotrigonia*' *pygoscelium*, -200m, ^{87}Sr/^{86}Sr = 0.707831. Additional ^{87}Sr/^{86}Sr data used in age model construction from belemnite *Dimitobelus* (*D.*) *seymouriensis* -636 m (Crame et al., 2004), ^{87}Sr/^{86}Sr = 0.707787. All values confirm a Maastrichtian age when compared to Sr isotope data from lower latitudes (Vonhof et al., 2011). b, dinoflagellate cyst biostratigraphy (Bowman et al., 2015; Bowman et al., 2012; Bowman et al., 2013), *M.b.* IZ = *Manumiella bertodano* Interval Zone, *M. d.* RZ = *Manumiella druggii* Range Zone, *H. t.* AZ = *Hystrichosphaeridium tubiferum* Acme Zone, *T. e.* AZ = *Trithyrodinium evittii* Acme Zone. Paleocene dinoflagellate cyst zones from Antarctica are correlated to New Zealand zones NZDP1 and NZDP2 (Bowman et al., 2015). c, ammonite biostratigraphy (Witts et al., 2015; Macellari, 1986), ammonite assemblage zones (11–14) from Olivero, 2012. 11, *Maorites tuberculatus*, 12, *Pachydiscus* (*Pachydiscus*) '*ootacodensis*', 13, *Pachydiscus* (*Pachydiscus*) *riccardii*, 14, *Pachydiscus* (*Pachydiscus*) *ultimus*. d, foraminiferal biostratigraphy (Huber, 1988). e, silicoflagellate biostratigraphy (Harwood, 1988). Dissolution facies above the K–Pg boundary defined by Huber, 1988 to account for non-preservation of calcareous microfossils. For further details on the development of this age model see Bowman et al., 2012; Bowman et al., 2013; Witts et al., 2015).
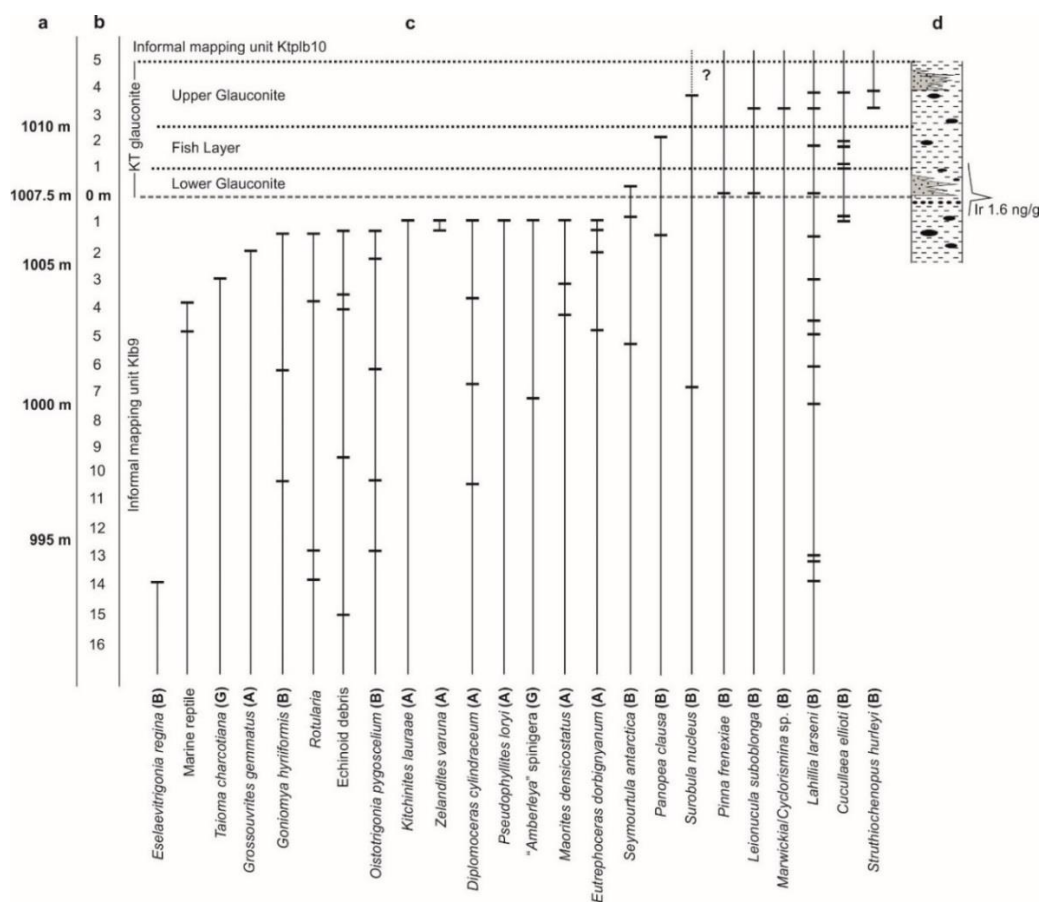
Figure B.6 Faunal range and occurrence data, and lithostratigraphy modified from the study of Zinsmeister, 1998. Data based on a compilation from 20 short measured section lines across the K–Pg boundary. a, correlation between Zinsmeister, 1998 and BAS composite section, assuming base of the "Lower Glauconite" is equivalent to the K–Pg boundary in our composite section (1007.5 m) (Bowman et al., 2015; Bowman et al., 2012; Witts et al., 2015; Bowman et al., 2014). b, stratigraphic height relative to the base of the "Lower Glauconite"/K–Pg boundary. c, stratigraphic nomenclature from Zinsmeister, 1998 and Macellari, 1988, along with faunal range and occurrence data, black lines represent species ranges, horizontal ticks are occurrences and last occurrences in different measured sections, only last occurrences used to extend ranges of taxa in BAS sections. All occurrences used in stratigraphic abundance calculations. Some species names have been changed to bring them into line with revised taxonomy (see Crame et al., 2014, Section B.1) (B), bivalve, (G), gastropod, (A), ammonite, '?' next to Surobula nucleus illustrates that this species does not range through into the Danian in our composite section. d, sedimentary log and lithostratigraphy from Zinsmeister, 1998, iridium (Ir) anomaly in "Lower Glauconite" only from Elliot et al., 1994.
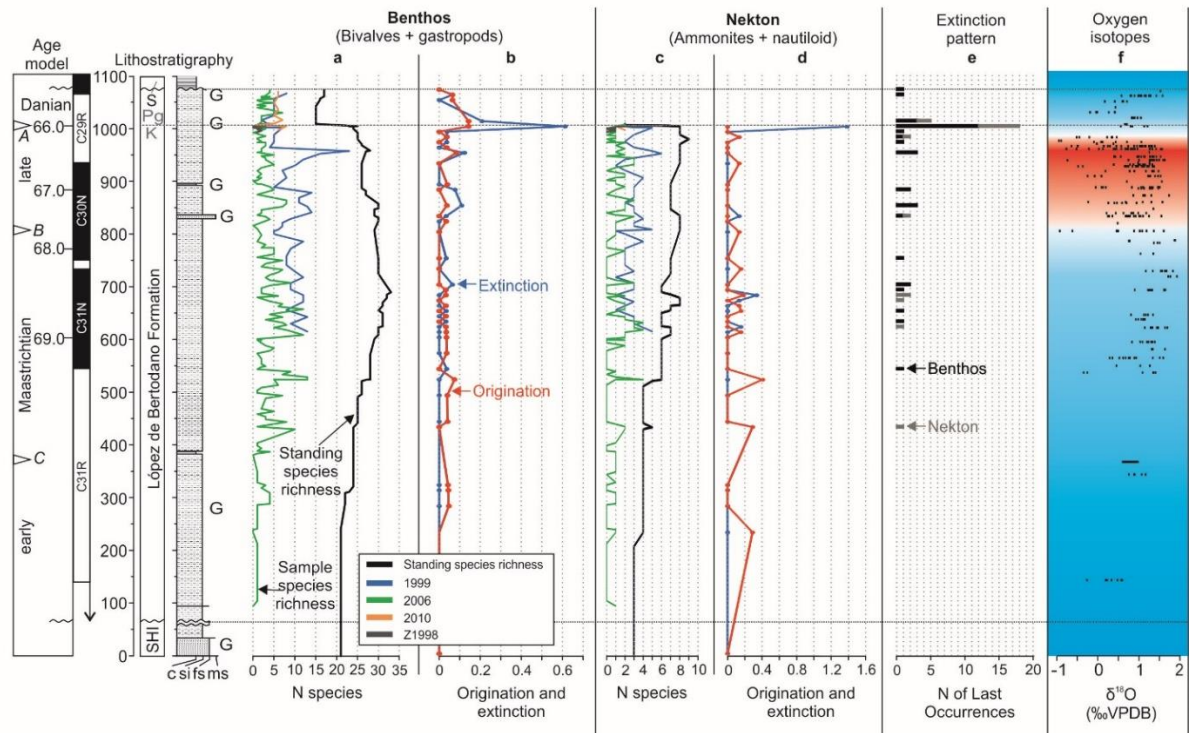
Figure B.7 Expanded molluscan diversity and palaeoenvironmental data.
Molluscan species richness variations within individual section
lines, standing species richness based on composite range-through
data (a, c) and estimated rates of origination and extinction in 10 m
binned intervals (b, d), divided into benthos (a, b) and nekton (c, d)
(species richness variations in individual sections based on
occurrences in Fig. B.3-B.6, see Section B.1). e, histogram
illustrating pattern of extinction as defined by the number of last
occurrences within 10 m binned intervals through the
Maastrichtian–Paleocene interval, divided into benthos (black) and
nekton (grey). The pattern is consistent with a sudden extinction
event at the K–Pg boundary at 1007.5 m, taking into account the
Signor-Lipps effect. f, raw oxygen isotope data taken from Tobin et
al., 2012 and Dutton et al., 2007), used as a proxy for marine
palaeotemperature. Blue = cooler overall temperatures, red =
warmer overall temperatures, as defined by other palaeoclimate
records (Bowman et al., 2013; Bowman et al., 2014). All data plotted
against age model and lithostratigraphy. See Figs. B.1 and B.5 for
details and lithostratigraphic key.

277
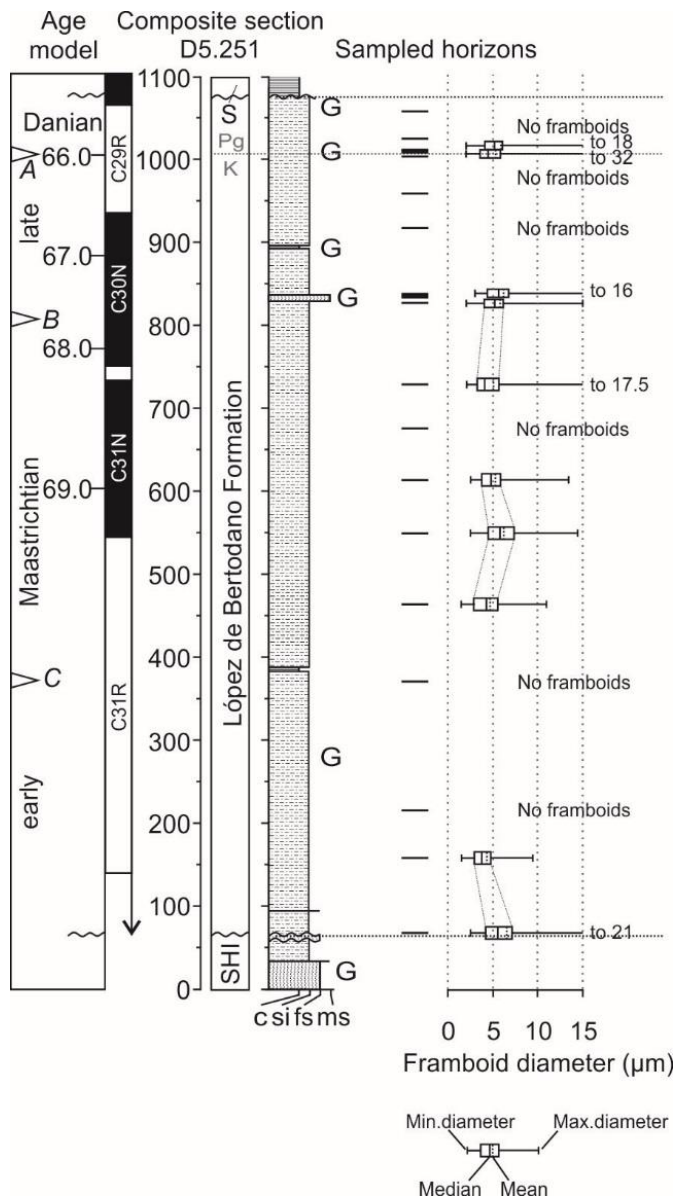
Figure B.8 Pyrite framboid data derived from section D5.251 illustrated against lithostratigraphy and age model. Data are illustrated as 'box and whisker' plots (Bond and Wignall, 2010). See Figs. B.1 and B.5 for details of age model and lithostratigraphic key.

Table B.1. Identification of range-through taxa from Campanian–Maastrichtian strata stratigraphically below the López de Bertodano Formation on Seymour Island.

#	Species *	Location, (Formation, member) □	Reference
1	*Leionucula suboblonga* (B)	Snow Hill Island (SHIF, Karlsen Cliffs Mbr)	Zinsmeister and Macellari, 1988; Wilckens 1910
2	*Solemya rossiana* (B)	Snow Hill Island (SHIF, Karlsen Cliffs Mbr)	Zinsmeister and Macellari, 1988; Wilckens 1910; Little et al., 2015
3	*Modiolus pontotcensis* (B)	Vega Island (SHIF, Cape Lamb Mbr)	Zinsmeister and Macellari, 1988; Del Valle and Medina 1980; Olivero, 1992
4	*Nordenskjoldia nordenskjoldi* (B)	Vega Island (SHIF, Cape Lamb Mbr)	Olivero, 1992
5	*Austrocucullaea oliveroi* (B)	Vega Island (SHIF, Cape Lamb Mbr)	Olivero, 1992
6	*Cucullaea antarctica* (B)	Vega Island (SHIF, Cape Lamb Mbr)	Olivero, 1992
7	*Pycnodonte* (*Phygraea*) *vesicularis vesicularis* (B)	Cockburn Island (SHIF, undifferentiated)	Askin et al., 1991; Stilwell 2002
8	*Seymourtula antarctica* (B)	Cockburn Island (SHIF, undifferentiated)	Askin et al., 1991; Stilwell 2002
9	*Oistotrigonia pygoscelium* (B)	Vega Island (SHIF, Cape Lamb Mbr)	Olivero, 1992
10	*Eselaevitrigonia regina* (B)	Vega Island (SHIF, Cape Lamb Mbr); Snow Hill Island (SHIF, Haslum Crag Mbr)	Pirrie et al., 1997; Zinsmeister and Macellari, 1988; Wilckens 1910; Olivero, 1992
11	"*Lucina*" *scotti* (B)	Snow Hill Island (SHIF, Karlsen Cliffs and Haslum Crag mbrs)	Zinsmeister and Macellari, 1988; Wilckens 1910; Little et al., 2015
12	"*Thyasira*" *townsendi* (B)	Snow Hill Island (SHIF, Karlsen Cliffs and Haslum Crag mbrs)	Zinsmeister and Macellari, 1988; Wilckens 1910; Little et al., 2015
13	*Cyclorismina/Marwickia* sp. (B)	Snow Hill Island (SHIF ?Karlsen Cliffs Mbr)	Zinsmeister and Macellari, 1988; Wilckens 1910;
14	*Panopea clausa* (B)	Humps Island (SHIF, undifferentiated)	Stilwell and Zinsmeister, 1987a
15	*Thracia askinae* (B)	Vega Island (SHIF, Cape Lamb Mbr)	Zinsmeister and Macellari, 1988; Del Valle and Medina 1980; Olivero, 1992
16	"*Amberleya*" *spinigera* (G)	Ula Point, James Ross Island (SHIF, undifferentiated)	Stilwell and Zinsmeister, 1987b
17	"*Vanikoropsis*" *arktowskiana* (G)	Snow Hill Island (SHIF, ?Karlsen Cliffs Mbr)	Crame et al., 2014; Wilckens, 1910

18	"Cassidaria" mirabilis (G)	Snow Hill Island (SHIF, ?Karlsen Cliffs Mbr)	Crame et al., 2014; Wilckens, 1910
19	?Cryptorhytis phillippiana (G)	Snow Hill Island (SHIF, ?Karlsen Cliffs Mbr)	Crame et al., 2014; Wilckens, 1910
20	Taioma charcotiana (G)	Snow Hill Island (SHIF, ?Karlsen Cliffs Mbr)	Crame et al., 2014; Wilckens, 1910
21	Pseudophyllites loryi (A)	Vega Island (SHIF, Cape Lamb Mbr)	Gradstein et al., 2012; McArthur et al., 1998; Olivero, 1992
22	Diplomoceras cylindraceum (A)	Vega Island (SHIF, Cape Lamb Mbr), Snow Hill Island (SHIF, Sanctuary Cliffs, Karlsen Cliffs, Haslum Crag mbrs)	Gradstein et al., 2012; McArthur et al., 1998; Pirrie et al., 1997; Bowman et al., 2013
23	Eutrephoceras dorbignyanum (N)	Vega Island (SHIF, Cape Lamb Mbr), James Ross Island (SMF, Lachman Crags Mbr)	Gradstein et al., 2012; Olivero, 1992; Cichowolski et al., 2005

Key: *(B), bivalve, (G), gastropod, (A), ammonite, (N), nautiloid.

◻ SHIF, Snow Hill Island Formation, SMF, Santa Marta Formation.

For information on the overall lithostratigraphy of the James Ross Basin see references and references therein (Crame et al., 2004; Bowman et al., 2015; Bowman et al., 2012; Witts et a;., 2015; Bowman et al., 2014; Crame et al., 2014; McArthur et al., 1998; Olivero, 2012; Pirrie et al., 1997; Bowman et al., 2013).

Table B.2 Pyrite framboid data taken from stratigraphic section D5.251.

Sample #	Stratigraphic height in composite section D5.251 (m)	N	Mean	S.D.	Min. F.D.	Max. F.D.
D5.1351.1	1058	N.A.	N.A.	N.A.	N.A.	N.A.
D5.1308.1	1023	N.A.	N.A.	N.A.	N.A.	N.A.
D5.1295.1	1007-1010	105	5.95	2.58	2	18
D5.1296.1	1010	104	5.17	1.65	2.5	13.5
D5.1294.1	1009	103	4.97	2.19	2	12.5
D5.1293.1	1008	103	5.26	3.17	1	31
D5.1292.1	1007	N.A.	N.A.	N.A.	N.A.	N.A.
D5.1290.1	1002	N.A.	N.A.	N.A.	N.A.	N.A.
D5.1237.1	958	N.A.	N.A.	N.A.	N.A.	N.A.
D5.1213.1	916	N.A.	N.A.	N.A.	N.A.	N.A.
D5.1164.1	832	102	5.99	1.84	3	14.5
D5.1163.1	831	99	6.2	2.3	3	16
D5.1160.1	826	104	5.82	2.3	2	15.5
D5.1108.1	728	102	5.02	2.41	2	17.5
D5.1053.1	674	N.A.	N.A.	N.A.	N.A.	N.A.
D5.696.1	612	104	5.27	1.92	2.5	13.5
D5.370.1	549	101	6.21	2.33	2.5	14
D5.985.1	462	104	4.69	1.92	1.5	11
D5.902.1	380	N.A.	N.A.	N.A.	N.A.	N.A.
D5.892.1	370	N.A.	N.A.	N.A.	N.A.	N.A.
D5.535.1	213	N.A.	N.A.	N.A.	N.A.	N.A.
D5.481.2	158	105	4.31	1.57	1.5	9.5
D5.406.1	68	100	6.56	3.2	2.5	21

N, number of framboids measured in sample, Mean, mean framboid diameter, S.D., standard deviation of framboid diameters, Min. F.D., minimum framboid diameter, Max F.D., maximum framboid diameter.

B.1 Taxonomy and field data

Classification of benthic molluscan taxa from the Maastrichtian–Danian López de Bertodano Formation and taxonomic remarks, bivalves arranged in taxonomic order according to Bouchet and Rocroi, (2010) and Bieler et al. (2014), and gastropods according to Bouchet and Rocroi, (2005) and Ponder and Limberg, (2008). See also Crame et al. (2014); Zinsmeister and Macellari, (1988); Stilwell et al. (2004); and Beu, (2009), for further discussion and full descriptions of Cretaceous–Paleogene molluscan taxa from Antarctica.

Photographs and information on specimens collected and described by other authors from Seymour Island (Crame et al., 2014; Zinsmeister and Macellari, 1988; Stilwell et al., 2004) currently held in the collections of the Paleontological Research Institute (PRI), Ithaca, NY, USA are available online at: http://www.pricollectionsdatabase.org/

Class: Bivalvia

Leionucula suboblonga (Crame et al., 2014; Zinsmeister and Macellari, 1988; Wilckens, 1910; Stilwell et al. 2004; Beu 2009)

Solemya rossiana (Little et al, 2015)

Jupiteria? sp. (Stilwell et al. 2004; Beu 2009

Neilo casei (Zinsmeister and Macellari, 1988; Beu 2009)

Neilo gracilis (Zinsmeister and Macellari, 1988; Beu 2009)

Modiolus cf. *pontotocencis* (Zinsmeister and Macellari, 1988)

Nordenskjoldia nordenskjoldi (Zinsmeister and Macellari, 1988)

Austrocucullaea oliveroi (Zinsmeister and Macellari, 1988)

Cucullaea Antarctica (Zinsmeister and Macellari, 1988)

Cucullaea ellioti (Zinsmeister and Macellari, 1988; Stilwell et al., 2004)
- In the BAS composite section specimens of *Cucullaea ellioti* occur only above the K–Pg boundary, whereas Zinsmeister (1998) records several

examples from immediately below the Ir-bearing Lower Glauconite horizon.

Limopsis (*Limopsis*) *Antarctica* (Zinsmeister and Macellari, 1988; Whittle et al., 2011)

Phelopteria feldmanni (Zinsmeister and Macellari, 1988)

Pulvinites Antarctica (Zinsmeister and Macellari, 1988; Zinsmeister, 2009)

Pinna frenexiae (Zinsmeister and Macellari, 1988)

Pycnodonte (*Phygraea*) *vesicularis vesicularis* (Zinsmeister and Macellari, 1988; Machalski, 1988; Wilmsen and Voight, 2006)
- Two distinct species of *Pycnodonte* have been described from Seymour Island by Zinsmeister and Macellari, 1988, they recognised the high degree of morphological plasticity shown by both. It is likely that all specimens from the López de Bertodano and Sobral Formations are ecomorphs of a single, highly variable species (Machalski, 1988), the widespread *Pycnodonte* (*Phygraea*) *vesicularis vesicularis* (see Wilmsen and Voight, 2006 for discussion).

"*Entolium*" cf. *membranaceum* (Zinsmeister and Macellari, 1988; Waller, 2006; Stilwell, 1998) See Waller (2006) for discussion of the current problems associated with pectinid taxonomy. BAS specimens are too poorly preserved to separate into two species as per Zinsmeister and Macellari, (1988). "*Entolium*" s.s. is used to describe many smooth Late Cretaceous pectinids, with "*E.*" *membranaceum* often considered a cosmopolitan latest Cretaceous species (D'Hondt, 1971; Stilwell, 1998).

Limatula sp. (Crame et al, 2014; Stilwell et al., 2004)
- This is the same as the specimens referred to as *Limatula* sp. nov in Crame et al. (2014).

Acesta shackletoni (Zinsmeister and Macellari, 1988)

Acesta webbi (Zinsmeister and Macellari, 1988)

Seymourtula Antarctica (Zinsmeister and Macellari, 1988)

Oistotrigonia pygoscelium (Zinsmeister and Macellari, 1988)

Eselaevitrigonia regina (Zinsmeister and Macellari, 1988)

"*Lucina*" *scotti* (Zinsmeister and Macellari, 1988; Little et al., 2015)

"*Saxolucina*" sp. (Stilwell et al., 2004; Beu, 2009)

"*Thyasira*" *townsendi* (Zinsmeister and Macellari, 1988; Little et al., 2015)

Dozyia drygalskiana (Zinsmeister and Macellari, 1988)

Lahillia larseni (Zinsmeister and Macellari, 1988 and Stilwell et al., 2004)

Cyclorismina/Marwickia sp. (Zinsmeister and Macellari, 1988; Stilwell et al., 2004; Beu, 2009)
- Taxa from Seymour Island assigned to these two genera were separated based on differences in size, shape of the umbo, and presence of anterior lateral tooth in "*Marwickia woodburnei*", but only articulated specimens with no dentition visible have been illustrated (Zinsmeister and Macellari, 1988; Stilwell et al., 2004). The majority of BAS specimens are also articulated, in many cases exhibit rather poor preservation and externally appear identical. We are thus unable to resolve the material in this collection into two distinct genera or species.

Surobula nucleus (Zinsmeister and Macellari, 1988)

Panopea clausa (Zinsmeister and Macellari, 1988)

Goniomya hyriiformis (Zinsmeister and Macellari, 1988)

Thracia askinae (Zinsmeister and Macellari, 1988)

Class: Gastropoda

Leptomaria cf. *seymouriensis* (Harasewych et al., 2009)

Leptomaria hickmanae (Harasewych et al., 2009)

Leptomaria antipodensis (Harasewych et al., 2009)

"*Amberleya*" *spinigera* (Crame et al., 2014; Ferrari et al., 2014)
- *Amberleya* sensu stricto is now restricted to the Jurassic type species (Ferrari et al., 2014). "*A.*" *spinigera* is probably a member of

> *Ambercyclus* - with morphology intermediate between the genera
> *Amberleya* and *Eucyclus* (Ferrari et al., 2014).

Haustator? sp.
- High-spired turritellid gastropod with flat whorl sides. Overall
  morphology suggests placement of two worn specimens from the
  interval beneath the K–Pg boundary in the genus *Haustator*. But the
  material is too poorly preserved for a definitive identifiation. Turritellid
  gastropods appear rare in the López de Bertodano and Sobral
  Formations (Stilwell et al., 2004; Beu, 2009).

"*Vanikoropsis*" *arktowskiana* (Crame et al., 2014)

Austroaporrhais sp. (Zinsmeister and Griffin, 1995)
- Material in BAS collections is too poorly preserved to be separated into
  the various Maastrichtian species of *Austroaporrhais* previously
  identified from Seymour Island (Zinsmeister and Griffin, 1995).

Perissodonta austerocallosa (Crame et al., 2014; Beu, 2009)

Struthiochenopus hurleyi (Stilwell et al., 2004; Zinsmeister and Griffin, 1995)

Neogastropod new genus A (Crame et al., 2014)

Neogastropod new genus B (Crame et al., 2014)

Austrosphaera bulloides (Crame et al., 2014; Oleinik and Zinsmeister, 1996)

"*Cassidaria*" *mirabilis* (Crame et al., 2014)

Heteroterma? sp. 1 (Crame et al., 2014)

Heteroterma? sp. 2 (Crame et al., 2014)

Heteroterma sp. (Crame et al., 2014)

Taioma charcotiana (Crame et al., 2014)

Cryptorhytis? *Phillippiana* (Crame et al., 2014)

Acteon (*Tenuiacteon*) *antarctihadrum* (Stilwell and Zinsmeister, 2002)

Raw field data relevant to this appendix is attached to the thesis on the
accompanying CD.

Table B.3 Composite first and last occurrence data, location of last occurrence relative to K–Pg boundary, stratigraphic abundance (S) for all molluscan taxa. Data sorted by last appearance (LA) in composite section.

#		FA 99	LA 99	N_{Ooo} 99	FA 06	LA 06	N_{Ooo} 06	FA 10	LA 10	N_{Ooo} 10
1	Austrocucullaea oliveroi	-	-	0	540	540	1	-	-	0
2	Leptomaria hickmanae	-	-	0	626	631	1	-	-	0
3	Leptomaria antipodensis	610	651	2	626	631	1	-	-	0
4	Pulvinites antarctica	680	690.5	1	-	-	0	-	-	0
5	Nordenskjoldia nordenskjoldi	610	702	3	194	676	15	-	-	0
6	Heteroterma ? sp. 1	690.5	702	1	-	-	0	-	-	0
7	Neogastropod new genus A	680	713.5	3	602	754	9	-	-	0
8	Limopsis (Limopsis) antarctica	-	-	0	289	832	3	-	-	0
9	Thracia askinae	624	858.5	4	492	711	2	-	-	0
10	Modiolus pontotocensis	848	858.5	1	850	856	1	-	-	0
11	Acteon (Tenuiacteon) antarctihadrum	848	858.5	1	572	577	1	-	-	0
12	"Entolium" cf. membranaceum	836	883	3	826	836	2	-	-	0
13	Dozyia drygalskiana	665	883	7	706	888	2	-	-	0
14	"Lucina" scotti	836	959.5	4	512	661	2	-	-	0
15	Solemya rossiana	949	959.5	2	525	661	4	-	-	0
16	Heteroterma ? sp. 2	821	959.5	3	527	532	1	-	-	0
17	Austroaporrhais sp.	610	971.5	23	322	954	23	-	-	0
18	Phelopteria feldmanni	958	981	2	-	-	0	-	-	0
19	Eselaevitrigonia regina	610	959.5	25	388	868	11	-	-	0
20	Acesta shackletoni	1003.5	1003.5	1	966	972	1	-	-	0
21	Taioma charcotiana	638.5	959.5	21	242	978	25	-	-	0
22	Oistotrigonia pygoscelium	638.5	958	19	105	856	26	-	-	0
23	Goniomya hyniformis	610	998	4	497	661	7	-	-	0
24	'Amberleya' spinigera	610	981	30	492	984	23	-	-	0
25	Cucullaea antarctica	638.5	1007	18	427	998	28	-	-	0
26	Limatula n. sp. ?	-	-	0	-	-	0	1004	1007.5	1
27	Neogastropod new genus B	702	959.5	8	442	778	12	1004	1007.5	1
28	"Cassidaria" mirabilis	610	959.5	14	289	980	45	1004	1007.5	1
29	Haustator ? Sp.	-	-	0	-	-	0	989.5	1007.5	2
30	Cryptorhytis ? phillippiana	610	1006	27	427	978	26	989.5	1007.5	2
31	Panopea clausa	610	1007	20	310	894	10	-	-	0
32	Surobula nucleus	779	935.5	5	641	1004	8	-	-	0
33	Seymourtula antarctica	875.5	949	5	882	1016	3	-	-	0

#	FA Z98	LA Z98	N$_{Oo}$ Z98	FA COMP	LA COMP	LA - KPg	S (stratigraphic abundance)	Total number of occurrences
1	-	-	0	540	540	-467.5	0.396825397	1
2	-	-	0	626	631	-376.5	0.396825397	1
3	-	-	0	610	651	-356.5	1.19047619	3
4	-	-	0	680	690.5	-317	0.396825397	1
5	-	-	0	194	702	-305.5	7.142857143	18
6	-	-	0	690.5	702	-305.5	0.396825397	1
7	-	-	0	602	754	-253.5	4.761904762	12
8	-	-	0	289	832	-175.5	1.19047619	3
9	-	-	0	492	858.5	-149	2.380952381	6
10	-	-	0	848	858.5	-149	0.793650794	2
11	-	-	0	572	858.5	-149	0.793650794	2
12	-	-	0	826	883	-124.5	1.984126984	5
13	-	-	0	665	888	-119.5	3.571428571	9
14	-	-	0	512	959.5	-48	2.380952381	6
15	-	-	0	525	959.5	-48	2.380952381	6
16	-	-	0	529.5	959.5	-48	1.587301587	4
17	-	-	0	322	971.5	-36	18.25396825	46
18	-	-	0	959.5	981	-26.5	0.793650794	2
19	993.5	993.5	1	388	993.5	-14	14.68253968	37
20	-	-	0	969.5	1003.5	-4	0.793650794	2
21	1004.5	1004.5	1	242	1004.5	-3	18.65079365	47
22	994.5	1006	4	105	1006	-1.5	19.44444444	49
23	997	1006	3	497	1006	-1.5	5.555555556	14
24	1000	1006.5	2	492	1006.5	-1	21.82539683	55
25	-	-	0	427	1007	-0.5	18.25396825	46
26	-	-	0	1004	1007.5	0	0.396825397	1
27	-	-	0	442	1007.5	0	7.53968254	19
28	-	-	0	289	1007.5	0	23.80952381	60
29	-	-	0	989.5	1007.5	0	0.793650794	2
30	-	-	0	430.5	1007.5	0	21.82539683	55
31	1006	1009.5	2	310	1009.5	2	12.6984127	32
32	1000.5	1011	2	641	1011	3.5	5.952380952	15
33	1002	1008	3	875.5	1016	8.5	4.365079365	11

	#	FA 99	LA 99	N$_{Ooo}$ 99	FA 06	LA 06	N$_{Ooo}$ 06	FA 10	LA 10	N$_{Ooo}$ 10
Leptomaria cf. seymouriensis	34	-	-	0	1070	1074	2	-	-	0
Leionucula suboblonga	35	610	1073	9	115	1063	41	1008.35	1069.35	6
"Vanikoropsis" arktowskiana	36	610	1073	21	165	1070	42	989.5	1021.35	3
Marwickia /Cyclorisma sp.	37	665	1073	18	208	1074	18	1007.35	1073.35	8
Pinna freneixae	38	610	1007	17	310	1034	17	-	-	0
Pycnodonte (Phygraea) vesicularis vesicularis	39	610	1073	22	312	1058	49	989.5	1007.5	2
"Thyasira" townsendi	40	949	959.5	2	512	661	4	-	-	0
Neilo casei	41	-	-	0	289	289	1	-	-	0
Heteroterma sp.	42	926.5	959.5	2	522	617	3	989.5	1007.35	1
Lahillia larseni	43	864.5	1073	21	850	1074	36	989.5	1073.35	10
Neilo gracilis	44	-	-	0	896	1004	2	-	-	0
Acesta webbi	45	958	959.5	1	1063	1063	1	-	-	0
Cucullaea ellioti	46	1007	1073	6	1028	1070	7	1005.85	1073.35	7
Struthiochenopus hurleyi	47	1007	1073	8	1022	1074	17	1005.85	1073.35	8
?Jupiteria sp.	48	-	-	0	1028	1034	1	1013.35	1043.5	3
"Saxolucina" sp.	49	1019	1062.5	3	-	-	0	-	-	0
Perissodonta austerocalliosa	50	-	-	0	-	-	0	1055.85	1073.35	2
Austrosphaera bulloides	51	1062.5	1073	1	-	-	0	1069.35	1073.35	1
Maorites tuberculatus	52	-	-	0	234.5	434	6	-	-	0
Maorites cf. weddelliensis	53	610	624	1	522	621	3	-	-	0
Pachydiscus (Pachydiscus) cf. 'ootacodensis'	54	-	-	0	666	671	1	-	-	0
Kitchinites sp.	55	610	880	4	522	876	12	-	-	0
Maorites seymourianus	56	610	880	4	434	886	18	-	-	0
Pachydiscus (Pachydiscus) riccardii	57	808.5	836	4	832	836	1	-	-	0
Pachydiscus (Pachydiscus) ultimus	58	935.5	981	5	942	980	5	-	-	0
Grossouvrites joharae	59	610	971.5	23	617	954	15	-	-	0
Pseudophyllites cf. loryi	60	890.5	898	4	327	832	3	-	-	0
Kitchinites laurae	61	880	824	6	681	989	4	-	-	0
Maorites densicostatus	62	725.5	1008	26	760	978	26	-	-	0
Anagaudryceras seymouriense	63	779	1007	9	656	836	3	-	-	0
Zelandites varuna	64	981	1007	1	-	-	0	-	-	0
Eutrephoceras dorbignyanum	65	610	1007	8	522	1010	9	989.5	989.5	1
Diplomoceras cylindraceum	66	702	1003.5	19	95	1010	12	989.5	1007.5	2
		N$_{sample\ 99}$	N$_{sample\ 99}$	N$_{sample\ 10}$	N$_{sample\ 288}$					
		46	175	11	20					

#	FA Z98	LA Z98	N$_{Occ}$ Z98	FA COMP	LA COMP	LA - KPg	S (stratigraphic abundance)	Total number of occurrences
34	-	-	0	1070	1074	66.5	0.793850794	2
35	1007.5	1010.5	2	115	1073	65.5	23.01587302	58
36	-	-	0	165	1073	65.5	26.19047619	66
37	-	-	0	208	1074	66.5	17.46031746	44
38	1007.5	1007.5	1	310	1031	23.5	13.88888889	35
39	-	-	0	312	1073	65.5	28.96825397	73
40	-	-	0	512	959.5	-48	2.380952381	6
41	-	-	0	289	289	-718.5	0.396825397	1
42	-	-	0	524.5	1007.35	-0.15	2.380952381	6
43	994.5	1011	12	850	1074	66.5	31.34920635	79
44	-	-	0	896	1001	-6.5	0.793850794	2
45	-	-	0	958	1063	55.5	0.793850794	2
46	1006	1011	5	1005.85	1073.35	65.85	9.920634921	25
47	1010.5	1011	2	1005.85	1074	66.5	13.88888889	35
48	-	-	0	1013.35	1043.5	36	1.587301587	4
49	-	-	0	1019	1062.5	55	1.19047619	3
50	-	-	0	1055.85	1073.35	65.85	0.793850794	2
51	-	-	0	1062.5	1073.35	65.85	0.793850794	2
52	-	-	0	234.5	434	-573.5	2.380952381	6
53	-	-	0	524.5	624	-383.5	1.587301587	4
54	-	-	0	666	671	-336.5	0.396825397	1
55	-	-	0	522	680	-327.5	6.349206349	16
56	-	-	0	434	686	-321.5	8.73015873	22
57	-	-	0	808.5	836	-171.5	1.984126984	5
58	-	-	0	935.5	981	-26.5	3.968253968	10
59	1005.5	1005.5	1	610	1005.5	-2	15.47619048	39
60	1006.5	1006.5	1	327	1006.5	-1	3.174603175	8
61	1006.5	1006.5	1	680	1006.5	-1	4.365079365	11
62	1003	1006	3	725.5	1006.5	-1	21.82539683	55
63	-	-	0	656	1007	-0.5	4.761904762	12
64	1006	1006.5	2	981	1007	-0.5	1.19047619	3
65	1003	1006.5	4	522	1010*	2.5	8.73015873	22
66	997	1006.5	4	95	1010*	2.5	14.68253968	37

Italics = FAD or LAD above/below study interval (range-through)

*Two species of cephalopod have LAD above the K-Pg boundary due to their last occurrence in a bin that straddles the boundary interval (see sheet B - 2006)

References

Askin, R. A., Elliot, D. H., Stilwell, J. D. & Zinsmeister, W. J., 1991. Stratigraphy and paleontology of Campanian and Eocene sediments, Cockburn Island, Antarctic Peninsula. *Journal of South American Earth Sciences* **4**, 99–117.

Beu, A. G., 2009. Before the ice: biogeography of Antarctic Paleogene molluscan faunas. *Palaeogeography, Palaeoclimatology, Palaeoecology* **284**, 191–226.

Bieler, R., Mikkelsen, P.M., Collins, T.M., Glover, E.A., González, V.L., Graf, D.L., Harper, E.M., Healy, J., Kawauchi, G.Y., Sharma, P.P., Staubach, S., Strong, E.E., Taylor, J.D., Tëmkin, I., Zardus, J.D., Clark, S., Guzmán, A., McIntyre, E., Sharp, P., Giribet, G., 2014. Investigating the bivalve tree of life – an exemplar-based approach combining molecular and novel morphological characters. *Invertebrate Systematics* **28**, 32-115.

Bond, D. P. G. & Wignall P. B., 2010. Pyrite framboid study of marine Permian–Triassic boundary sections: a complex anoxic event and its relationship to contemporaneous mass extinction. *Geological Society of America Bulletin* **122,** 1265–1279.

Bouchet, P. & Rocroi, J-P., 2005. Classification and nomenclator of gastropod families. *Malacologia* **47**, 1–397.

Bouchet, P. & Rocroi, J-P., 2010. Nomenclator of bivalve families. *Malacologia* **52**, 1–184.

Bowman, V. C., Francis, J. E. & Riding, J. B. 2013. Late Cretaceous winter sea ice in Antarctica? *Geology* **41**, 1227–1230.

Bowman, V. C., Francis, J. E., Askin, R. A., Riding, J. B. & Swindles, G. T., 2014. Latest Cretaceous–earliest Paleogene vegetation and climate change at the high southern latitudes: palynological evidence from Seymour Island, Antarctic Peninsula. *Palaeogeography, Palaeoclimatology, Palaeoecology* **408**, 26–47.

Bowman, V. C., Francis, J. E., Riding, J. B., Hunter, S. J. & Haywood, A. M., 2012. A latest Cretaceous to earliest Paleogene dinoflagellate cyst zonation from Antarctica, and implications for phytoprovincialism in the high southern latitudes. *Review of Palaeobotany and Palynology* **171,** 40–56.

Bowman, V. C., Riding, J. B., Francis, J. E., Crame, J. A. & Hannah, M., 2013. The taxonomy and palaeobiogeography of small chorate dinoflagellate cysts from the Late Cretaceous to Quaternary of Antarctica. *Palynology* **37**, 151–169.

Bowman, V.C., Ineson, J.R., Riding, J.B., Crame, J.A., Francis, J.E., Condon, D., Whittle, R., Ferraccioli, F., 2015. The Paleocene of Antarctica: Dinoflagellate cyst biostratigraphy, chronostratigraphy and implications for the palaeo-Pacific margin of Gondwana. *Gondwana Research* doi:10.1016/j.gr.2015.10.018.

Cichowolski, M., Ambrosio, A. & Concheyro, A., 2005. Nautilids from the upper Cretaceous of the James Ross Basin, Antarctic Peninsula. *Antarctic Science* **17**, 267–280.

Crame, J. A., Beu, A. G., Ineson, J. R., Francis, J. E., Whittle, R. J. & Bowman, V. C., 2014. The early origins of the Antarctic marine fauna and its evolutionary implications. *PLoS ONE* **9**, e114732.

Crame, J. A., Francis, J. E., Cantrill, D. J. & Pirrie, D., 2004. Maastrichtian stratigraphy of Antarctica. *Cretaceous Research* **25**, 411–423.

Crame, J. A., McArthur, M. A., Pirrie, D. & Riding, J. B., 1999. Strontium isotope correlation of the basal Maastrichtian stage in Antarctica to the European and US biostratigraphic schemes. *Journal of the Geological Society London* **156**, 957–964.

D'Hondt A., 1971. Systematic revision of *Entolium*, *Propeamussium* (Amusiidae) and *Syncyclonema* (Pectinidae, Bivalvia, Mollusca) of the European Boreal Cretaceous. *Bulletin de l'Institut Royal des Sciences Naturelles de Belgique* **47**, 1–95.

Del Valle, R. & Medina, F. A., 1980. Nuevos invertebrados fósiles de Cabo Lamb (Isla Vega) y Cabo Morro (Isla James Ross). *Contribuciones del Instituto Antárctico Argentino* **228**, 51–67.

Dutton, A., Huber, B. T., Lohmann, K. C. & Zinsmeister, W. J., 2007. High-resolution stable isotope profiles of a dimitobelid belemnite: implications for paleodepth habitat and late Maastrichtian climate seasonality *Palaios* **22**, 642–650.

Elliot, D. H., Askin, R. A., Kyte, F. T. & Zinsmeister, W. J., 1994. Iridium and dinocysts at the Cretaceous–Tertiary boundary on Seymour Island, Antarctica: implications for the K–T event. *Geology* **22**, 675–678.

Ferrari, S. M., Kaim, A. & Damborenea, S. E., 2014 The genera *Calliotropis* Seguenza and *Ambercyclus* n. gen. (Vetigastropoda, Eucyclidae) from the early Jurassic of Argentina. *Journal of Paleontology* **88**, 1174–1188.

Gradstein, F. M., Ogg, J. G., Schmitz, M. & Ogg, G. The Geological Time Scale 2012 Elsevier Science Ltd: Boston, (2012).

Harasewych, M. G., Oleinik, A. & Zinsmeister, W. J., 2009. The Cretaceous and Paleocene Pleurotomariid (Gastropoda: Vetigastropoda) fauna of Seymour Island, Antarctica. *Journal of Paleontology* **83**, 750–766.

Harwood, D. M., 1988. Upper Cretaceous and lower Paleocene diatom and silicoflagellate biostratigraphy of Seymour Island, eastern Antarctic Peninsula. In: Feldmann, R.M., Woodburne, M.O. (Eds.), *Geology and Paleontology of Seymour Island, Antarctic Peninsula*. Geological Society of America, Memoirs **169,** 55–130.

Huber, B. T., 1988. Upper Campanian–Paleocene foraminfera from the James Ross Island region, Antarctic Peninsula. In: Feldmann, R.M., Woodburne, M.O. (Eds.), *Geology and Paleontology of Seymour Island, Antarctic Peninsula*. Geological Society of America, Memoirs **169,** 163–252.

Little, C.T.S., Birgel, D., Boyce, A.J., Crame, J.A., Francis, J.E., Kiel, S., Peckmann, J., Pirrie, D., Rollinson, G.K., Witts, J.D., 2015. Late

Cretaceous (Maastrichtian) shallow water hydrocarbon seeps from Snow Hill and Seymour Islands, James Ross Basin, Antarctica. *Palaeogeography Palaeoclimatology Palaeoecology* **418**, 213–228.

Macellari, C.E., 1988. Stratigraphy, sedimentology and paleoecology of Upper Cretaceous/Paleocene shelf-deltaic sediments of Seymour Island (Antarctic Peninsula). In: Feldmann, R.M., Woodburne, M.O. (Eds.), *Geology and Paleontology of Seymour Island, Antarctic Peninsula*. Geological Society of America, Memoirs **169**, pp. 25–53.

Macellari, C.E., 1986. Late Campanian-Maastrichtian ammonite fauna from Seymour Island (Antarctic Peninsula). *Memoir (The Paleontological Society)* **18**, pp. 1–55.

Machalski, M., 1988. Redescription of a Danian oyster *Pycnodonte simile* (Pusch, 1837) from Poland. *Acta Palaeontologica Polonica* **33**, 73–83.

Marshall, C. R., 2010. in: *Quantitative methods in paleobiology.* (eds Alroy, J. and Hunt, G.) The Palentological Society Papers **16**, 291–316.

McArthur, J. M., Thirlwall, M. F., Engkilde, M., Zinsmeister, W. J. & Howarth, R. J. 1998. Strontium isotope profiles across K/T boundary sequences in Denmark and Antarctica. *Earth and Planetary Science Letters* **160**, 179–192.

Meldahl, K.H., 1990. Sampling, species abundance, and the stratigraphic signature, of mass extinction: a test using Holocene tidal flat molluscs. *Geology* **18**, 890–893.

Oleinik, A. E. & Zinsmeister, W. J., 1996. Paleocene diversification of bucciniform gastropods on Seymour Island, Antarctica. *Journal of Paleontology* **70**, 923–934.

Olivero, E. B., 2012. Sedimentary cycles, ammonite diversity and palaeoenvironmental changes in the Upper Cretaceous Marambio group, Antarctica. *Cretaceous Research* 34, 348–**366**.

Olivero, E. B., Martinioni, D. & Mussel, F., 1992. In: *Geología de la Isla James Ross* (ed. Rinaldi, C. A.), pp. 125–145 (Publicacion Especial del Instituto Antartico Argentin, Buenos Aires).

Pirrie, D., Crame, J. A., Lomas, S. A. & Riding, J. B., 1997. Late Cretaceous stratigraphy of the Admiralty Sound region, James Ross Basin, Antarctica. *Cretaceous Research* **18,** 109–137.

Ponder, W. F. & Limberg, D. R., 2008. *Phylogeny and evolution of the Mollusca.* 469 p. (University of California Press).

Stilwell, J. D. & Zinsmeister, W. J., 2002. A new, large, Acteonid gastropod (Mollusca) from the latest Cretaceous of Antarctica. *Journal of Paleontology* **76**, 1102–1105.

Stilwell, J. D. & Zinsmeister, W. J., 1987[a]. Late Cretaceous faunal assemblage of Humps Island collected during the 1986–1987 expedition to the Antarctic Peninsula. *Antarctic Journal of the United States* **12**, 9–10.

Stilwell, J. D. & Zinsmeister, W. J., 1987[b]. Late Cretaceous fossils from Ula Point, James Ross Island, collected during the 1986–1987 expedition to the Antarctic Peninsula. *Antarctic Journal of the United States* **12**, 8–9.

Stilwell, J. D., 2002. Geological exploration of Cockburn Island, Antarctic Peninsula. *Polish Polar Research* **23,** 47–73.

Stilwell, J. D., 1998. Late Cretaceous Mollusca from the Chatham Islands, New Zealand. *Alcheringa* **22**, 29–85.

Stilwell, J. D., Zinsmeister, W. J. & Oleinik, A. E., 2004. Early Paleocene mollusks of Antarctica: systematics, paleoecology and paleogeographic significance. *Bulletins of American Paleontology* **367**, 1–89.

Tobin, T. S., Ward, P.D., Steig, E.J., Olivero, E.B., Hilburn, I.A., Mitchell, R.N., Diamond, M.R., Raub, T.D., Kirschvink, J.L., 2012. Extinction patterns, $\delta^{18}O$ trends, and magnetostratigraphy from a southern high-latitude Cretaceous–Paleogene section: links with Deccan volcanism. *Palaeogeography Palaeoclimatology Palaeoecology* **350–352**, 180–188.

Vonhof, H.B., Jagt, J.W.M., Immenhauser, A., Smit, J., Van Den Berg, Y.W., Saner, M., Keutgen, N., Reijmer, J.J.G., 2011. Belemnite-based strontium, carbon, and oxygen isotope stratigraphy of the type area of the Maastrichtian stage. *Netherlands Journal of Geosciences* **90**, 259–270.

Waller, T. R., 2006. Phylogeny of families in the Pectinoidea (Mollusca: Bivalvia) importance of the fossil record. *Zoological Journal of the Linnean Society* **148**, 313–342.

Whittle, R. J., Linse, K. & Griffiths, H. J., 2011. The fossil record of *Limopsis* (Bivalvia: Limopsidae) in Antarctica and the southern high latitudes. *Palaeontology* **54**, 935–952.

Wilckens, O., 1910. Die Anneliden, Bivalven und Gastropoden der antarktischen Kreideformation. *Wiss. Ergeb. Schwed. Südpolarexp* **3**, 1–132.

Wilmsen, M. & Voigt, T., 2006. The middle-upper Cenomanian of Zilly (Sachsen-Anhalt, northern Germany) with remarks on the *Pycnodonte* event. *Acta Geologica Polonica* **56**, 17–31.

Witts, J. D., Bowman, V. C., Wignall, P. B., Crame, J. A., Francis, J. E. & Newton, R. J., 2015. Evolution and extinction of Maastrichtian (Late Cretaceous) cephalopods from the López de Bertodano Formation, Seymour Island, Antarctica. *Palaeogeography, Palaeoclimatology, Palaeoecology* **418**, 193–212.

Zinsmeister, W. J. & Griffin, M., 1995. Late Cretaceous and Tertiary aporrhaid gastropods from southern rim of the Pacific Ocean. *Journal of Paleontology* **69**, 692–702.

Zinsmeister, W. J. & Macellari, C. E., 1988. Bivalvia (Mollusca) from Seymour Island, Antarctic Peninsula. *Geological Society of America Memoirs* **169,** 25–53.

Zinsmeister, W. J., 1998. Discovery of fish mortality horizon at the K–T boundary on Seymour Island: re-evaluation of events at the end of the Cretaceous. *Journal of Palaeontology* **72**, 556–571.

Zinsmeister, W. J., 1978. Three new species of *Pulvinites* (Mollusca: Bivalvia) from Seymour Island (Antarctic Peninsula) and southern California. *Journal of Paleontology* **52**, 565–569.

Appendix C   Supplementary data for Chapter 5

C.1   Table C1 Sulphur isotope data

Sample #	BAS Sample #	Comp. Strat. Height (M)	ID	δ³⁴S_CAS (‰VCDT)	δ¹⁸O_CAS (‰VSMOW)	δ³⁴S_hypochlorite-S (‰VCDT)	[CAS] ppm
39-1	D5.1379.2	1074	*Lahillia*	18.70	10.00	8.0	148.14
38-1	D5.1375.2	1070	*Lahillia*	17.65	10.9	-10.5*	194.00
37-1	D5.1363.2	1064	*Lahillia*	13.48	9.2	-	149.47
36-1	D5.1359.2	1062	*Lahillia*	14.69	7.6	-4.3	74.61
35-1	D5.1355.2	1060	*Lahillia*	14.24	6.9	-9.6	116.61
34-1	D5.1351.2	1058	*Lahillia*	57.70	16.9	-17	109.31
33-1	D5.1343.2	1054	*Lahillia*	29.81	10.4	-6.5	109.14
32-1	D5.1339.2	1052	*Lahillia*	35.8	-	-8.8*	272.49
30-1	D5.1336.2	1049	*Lahillia*	12.6	-	-	80.97
29-1	D5.1334.2	1047	*Lahillia*	0.72	-1.4	-2.2	527.97
24-1	D5.1313.2	1022-1028	*Lahillia*	9.2	5.3	-4.6*	301.34
23-1	D5.1307.2	1019	*Lahillia*	19.4	-	-8.1	90.94
22-1	D5.1301.2	1010-1016	*Lahillia*	17.72	8.5	0.4*	75.15
21-1	D5.1295.2	1007-1010	*Pycnodonte*	18.22	9.6	6.1	1402.5
20-1	D5.1289.2	1004	*Lahillia*	-10.72	-0.6	-11.6	24318.6
18-1	D5.1277.2	986-992	*Pycnodonte*	17.78	8.5	-3.3*	1108.84
16-1	D5.1270.2	980-986	*Pycnodonte*	18.38	10.3	-10.1	591.89
15-1	D5.1251.2	978-984	*Pycnodonte*	18.76	9.9	3.1*	1232.15
14-1	D5.1248.2	972-978	*Pycnodonte*	17.02	9.4	7.5*	578.01
13-1	D5.1245.2	966-972	*Pycnodonte*	17.79	10.3	-10.6*	1472.26
12-1	D5.1241.2	960-966	*Pycnodonte*	17.00	8.4	15.0	1047.12
11-1	D5.1238.2	954-960	*Pycnodonte*	17.62	8.8	-5.5	1407.32
10-1	D5.1236.2	956	*Pycnodonte*	16.82	9.5	-0.2	370.32
9-1	D5.1234.2	948-954	*Pycnodonte*	18.28	9.4	13.8	1134.50
8-1	D5.1229.2	942-948	*Pycnodonte*	17.41	8.4	8.0	842.05
5-1	D5.1220.2	924-930	*Pycnodonte*	17.51	8.6	-3.5	1080.93
4-1	D5.1217.2	918-924	*Lahillia*	18.36	10.1	13.1*	2341.82
3-1	D5.1214.2	912-918	*Lahillia*	17.95	10	17.1	1713.99
22-2	D5.1197.2	882-888	*Pycnodonte*	16.34	12.8	-0.5	658.56
19-2	D5.1138.2	772-778	*Cucullaea*	15.20	-	-	156.25
18-2	D5.1111.2	726-731	*Eselaevitrigonia*	16.01	11.0	-	282.27
16-2	D5.1040.2	656-661	*Cucullaea*	-5.16	6.9	-28.2	1058.61
15-2	D5.1021.2	636-641	*Cucullaea*	11.86	-	-11.7	128.42
14-2	D5.1006.2	621-626	*Pycnodonte*	18.00	12.1	-16.7	1811.69
13-2	D5.696.2	607-612	*Cucullaea*	16.27	-	-	44.98
12-2	D5.672.2	582-587	*Cucullaea*	18.11	12.1	-4.3*	140.63
11-2	D5.370.2	549	*Pycnodonte*	18.03	10.2	-1.4*	2134.57
9b-2	D5.347.2	522-527	*Leionucula*	5.4	-	-23.9	69.54
7-2	D5.970.2	442-447	*Oistotrigonia*	-2.94	4.1	-13.1	652.06
6-2	D5.955.2	427-434	Cucullaeidae	15.80	11.3	-1.0*	92.50
2-2	D5.490.2	166	*Pycnodonte*	16.70	11	-2.5	767.90

C.2   Table C2 Carbonate isotope and trace element data

Sample #	Strat. Height (M)	Generic ID	δ¹⁸O$_{carb}$ (‰VSMOW)	δ¹³C$_{carb}$ (‰VCDT)	Mg (ppm)	Ca (ppm)	Mn (ppm)	Fe (ppm)	Sr (ppm)	Ba (ppm)
D5.1379.2	1074	*Lahillia*	1.42	1.24	1242	398600	206.9	839.9	1836	34.88
D5.1375.2	1070	*Lahillia*	1.18	-1.79	4943	357000	615	3842	1748	50.87
D5.1363.2	1064	*Lahillia*	1.01	-1.21	1195	383200	397.2	1339	2513	100.4
D5.1359.2	1062	*Lahillia*	1.38	0.78	753	369700	356.6	989.3	2124	52.85
D5.1355.2	1060	*Lahillia*	1.40	0.86	292.5	400000	115.2	339.3	2921	62.75
D5.1351.2	1058	*Lahillia*	1.43	-7.19	6275	358200	888.9	3947	1507	52.86
D5.1343.2	1054	*Lahillia*	0.99	-0.38	1791	314100	704.5	2149	1846	51.31
D5.1339.2	1052	*Lahillia*	1.09	-3.40	2905	362900	743.5	1992	2015	47.11
D5.1336.2	1049	*Lahillia*	0.93	-6.41	8230	353100	1531	8179	2972	88.84
D5.1334.2	1047	*Lahillia*	1.17	1.85	125.3	388700	55.59	237.2	4614	49.91
D5.1313.2	1022-1028	*Lahillia*	1.53	1.28	1808	324300	501	19200	1976	37.18
D5.1307.2	1019	*Lahillia*	1.13	-1.00	2316	323200	321.1	1114	1466	34.41
D5.1301.2	1010-1016	*Lahillia*	0.72	1.60	658.2	356800	248.6	1902	2126	68.38
D5.1295.2	1007-1010	*Pycnodonte*	0.10	3.04	1329	365700	345.7	624.8	508	5.672
D5.1289.2	1004	*Lahillia*	1.18	2.05	227.9	368100	204.1	320.4	1612	44.9
D5.1277.2	986-992	*Pycnodonte*	0.91	3.61	1729	381900	309.4	784.3	614	8.003
D5.1270.2	980-986	*Pycnodonte*	-0.58	0.37	5906	391500	1222	3599	494	13.96
D5.1251.2	978-984	*Pycnodonte*	-0.07	0.77	5974	405200	1873	3819	511	10.19
D5.1248.2	972-978	*Pycnodonte*	0.48	3.32	1150	381900	257.8	344.6	592	5.098
D5.1245.2	966-972	*Pycnodonte*	-0.15	3.03	1986	404800	660.8	1035	538	4.862
D5.1241.2	960-966	*Pycnodonte*	0.45	-0.88	11930	368400	96.62	213.9	652	6.869
D5.1238.2	954-960	*Pycnodonte*	-0.30	3.31	2588	367100	856.9	1998	554	7.134
D5.1236.2	956	*Pycnodonte*	0.19	2.97	2645	391100	710.5	1734	642	7.224
D5.1234.2	948-954	*Pycnodonte*	-0.51	0.94	8472	351400	638.8	3596	506	10.96
D5.1229.2	942-948	*Pycnodonte*	0.20	1.67	2267	387300	213.1	325.5	667	5.326

D5.1220.2	924-930	*Pycnodonte*	0.04	2.03	3560	354400	656.7	2309	526	9.85
D5.1217.2	918-924	*Lahillia*	0.62	4.13	1058	357600	124	805.4	624	10.19
D5.1214.2	912-918	*Lahillia*	0.78	1.35	1464	458900	97.61	207.8	7603	138
D5.1197.2	882-888	*Pycnodonte*	0.74	2.91	6975	384600	430.3	6962	737	26.92
D5.1138.2	772-778	*Cucullaea*	1.05	1.66	86.09	389500	10.77	238.5	2160	44.53
D5.1111.2	726-731	*Eselaevitrigonia*	1.27	1.83	64.76	375800	7.195	183.8	1702	24.12
D5.1040.2	656-661	*Cucullaea*	0.75	-0.86	1530	371400	834.2	2114	5999	161
D5.1021.2	636-641	*Cucullaea*	0.51	-0.82	522	267000	62.9	1464	3081	125.2
D5.1006.2	621-627	*Pycnodonte*	-0.02	3.02	5678	372400	198.1	696.7	647	17.23
D5.696.2	607-612	*Cucullaea*	1.31	2.45	93.77	383800	53.7	154.5	1859	45.34
D5.672.2	582-587	*Cucullaea*	1.36	-2.45	172.2	380900	19.21	299.4	4500	106.9
D5.370.2	549	*Pycnodonte*	0.39	3.12	16240	379100	241.9	2052	744	28.12
D5.347.2	522-527	*Leionucula*	2.15	-0.18	241.4	383700	505.4	347.7	3986	45.99
D5.970.2	442-447	*Oistotrigonia*	1.35	1.54	131.9	357100	33.05	216.2	1722	26.95
D5.955.2	427-434	Cucullaeidae	1.28	0.79	299.3	353600	15.44	127.7	2734	58.35
D5.490.2	166	*Pycnodonte*	0.93	2.79	1241	377000	219.5	1922	700	39.38

C.3 Sedimentary geochemistry and pyrite sulphur isotope data

Comp. Height (m)	Strat. Height (m)	Sample Number	Sub-section	TOC (wt %)	Bulk δ13C VPDB	Total S (wt %)	Py-S (wt %)	δ34SPyrite (VCDT)
1074	100	D5.1379.1	D5.229				0.00	-4.63
1072	98	D5.1377.1	D5.229	0.45	-26.14	0.32	0.01	-8.44
1069	95	D5.1373.1	D5.229	0.29	-25.98			
1064	90	D5.1363.1	D5.229	0.27	-26.04			
1062	88	D5.1359.1	D5.229				0.01	-6.51
1059	85	D5.1353.1	D5.229	0.13	-26.08			
1058	84	D5.1351.1	D5.229				0.00	-9.90
1056	82	D5.1347.1	D5.229	0.27	-25.77			
1054.5	80.5	D5.1344.1	D5.229				0.02	-21.67
1052	78	D5.1339.1	D5.229	0.44	-25.62	0.24	0.01	-10.52
1047	73	D5.1334.1	D5.229				0.00	-21.50
1044	70	D5.1331.1	D5.229	0.43	-24.96			
1034	60	D5.1320.1	D5.229	0.30	-24.81			
1032	58	D5.1318.1	D5.229	0.41	-24.86	0.29	0.00	1.96
1027	53	D5.1312.1	D5.229	0.22	-25.16			
1024	50	D5.1309.1	D5.229				0.00	-16.77
1023	49	D5.1308.1	D5.229				0.00	-16.46
1022	48	D5.1307.1	D5.229	0.34	-24.73	0.22	0.00	-10.69
1019	45	D5.1304.1	D5.229	0.16	-25.73			
1013	39	D5.1298.1	D5.229	0.14	-25.00		2.52	-14.25
1012	38	D5.1297.1	D5.229	0.36	-23.98	0.16	0.00	-5.98
1011	37	D5.1296.1	D5.229	0.26	-24.94	0.25	0.14	-13.90
1009	35	D5.1294.1	D5.229	0.14	-24.77	0.18	0.12	-14.50
1008	34	D5.1293.1	D5.229	0.43	-22.37	0.33	0.13	-23.86
1007	33	D5.1292.1	D5.229	0.39	-24.70	0.40	0.00	-17.33
1006	32	D5.1291.1	D5.229	0.29	-24.29	0.34	0.23	-4.86
1005	31	D5.1290.1	D5.229	0.36	-24.98	0.34	0.00	-16.20
1004	30	D5.1289.1	D5.229	0.40	-25.30	0.32	0.00	-21.04
1003	29	D5.1288.1	D5.229	0.37	-24.61		0.00	-5.36
1000	26	D5.1285.1	D5.229	0.24	-25.20			
995	21	D5.1280.1	D5.229	0.37	-24.32			
990	16	D5.1275.1	D5.229	0.57	-25.10			

989	15	D5.1274.1	D5.229	0.38	-24.75	0.18	0.00	-13.31
985	11	D5.1269.1	D5.229	0.27	-24.86			
983	9	D5.1267.1	D5.229				0.01	-16.51
980	6	D5.1264.1	D5.229	0.20	-25.42			
975	1	D5.1259.1	D5.229	0.32	-25.06	0.42	0.00	-11.85
974	0	D5.1258.1	D5.229	0.29	-24.96			
970	22	D5.1244.1	D5.222		-25.38			
969	21	D5.1243.1	D5.222				0.03	26.82
966	18	D5.1241.1	D5.222	0.30	-25.50		0.00	-7.17
963	16	D5.1240.1	D5.222	0.21	-25.11	0.24	0.01	-14.73
960	12	D5.1238.1	D5.222	0.37	-24.54			
958	10	D5.1236.1	D5.222				0.01	-9.52
954	6	D5.1234.1	D5.222	0.28	-23.35			
950	4	D5.1232.1	D5.222	0.22	-24.72		0.00	
944	74	D5.1227.1	D5.220	0.29	-24.83	0.62	0.01	11.85
940	70	D5.1225.1	D5.220	0.21	-22.93			
934	64	D5.1222.1	D5.220	0.22	-23.74			
930	60	D5.1220.1	D5.220	0.14	-24.84			
926	56	D5.1218.1	D5.220	0.22	-24.28		0.00	13.62
924	54	D5.1217.1	D5.220	0.30	-22.36	0.84	0.03	25.20
920	50	D5.1215.1	D5.220	0.18	-25.45			
916	46	D5.1213.1	D5.220				0.01	15.46
914	44	D5.1212.1	D5.220	0.31	-24.34			
910	40	D5.1210.1	D5.220	0.18	-25.26			
904	34	D5.1207.1	D5.220	0.33	-23.96	0.17	0.00	-9.06
900	30	D5.1205.1	D5.220	0.21	-25.26			
890	20	D5.1198.1	D5.220	0.21	-23.81			
886	16	D5.1196.1	D5.220	0.25	-25.04		0.00	-22.86
883	13	D5.1194.1	D5.220	0.33	-25.05	0.19	0.12	-41.63
880	10	D5.1192.1	D5.220	0.27	-25.13			
876	6	D5.1190.1	D5.220	0.38	-24.68			
864	178	D5.1183.1	D5.219	0.42	-24.48	0.47		
844	158	D5.1173.1	D5.219	0.17	-25.09	0.38	0.01	-5.29
837	151	D5.1169.1	D5.219	0.27	-24.70			
834	148	D5.1166.2	D5.219	0.22	-24.95			
832	146	D5.1164.1	D5.219	0.27	-25.54		0.15	39.77
831	145	D5.1163.1	D5.219	0.19	-24.26		0.12	-41.22
830	144	D5.1162.1	D5.219	0.19	-24.63			
826	140	D5.1160.1	D5.219				0.15	-45.50
824	138	D5.1159.1	D5.219	0.24	-25.04	0.17	0.12	-47.27

808	121	D5.1151.1	D5.219				0.12	-47.27
800	114	D5.1150.1	D5.219	0.26	-25.10	0.13		
784	98	D5.1141.1	D5.219	0.34	-24.63	0.03		
764	78	D5.1131.1	D5.219	0.42	-23.84	0.38		
744	58	D5.1120.1	D5.219	0.53	-24.24	0.43		
728	42	D5.1108.1	D5.219				0.05	-4.66
724	38	D5.1104.1	D5.219	0.35	-24.78	0.34		
723	37	D5.1103.1	D5.219	0.41	-24.87			
722	36	D5.1102.1	D5.219	0.50	-24.60			
721	35	D5.1101.1	D5.219	0.34	-24.81			
720	34	D5.1100.1	D5.219	0.45	-24.94			
719	33	D5.1099.1	D5.219	0.49	-21.74			
718	32	D5.1098.1	D5.219	0.28	-23.85			
717	31	D5.1097.1	D5.219	0.31	-24.66			
716	30	D5.1096.1	D5.219	0.27	-23.22			
704	18	D5.1085.1	D5.219	0.24	-24.52	0.08		
683	62	D5.1063.1	D5.218	0.32	-24.67	0.48	0.04	-14.45
663	42	D5.1042.1	D5.218	0.30	-24.50	0.59	0.00	-21.40
654	33	D5.1033.1	D5.218	0.32	-24.91			
653	32	D5.1032.1	D5.218	0.28	-24.70			
651	30	D5.1031.1	D5.218		-24.37			
649	28	D5.1030.1	D5.218	0.39	-23.70			
648	27	D5.1029.1	D5.218	0.36	-24.85			
647	26	D5.1028.1	D5.218	0.26	-23.72			
646	25	D5.1027.1	D5.218	0.28	-24.57			
645	24	D5.1026.1	D5.218	0.24	-24.43			
644	23	D5.1025.1	D5.218		-24.25			
643	22	D5.1024.1	D5.218	0.29	-24.83	0.18		
624	3	D5.1004.1	D5.218	0.44	-24.63		0.01	-31.61
623	2	D5.1003.1	D5.218	0.32	-24.24	0.24		
622	1	D5.1002.1	D5.218	0.45	-24.50			
621	0	D5.1001.1	D5.218	0.34	-24.82			
620	233	D5.704.1	D5.215	0.69	-23.59			
619	232	D5.703.1	D5.215	0.68	-24.57			
618	231	D5.702.1	D5.215	0.50	-24.49			
617	230	D5.701.1	D5.215	0.62	-24.59			
612	225	D5.696.1	D5.215				0.12	-41.06
603	216	D5.687.1	D5.215	0.48	-24.29	0.26		
583	196	D5.668.1	D5.215	0.51	-25.09	0.75	0.01	-12.08
563	176	D5.384.1	D5.215	0.65	-25.00	0.10		

549	162	D5.370.1					0.16	-34.36
543	156	D5.364.1	D5.215	0.60	-25.14	0.72		
528	141	D5.348.1	D5.215	0.52	-24.89			
527	140	D5.347.1	D5.215	0.56	-25.10			
526	139	D5.346.1	D5.215	0.51	-24.35			
525	138	D5.345.1	D5.215	0.61	-25.37			
524	137	D5.344.1	D5.215	0.57	-25.14			
523	136	D5.343.1	D5.215	0.58	-25.45	1.23	0.01	-14.11
522	135	D5.342.1	D5.215	0.66	-25.30			
521	134	D5.341.1	D5.215	0.63	-25.38			
520	133	D5.340.1	D5.215	0.62	-25.38			
503	116	D5.323.1	D5.215	0.45	-24.96	0.70	0.02	
481	94	D5.303.1	D5.215	0.57	-25.39	2.30		
461	74	D5.984.1	D5.215	0.47	-25.35	0.72	0.01	-26.53
443	56	D5.966.1	D5.215	0.65	-25.60	0.77	0.01	-23.54
438	51	D5.961.1	D5.215	0.09	-25.00			
433	46	D5.956.1	D5.215	0.09	-25.33			
428	41	D5.951.1	D5.215	0.81	-25.31			
423	36	D5.946.1	D5.215	0.77	-24.94	1.43		
418	31	D5.941.1	D5.215	0.79	-25.16			
413	26	D5.936.1	D5.215	0.47	-24.76			
408	21	D5.931.1	D5.215	0.48	-25.16			
403	16	D5.926.1	D5.215	0.82	-25.04			
398	11	D5.921.1	D5.215	0.66	-25.04			
393	6	D5.916.1	D5.215	0.51	-24.88			
390	3	D5.913.2	D5.215	0.97	-25.24			
387	0	D5.910.11	D5.215	0.53	-24.70	0.25		
370	307	D5.892.1	D5.212				0.00	2.53
366	303	D5.889.1	D5.212	0.53	-25.44			
356	293	D5.879.1	D5.212	0.52	-25.02			
346	283	D5.869.1	D5.212	0.39	-25.46	0.04	0.00	-14.71
337	274	D5.860.1	D5.212	0.24	-25.05			
316	253	D5.839.1	D5.212	0.37	-25.36			
309	246	D5.832.1	D5.212	0.45	-25.95	0.46		
246	183	D5.570.1	D5.212	0.28	-25.33	0.15	0.16	-25.00
206	143	D5.528.1	D5.212	0.50	-25.03	0.52		
165	102	D5.489.3	D5.212	0.24	-25.73	0.08	0.09	-22.99
158	95	D5.481.2	D5.212				0.03	-27.78

C.4   Quantified XRD data

Sample #	Strat. height (m)	ID	%aragonite	%calcite	%other
D5.1379.2	1074	*Lahillia*	93.17	6.16	0.67
D5.1375.2	1070	*Lahillia*	75.09	18.03	6.87
D5.1363.2	1064	*Lahillia*	89.23	9.05	1.73
D5.1359.2	1062	*Lahillia*	94.85	5.03	0.12
D5.1355.2	1060	*Lahillia*	95.59	2.96	1.45
D5.1351.2	1058	*Lahillia*	47.53	36.99	15.48
D5.1343.2	1054	*Lahillia*	81.28	16.87	1.84
D5.1339.2	1052	*Lahillia*	73.08	26.16	0.76
D5.1336.2	1049	*Lahillia*	63.19	36.81	0
D5.1307.2	1019	*Lahillia*	85.63	13.45	0.91
D5.1301.2	1010-1016	*Lahillia*	94.06	5.74	0.2
D5.1295.2	1007-1010	*Pycnodonte*	0	99.42	0.58
D5.1277.2	986-992	*Pycnodonte*	0	96.92	3.09
D5.1270.2	980-986	*Pycnodonte*	0.79	94.06	5.15
D5.1251.2	978-984	*Pycnodonte*	0	94.65	5.35
D5.1248.2	972-978	*Pycnodonte*	0	98.15	1.86
D5.1245.2	966-972	*Pycnodonte*	0	75.14	24.86
D5.1241.2	960-966	*Pycnodonte*	0	83.46	16.54
D5.1238.2	954-960	*Pycnodonte*	0	97.35	1.17
D5.1236.2	956	*Pycnodonte*	0	97.55	1.77
D5.1234.2	948-954	*Pycnodonte*	0	92.98	7.23

D5.1229.2	942-948	*Pycnodonte*	0.98	97.38	1.65
D5.1220.2	924-930	*Pycnodonte*	0	96.21	3.79
D5.1217.2	918-924	*Lahillia*	0	98.3	1.71
D5.1214.2	912-918	*Lahillia*	33.72	65.46	0.81
D5.1197.2	882-888	*Pycnodonte*	0	93.01	6.99
D5.1138.2	772-778	*Cucullaea*	97.40	2.60	0
D5.1111.2	726-731	*Eselaevitrigonia*	96.42	3.58	0
D5.1021.2	636-641	*Cucullaea*	96.80	3.17	0.03
D5.1006.2	621-627	*Pycnodonte*	0	92.07	7.93
D5.696.2	607-612	*Cucullaea*	99.07	0.93	0
D5.672.2	582-587	*Cucullaea*	96.13	3.87	0
D5.370.2	549	*Pycnodonte*	94.23	5.45	0.32
D5.955.2	427-434	Cucullaeid	92.97	7.03	0
D5.490.2	166	*Pycnodonte*	0	99.91	0.09

C.5 Δ³⁴S data

Strat. Height (Comp.) (m)	Strat Height (m)	Sample # BAS	δ34S_Pyrite	δ34S_CAS	Δ³⁴S
165	D5.212 - 102m	D5.489.3	-22.99		
166	D5.212 - 103m	D5.490.2		16.7	39.6863
549	D5.215 - 162m	D5.370.1	-34.3623		
549	D5.215 - 162m	D5.370.2		18.03	52.3923
583	D5.215 - 196m	D5.668.1	-12.08		
582 - 587	D5.215 - 195 - 200m	D5.672.2		18.11	30.1901
612	D5.215 - 225m	D5.696.1	-41.06		
607 - 612	D5.215 - 220 - 225m	D5.696.2		16.27	57.3252
624	D5.218 - 3m	D5.1004.1	-31.6092		
621 - 626	D5.218 - 0 - 6m	D5.1006.2		18	49.6092
728	D5.219 - 42m	D5.1108.1	-4.66477		
726 - 731	D5.219 - 40 - 45m	D5.1111.2		16.01	20.6748
883	D5.220 - 13m	D5.1194.1	-41.628		
886	D5.220 - 16m	D5.1196.1	-22.86		
882 - 888	D5.220 - 12 - 18m	D5.1197.2		16.3375	48.5804
916	D5.220 - 46m	D5.1213.1	15.46		
912 - 918	D5.220 - 42 - 48m	D5.1214.2		17.95	
924	D5.220 - 54m	D5.1217.1	25.20		
918 - 924	D5.220 - 48 - 54m	D5.1217.2		18.36	
926	D5.220 - 56m	D5.1218.1	13.62267		
924 - 930	D5.220 - 54 - 60m	D5.1220.2		17.51	
944	D5.220 - 74m	D5.1227.1	11.85		
942 - 948	D5.220 - 72 - 78m	D5.1229.2		17.41	
958	D5.222 - 10m	D5.1237.1	-9.52		
954 - 960	D5.222 - 6 - 12m	D5.1238.2		17.62	27.1403
963	D5.222 - 16m	D5.1240.1	-14.7317		
966	D5.222 - 18m	D5.1241.1	-7.17		
960 - 966	D5.222 - 12 - 18m	D5.1241.2		17	24.1706
969	D5.222 - 21m	D5.1243.1	26.82		
966 - 972m	D5.222 - 18 - 24m	D5.1245.2		17.7933	
975	D5.229 - 1m	D5.1259.1	-11.85		
972 - 978	D5.222 -24 - 30m	D5.1248.2		17.02	28.8718
983	D5.229 - 9m	D5.1267.1	-16.51		
980 - 986	D5.229 - 6 - 12m	D5.1270.2		18.38	34.8935
989	D5.229 - 15m	D5.1274.1	-13.31		

986 - 992m	D5.229 - 12 - 18m	D5.1277.2		**17.78**	**31.0946**
1007	D5.229 - 33m	D5.1292.1	**-17.3251**		
1008	D5.229 - 34m	D5.1293.1	**-23.86**		
1009	D5.229 - 35m	D5.1294.1	**-14.50**		
1007 - 1010	D5.229 - 33 - 36m	D5.1295.2		**18.22**	**36.7829**
1011	D5.229 - 37m	D5.1296.1	**-13.8962**		
1012	D5.229 - 38m	D5.1297.1	**-5.98**		
1013	D5.229 - 39m	D5.1298.1	**-14.25**		
1010 - 1016	D5.229 - 36 - 42m	D5.1301.2		**17.72**	**29.0947**
1022	D5.229 - 48m	D5.1307.1	*-10.6948*		
1023	D5.229 - 49m	D5.1308.1	*-16.46*		
1024	D5.229 - 50m	D5.1309.1	*-16.77*		
1062	D5.229 - 88m	D5.1359.1	**-6.51427**		
1062	D5.229 - 88m	D5.1359.2		**14.69**	**24.5885**
1074	D5.229 - 100m	D5.1379.1	**-4.63**		
1074	D5.229 - 100m	D5.1379.2		**18.7044**	**25.2187**

Appendix D   Late Cretaceous (Maastrichtian) shallow water hydrocarbon seeps from Snow Hill and Seymour Islands, James Ross Basin, Antarctica

This appendix has been published as;

Little, C.T.S., Birgel, D., Boyce, A.J., Crame, J.A., Francis, J.E., Kiel, S., Peckmann, J., Pirrie, D., Rollinson, G.K., **Witts**, **J.D.** 2015. Late Cretaceous (Maastrichtian) shallow water hydrocarbon seeps from Snow Hill and Seymour Islands, James Ross Basin, Antarctica. *Palaeogeography, Palaeoclimatology, Palaeoecology* **418**, 213–228.

The paper is attached to the thesis on the accompanying CD.

Appendix E   Sedimentary carbon cycling in a low sulfate ocean: Evidence of episodic seasonally modulated methane oxidation in the Cretaceous-Paleogene Antarctic

This appendix is in preperation for publication;

Hall, J.L.O., Newton, R.J., **Witts**, **J.D.,** Francis, J.E, Harper, E.M., Crame, J.A., Haywood, A.M., Hunter, S.J., In prep. Sedimentary carbon cycling in a low sulfate ocean: evidence of episodic seasonal methane oxidation in the Cretaceous Antarctic. To be submitted to: *Proceedings of the National Academy of Science*.

E.1   Abstract

Sulfate exerts a fundamental control on the pathways of organic carbon oxidation in modern marine sediments, particularly the oxidation of methane. However for the bulk of the Phanerozoic, oceans had much lower sulfate concentrations than modern, and the effects of this on the methane cycle have received little attention. Here, we examine the carbonate-carbon isotope record from well-preserved shallow-infaunal bivalves with sub-annual resolution sampling which allows us to examine not only stratigraphic trends but annual variability in sedimentary carbon cycling. The location across the Cretaceous-Palaeogene boundary of the James Ross Basin represents a time interval characterized by substantially lower oceanic sulfate and with existing evidence for seafloor methane release. Exceptionally negative carbon isotope compositions, considerably outside the reported marine range, appear at several intervals in the section. During these intervals, the annually-resolved records display large amplitude cycles of carbon isotopic variability, with the most negative values, as low as −34‰ in the spring. We interpret these signals as periods where carbon derived from methane oxidation dominated the bottom water dissolved inorganic carbon pool. The cyclic nature of the signal indicates that the system of methane production or oxidation must have been sensitive to environmental

variables on a seasonal time scale. This sensitivity likely precludes control by methane-hydrates and we argue that this indicates the shallowing and increased importance of methanogenesis in the sediments. This style of sedimentary biogeochemical cycling is likely to apply to much of the Phanerozoic where sulfate concentrations are routinely lower than in the modern ocean.

E.2   **Significance statement**

Marine sulfate plays a major role in carbon cycling, strongly influencing sedimentary methane production and breakdown. However, the behaviour of the marine methane cycle under low sulfate conditions is poorly understood. Here, we sample stable isotope records from infaunal marine bivalves with sub-annual resolution, affording records of bottom-water temperature and DIC isotopic composition during the mid-Cretaceous to Eocene low sulfate interval. This approach gives insight into both stratigraphic trends and annual variability in sedimentary carbon cycling. We observed exceptionally negative seasonal carbon isotopic signals; which suggest a radically different, more environmentally responsive methane oxidation mechanism than that observed in modern oceans. This mechanism likely applies to large tracts of the Phanerozoic, where sulfate levels were significantly lower than modern.

In the modern ocean, sulfate plays a key role in the oxidation of organic carbon in ocean sediments via the process of microbial sulfate reduction (MSR). In modern near shore settings MSR can account for up to ~80% of organic carbon oxidation (Jørgensen and Kasten, 2006). Simplistically, only organic carbon that survives mineralisation by MSR to below the sedimentary zone where sulfate concentrations have been reduced to zero is then available for methanogenesis. Ocean sulfate concentrations will therefore exert a first order control on both the amount of organic carbon available for methanogenesis and the sedimentary depth at which methanogenesis becomes the dominant mineralisation process. High sulfate plays an additional role in regulating methane release from sediments via the process of anaerobic methane oxidation (AOM). During AOM, consortia of archaea and bacteria oxidize methane using sulfate to produce hydrogen sulfide; a reaction which provides an effective barrier to methane diffusion from the sediment to the water column in the modern ocean (Hinrichs and Boetius, 2002; Reeburgh, 2007).

The chemistry of the oceans has varied considerably over Earth's history, with sulfate in particular fluctuating between ~5 and 28 mM across the Phanerozoic (Horita et al., 2002; Holt et al., 2014). It is therefore reasonable to hypothesize that the lower sulfate oceans of the past would have been characterized by greater methane production in ocean sediments, with methanogenesis occurring at shallower depths in the sediment, and a greater diffusional flux of this methane from the sediment to the water column. In this scenario it is possible to envisage methane production and oxidation becoming more susceptible to seasonal factors such as organic matter delivery and temperature fluctuations. Here we explore this hypothesis by applying high resolution carbon isotope analysis to the shells of late Cretaceous bivalves, from a high palaeo-latitude section from Seymour Island (65°S (Lawver et al., 1992)), with the aim of detecting the characteristically negative signatures of methane-derived carbon after it has been oxidized to dissolved inorganic carbon (DIC).

The Cretaceous is part of a ~140 Myr time period characterized by low sulfate concentrations; data from halite fluid inclusion analyses suggest that concentrations were less than half modern (<14mM) for most of this period, although the error bars on these analyses are large (Horita et al., 2002). Subsequent records of carbonate

associated sulfate-sulfur isotopic composition combined with sulfur-cycle modelling, mostly focused on the early Cretaceous and its OAE intervals, suggest that sulfur concentrations were variable and nearer the lower end of previous estimates (Wortmann and Chernyavsky, 2007; Adams et al., 2010; Owens et al., 2013; Poulton et al., 2015; Gomes et al., 2015).

This study focuses on fossils of the López de Bertodano formation of Seymour Island, Antarctica for several reasons: the Late Cretaceous age (Crame et al., 2004; Bowman et al., 2014 and supplementary for age model) means that ocean sulfate concentrations are likely to have been low, and muted indicators of methane production and oxidation have already been observed at discrete levels in the succession. These take the form of repeated occurrences of thyasirid, lucinid and solemyid bivalve taxa known to host chemosymbiotic bacteria and occur at sites of methane seepage; and burrow-filling carbonates with distinctly negative carbon isotope compositions. ($\delta^{13}C$ = −24 to −58‰, (Little et al., 2015). The abundance of authigenic carbonate produced at many sites of focused methane seepage is entirely absent from this formation, although it has been observed in Campanian sediments on nearby Snow Hill Island (Little et al., 2015).

Infaunal bivalves have been established as good archives of environmental stable isotope data; *Cucullaea* from the Eocene of Seymour Island have previously been used for high resolution seasonal studies (Dutton et al., 2002; Buick and Ivany, 2004). The active pumping of water to supply food particles, oxygen and ions for biomineralization means that the isotope signatures produced in modern shells are dominated by bottom water rather than sedimentary signatures (Klein et al., 1996). Some species do incorporate a small amount of respired organic carbon into their shell carbonate, however the majority is precipitated from the dissolved inorganic carbon (DIC) in inhalant seawater with little fractionation (McConnaughey et al., 1997; Poulain et al., 2010). Even bivalves which derive nutrition from chemosymbiotic methane oxidizing bacteria at modern seeps, have shell carbon isotope compositions dominated by DIC from the ambient seawater, and display a depleted $\delta^{13}C$ signal only in their soft tissues. (Paull et al. 1989; Fisher 1995). Bivalves are therefore ideal to capture signals of methane-oxidation present in the benthic boundary layer of the water column. Examples of the infaunal genera *Lahillia*

and *Cucullaea* were chosen for this study due to their abundance in pre- and post-extinction faunas and the preservation of their original aragonite shell material, verified by electron and cathodoluminescence microscopy and x-ray diffraction (Fig. S2-S3). Their large shell size has enabled microsampling for isotopic analysis within growth bands thus affording records of temperature and DIC isotopic composition at approximately monthly resolution. This allows us to examine not only stratigraphic trends but annual variability in Late Cretaceous sedimentary carbon cycling.

E.3   Results

Carbon isotopic records in the bivalves show strong seasonal trends related to the annual growth bands, with 9 of the 19 shells examined at high resolution presenting a consistent pattern of abnormally depleted $\delta^{13}C$ values, (as low as −34‰) at the beginning of each growth phase, with a trend towards less negative values throughout the growing period (Fig. 1).. Mean average $\delta^{13}C$ for these specimens is between −23.8 and −0.5‰, with up to 23.5‰ variation within one shell. The other 10 shells exhibit signals with much more positive $\delta^{13}C$ averages of between −2.3 and +4.2‰ with periodic variations within each specimen averaging 1.7‰, which is typical of productivity-influenced signals observed in modern shells (Schöne et al., 2005; Toland et al., 2000; Carré et al., 2005) .

Oxygen isotopic data were used to establish the seasonality of the carbon isotope signals. Individual $\delta^{18}O$ records in both species have cuspate trajectories truncated against visible major growth lines. A characteristic trend toward more negative $\delta^{18}O$ during the growth seasons indicates shell production throughout the warming spring and summer with growth ceasing shortly after summer peak temperatures were reached each year (Fig. 1).

The strong seasonal carbon isotope excursions are present in both species and appear to be clustered in time. There are several horizons containing bivalves with extreme carbon isotope depletion which occur close to, or overlap occurrences of putatively chemosymbiotic bivalves (Little et al., 2015). These are separated by stratigraphic sections containing shells displaying typical low-amplitude isotopic variation well within the range of contemporary marine DIC values (Fig. 2). Bulk

organic carbon isotopic values ($\delta^{13}C_{org}$) are within expected values for photosynthetic activity and show little variation through these active horizons, and total organic carbon (TOC) ranges between 0.14 and 0.65% throughout the section (Fig. 2).

E.4   Discussion

E.4.1   Signal veracity

The carbon isotope variability within the shells is considered to be a primary signal for a number of reasons. Shells are preserved in their original aragonite with well-preserved microstructures. Aragonite is likely to have recrystallized to calcite during any wholesale isotopic resetting; a process which would have obliterated any original microstructure. The seasonal signals preserved in the $\delta^{18}O$ records are more susceptible to diagenetic resetting than carbonate carbon isotopes and plot in a similar range to previously published bulk data sets (Tobin et al., 2012; Dutton et al., 2007). Simple $\delta^{18}O$ conversion (Grossman and Ku, 1986) gives mean recorded temperatures of 7.2 to 18.0°C which is in line with other temperature proxies from the Antarctic Peninsula (Kemp et al., 2014).

We used simple isotopic mass balance models (Fig. 3a and methods) to determine whether the shell records were likely to be an accurate reflection of environmental DIC composition, or if the unusually light signals could have originated from the incorporation of isotopically depleted metabolic carbon from a particulate organic carbon (POC) food source. Isotopic mass balance using the most extreme reported modern values for the proportional incorporation of POC into bivalve carbonate (37%) and a range of seawater DIC and POC isotope compositions (DIC: 0 to +2.5‰, POC: −28 to −20‰) shows that only values heavier than −11‰ may be accounted for by a pure photosynthetic component. The annual $\delta^{13}C$ excursions in many of the examined shells are far too negative to be accounted for without the contribution of an additional source of depleted carbon. The most likely source is

methanogenic carbon, which is much lighter than photosynthetic-derived POC. Methane cannot be incorporated directly into shell carbonate, unless it is first oxidized to DIC.

It is therefore likely that the signals in the shells are an accurate reflection of the DIC composition of the water sourced by the bivalves for shell mineralization. Similar negative signals are, however, not seen in the bulk organic $\delta^{13}C$ data, suggesting the bivalves are recording a localized bottom-water DIC signal rather than a record of depletion in the entire water column.

E.4.2   Origin and seasonality

The presence of cyclic isotopic depletion in these bivalves can therefore also be linked to annual changes in the isotopic composition of bottom-water DIC. Seasonal depletion may be introduced by variation of the $\delta^{13}C$ of the methane itself or by seasonal modulation of the rate of methane release and breakdown. Winter $\delta^{13}C$ depletion of up to 10‰ has been observed in biogenic methane from marine sediments (Martens et al., 1986), but this is clearly insufficient to explain the seasonal variations reported, which can be as great as 23.5‰ even within the truncated period of active spring-summer shell growth. Since variability within the methane itself is unlikely to explain the observed signals, we consider mechanisms by which methane flux may be pulsed annually.

The destabilization of methane clathrates may be triggered by annual changes in pressure or temperature in the water column. However, at around 200m water depth, the accepted continental shelf-edge setting for the bivalves under study would not have produced sufficient pressures for the formation of sea-bed clathrates at temperatures greater than around −2°C without the influence of a marine-based ice sheet (Kvenvolden, 1993). One-dimensional sedimentary geotherm modelling (see supplementary) using mean annual temperatures from our $\delta^{18}O$ data suggests that temperatures were too high to allow clathrate formation at sediment depths which could realistically be affected by seasonal variations in temperature and pressure, unless brief periods of cooler bottom water were present.

Precluding control by methane clathrates, we conclude that the bivalve shells are recording a direct signal of enhanced springtime methane input to DIC. Shell δ^{13}C values of the magnitude we observe have not been recorded in any modern methane seep material (Hein et al., 2006; Lartaud et al., 2010), and no comparable evidence has been found for such pronounced seasonality. Modern areas of prolific seasonal methanogenesis tend to occur in shallow-waters such as swamps and marginal marine estuaries with extremely high organic carbon sedimentation, many of which also have lower than marine sulfate levels (Crill and Martens, 1983; Van der Nat and Middelburg; Zhang et al., 2008). However, to find similar seasonal release in high-biodiversity fully marine environments with relatively low sedimentary TOC (Fig. 2) and no evidence for widespread shallow sedimentary anoxia is extremely unusual. We extend the mass balance approach to estimate the amount of methane-derived material required to produce signals of this magnitude. Using a range of possible methane δ13C values, we calculate that methane-derived DIC may have accounted for a remarkable 30 to 85% of local bottom water DIC during the peak spring depletion (methods section).

This unusual DIC signal hints at a style of marine methane breakdown and release within these Cretaceous sediments which is fundamentally different from biogeochemical cycles observed in modern systems. The strength of the isotopic signals are consistent with our original hypothesis that the low-sulfate conditions of the Late Cretaceous allowed for a greatly increased flux of methane-derived DIC to bottom-waters. A conceptual model of the normal modern and hypothetical low-sulfate Cretaceous conditions is explored in Figure 3. The depleted Cretaceous bottom-waters recorded by bivalve shells are likely to result from some combination of enhanced methane production, and oxidation to bottom-water DIC, but it would be difficult to decouple the two effects without further biogeochemical modelling. It is also difficult to determine the balance of methane-derived bottom-water DIC produced by AOM vs aerobic oxidation of methane, but it is likely that less AOM occurs under low sulfate conditions, allowing methane to survive to a shallower depth in the sediment where it is able to diffuse or be transported by fluids into bottom waters faster. We also tentatively suggest that an increased flux of methane

gas to the atmosphere may have been possible during low sulfate conditions, which may be of interest for climate modelling simulations.

In this scenario the seasonality of methane flux may have been enhanced by increased surface production of organic matter in spring (Iversen and Jorgensen, 1985; Bange et al., 2010), or by temperature or pressure effects influencing the depth of the methanogenic zone through the year (Crill and Martens, 1983). The mixing ratios of bulk seawater and local bottom-water may also be affected by seasonal salinity and stratification effects which could contribute to the domination of bottom-waters by such a strong DIC signal. These effects are beginning to be incorporated into models for the mechanism of methane release in modern systems (Mau et al., 2014; Gentz et al., 2014). It is also possible that the high sedimentation rates in the James Ross Basin (up to 0.1 – 0.2mm/yr) may have enhanced pore space compaction, increasing the fluid flux rate and allowing more methane-derived DIC to be released from sediments, contributing to the extremity of this signal.

The episodic nature of methane release throughout the stratigraphic section is more difficult to justify, as an increased methane flux due to a low sulfate biogeochemical regime might be expected to operate throughout the whole mid-Cretaceous to Eocene low-sulfate interval. The onset of increased methane flux to DIC may be linked to a proposed period of local climate warming observed through the latest part of this stratigraphic section (Tobin et al., 2012; Bowman et al., 2013; Kemp et al., 2014; Bowman et al., 2014). It is also possible that small changes in the regional sulfate concentration of the ocean may have been enough to drive the change in regime seen here. The development of regional differences in sulfate concentration have been demonstrated for the early Jurassic (Newton et al, 2011) and may be important in other intervals during the Phanerozoic.

Given the prevalence of low sulfate conditions through the Phanerozoic, the question arises as to why similar extreme shell carbon values have not been documented in previous studies. However, it is rare for bivalve shells to be sufficiently well-preserved for stable isotope analysis as deep in the fossil record as the mid-Cretaceous to Eocene low-sulfate interval or earlier. It is also likely that there will have been a tendency to discount unusual isotopic signals from single analyses of bulk shell material as the result of poor preservation, especially if, as is seen here,

the signals are sporadic in nature and only present in a subset of shells analyzed. Our method of micro-analysis gives confidence in the primary nature of the signals and allows the repetitive patterns within shells to be seen. This approach is rarely used for fossil shell material (Buick and Ivany, 2004; Krantz et al., 1987), but may be required to produce the temporal resolution to detect the extreme seasonal signals which we have used in our calculations to provide diagnostic indicators of methanogenic input to DIC.

E.5   Conclusion

These isotopic records from latest Cretaceous bivalves in Antarctica represent the first time that negative carbon isotope signals of this nature have been documented in the fossil record and resolved on a sub-annual scale, allowing the timing of seasonal and stratigraphically-pulsed $\delta^{13}C$ flux to be determined. The shell carbonate-carbon signals are likely to be reflective of local DIC composition, with extreme springtime carbon isotope depletion suggesting a dominance of bottom-water DIC by marine methane oxidation products. However, bulk sediment organic-carbon isotopes indicate that the influence of this process did not extend to the upper water column. The presence of pronounced annual cyclicity suggests intervals of strong environmental control on methane flux to the bottom-water DIC pool. A methane-clathrate mechanism appears unlikely at the temperatures and water depths indicated for this site, so the signal is more likely due to a combination of enhanced methane production rate and oxidation, facilitated by the low sulfate concentrations of a Cretaceous ocean.

E.6   Methods

Specimens of bivalves of the genus Lahillia and Cucullaea were collected from several measured stratigraphic sections perpendicular to strike during field excursions across southern Seymour Island (Fig. S1). The sections have been correlated by using stratigraphic tie-points, including the well-defined K-Pg boundary layer and a prominent glauconitic horizon ~170 m below as a datum. Both genera

are likely to have been shallow-burrowing mobile infaunal suspension feeders (Zinsmeister and Macellari, 1988).

E.6.1 Preservation tests

Bivalve shell material was tested to confirm the presence of original shell material and rule out diagenetic resetting of stable isotope values. Authigenic carbonate in the sediment is calcite, and both species studied produce aragonite shells. 11 specimens were examined on a cold cathode cathodoluminescence system (CITL 8200 Mk 3A mounted on a Nikon Optiphot petrological microscope) to identify areas of recrystallized carbonate. 5 specimens were examined under scanning electron microscope as polyester resin-mounted polished blocks or fractured surfaces, which were etched to show shell microstructures. Analysis of 8 bulk powders collected by MicroMill from different shell layers was carried out using x-ray diffraction (Bruker D8 diffractometer scanning from 20° to 60° with a 0.02° step size). Results were interpreted using Topas software to indicate proportions of original aragonite and recrystallized calcite. Standard methodology was used for all analyses (SI methods). Diagenetic alteration was found to be limited to the surface layers only, and shells were polished or sectioned for sampling to minimize contamination. Full preservation test results are presented in supporting information.

E.6.2 Stable Isotope Analysis

High resolution stable carbon and oxygen isotope microanalysis was performed for 19 well-preserved specimens. *Lahillia* were polished by dremel to remove any surface alteration and sampled on the outer surface. *Cucullaea* were sectioned along the line of maximum growth and sampled from the cut face to avoid the intermittent periostracal layer identified by SEM. Specimens were microsampled following standard procedures (Dettman & Lohmann 1995) using a Merchantek MicroMill at a resolution of between 5 and 10 samples per visible growth band using an adaptive sampling strategy, i.e. low sampling resolution in fast-growing shell portions, higher resolution in slow-growing portions. The stable oxygen and carbon isotope

compositions of the resulting powders were determined using a Micromass Multicarb Sample Preparation System attached to a VG SIRA Mass Spectrometer. The results are reported with reference to the international standard V-PDB and the precision is better than ±0.06‰ for $\delta^{13}C$ and ±0.08‰ for $\delta^{18}O$. Bulk shell powders produced by grinding shell fragments were also tested for stable isotope composition (Fig. 2) following the same method. To remove obvious outliers, which may be a result of sampling small patches of diagenetically altered material in microborings or cracks, mean and 3σ values were calculated for the oxygen isotope data from each specimen and any outliers were removed from both the oxygen and carbon datasets. This removed a total of 5 data points out of the 564 stable isotope studies performed, all of which are visible in Fig. 1.

E.6.3 Organic Carbon Analysis

133 samples of bulk sediment from composite section D5.251 were analyzed for organic carbon isotope content. Samples were prepared by acidification following standard techniques to remove all carbonate and non-organic material (SI Methods) and analyzed using a Micromass Isoprime continous flow mass spectrometer coupled to a Eurovector or Elementar Pyrocube Elemental Analyser. $^{13}C/^{12}C$ ratios were calibrated using the international standards ANU-sucrose and IAEA-CH7 to the V-PDB scale with a precision of better than ±0.25‰ for repeat analysis of standard materials during the runs. Calculation of weight percent organic carbon was derived from the mass spectrometer traces, and corrected for weight loss during the acidification process.

E.6.4 Carbon Isotope Mass Balance Calculations

Mollusc shells incorporate carbon both from the DIC pool and from POC metabolized as a food source. To explore whether our shell carbon isotope compositions could be explained by this process we used a simple isotope mass balance equation, where F is the proportion of metabolic carbon incorporated into shells, $\delta^{13}C_{shell}$ $\delta^{13}C_{DIC}$, and

$\delta^{13}C_{POC}$ are the $\delta^{13}C$ values of the aragonite shell, the DIC incorporated directly into the shell and the POC incorporated from metabolic processes respectively:

$$\delta^{13}C_{shell}= F\ \delta^{13}C_{DIC} +(1-F)\delta^{13}C_{POC}$$

The normal contribution of respired carbon to bivalve shell carbonate (F) is around 10% (McConnaughey et al., 1997), which typically produces a shell $\delta^{13}C$ depletion of less than 2‰ relative to seawater. An average ocean surface DIC composition of +2.5‰ (Voigt et al., 2012) can be estimated from marine bulk carbonate $\delta^{13}C_{DIC}$ (Fig. 2). Bottom waters may be depleted relative to surface waters so we used a value of 0‰ to represent a lower limit. Modern temperate marine phytoplankton produces organic carbon with a $\delta^{13}C_{POC}$ of around −20‰, whereas Antarctic phytoplankton produces a greater depletion of around −28‰, (Mook and Tan 1991). This range encompasses the observed bulk $\delta^{13}C_{org}$ data presented in the main text (Fig. 2). Applying these values produces expected $\delta^{13}C_{shell}$ values between +2.5 and −2.8‰. Even using an extreme maximum value for F (37% Gillikin et al. 2007); our calculations still only produce a minimum $\delta^{13}C_{shell}$ of −10.4‰ (Table S1). These calculations demonstrate that we must invoke a highly ^{13}C depleted carbon source to explain our data.

The same equation was used to explore the contribution of methane derived DIC to the bottom-water DIC pool, this time using representative shell values of −10 and −34‰ and solving for $\delta^{13}C_{DIC}$ to produce an estimate of bottom-water DIC $\delta^{13}C$. Using the same range of proportional metabolic POC input (0 to 37%) yields bottom water DIC estimates of between −35.0‰ and −42.2‰ required to explain our most negative observed shell signals (Table S2).

$$\delta^{13}C_{bottom\ water\ DIC}= F\ \delta^{13}C_{methane-derived\ DIC} +(1-F)\delta^{13}C_{oceanic\ DIC}$$

We have used a similar mass balance equation (above) to estimate local bottom water DIC sources. If we assume that local bottom water DIC is produced by combining ocean DIC in our expected isotopic range (0 to +2.5‰) with DIC derived from the oxidation of methane, we can work out the fraction of each component that is required to account for the range of bottom water DIC isotopes from the previous calculation. Biogenic methane $\delta^{13}C$ spans −50 to −110‰ (Whiticar 1999). Using these values, between 30-85% methane derived DIC is required to account for the most extreme negative shell values. Results tables for all calculations are available in the supplementary information (Tables S1-S3).

E.7 Acknowledgments

E.8 References cited

Adams, D.D., Hurtgen, M.T., and Sageman, B.B., 2010, Volcanic triggering of a biogeochemical cascade during Oceanic Anoxic Event 2: Nature Geoscience, v. 3, p. 1–4.

Bange, H.W., Bergmann, K., Hansen, H.P., Kock, A., Koppe, R., Malien, F., and Ostrau, C., 2010, Dissolved methane during hypoxic events at the Boknis Eck time series station (Eckernförde Bay, SW Baltic Sea): Biogeosciences, v. 7, p. 1279–1284.

Bowman, V.C., Francis, J.E., Askin, R. a., Riding, J.B., and Swindles, G.T., 2014, Latest Cretaceous–earliest Paleogene vegetation and climate change at the high southern latitudes: palynological evidence from Seymour Island, Antarctic Peninsula: Palaeogeography, Palaeoclimatology, Palaeoecology, v. 408, p. 26–47.

Bowman, V.C., Francis, J.E., and Riding, J.B., 2013, Late Cretaceous winter sea ice in Antarctica? Geology, v. 41, p. 1227–1230.

Buick, D.P., and Ivany, L.C., 2004, 100 years in the dark: Extreme longevity of Eocene bivalves from Antarctica: Geology, v. 32, p. 921.

Carré, M., Bentaleb, I., Blamart, D., Ogle, N., Cardenas, F., Zevallos, S., Kalin, R.M., Ortlieb, L., and Fontugne, M., 2005, Stable isotopes and sclerochronology of the bivalve Mesodesma donacium: Potential application to Peruvian paleoceanographic reconstructions: Palaeogeography, Palaeoclimatology, Palaeoecology, v. 228, p. 4–25.

Crill, P.M., and Martens, C.S., 1983, Spatial and temporal fluctuations anoxic coastal marine sediments of methane production in anoxic coastal marine sediments: Limnology and Oceanography, v. 28, p. 1117–1130.

Dettman, D.L., and Lohmann, K.C., 1995, Microsampling carbonates for stable isotope and minor element analysis; physical separation of samples on a 20 micrometer scale: Journal of Sedimentary Research, v. 65, p. 566–569.

Dinarès-Turell, J., Westerhold, T., Pujalte, V., Röhl, U., and Kroon, D., 2014, Astronomical calibration of the Danian stage (Early Paleocene) revisited: Settling chronologies of sedimentary records across the Atlantic and Pacific Oceans: Earth and Planetary Science Letters, v. 405, p. 119–131.

Dutton, A.L., Huber, B.T., Lohmann, K.C., and Zinsmeister, W.J., 2007, High-resolution stable isotope profiles of a Dimitobelid Belemnite implications for paleodepth habitat and Late Maastrichtian climate Sensitivity: Palaios, v. 22, p. 642–650.

Dutton, A.L., Lohmann, K.C., and Zinsmeister, W.J., 2002, Stable isotope and minor element proxies for Eocene climate of Seymour Island, Antarctica: Paleoceanography, v. 17, p. 1–7.

Gentz, T., Damm, E., Schneider von Deimling, J., Mau, S., McGinnis, D.F., and Schlüter, M., 2014, A water column study of methane around gas flares located at the West Spitsbergen continental margin: Continental Shelf Research, v. 72, p. 107–118.

Gomes, M.L., Hurtgen, M.T., and Sageman, B.B., 2015, Biogeochemical sulfur cycling during Cretaceous oceanic anoxic events: A comparison of OAE1a and OAE2: , p. 233–251.

Grossman, E.L., and Ku, T.-L., 1986, Oxygen and carbon isotope fractionation in biogenic aragonite: Temperature effects: Chemical Geology: Isotope Geoscience section, v. 59, p. 59–74.

Hinrichs, K.-U., and Boetius, A., 2002, The Anaerobic Oxidation of Methane: New Insights in Microbial Ecology and Biogeochemistry, *in* Wefer, G., Billett, D., Hebbeln, D., Jørgensen, B.B., Schlüter, M., and van Weering, T.C.E. eds., Ocean Margin Systems, Berlin, Heidelberg, Springer Berlin Heidelberg, p. 457–477.

Holt, N.M., García-Veigas, J., Lowenstein, T.K., Giles, P.S., and Williams-Stroud, S., 2014, The major-ion composition of Carboniferous seawater: Geochimica et Cosmochimica Acta, v. 134, p. 317–334.

Horita, J., Zimmermann, H., and Holland, H.D., 2002, Chemical evolution of seawater during the Phanerozoic: Geochimica et Cosmochimica Acta, v. 66, p. 3733–3756.

Iversen, N., and Jorgensen, B.B., 1985, Anaerobic methane oxidation rates at the sulfate-methane transition in marine sediments from Kattegat and Skagerrak (Denmark)': v. 1983, p. 944–955.

Jørgensen, B.B., and Kasten, S., 2006, Sulfur Cycling and Methane Oxidation, *in* Schulz, H.D. and Zabel, M. eds., Marine Geochemistry, Berlin/Heidelberg, Springer-Verlag, p. 271–309.

Kemp, D.B., Robinson, S. a., Crame, J. a., Francis, J.E., Ineson, J., Whittle, R.J., Bowman, V., and O'Brien, C., 2014, A cool temperate climate on the Antarctic Peninsula through the latest Cretaceous to early Paleogene: Geology, v. 42, p. 583–586.

Klein, R.T., Lohmann, K.C., and Thayer, C.W., 1996, SrCa and 13C12C ratios in skeletal calcite of Mytilus trossulus: Covariation with metabolic rate, salinity, and carbon isotopic composition of seawater: Geochimica et Cosmochimica Acta, v. 60, p. 4207–4221.

Krantz, D.E., Williams, D.F., and Jones, D.S., 1987, Ecological and paleoenvironmental information using stable isotope profiles from living and fossil molluscs: Palaeogeography, Palaeoclimatology, Palaeoecology, v. 58, p. 249–266.

Kvenvolden, K.A., 1993, Gas hydrates—geological perspective and global change: Reviews of Geophysics, v. 31, p. 173.

Lawver, L.A., Gahagan, L.M., and Coffin, M.F., 1992, The development of paleoseaways around Antarctica, *in* Kennett, J.P. and Warnke, D.A. eds., The Antarctic Paleoenvironment: A Perspective on Global Change Antarctic Research Series, p. 7–30.

Little, C.T.S., Birgel, D., Boyce, A.J., Crame, J.A., Francis, J.E., Kiel, S., Peckmann, J., Pirrie, D., Rollinson, G.K., and Witts, J.D., 2015, Late Cretaceous (Maastrichtian) shallow water hydrocarbon seeps from Snow Hill and Seymour Islands, James Ross Basin, Antarctica: Palaeogeography, Palaeoclimatology, Palaeoecology, v. 418, p. 213–228.

Macellari, C.E., 1988, Stratigraphy, sedimentology, and paleoecology of Upper Cretaceous / Paleocene shelf-deltaic sediments of Seymour Island: Geological Society of America Memoirs, v. 169, p. 25–54.

Martens, C., Blair, N., Green, C., and Des Marais, D., 1986, Seasonal variations in the stable carbon isotopic signature of biogenic methane in a coastal sediment: Science, v. 233, p. 1300–1303.

Mau, S., Gentz, T., Körber, J.H., Torres, M., Römer, M., Sahling, H., Wintersteller, P., Martinez, R., Schlüter, M., and Helmke, E., 2014, Seasonal methane accumulation and release from a gas emission site in the central North Sea: Biogeosciences Discussions, v. 11, p. 18003–18044.

McConnaughey, T.A., Burdett, J., Whelan, J.F., and Paull, C.K., 1997, Carbon isotopes in biological carbonates: Respiration and photosynthesis: Geochimica et Cosmochimica Acta, v. 61, p. 611–622.

Van der Nat, F.-J., and Middelburg, J.J. Methane emission from tidal freshwater marshes: Biogeochemistry, v. 49, p. 103–121.

Owens, J.D., Gill, B.C., Jenkyns, H.C., Bates, S.M., Severmann, S., Kuypers, M.M.M., Wood, R.G., and Lyons, T.W., 2013, Sulfur isotopes track the global extent and dynamics of euxinia during Cretaceous Oceanic Anoxic Event 2: v. 110.

Paull, C.K., Martens, C.S., Chanton, J.P., Neumann, A.C., Coston, J., Jull, A.J.T., and Toolin, L.J., 1989, Old carbon in living organisms and young CaC03 cements from abyssal brine seeps: Nature, v. 342, p. 166–168.

Poulain, C., Lorrain, a., Mas, R., Gillikin, D.P., Dehairs, F., Robert, R., and Paulet, Y.-M., 2010, Experimental shift of diet and DIC stable carbon isotopes: Influence on shell δ13C values in the Manila clam Ruditapes philippinarum: Chemical Geology, v. 272, p. 75–82.

Poulton, S.W., Henkel, S., März, C., Urquhart, H., Flögel, S., Kasten, S., Jaap, S., Damsté, S., Wagner, T., Ozeanforschung, H., and Geomar, K., 2015, A continental-weathering control on orbitally driven redox-nutrient cycling during Cretaceous Oceanic Anoxic Event 2: v. 43, p. 963–966.

Reeburgh, W.S., 2007, Oceanic methane biogeochemistry.: Chemical reviews, v. 107, p. 486–513.

Schöne, B.R., Fiebig, J., Pfeiffer, M., Gleβ, R., Hickson, J., Johnson, A.L.A., Dreyer, W., and Oschmann, W., 2005, Climate records from a bivalved Methuselah (Arctica islandica, Mollusca; Iceland): Palaeogeography, Palaeoclimatology, Palaeoecology, v. 228, p. 130–148.

Thibault, N., Husson, D., Harlou, R., Gardin, S., Galbrun, B., Huret, E., and Minoletti, F., 2012, Astronomical calibration of upper Campanian–Maastrichtian carbon isotope events and calcareous plankton biostratigraphy in the Indian Ocean (ODP Hole 762C): Implication for the age of the Campanian–Maastrichtian boundary: Palaeogeography, Palaeoclimatology, Palaeoecology, v. 337-338, p. 52–71.

Tobin, T.S., Ward, P.D., Steig, E.J., Olivero, E.B., Hilburn, I.A., Mitchell, R.N., Diamond, M.R., Raub, T.D., and Kirschvink, J.L., 2012, Extinction patterns, δ18 O trends, and magnetostratigraphy from a southern high-latitude Cretaceous–Paleogene section: Links with Deccan volcanism: Palaeogeography, Palaeoclimatology, Palaeoecology, v. 350, p. 180–188.

Toland, H., Perkins, B., Pearce, N., Keenan, F., and Leng, M.J., 2000, A study of sclerochronology by laser ablation ICP-MS: Journal of Analytical Atomic Spectrometry, v. 15, p. 1143–1148.

Voigt, S., Gale, A.S., Jung, C., and Jenkyns, H.C., 2012, Global correlation of Upper Campanian – Maastrichtian successions using carbon-isotope stratigraphy: development of a new Maastrichtian timescale: Newsletters on Stratigraphy, v. 45, p. 25–53.

Wortmann, U.G., and Chernyavsky, B.M., 2007, Effect of evaporite deposition on Early Cretaceous carbon and sulphur cycling: v. 446, p. 17–19.

Zhang, G., Zhang, J., Liu, S., Ren, J., Xu, J., and Zhang, F., 2008, Methane in the Changjiang (Yangtze River) Estuary and its adjacent marine area: riverine input, sediment release and atmospheric fluxes: Biogeochemistry, v. 91, p. 71–84.

Zinsmeister, W.J., and Macellari, C.E., 1988, Bivalvia (Mollusca) from Seymour Island , Antarctic Peninsula: Geological Society of America Memoirs,.
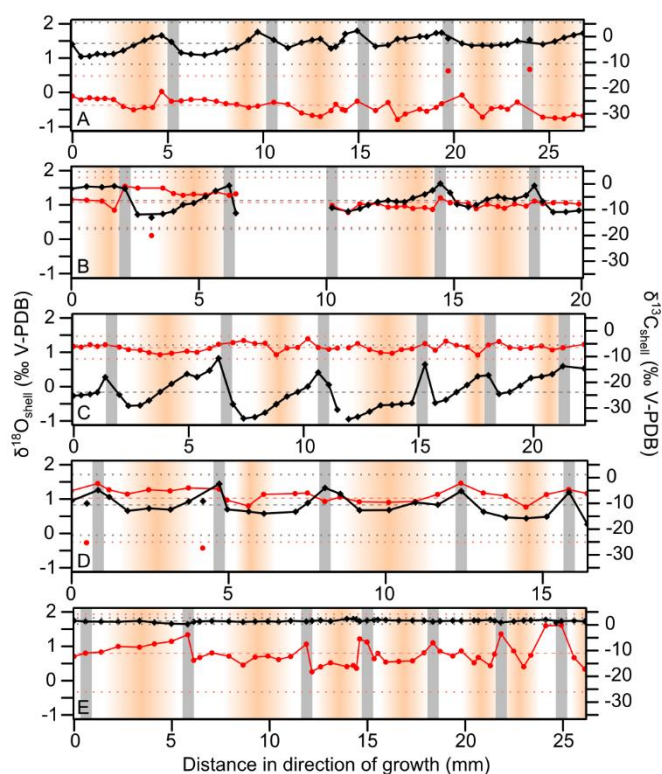
Figure 1. Stable isotope shell profiles of selected *Lahillia* specimens.
(A) D9.207.1, 1026m; (B) D9.206.152 1011m; (C) DJ.953.456, 959m; (D) DJ.953.335, 959m; (E) D5.219.1182.2, 859m. Stable oxygen (red dots) and carbon (black diamonds) isotopes are plotted with most enriched values towards the top of the y axis using the same vertical scales for each specimen. Distance axis begins at an arbitrary point within shell growth due position of cracks and abrasion of earlier growth years from the umbo. Vertical gray bars locate positions of annual growth bands. Horizontal dashed lines represent mean and 3σ values. Orange shading highlights the peak summer δ^{18}O values. Sawtooth variation of δ^{13}C is assumed to represent springtime dominance of DIC by methane derived carbon. Machine errors of ±0.06‰ for δ^{13}C and ±0.08‰ for δ^{18}O do not plot at this resolution.
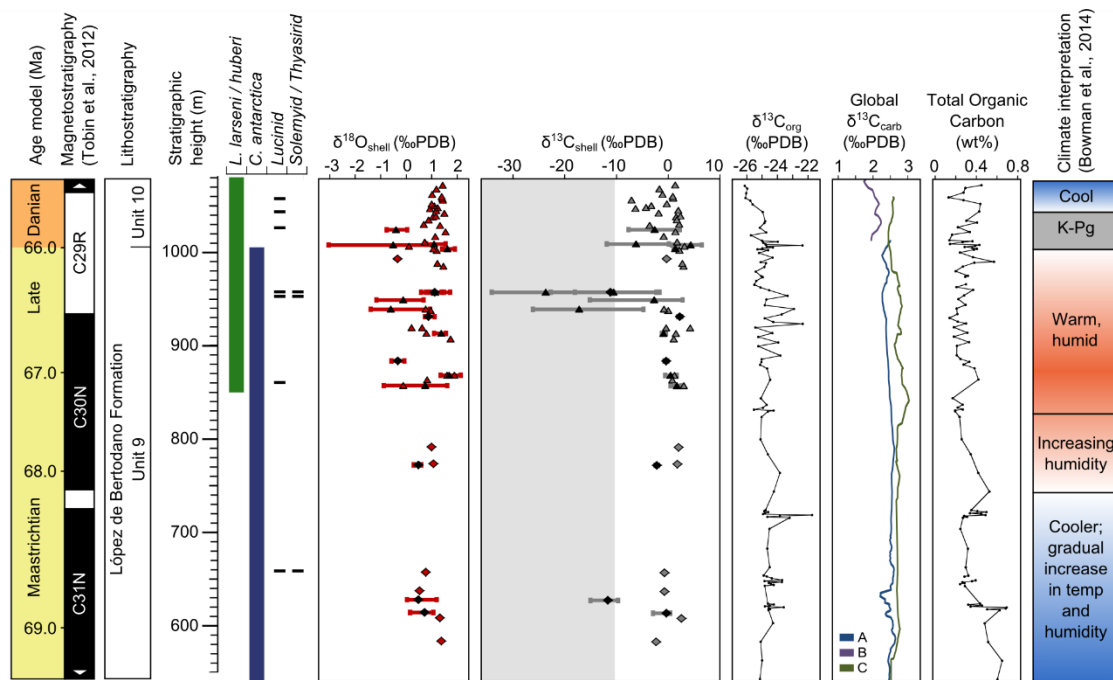
Figure 2. Stable isotope data from Seymour Island.

From left to right: magnetostratigraphy (Tobin et al., 2012) and age model (Macellari, 1988). Stratigraphic ranges for selected bivalve species including recorded horizons of chemosymbiotic-associated lucinids, thyasirids and solemyids. Bulk $\delta^{18}O$ and $\delta^{13}C$ values from *Lahillia* (triangles) and *Cucullaea* (diamonds), horizontal bars with black markers indicate seasonal range and mean values from specimens sampled at high resolution and are not error bars; the shaded field contains $\delta^{13}C$ values lighter than −11‰ which require methane-derived carbon input. $\delta^{13}C$ from organic sedimentary material. Contemporary bulk carbonate $\delta^{13}C$ values; (A) Voigt et al. 2012; (B) Dinarès-Turell et al., 2014; (C) Thibault et al., 2012
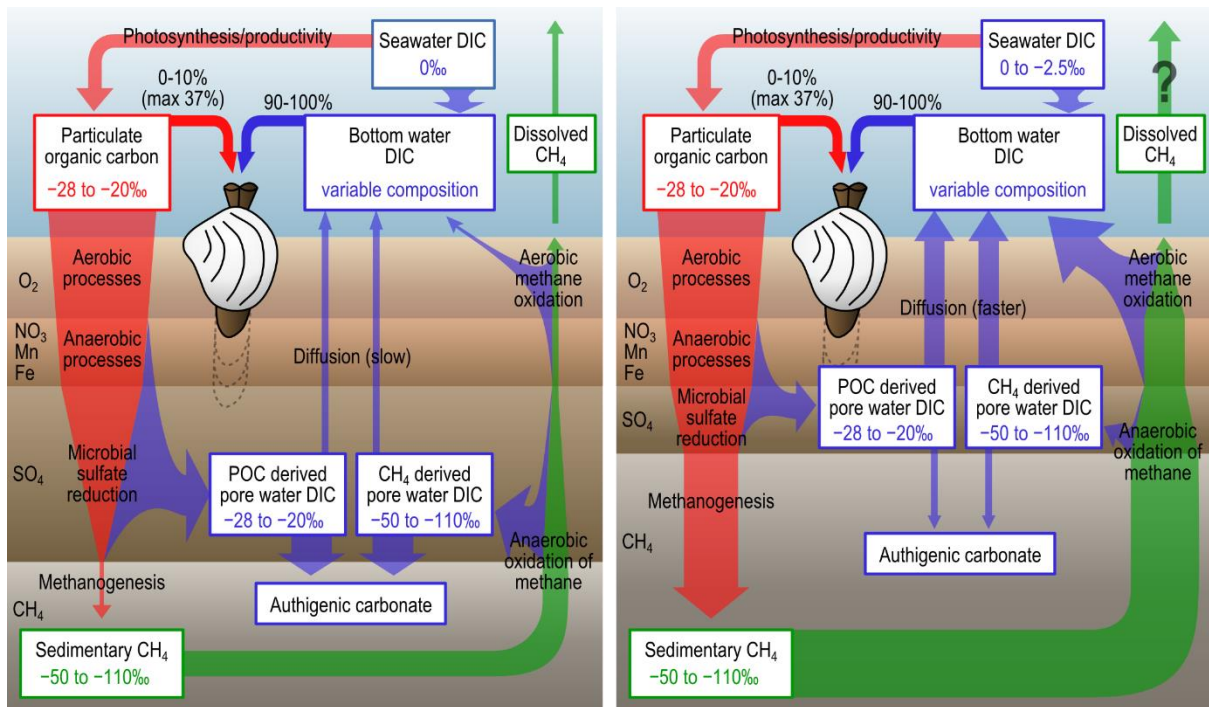
Figure 3. Conceptual model of sedimentary carbon cycle under high and low sulfate conditions

Conceptual diagram of fluxes of POC (red), DIC (blue) and methane (green) under (A) modern high sulfate conditions (B) Cretaceous lower sulfate conditions. Thickness of arrows represents relative strength of flux to each reservoir (not to scale). Depth scales are arbitrary; bottom-water reservoir refers to the benthic boundary layer sampled by bivalves and is likely to be only 5-10cm in depth. The depth to the sulfate zone is variable in modern marine sediments depending on factors such as porewater flow and bioturbation. The proportion of pore water DIC that diffuses into bottom water versus burial as authigenic carbonate is unknown, but likely to relate to depth of DIC production, and pore fluid flux from the sediment to bottom water, thus is likely to be faster in low sulfate systems. Little authigenic carbonate has been found at horizons where we see evidence for increased methane flux to bottom-water DIC